A. DuBois

LBL-8313
SAC-25
UC-70

SWEDISH-AMERICAN COOPERATIVE PROGRAM ON RADIOACTIVE WASTE STORAGE IN MINED CAVERNS IN CRYSTALLINE ROCK

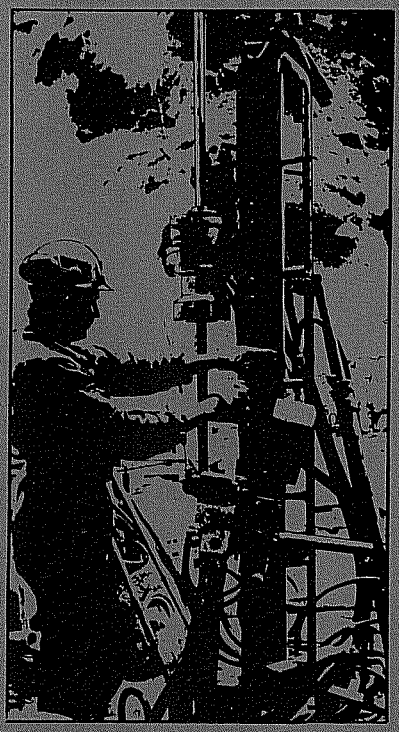

Technical Information Report No. 25

INSTRUMENT EVALUATION, CALIBRATION, AND INSTALLATION FOR THE HEATER EXPERIMENTS AT STRIPA

T. Schrauf, H. Pratt, E. Simonson, and W. Hustrulid
Terra Tek
Salt Lake City, Utah 84108

P. Nelson, A. DuBois, E. Binnall, and R. Haught
Lawrence Berkeley Laboratory
University of California
Berkeley, California 94720

December 1979

A Joint Project of

Swedish Nuclear Fuel Supply Co.
Fack 10240 Stockholm, Sweden

Operated for the Swedish
Nuclear Power Utility Industry

Lawrence Berkeley Laboratory
Earth Sciences Division
University of California
Berkeley, California 94720, USA

Operated for the U.S. Department of
Energy under Contract W-7405-ENG-48

This report was prepared as an account of work sponsored by the United States Government and/or the Swedish Nuclear Fuel Supply Company. Neither the United States nor the U.S. Department of Energy, nor the Swedish Nuclear Fuel Supply Company, nor any of their employees, nor any of their contractors, subcontractors, or their employees, makes any warranty, express or implied or assumes any legal liability or responsibility for the accuracy, completeness or usefulness of any information, apparatus, product or process disclosed, or represents that its use would not infringe privately owned rights.

Printed in the United States of America
Available from
National Technical Information Service
U.S. Department of Commerce
5285 Port Royal Road
Springfield, VA 22161
Price Code: A09

This report is part of a cooperative Swedish-American project supported by the U.S. Department of Energy and/or the Swedish Nuclear Fuel Supply Company. Any conclusions or opinions expressed in this report represent solely those of the author(s) and not necessarily those of The Regents of the University of California, the Lawrence Berkeley Laboratory, the Department of Energy, or the Swedish Nuclear Fuel Supply Company.

Reference to a company or product name does not imply approval or recommendation of the product by the University of California or the U.S. Department of Energy to the exclusion of others that may be suitable.

TECHNICAL INFORMATION DEPARTMENT
LAWRENCE BERKELEY LABORATORY
UNIVERSITY OF CALIFORNIA
BERKELEY, CALIFORNIA 94720

LBL-8313
SAC-25
UC-70

INSTRUMENT EVALUATION, CALIBRATION, AND INSTALLATION FOR THE HEATER EXPERIMENTS AT STRIPA

T. Schrauf, H. Pratt, E. Simonson and W. Hustrulid
Terra Tek
Salt Lake City, Utah 84108

P. Nelson, A. DuBois, E. Binnall and R. Haught
Lawrence Berkeley Laboratory
University of California
Berkeley, California 94720

December 1979

This report was prepared by the Lawrence Berkeley Laboratory under the University of California Contract W-7405-ENG-48 with the U.S. Department of Energy. Funding for this project is administered by the Office of Nuclear Waste Isolation at Battelle Memorial Institute.

PREFACE

This report is one of a series documenting the results of the Swedish-American cooperative research program in which the cooperating scientists explore the geological, geophysical, hydrological, geochemical, and structural effects anticipated from the use of a large crystalline rock mass as a geologic repository for nuclear waste. This program has been sponsored by the Swedish Nuclear Power Utilities through the Swedish Nuclear Fuel Supply Company (SKBF), and the U.S. Department of Energy (DOE) through the Lawrence Berkeley Laboratory (LBL).

The principal investigators are L. B. Nilsson and O. Degerman for SKBF, and N. G. W. Cook, P. A. Witherspoon, and J. E. Gale for LBL. Other participants will appear as authors of the individual reports.

Previous technical reports in this series are listed below.

1. Swedish-American Cooperative Program on Radioactive Waste Storage in Mined Caverns by P. A. Witherspoon and O. Degerman. (LBL-7049, SAC-01).

2. Large Scale Permeability Test of the Granite in the Stripa Mine and Thermal Conductivity Test by Lars Lundstrom and Haken Stille. (LBL-7052, SAC-02).

3. The Mechanical Properties of the Stripa Granite by Graham Swan. (LBL-7074, SAC-03).

4. Stress Measurements in the Stripa Granite by H. Carlsson. (LBL-7078, SAC-04).

5. Borehole Drilling and Related Activities at the Stripa Mine by Pavel J. Kurfurst, T. Hugo-Persson, and G. Rudolph. (LBL-7080, SAC-05).

6. A Pilot Heater Test in the Stripa Granite by Hans Carlsson. (LBL-7086, SAC-06).

7. An Analysis of Measured Values for the State of Stress in the Earth's Crust by Dennis B. Jamison and Neville G. W. Cook. (LBL-7071, SAC-07).

8. Mining Methods Used in the Underground Tunnels and Test Rooms at Stripa by B. Andersson and P. A. Halen. (LBL-7081, SAC-08).

9. Theoretical Temperature Fields for the Stripa Heater Project by Tin Chan, Neville G. W. Cook, and Chin-Fu Tsang. (LBL-7082, SAC-09).

10. Mechanical and Thermal Design Considerations for Radioactive Waste Repositories in Hard Rock. Part I: An Appraisal of Hard Rock for Potential Underground Repositories of Radioactive Wastes by Neville G. W. Cook; Part II: In Situ Heating Experiments in Hard Rock: Their Objectives and Design by Neville G. W. Cook and Paul A. Witherspoon. (LBL-7073, SAC-10).

11. Full-Scale and Time-Scale Heating Experiments at Stripa: Preliminary Results by Neville G.W. Cook and Michael Hood. (LBL-7072, SAC-11).

12. Geochemistry and Isotope Hydrology of Groundwaters in the Stripa Granite: Results and Preliminary Interpretation by P. Fritz, J.F. Barker, and J.E. Gale. (LBL-8285, SAC-12).

13. Electrical Heaters for Thermo-mechanical Tests at the Stripa Mine by R. H. Burleigh, E. P. Binnall, A. O. DuBois, D. U. Norgren, and A. R. Oritz. (LBL-7063, SAC-13).

14. Data Acquisition, Handling, and Display for the Heater Experiments at Stripa by Maurice B. McEvoy. (LBL-7062, SAC-14).

15. An Approach to the Fracture Hydrology at Stripa: Preliminary Results by J. E. Gale and P. A. Witherspoon. (LBL-7079, SAC-15).

16. Preliminary Report on Geophysical and Mechanical Borehole Measurements at Stripa by P. Nelson, B. Paulsson, R. Rachiele, L. Andersson, T. Schrauf, W. Hustrulid, O. Duran, and K. A. Magnusson. (LBL-8280, SAC-16).

17. Observations of a Potential Size-Effect in Experimental Determination of the Hydraulic Properties of Fractures by P. A. Witherspoon, C. H. Amick, J. E. Gale, and K. Iwai. (LBL-8571, SAC-17).

18. Rock Mass Characterization for Storage of Nuclear Waste in Granite by P. A. Witherspoon, P. Nelson, T. Doe, R. Thorpe, B. Paulsson, J. Gale, and C. Forster (LBL-8570, SAC-18).

19. Fracture Detection in Crystalline Rock Using Shear Waves by K. H. Waters, S. P. Palmer, and W. E. Farrell. (LBL-7051, SAC-19).

20. Characterization of Discontinuities in the Stripa Granite -- Time-Scale Heater Experiment by Richard Thorpe (LBL-7083, SAC-20).

21. Geology and Fracture System at Stripa by A. Olkiewicz, J. E. Gale, R. Thorpe, and B. Paulsson. (LBL-8907, SAC-21).

22. Calculated Thermally Induced Displacements and Stress for Heater Experiments at Stripa by T. Chan and N. G. W. Cook. (LBL-7061, SAC-22).

23. Validity of Cubic Law for Fluid Flow in a Deformable Rock Fracture by P. A. Witherspoon, J. S. Y. Wang, K. Iwai, and J. E. Gale. (LBL-9557, SAC-23).

24. Determination of In-Situ Thermal Properties of Stripa Granite from Temperature Measurements in the Full-Scale Heater Experiments: Method and Preliminary Results by J. A. Jeffry, T. Chan, N. G. W. Cook, and P. A. Witherspoon. (LBL-8423, SAC-24).

TABLE OF CONTENTS

Page

LIST OF FIGURES ix

LIST OF TABLES xii

ABSTRACT 1

1. INTRODUCTION 3

2. ROD EXTENSOMETERS 11

2.1 Description of the Instrument 11

2.2 Laboratory Evaluation of Temperature Effects 15

2.2.1 Anchor System 16

2.2.2 Connecting Rock Tests 23

2.3 Data Reduction Scheme 31

2.4 Data Storage 36

2.5 Field Installation 37

2.6 Field Calibration 40

3. USBM BOREHOLE DEFORMATION GAGES 43

3.1 Description of the Instrument 43

3.2 Laboratory Evaluation of Temperature Effects 47

3.3 Computation of Displacement and Stress 54

3.4 Data Storage 59

3.5 Field Calibration and Installation 59

3.6 Sensitivity Analysis 61

3.7 Summary 62

4. IRAD VIBRATING WIRE STRESSMETER 65

4.1 Description of the Instrument 65

4.2 Gage Calibration and Evaluation of Temperature Effects 67

4.3 Interpretation of Gage Reading 78

Page

4.4 Data Storage 83

4.5 Field Installation 84

4.6 Summary 86

5. THERMOCOUPLES 87

5.1 Introduction 87

5.2 Low-Temperature Thermocouples 88

5.3 Medium-Temperature Thermocouples 91

5.4 High-Temperature Thermocouples 94

5.5 Data Storage 96

5.6 Field Installation 96

6. DEWATERING SYSTEM 97

6.1 Introduction 97

6.2 Thermocouple Holes 99

6.3 IRAD Holes 102

6.4 USBM Holes 104

6.5 Dewatering Control System 107

7. WORK IN PROGRESS 109

8. ACKNOWLEDGMENTS 111

9. APPENDICES 112

A. Sensor Locations 112

B. Sensor Parameter File 138

C. Properties of Pressurizing Fluids for Extensometer Anchors 141

D. Extensometer Calibration Coefficients 145

E. USBM Gage Test Data, Calibration Data, and Error Analysis 147

F. IRAD Gage Installation Data 164

G. Thermocouple Calibration Coefficients 165

10. REFERENCES 174

LIST OF FIGURES

Page

1. Plan view of experimental areas 340 m underground at Stripa, showing location of instrument boreholes. 3
2. Sectional view along profile AA' in Fig. 1, showing thermocouple and extensometer anchor locations. 7
3. Sectional view along profile BB' of Fig. 1. 8
4. Sectional view along profile CC' of Fig. 1. 9
5. Foreshortened sectional view of a simplified, two-anchor extensometer. 11
6. Schematic of extensometer anchor hydraulic system. . . . 12
7. Extensometer anchor, installed. 13
8. Superinvar rod connection, cutaway view; and thermocouple attachment. 14
9. Anchor creep test configuration. 18
10. Anchor pressure versus temperature for four anchors filled with Dowtherm A. 18
11. Anchor creep versus time under load at 190°C for three anchors set with different grouts. 20
12. Apparatus for thermal expansion measurements. 24
13. Comparison of superinvar thermal expansion curves. . . . 24
14. Superinvar thermal expansion data. 25
15. Borehole simulation model. 27
16. Time sequence temperature profiles of the borehole model during one of the heating trials. 29

Page

17. Mechanical system for exercising DCDT transducer. . . . 17
18. Two cases for extensometer installation. 32
19. Comparison of theoretical and spline-fit temperature profiles for two extensometer installations. 34
20. Extensometer anchor connection rods and segments for thermal expansion calculations. 35
21. Pressure-checking the anchor system. 38
22. Placing extensometer in borehole. 39
23. Extensometer calibration set-up. 40
24. Displacement versus output voltage obtained from extensometer calibration. 43
25. U.S. Bureau of Mines (USBM) borehole deformation gage . . 44
26. Schematic of strain-gage bridge wiring on a cantilever pair for the measurement of one component of diametral deformation. 45
27. USBM calibration fixture. 48
28. USBM gage response at two temperatures. 50
29. USBM gage calibration factor as a function of temperature. 51
30. Change in strain reading with temperature, cantilevers in no-load condition. 53
31. General form of USBM gage calibration curves. 55
32. Displacement and stress nomenclature for USBM gages. . . 58
33. Displacement versus output voltage of USBM gage. 60

Page

34. Vibrating wire stressmeter: photograph of assembled gage, and exploded sectional view. 66
35. Distribution of initial IRAD stressmeter readings. . . . 68
36. Average response of IRAD gages when subjected to elevated temperatures. 70
37. Granite sample for calibration of IRAD gages under uniaxial compression 71
38. Calibration curves for IRAD gage 3-18. 72
39. Coefficients C_1 and C_2 versus temperature 77
40. Illustration of ΔR offset as used for elevated temperature data-reduction. 79
41. Comparison of calculated versus calibrated stress change values. 81
42. Sign convention for angular measurements. 82
43. Sample plot and listing of a thermocouple calibration. . . 92
44. Thermocouple hole dewatering tubes. 100
45. IRAD gages and dewatering tubes. 103
46. USBM gage and dewatering tubes. 105
47. Dewatering control station. 108
A-1. Relationships among coordinate systems. 113
A-2. Borehole layout in the time-scaled drift. 115
A-3. Borehole layout in the full-scale drift. 116
A-4. Borehole layout in the extensometer drift. 117
C-1. Thermal expansion for several heat-transfer fluids. . . . 144

LIST OF TABLES

Page

1. Viscosity changes for fluids held 36 days at 200°C . . . 17
2. Measured room temperature grout strength versus aging time and temperature. 21
3. Thermal strain data for superinvar rod. 26
4. DCDT stability test environments. 31
5. Data from sample extensometer calibration, performed after installation with 5.0-mm step blocks. 42
6. Change in calibration factor with temperature for USBM gage 401. 51
7. Estimated errors in stresses computed from a USBM gage measurement. 63
8. IRAD gage calibration test results 73
9. Pressurized hole groupings for dewatering 109

A-1. Transform equations relating to the mine and experimental coordinate systems. 114

A-2. List of all sensors and their locations for the three heater experiments at Stripa. 121

C-1. Thermal degradation of five heat-transfer oils. 142

C-2. Physical properties of heat-transfer fluids. 143

E-1. USBM gage-temperature calibration listing. 148

E-2. USBM gage-drift measurements. 151

E-3. USBM gage-offset measurements. 152

E-4. Summary of estimated errors in the USBM gage measurement of borehole displacement. 160

E-5. Estimated errors in stresses computed from a USBM gage measurement. 163

ABSTRACT

Borehole instrumentation for the measurement of temperature, displacement, and stress was evaluated, modified, calibrated, and installed in an underground site at Stripa, Sweden where experiments are currently underway to investigate the suitability of granite as a storage medium for nuclear waste. Three arrays of borehole instrumentation measure the thermomechanical effects caused by electrical heaters which simulate the thermal output of canisters of radioactive waste. Quantities of each instrument type are as follows: thermocouples, (389); rod extensometers, (35); U.S.Bureau of Mines (USBM) borehole deformation gages, (30); and IRAD vibrating wire stressmeters, (26).

Because most rock mechanics investigations are carried out at modest temperatures, a sustained operating temperature as high as 200°C was an unusual and most important criterion governing the instrumentation program. Extensive laboratory experiments were conducted to determine the effect of high temperature on instrument behavior and also to develop calibration and data-reduction procedures. Temperatures up to 200°C and stresses up to 14 MPa (2,000 psi) were attained during the laboratory evaluation. Based on this work, algorithms suitable for computer implementation were formulated. Significant aspects regarding the individual instrumentation types are:

The rod extensometers were tested for anchor creep, the selection of a suitable high-temperature pressurizing fluid, and the thermal stability of the grout. Superinvar was substituted for invar for the connecting rods. Five temperature measurements along the full extensometer length are used to correct for the rod thermal expansion using an interpolation scheme.

- Four temperature corrections are incorporated into the data reduction of the USBM borehole deformation measurement: the bridge voltage offset correction, the change in calibration factor induced by temperature, and the thermal expansion of the gage and of the rock. Uncertainties in the computed stress introduced by these correction factors appear to be less than uncertainties in the values of the mechanical moduli.

- The vibrating wire gages were calibrated in the laboratory by loading gages installed in a granite block at pressures up to 13 MPa and at temperatures ranging from 20° to 200°C. Both the slope and offset of the response equation are corrected for temperature effects. These corrections were treated statistically because not all gages were fully calibrated individually.

- Most thermocouples were calibrated in an oven at the field site, with the response then represented by a fourth order polynomial with the coefficients stored in the computer for reduction of the temperature measurements. Thermocouples were emplaced with individual gages and into holes backfilled with sand or grout.

- Some of the vertical boreholes were outfitted with a dewatering system to minimize instrument degradation and temperature anomalies due to fluid convection.

1. INTRODUCTION

Experiments to assess the feasibility of using crystalline rock for high-level nuclear waste storage are presently underway in a granitic stock at Stripa, Sweden. In an attempt to determine the thermomechanical response of a typical granite to the thermal loading of actual nuclear waste canisters, canisters containing electrical heaters which simulate the power output from the decay of radioactive materials have been installed at three test areas illustrated in Fig. 1. Measurement of the thermomechanical response of the rock mass surrounding the heaters places new requirements upon the standard instrumentation used for rock mechanic investigations, especially in terms of long-term stability and high operating temperatures.

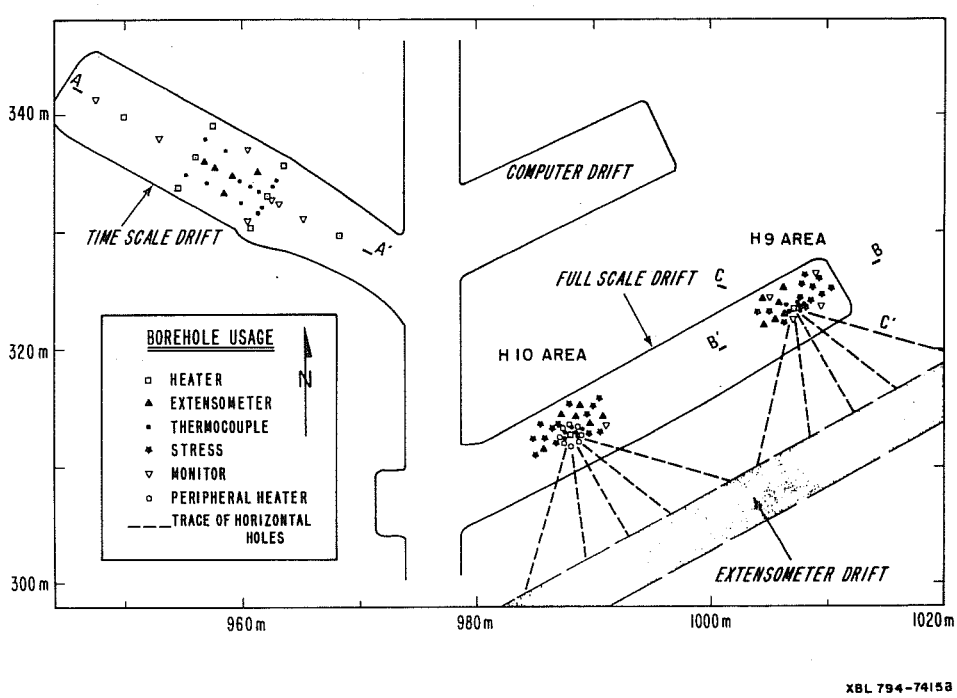

Fig. 1. Plan view of experimental areas 340 m underground at Stripa, showing location of instrument boreholes.

The current tests in Stripa, designed to determine the three-dimensional response of a jointed rock mass, use over 700 channels of temperature- , stress- , and displacement-measuring instrumentation. Theoretical models based on the theory of thermo-elasticity predicted relatively small displacements, significant thermal gradients, and temperatures of 200°C. Rock mechanics programs associated with large civil works projects (dams, power plants), mines, and defense related programs (nuclear or nuclear-simulation tests) have usually been less comprehensive in the number of channels, the sensitivity of the measurements, the long duration of the test, and the severity of the thermal environment.

Rock mechanics test programs at large civil works projects are aimed at obtaining in-situ rock mass properties during site evaluation. A variety of tests (deformation, shear-strength, in-situ velocity, etc.) are usually conducted at critical locations where problems are likely to occur or where an "average" value can be obtained. The change in rock mass response is not usually measured for long time periods, and especially not with the sensitivity and redundancy of instrumentation used at Stripa. The tests conducted during nuclear-related programs of the U.S. Department of Defense are designed to obtain the high-pressure dynamic response of the rock mass. The instrumentation senses acceleration, velocity, and stress. The displacement fields are generally calculated from acceleration or velocity records rather than measured directly. The dynamic stress levels of interest are hundreds to thousands of megapascals above the stress-range of interest at Stripa. In the rock mechanics test programs mentioned above, temperature was not an important parameter. In the Stripa experiments the thermomechanical response of the host rock is the key phenomenon of interest.

This report deals specifically with the modification, calibration, and installation of the instrumentation emplaced in boreholes surrounding the heaters at Stripa to measure rock deformation and temperature, and to infer stress changes. It is one of three reports describing the engineering aspects of the experiments through the time of installation and early phases of operation. The design and early operation of the heaters is discussed by Burleigh et al. (1979). McEvoy (1979) describes the data acquisition system and also provides an overview of the data handling procedures for the heater experiments. Taken together, these three reports provide a comprehensive view of the design and installation of the heaters, the measurement instrumentation, and the data acquisition system at Stripa.

Terra Tek, Inc., under contract to and in cooperation with Lawrence Berkeley Laboratory, conducted a study beginning in May 1977 to (1) evaluate the suitability of state-of-the-art instrumentation to measure temperature, stress, and displacements, (2) recommend instrumentation types, (3) recommend a laboratory/field program to evaluate the long-term thermal and mechanical stability of the instrumentation, and (4) recommend a borehole instrumentation layout for the full-scale and time-scale heater tests. Several criteria were established for the instrumentation system in order to meet the specifications and schedule required by the program. These criteria were (1) deliverability by October 1977 in order to meet laboratory evaluation and calibration schedules; (2) availability of the instrumentation as off-the-shelf or modified equipment; (3) stability and reliability in a 200°C environment; (4) sensitivity enough to measure temperature, displacement, or stress to the levels estimated from preliminary calculations using laboratory data; and 5) reliability over the life of the tests, estimated to be 1 to 2

years. After excavation began at the Stripa mine it was recognized that the mine was wetter than anticipated. As a consequence, some additional modifications were made to the instrumentation. It was also realized that a dewatering system would be needed for the stress and temperature instrumentation in the vertical boreholes.

The four instrument types selected at the outset of the project are thermocouples for temperature measurement, U.S. Bureau of Mines (USBM) borehole deformation gages, and IRAD vibrating-wire stress gages for stress determination, and rod extensometers for displacement measurements. The USBM gage was selected as the primary stress indicator because of its availability and its favorable operational record. Further, it appeared that both it and the IRAD gage could be used with only modest modifications to operate in the high-temperature environment. The IRAD gage was selected as a backup for the USBM gages, and to provide comparison measurements.

The disposition of these sensors around the heaters is shown in Figs. 2, 3, and 4, which are vertical cross sections through the heater experiments, keyed to Fig. 1. Note the higher spatial density of instrumentation around the H9 and H10 full-scale sites as compared with the time-scale experiment. Also note the abundant use of thermocouples in holes drilled specifically for temperature determination, and also associated with individual USBM gages, IRAD gages, and extensometer anchor points. The exact position of all sensors as initially installed is given in Appendix A.

A second phase of the instrumentation program, beginning July 1977, included the modification, calibration, and installation of the selected

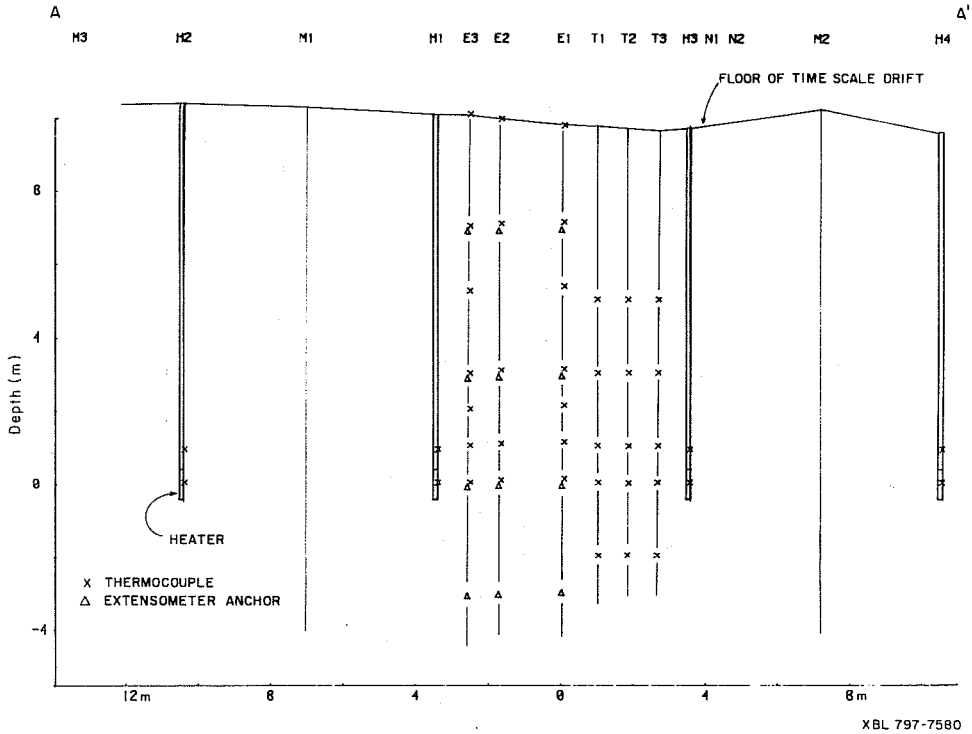

Fig. 2. Sectional view along profile AA' in Fig. 1, showing thermocouple and extensometer anchor locations.

borehole instrumentation, along with the integration of the instrumentation with the data retrieval system. The testing, modification, and preliminary calibration of the instruments began in July 1977 and was completed in late December 1977 when the instrumentation and associated data retrieval system were shipped to Sweden. The field calibration and installation of the instrumentation for the three in-situ heater tests occurred during January to August 1978.

Each of the four instrumentation types is discussed separately in the body of this report. Each section (sections 2 through 5) addresses the laboratory testing of components and sensors, the modifications performed as a

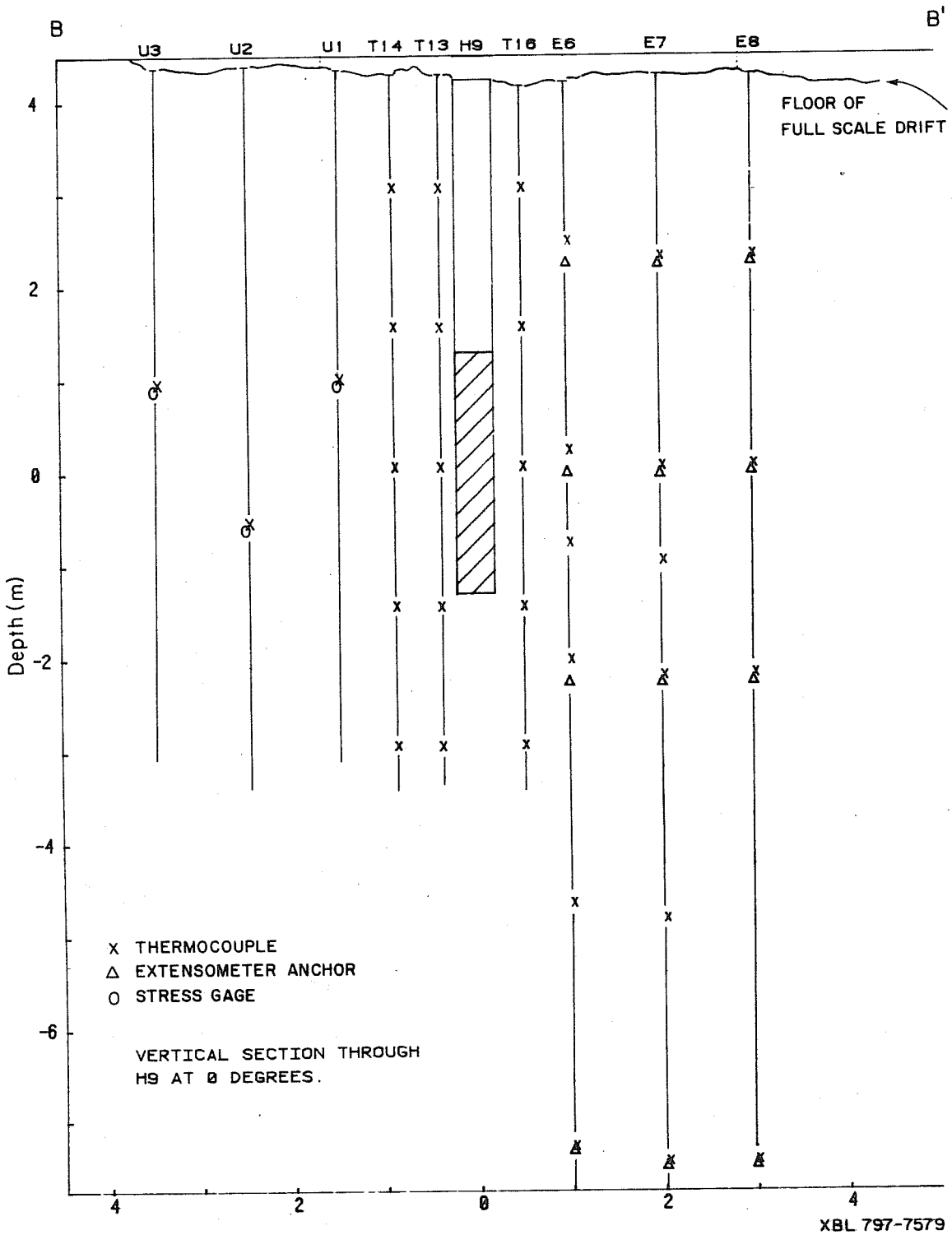

Fig. 3. Sectional view along profile BB' of Fig. 1.

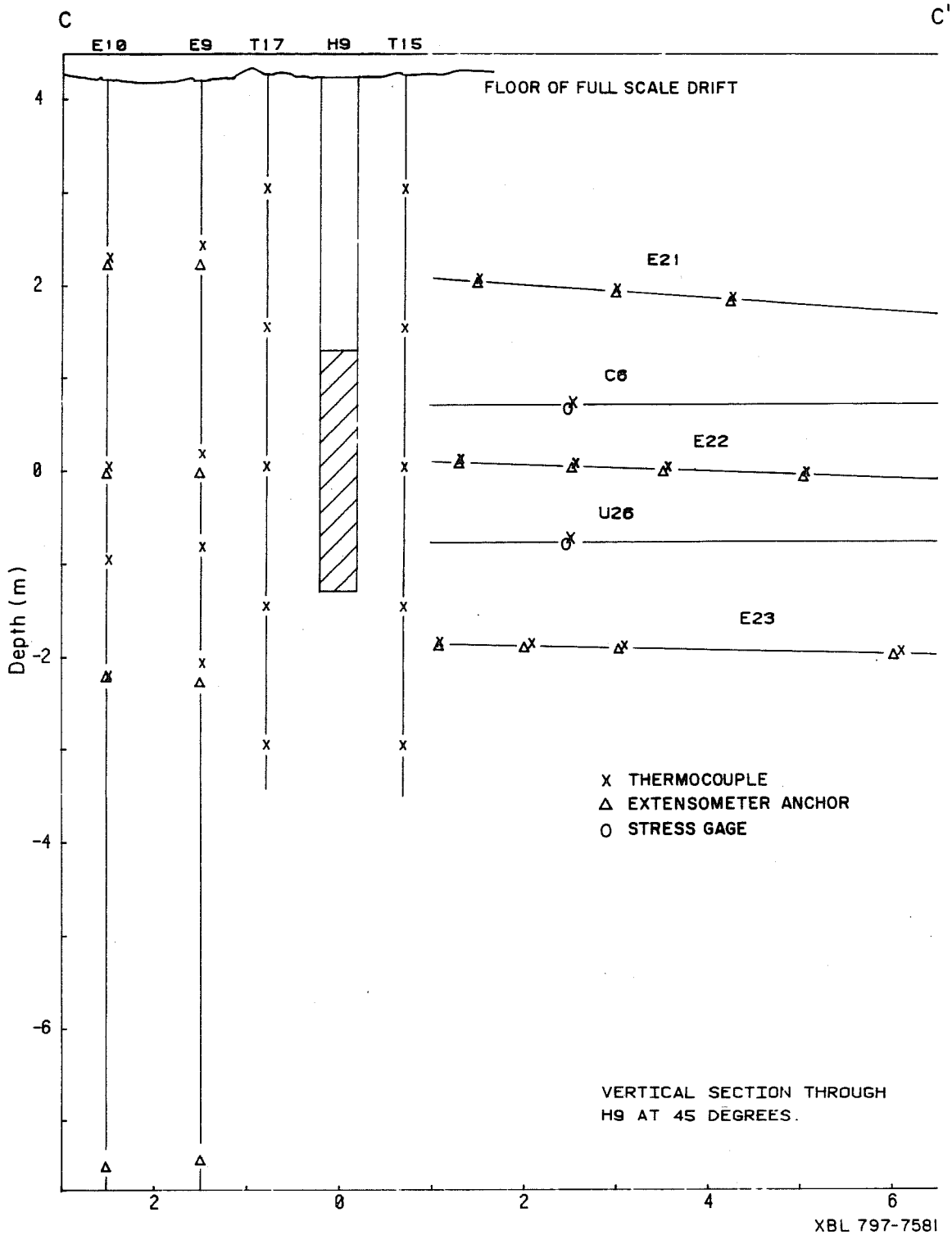

Fig. 4. Sectional view along profile CC' of Fig. 1.

result of the testing, and the calibration procedure established for field use. With the exception of the vibrating-wire stress gages, which were calibrated in the laboratory, all calibrations were performed at the field site with instruments connected to the computer-controlled data acquisition system. Calibration was done on line, using software routines developed especially for that purpose. The calibration data were stored in a sensor parameter file which is described in Appendix B. Calibration coefficients for individual sensors, as installed, are given in the appendices.

The installation of each sensor type is described in sections 2 through 5 of this report. Installation of the dewatering apparatus, which is sufficiently specialized to warrant separate discussion, is described in section 6. An instrument-installation wiring list identifies the data logger channel numbers, computer input, connector pins, transducer numbers, and sensor number of every sensor in the experiment. Because of its length it is not reproduced in this report, although McEvoy (1979) gives an example of its format (in Fig. 23 of that report). The sensor number uniquely identifies each sensor and in this report links the several appendices so the calibration data can be tied to a specific location.

Insofar as possible, each of the four instrument sections includes information on measurement precision and on specific problems. However, the emphasis of this report is on the findings and status at the completion of installation. Hence section 7 outlines some of the work on instrument performance currently in progress.

2. ROD EXTENSOMETERS

2.1 Description of the Instrument

An extensometer is a device for measuring changes in the axial length of a borehole. The rod-type extensometer selected for use at Stripa (Model 4C SLT manufactured by Terrametrics, Inc. of Golden, Colorado) measures the displacement of each of four downhole anchor points with respect to the borehole collar. One spring-tensioned rod connects each anchor point to one of the four displacement sensors which are located at the borehole collar.

The major elements of the rod extensometer (Fig. 5) are: (1) hydraulic anchoring system; (2) anchor-to-collar rod connections; (3) a head assembly that includes the rod tensioning system and the displacement transducers; and (4) thermocouples for sensing the temperature profile of the connection rods.

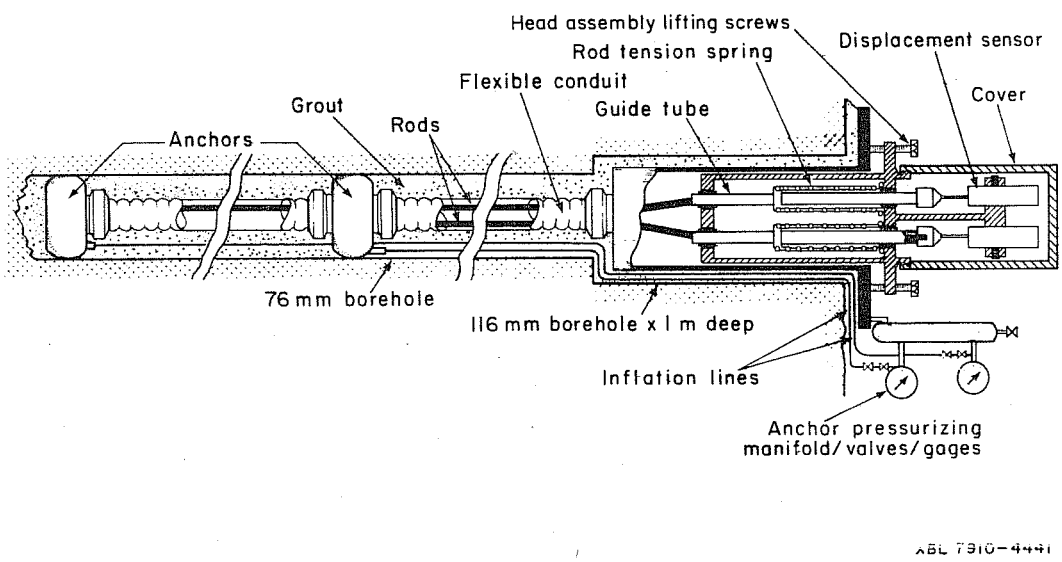

Fig. 5. Foreshortened sectional view of a simplified, two-anchor extensometer.

The hydraulic anchoring system is shown schematically in Fig. 6. Each borehole anchor creates a fixed point along the borehole to which the downhole end of one of the connecting rods is secured. A hole through the center of each anchor allows any connecting rod originating at a lower anchor point to pass through freely. These anchors (Fig. 7) consist of a flat jack (a short length of flattened copper tube which has been sealed at the ends) rolled around a retaining mandrel and fitted with an inflation line of copper-coated steel tubing. Each inflation line is connected to a fluid reservoir (manifold), at the borehole collar, through a pressure gage and two valves. Anchor pressure is manually maintained between 10 and 14 MPa (1,500 to 2,000 psi) through the use of this manifold. The anchors are secured into

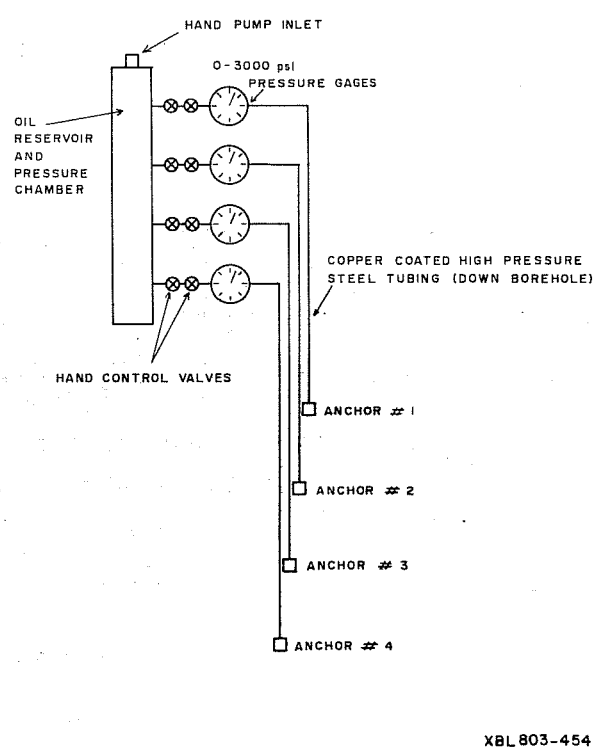

Fig. 6. Schematic of extensometer anchor hydraulic system.

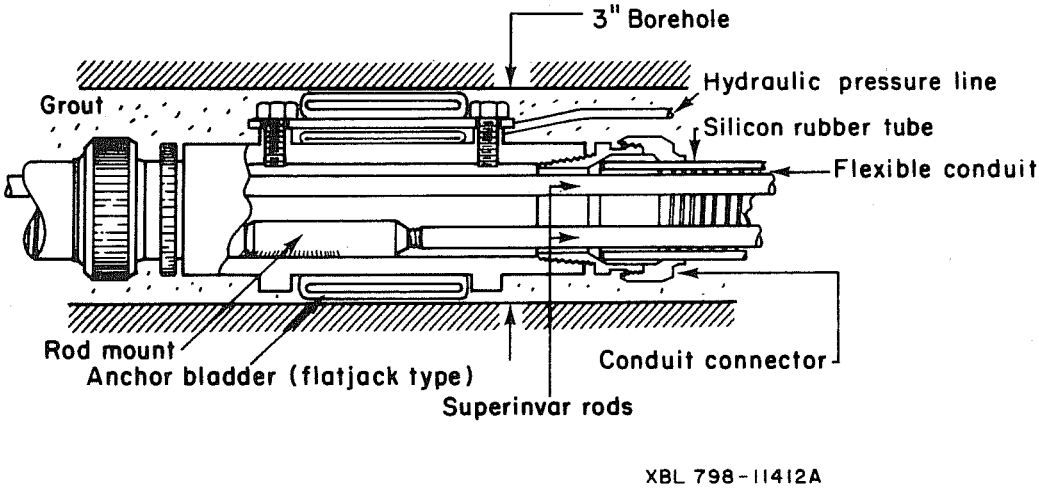

Fig. 7. Extensometer anchor, installed.

the borehole by grout as well as by the pressurizing system described above.

The connecting rods provide a linkage between the measuring head and the borehole anchors. Any axial displacement of an anchor relative to the borehole collar will be transmitted by its connecting rod to the collar, where a transducer senses the displacement. Connecting rods are trimmed to length from 12-ft sections of 1/4-inch-diameter superinvar rod. For connecting rods longer than 12 ft, multiple sections are butted together with threaded aluminum couplings (Fig. 8A). Type K thermocouple junctions are attached at several points along the longest of the four connecting rods (Fig. 8B). A 1-inch flexible steel conduit, jacketed by a waterproof silicone-rubber sleeve, spans the gap between anchors to protect both the rods and the thermocouples from groundwater and from the intrusion of grout. A fourth length of this flexible conduit protects the rods and thermocouples as they pass from the borehole collar to the first anchor.

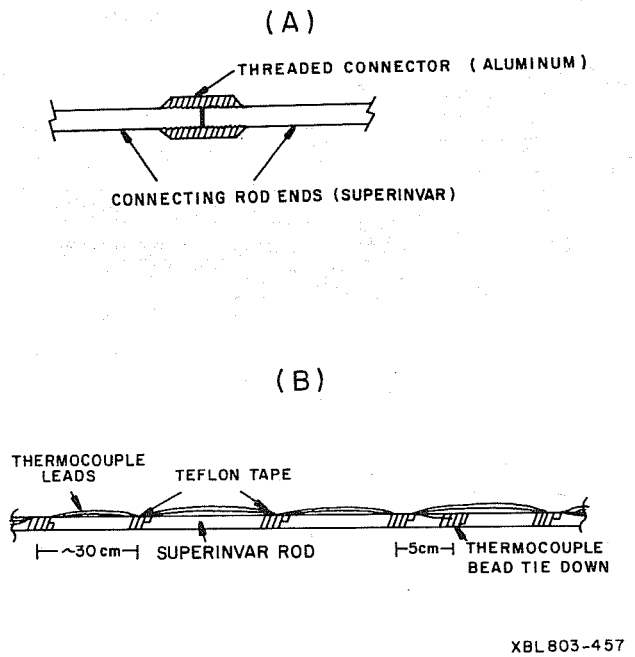

Fig. 8. (A) Superinvar rod connection, cutaway view; (B) thermocouple attachment.

The top of the fourth section of conduit terminates at a 1-m-long aluminum sleeve (collar stabilizer tube). This provides a rigid mount for the head assembly and for the pressure manifold. The head assembly mounts to the top flange of the collar stabilizer tube after the stabilizer tube has been grouted into the borehole. The head assembly contains four independent rod tensioning springs, four rod guide tubes, and four DCDT (direct current linear variable differential transformer) displacement measuring transducers. A spring tension of 455 N (100 lb) per rod minimizes rod sag, particularly in horizontal holes, and increases instrument sensitivity. The DCDTs produce a voltage output that is linear with the relative displacement between the transducer coil and its movable core. Each core is secured to the end of one of the four connecting rods. Thus, a change in output voltage of one of the

transducers, when multiplied by a predetermined calibration factor and corrected for the thermal expansion of the rod, indicates the relative displacement between the collar and the appropriate anchor.

In most previous applications, rod extensometers have been operated under constant temperature conditions, and these temperatures have rarely exceeded 50°C. As part of the work reported here, modifications were made so as to accommodate the elevated and variable temperatures expected at Stripa. These modifications include:

- Heat treated superinvar (64% Fe, 31% Ni, and 5% Co) was used for the connecting rods to minimize the magnitude of the thermal expansion effect.
- Four to six thermocouples were attached to the longest connecting rod to determine the rod temperature profile for thermal expansion corrections.
- Silicon-based fluid was used as an anchor pressurizing fluid for chemical stability at elevated temperatures.
- A pressure manifold was provided to allow for control of anchor pressure during periods of changing temperature.
- A silicone rubber sleeve was installed over the flex conduit, housing the connection rods, to maintain water proofing to 200°C.

2.2 Laboratory Evaluation of Temperature Effects

The rod extensometer components were tested to select suitable construction materials, to evaluate the instrument's response to environmental factors, and to determine a suitable technique for generating accurate corrections for thermal expansion.

2.2.1 Anchor System

The anchor system was tested to determine (1) a suitable anchor pressurizing fluid capable of withstanding a 200°C environment over long periods, (2) the magnitude of the creep to be expected for an anchor system operating under a rod tensioning load of 455 N, and (3) a grout that would not undergo excessive deterioration at temperatures up to 200°C.

Selection and Testing of Pressurizing Fluids. The literature has been reviewed to identify commercially available fluids which might be suitable for this high-temperature application. Several specialized petroleum oils were eliminated on the basis of probable degradation at the temperature expected in service at Stripa (See Appendix C). On the basis of this review of thermal stability and physical properties, three oils were selected for laboratory testing: (1) Dowtherm A, (2) Dowtherm G, and (3) Dow Corning X2-1162. These oils were tested for degradation at elevated temperature in the presence of copper and air. Details of the fluid properties are given in Appendix C.

Viscosity tests were performed on one sample of each oil before and after it had been held at 200°C for 36 days. Each sample was placed in a glass beaker containing a small piece of copper tubing and the beaker was covered loosely to allow for venting of vapors and exposure to atmospheric oxygen. The results of these tests are shown in Table 1. Note that the Dow Corning X2-1162 showed good stability at 200°C despite the presence of oxygen.

Anchor Pressuring and Creep Tests. Oven tests were conducted on three simulated anchor installations: 1) to evaluate the effectiveness of the fluid

Table 1. Viscosity changes for fluids held 36 days at 200°C.

Fluid	Viscosity (centipoise) at 23°C		Remarks
	Initial	Final	
Dowtherm A	4.1	--	Sample lost due to evaporation; only tar residue remained.
Dowtherm G	22.5	186.0	20% sample loss to evaporation; remainder is thick residue and tar.
Dow Corning X2-1162	10.2	13.7	No sample loss. Oil slightly cloudy with white precipitate.

manifold and anchor flat jack in maintaining the hydraulic pressure, 2) to evaluate the performance of the various grouts, and 3) to determine if elevated temperatures resulted in anchor movement.

To simulate a borehole, a 152-mm diameter x 152-mm long granite core was center cored to 76-mm diameter, and an aluminum ring was grouted to the outside of the core to accommodate hoop stress. A hydraulic anchor was then inflated in the simulated borehole and was grouted in place (see Fig. 9).

Three of these simulated anchor installations were constructed. All were filled with Dowtherm A fluid, which was used for the laboratory tests because it had an acceptable thermal stability (with absence of air) and it was readily available. It performed satisfactorily for these tests but was superseded by the superior Dow Corning X2-1162 for field application.

Each of the anchors was grouted with a different material. The three grouts used were 1) Masterflow 713 (a standard cement and sand mixture); 2) Celtite 42 Hi Flow (an epoxy resin with a fine sand filler); and 3) American Cyanamid AM-9 (a chemical gel suspension).

The three anchors were placed in an oven and heated, in approximately 50°C steps, to 150°C. The pressure of the inflation fluid, trapped in the anchor flat jack, increased from 2,000 psi to some higher pressure as the temperature was increased. Each time the pressure reached 3,000 to 4,000 psi, the hydraulic pressure was released again to 2,000 psi. The magnitude of each of these pressure rises was integrated to create the plot shown in Fig. 10. During periods of steady temperature, the pressure remained constant. The flat jacks were not ruptured and no leak was noted. Anchor #1 was subsequently emptied, evacuated to remove any trapped air, and refilled with Dowtherm A. That anchor was then cycled to 225°C. It experienced a 40%

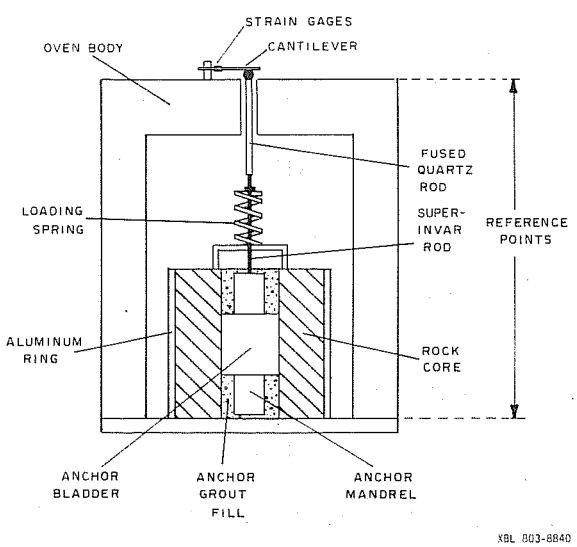

Fig. 9. Anchor creep test configuration.

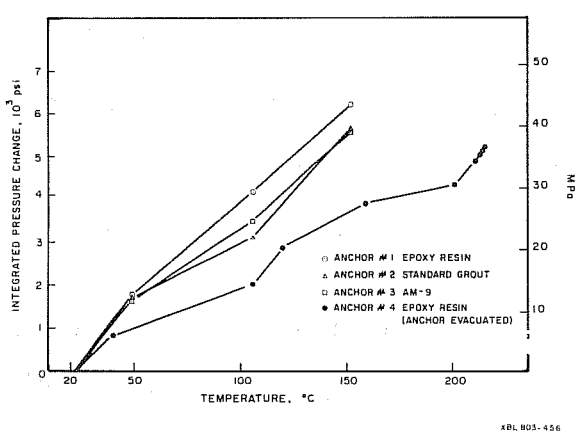

Fig. 10. Anchor pressure versus temperature for four anchors filled with Dowtherm A.

smaller integrated pressure rise to 150°C than was noted for the same anchor when filled without first evacuating the air. This behavior is shown as anchor #4 in Fig. 10.

For the second set of anchor tests, to evaluate creep at elevated temperatures, a short superinvar rod was attached to each anchor and it was spring loaded to 445-N tension. A fused quartz rod was connected from the top of the superinvar rod to a strain-gaged cantilever beam mounted from an external reference point atop the oven (see Fig. 9). The strain gage output had a sensitivity of 1×10^{-4} mm and it was calibrated over a deflection range of $\pm$ 0.1 mm.

The epoxy and standard-grout anchors were inflated to 14 MPa (2,000 psi). The AM-9 chemical grout exhibited extreme shrinkage upon long time curing and, because of this behavior, was selected for the test of a "worst case" situation, in which an anchor has both lost pressurization and experienced grout deterioration. Therefore, the AM-9 grouted anchor was not pressurized during this high-temperature creep test.

Each anchor was brought, in 50°C steps, to a temperature of 190°C. The oven was held at each temperature step for several hours. During each period of increasing temperature, the inflation pressure would rise; however, that pressure was manually bled off so as not to exceed 28 MPa (4,000 psi). During the periods of steady temperature, the pressure remained unchanged.

When the oven reached 190°C, the temperature was maintained for 15 days and the deflections of the three cantilever beams were continuously monitored. A record of deflection versus time for each of the three anchors is shown in

Fig. 11. The net change in deflection for the two pressurized anchors was zero, with an uncertainty in the reading of $\pm$ 4 x 10^{-4} mm. The net deflection for the unpressurized anchor increased by about 10 x 10^{-4} mm during the first 5 days, and then remained constant to within $\pm$ 2 x 10^{-4} mm for the remaining 10 days. These deflections were smaller than the precision limit (approximately 1 x 10^{-2} mm) expected for the installed gage.

Grout Compression Tests. Following these high-temperature creep tests, the three anchors were depressurized, removed from the oven, cooled, and the anchor mandrel was then axially loaded in a hydraulic press until it was seen to slip within the simulated borehole. The loads at which this slippage occurred were greater than 3,000 lb. for all three grouts. These values are

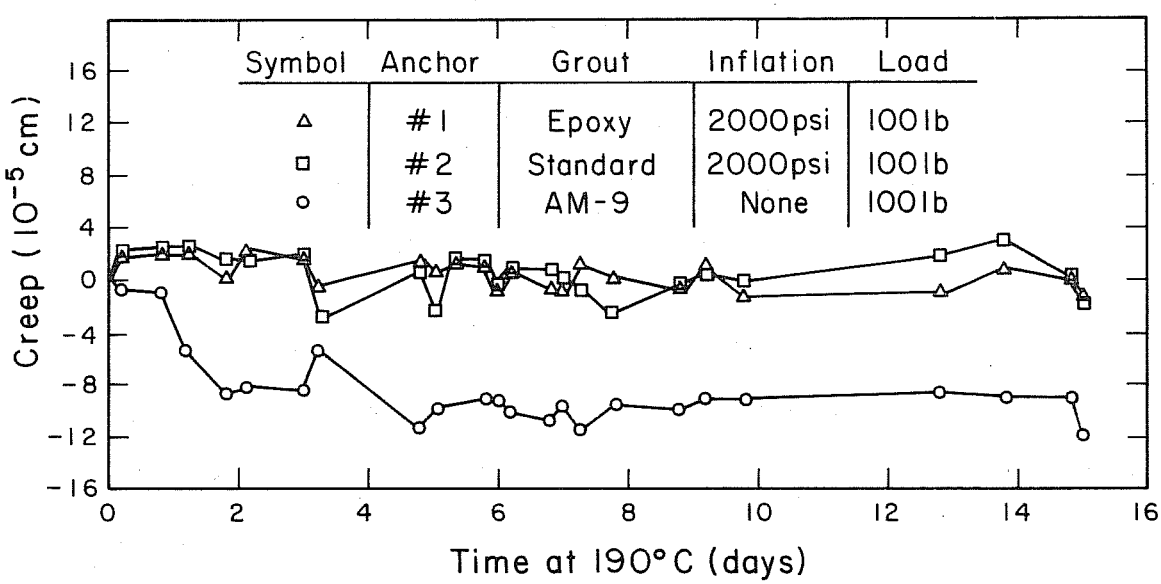

XBL 7911-13429

Fig. 11. Anchor creep versus time under load at 190°C for three anchors set with different grouts. One anchor was unpressurized.

all large compared to the nominal 445 N of axial load which is applied to each anchor during field use.

An additional test was performed to evaluate the effect of high-temperature aging upon the strength of epoxy and standard grout. Five cylindrical compression test cylinders (size 25-mm diameter x 50-mm long) were cast from each of these materials. The AM-9 grout had been eliminated from consideration on the basis of its excessive shrinkage.

Four samples of each material were placed in an oven and brought, in 50°C steps, to a maximum temperature of 200°C. One sample of each material was removed after the furnace had been held at 100°C for 53 hours, and a second sample of each was removed after the furnace had been held at 150°C for an additional 48 hours. The final two samples of each material were removed after an additional 365 hours and 864 hours at 200°C. Table 2

Table 2. Measured room temperature grout strength versus aging time and temperature.

Oven temperature (°C)	Time at temperature (hours)	Sample no. removed From furnace	Compressive strength (MPa)	
			Standard	Epoxy
Ambient	--	1	9.7	90
50	48	None	--	--
100	53	2	9.0	68
150	48	3	9.7	98
200	365	4	3.8	75
200	864	5	5.0	27

summarizes the subsequently measured room-temperature compressive strength of each sample.

The epoxy sample, after being heated for 864 hours at 200°C, exhibited visible swelling. When a fifth epoxy sample, previously unheated, was placed in the oven and heated to 225°C, it experienced a complete breakdown.

Conclusions from Anchor Tests. On the basis of the above tests, an anchoring system was specified which will provide an anchoring capacity exceeding that required to resist the 455-N rod-tensioning force for an extended test period at temperatures up to 200°C. Test results indicated an anchor creep of less than 2 microns even under conditions of anchor depressurization and grout deterioration. This resistance to creep may be due to the tendency of the soft-copper anchor bladders to seat themselves along the rough surface of the borehole wall.

Standard grout was specified for field installation of the extensometers, because it (1) exhibits the least relative volume change upon curing or during high-temperature aging; (2) appears to be adequately strong, after high-temperature aging, despite a marked reduction in strength when aged at temperatures over 150°C; (3) costs considerably less than epoxy; and (4) is much easier than epoxy to mix and place.

For pressurizing the anchors, Dow Corning X2-1162 oil was specified, because it: (1) exhibits good chemical stability even in air at elevated temperature; (2) has a relatively high fire point; (3) has a low volatility and generates no pervasive odor; and (4) undergoes only a small change in viscosity after long-time exposure at elevated temperatures.

2.2.2 Connecting Rod Tests

The thermal expansion of an extensometer anchor-to-transducer connecting rod results in a displacement of the core of the transducer. This thermal displacement must be added to the gross indicated displacement to obtain the net displacement of an anchor. Superinvar was selected for the connection rods because it is an alloy (64% Fe, 31% Ni, 5% Co) which has a small expansion over the temperature range of interest and would, therefore, minimize the magnitude of this correction for thermal expansion. The 3.66-m (12 ft)-long x 6.35-mm (0.25 inch)-diameter rod segments used for all of the connecting rods were fabricated from a single melt. The laboratory thermal strain measurements were made, as described below, upon several rods selected at random from this group. The average behavior of these rods was used to characterize all rods used.

Thermal Expansion Measurements. The thermal expansion measuring apparatus that was used for these tests is shown in Fig. 12. The apparatus consisted of: a horizontal oven 3.96-m long x 1.27-cm i.d.; a single superinvar rod with five (5) thermocouples attached to the rod at its end points, mid-point, and quarter points; and two LVDT displacement transducers mounted externally to the oven ends. Linkages between the rod ends and the LVDT cores were constructed from fused quartz. When a rod was cycled slowly to temperatures over 100°C, the thermal expansion of the superinvar changed. This is shown in Fig. 13 as three temperature-versus-thermal-strain curves for a single rod, as received from the vendor. Curve I shows the rod's expansion when heated rapidly (2 hours to 200°C); curve II, when heated slowly (8 hours to 200°C); and curve III, for all subsequent cycles, when

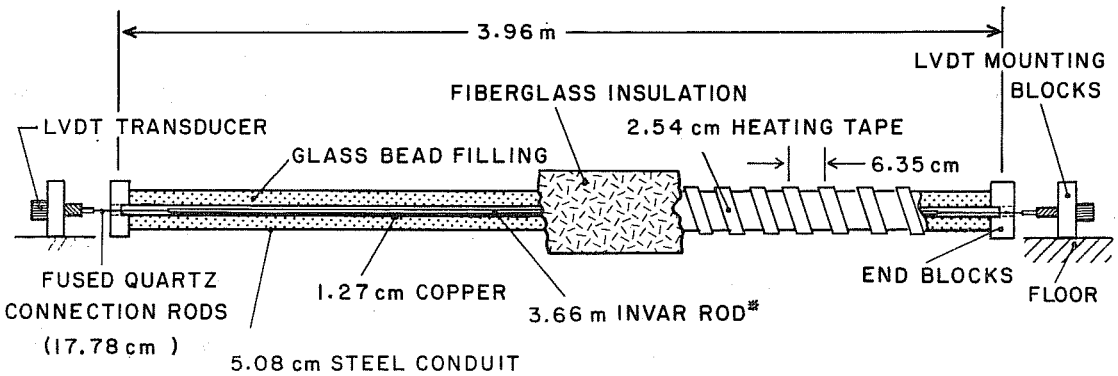

* 5 THERMOCOUPLES ATTACHED-(ONE AT EACH END, ONE AT MIDPOINT, ONE AT EACH QUARTER POINT)

XBL 803-8841

Fig. 12. Apparatus for thermal expansion measurements.

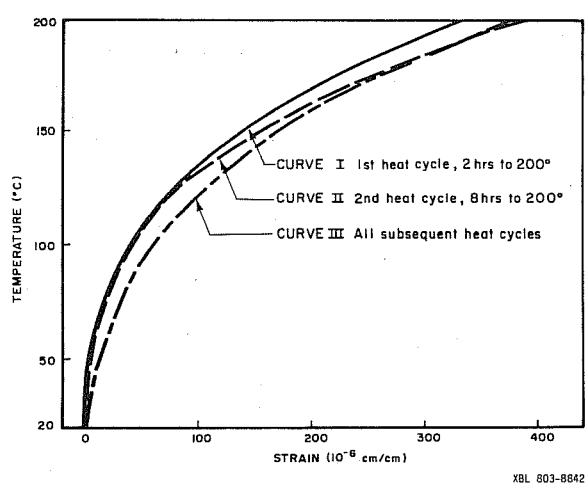

XBL 803-8842

Fig. 13. Comparison of superinvar thermal expansion curves.

heated either slowly or rapidly. Another rod, heated overnight (12 hours) to 250°C maximum, duplicated the expansion values shown in curve III. Thus, curve III represents a stable behavior for temperature cycles to temperatures in excess of 200°C. The change exhibited here between the "as received" rod and a rod which had been heated above 100°C for an extended period, has been

reported to be the results of the precipitation of carbon from the crystal lattice (Marshall and Maringer 1976). To establish this repeatable thermal-strain behavior, the rods were all heat treated. Fifty rods per batch were heated, in a cylindrical oven (250-mm diameter x 4-m long) to 225°C in 5 hours, and then allowed to cool, in the oven, overnight.

Seven rods were tested in the thermal expansion apparatus described above. Six rods were tested to determine the effect of thermal history on the measured rod expansion. One additional rod was selected from the heat-treated material and tested to assure that repeatable thermal-strain behavior had been obtained by the heat treatment. The measured thermal-strain-versus-temperature curves for all seven rods are shown in Fig. 14.

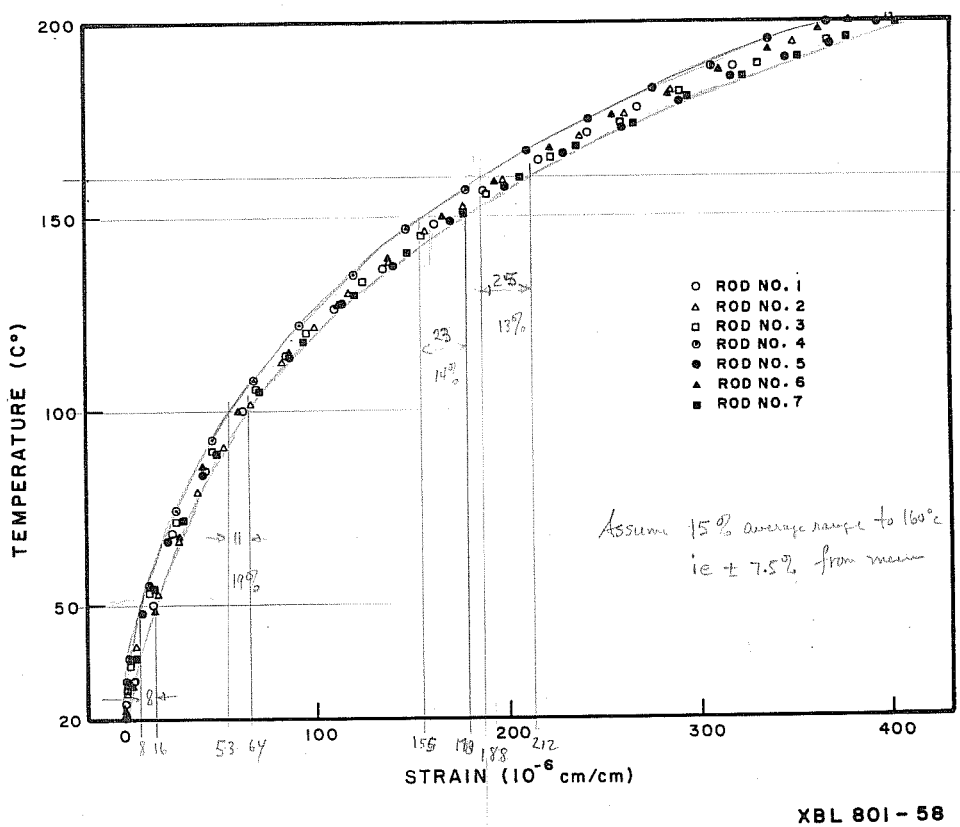

Fig. 14. Superinvar thermal expansion data.

The measured values of thermal expansion for the seven tested samples were averaged at each 10°C temperature increment from 20° to 200°C, and Table 3 was constructed from these averaged values. The thermal expansion values shown in Table 3 are used during the in-situ heater tests to calculate the total thermal expansion of each rod for its current temperature profile. Expansion values for temperatures intermediate to those shown in Table 3 are

Table 3. Thermal strain data for superinvar rod. α_t = Integrated thermal expansion per unit length as measured from a base value at 20°C.

T (°C)	α_t (mm/mm) x 10^{-6}
20	0
30	2
40	5
50	12
60	18
70	26
80	35
90	48
100	62
110	79
120	97
130	118
140	141
150	167
160	197
170	233
180	276
190	329
200	380

calculated by linear interpolation.

Simulated Borehole Test. A two-anchor extensometer was installed in a simulated borehole (see Fig. 15) to evaluate the degree to which one could expect that the temperature measured on one rod would track the temperature measured at the borehole wall, and on an adjacent rod.

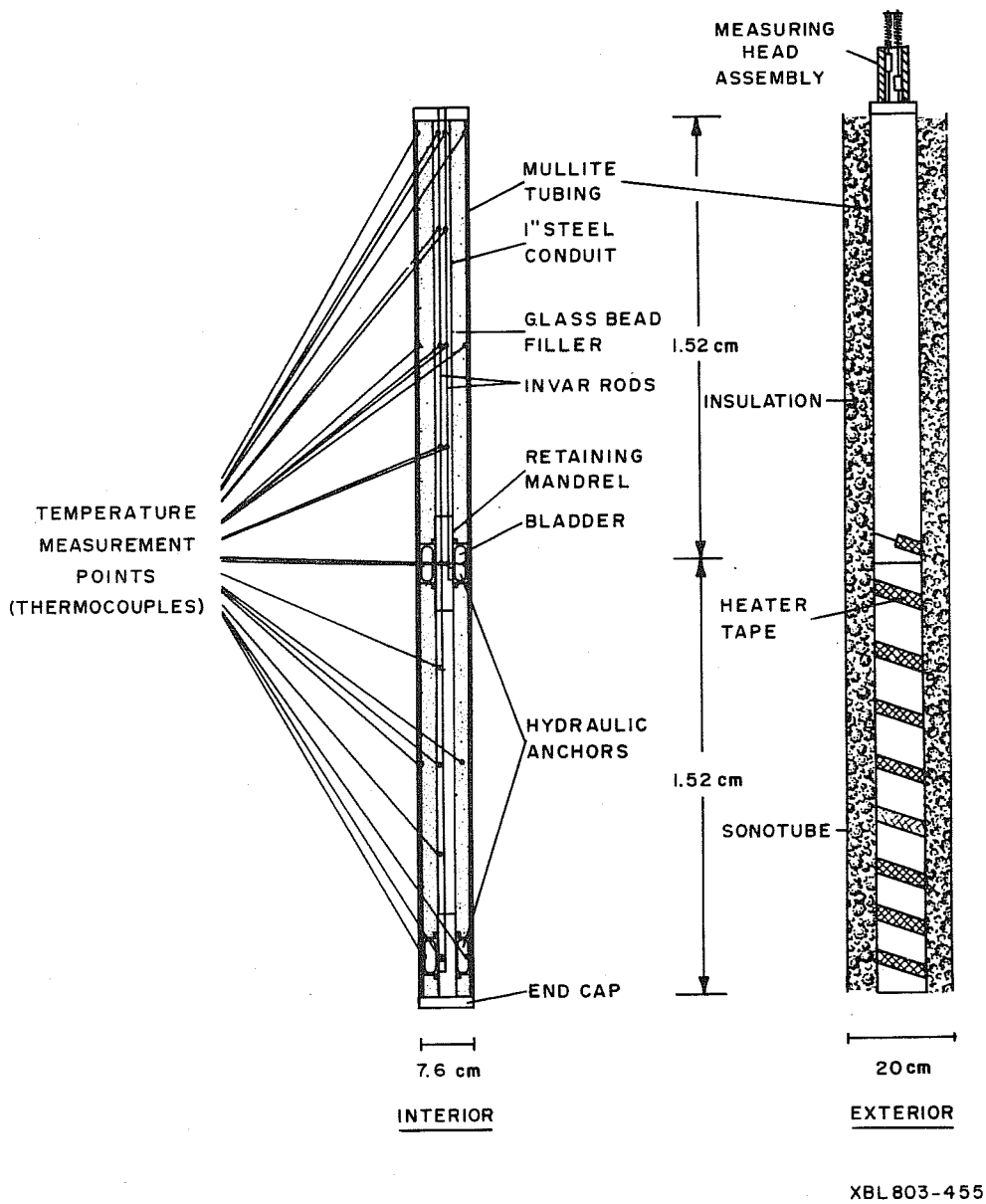

Fig. 15. Borehole simulation model.

The simulated borehole was constructed of two 1.52-m sections of 76-mm i.d. x 83-mm o.d. mullite ceramic tubing, which has a thermal conductivity similar to that of Stripa granite. Two extensometer anchors were grouted and inflated in place at positions 1.52 m and 3.04 m from one end of the tube. Steel conduits, 2.54 cm in diameter, were attached to the anchors and to the measuring head assembly. Inside the conduit two rods of superinvar, with thermocouples attached every 38 cm, were threaded into the anchor mounts. The space between the conduit and the mullite wall was filled with fine glass beads to simulate the heat transfer characteristic of the grout which would be filling this void in a field installation, while still allowing for recoverability of the extensometer components. Heater tape was wrapped around the bottom 1.52-m section of the borehole model, and thermocouples were placed at 38-cm intervals on opposing sides of the mullite tube. The entire apparatus was surrounded with 5-cm-thick glass fiber insulation encased in a rigid cardboard tube.

Five heating trials were conducted while the temperatures were monitored by an automatic data logger. An example of the temperature profiles obtained after various heating times is shown in Fig. 16. An equilibrium condition was approached after approximately 10 hours. Under field conditions at Stripa, the heat-up rate will be much slower and the temperature gradients along the borehole will be less severe than those shown in Fig. 16.

These temperature profiles demonstrated that one can expect the temperature of adjacent rods in a conduit to be within 2°C of each other; but that the borehole wall temperature could, in zones where temperature gradients are as large as 90°C per meter, be up to 15°C different. We believe that in

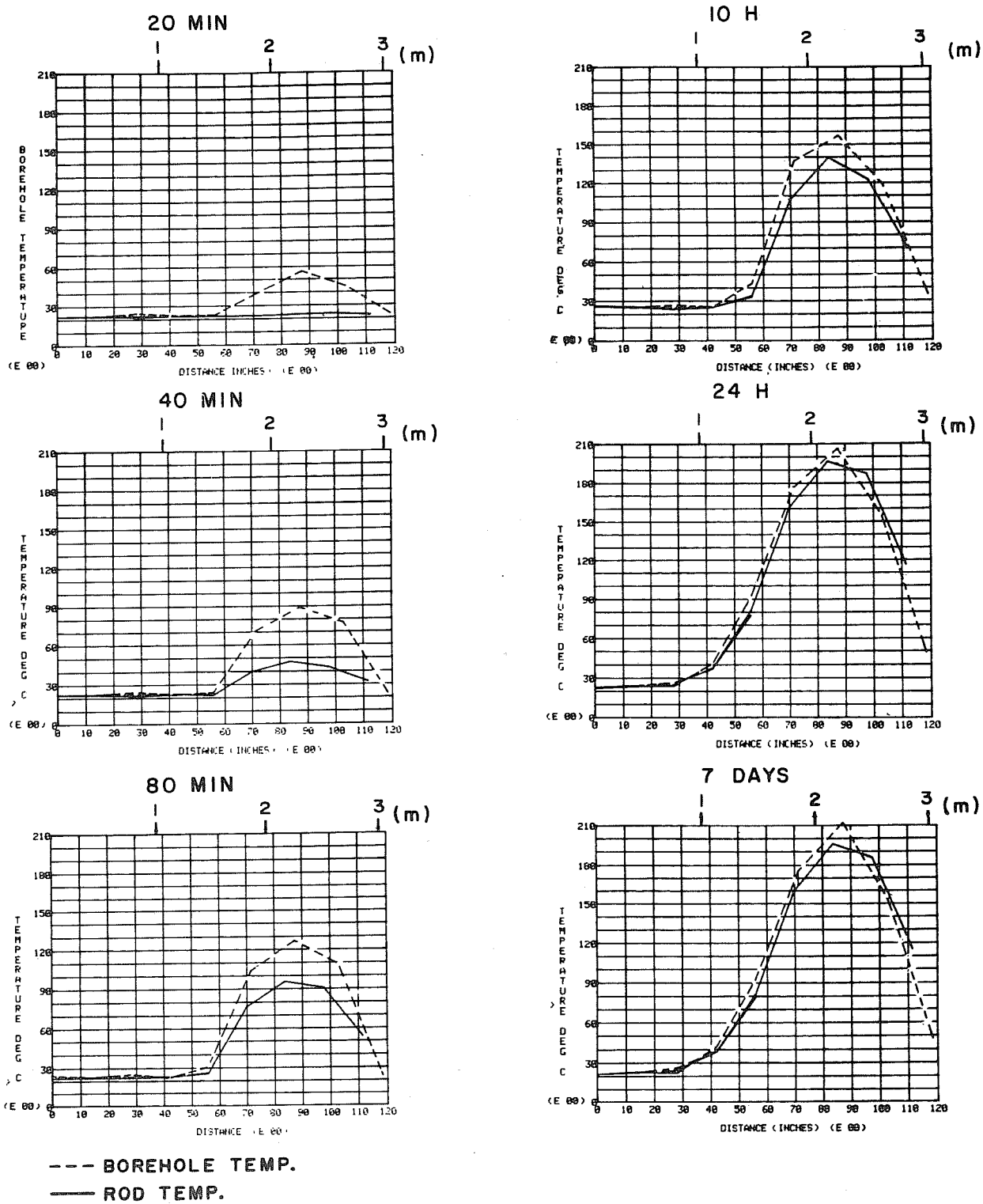

XBL 803-8843

Fig. 16. Time sequence temperature profiles of the borehole model during one of the heating trials.

practice the borehole wall temperatures will be closer to the rod temperatures because the grout has a higher conductivity than the loosely packed glass beads used in this test.

Displacement Sensor Test. A displacement transducer (DCDT) was tested in a variety of humidity and temperature conditions to determine the effect of these variables and of extensive cycling on the transducer output. The transducer was mounted on the cycling apparatus shown in Fig. 17, and the assembly was placed in a controlled environment chamber. Transducer input voltage was regulated by an external power supply constant to ± 0.01 V. Transducer output voltage was monitored by a strip chart recorder over the full test period. The DCDT was tested in the environments listed in Table 4.

No measurable change was observed in the maximum or minimum voltage produced by the extensometer cycling. All votage curves were smooth and demonstrated no disruption of the output voltage due to transducer failure or mechanical sticking.

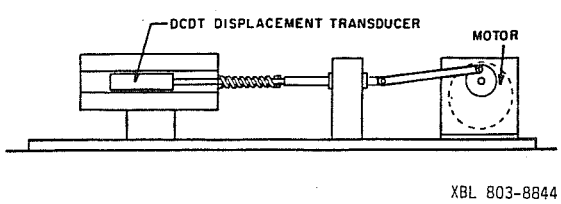

Fig. 17. Mechanical system for exercising DCDT transducer.

Table 4. DCDT stability test environments.

Temperature (°C)	Humidity (%)	Length of test (hours)
Ambient (23°C)	Ambient (11%)	24
25	50	24
25	75	24
25	100	21
35	75	24
35	100	72
50	75	24
50	100	72

NOTE: All tests showed no effect on the operation of the DCDT or its output voltage in any of the above environments.

2.3 Data Reduction Scheme

Extensometers used in the Stripa project measure the relative displacements between the head and each of four anchor points in an instrumentation borehole. Four spring-loaded rods, each attached to one of the four anchor points, extend to the collar of the hole, at which point the relative axial movements of the rods with respect to the collar are measured by four DCDTs. For isothermal conditions, the measured displacements are the true displacements. For non-isothermal conditions, as in the Stripa project, the displace-

ments sensed by the DCDTs must be corrected for the thermal expansion/contraction of the rods.

There are two cases of extensometer anchor placement at Stripa (see Fig. 18) which are treated separately. Case I identifies both vertical and horizontal extensometers where anchor points extend across the heater centerline; case II identifies an extensometer for which the anchor points are entirely on one side of the heater centerline. Vertical extensometer holes for case I are E1 through E17. Extensometer holes E20 and E29 are the only horizontal holes that extend across the heater centerline as in case I. All other horizontal extensometers (E18, E19, E21 through E28, and E30 through E35) are case II.

Chromel-Alumel thermocouples are attached to the longest superinvar rod in each extensometer to measure the rod temperatures. These temperatures are used to calculate the thermal expansion of the rods. Thermocouple locations are not necessarily at anchor locations. All thermocouple locations for extensometers as installed at Stripa are listed in Appendix A.

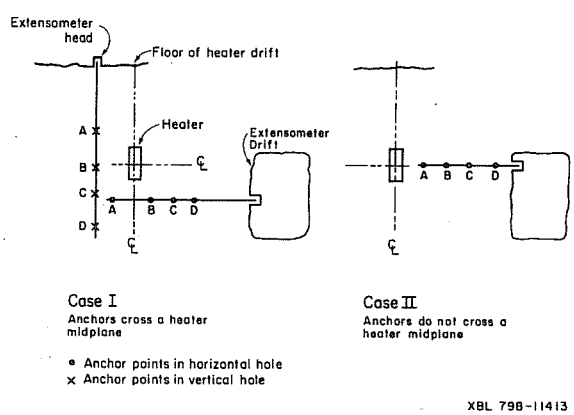

Fig. 18. Two cases for extensometer installation: where anchors do (Case I), and do not (Case II) cross a heater midplane.

To estimate the temperature of the rods at points between thermocouples, a smooth function must be calculated that closely approximates the actual temperature profile along the extensometer rod. A linear interpolation of the intermediate temperature is not sufficiently accurate for the calculation of the thermal expansion. Cubic spline functions were found to interpolate well between the discrete temperature points . At each of the temperature points, the spline function is continuous and has a continuous first derivative. End point slopes are required in order to evaluate these functions over the entire interval of interpolation. For case I type extensometers, symmetry was assumed and temperature measurements were reflected about the centerline. A zero slope condition at the centerline was also assumed, and the slope at the collar end was calculated by a least square fitted function of the form $T = Ae^{Bz}$ to the first three temperatures and differentiating this function at the endpoint. For case II type extensometers, the endpoint slopes were calculated by fitting a $T = Ae^{Bz}$ to the first three and last three temperature points. The resulting two equations were differentiated at the first and last temperature points to obtain the slopes. Figure 19 compares typical results from these spline-fit calculations for both types of temperature profile, along with theoretical calculations by Chan et al. (1978) for the temperature profiles approximately three months after heater turn on.

Keeping in mind the rod-temperature-profile calculation scheme described above, one can outline the data reduction scheme for calculating axial borehole displacements as follows:

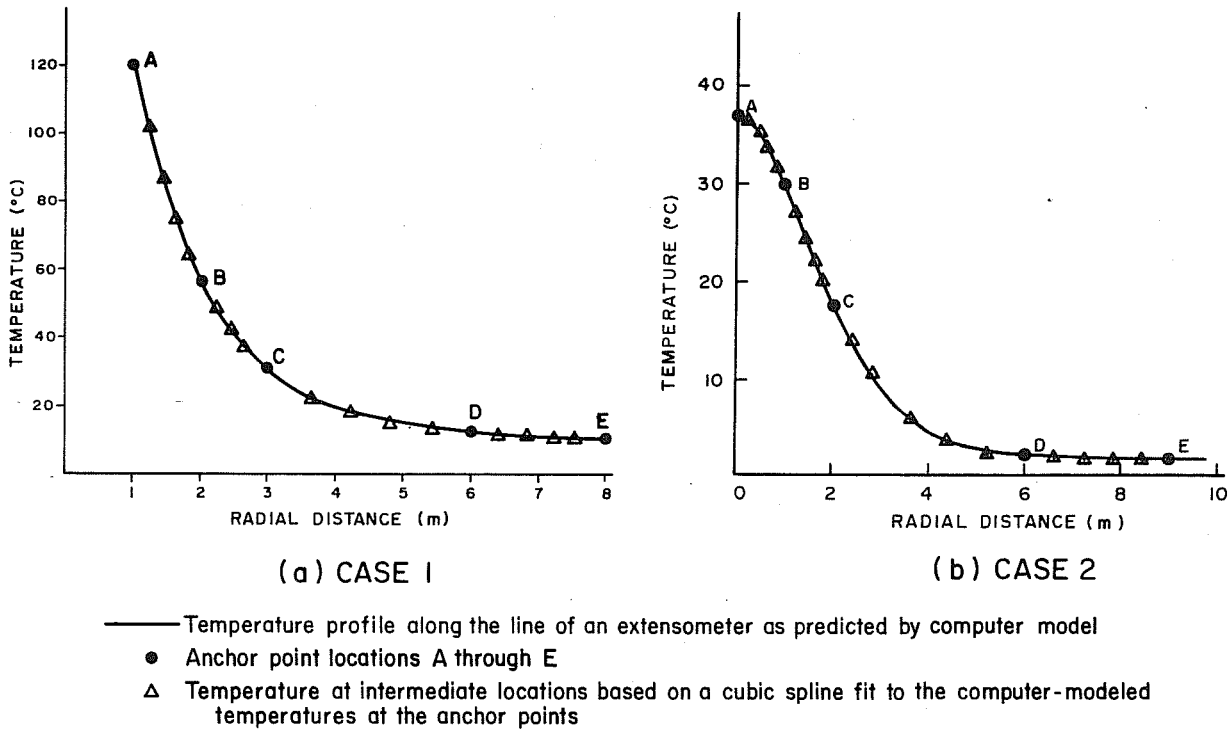

Fig. 19. Comparison of theoretical and spline-fit temperature profiles for Case I and Case II extensometer installations shown in Fig. 18.

Step 1: Record the voltage (V_i) from the appropriate rod displacement sensor (DCDT--see Fig. 20) and from this voltage calculate the gross displacement (D_G) of the associated anchor point, i.e.,

$$D_G = C_1 \left[V_i - V_o \right]$$

where C_1 = DCDT calibration value determined by in-situ calibration (mm/V), and

V_o = voltage measured before heater turn on.

Step 2: Record the collar temperature and all other temperatures measured on the longest rod in this borehole.

For Rod 4, $D_T = d_1 + d_2 + d_3 + d_4$

For Rod 3, $D_T = d_1 + d_2 + d_3$

For Rod 2, $D_T = d_1 + d_2$

For Rod 1, $D_T = d_1$

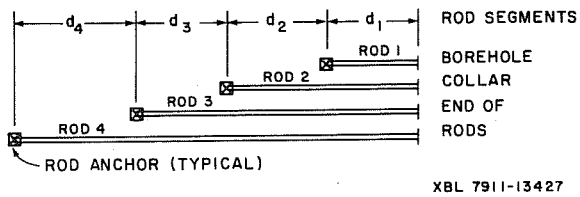

Fig. 20. Extensometer anchor connection rods and segments for thermal expansion calculations.

Step 3: Spline fit the data from Step 2 to allow calculation of anchor-point temperatures and 18 intermediate temperatures at points equally spaced between adjacent anchor points.

Step 4: Compute the total thermal expansion (d_k) for each of the four segments (between adjacent anchor points) of this longest rod., i.e.,

$$d_k = \ell \sum_{i=1}^{19} \alpha_i \qquad k = 1, \ldots, 4$$

where

ℓ = distance between adjacent anchor points divided by 19 (mm), and

α_i = net thermal strain, since time of installation, for each element of rod length ($^{mm}/mm$).

The α_i values can be calculated as:

$$\alpha_i = \alpha_i(T) - \alpha_i(T_o)$$

where

$\alpha_i(T_0)$ = thermal strain of the ith element of rod length between 0°C and the average temperature of the extensometer rods prior to heater turn on

$\alpha_i(T)$ = thermal strain of the ith element of rod length between 0°C and the current mean temperature between interpolated points.

Table 3 lists the experimentally determined thermal strain (mm/mm) as a function of temperature. The coefficients $\alpha_i(T_0)$ and $\alpha_i(T)$ are obtained by linear interpolation from this table.

Step 5: Compute the total thermal expansion, D_T, for the full length of each rod under consideration. The total thermal expansion for each rod is the sum of the expansions from Step 4 depending on anchor position (see Fig. 20).

Step 6: Thermal expansion of the rod and thermal expansion of the rock results in displacing the collar end of a rod in opposite directions. Therefore, to obtain the net anchor displacement (D_N), one must add the calculated thermal expansion of the appropriate rod (D_T) to the gross measured displacement (D_G) for that anchor point as calculated in Step 1.

2.4 Data Storage

Data for each extensometer displacement sensor (four per extensometer assembly) are stored by the computer in two ways. Short-term data, taken every 15 minutes, are stored on disk for 24 hours and can be viewed by the operators as hexadecimal values from the analog-to-digital converter, as DCDT output voltage, and as net anchor displacement in millimeters. After each

15-minute sample, the data are written to tape for permanent storage as a coded voltage.

Long-term data, an average of from 3 to 95 of the 15-minute samples, are stored on disk as millimeters of displacement relative to the borehole collar. These data are used by the graphics programs for plotting.

2.5 Field Installation

Extensometer construction and installation can be subdivided into three separate tasks: (1) assembly of the downhole hardware, (2) installation of this hardware into the borehole plus grouting and anchor pressurizing procedures, and (3) installation of the head assembly.

Construction of the downhole portion involved assembly of rods, anchors and pressurizing system, thermocouples, and conduit sections. This job was handled on a workbench 10 m in length by 1 m in width to accommodate the entire instrument during assembly (see Fig. 21). A two-man crew was required for the job. Procedure was as follows:

1. Rod sections joined, measured, and marked
2. Thermocouple leads attached at specific points along the longest rod
3. Anchors and protective conduits joined and placed around rods
4. Collar stabilizer tube attached to conduit
5. Anchor pressure lines strung and connected to anchors and pressure manifold
6. Anchor system pressure tested for leaks.

Placing the instrument in the borehole followed by grouting and setting of the anchor position was the next step. Due to the length of the instru-

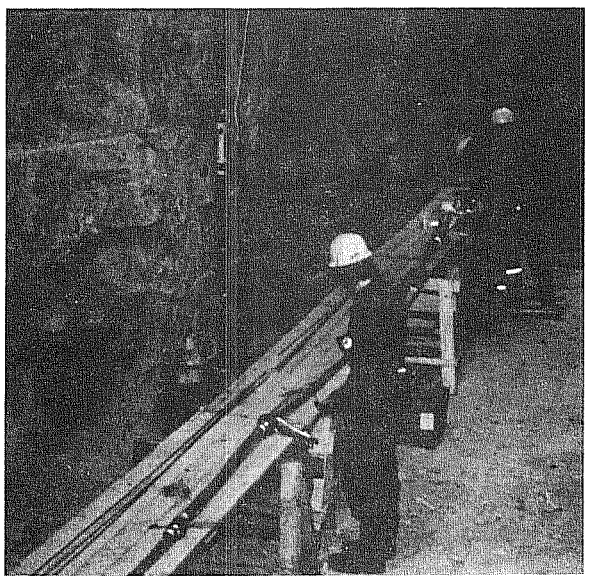

XBB 803-3397

Fig. 21. Pressure-checking the anchor system.

ment, a large crew (minimum six persons) is required to move the assembled extensometer and feed it into the borehole. Grouting operations required only a two-man crew. Procedure was as follows:

1. Grout mix prepared
2. Hole cleared of water and debris with a blast of compressed air
3. Instrument placed into borehole (Fig. 22)
4. Collar of hole packed off and the collar stabilizer tube flange secured to the rock wall (horizontal installations only)
5. Hole pumped full of grout
6. Deepest anchor positioned by pushing on the connecting rods and then inflating that anchor in place

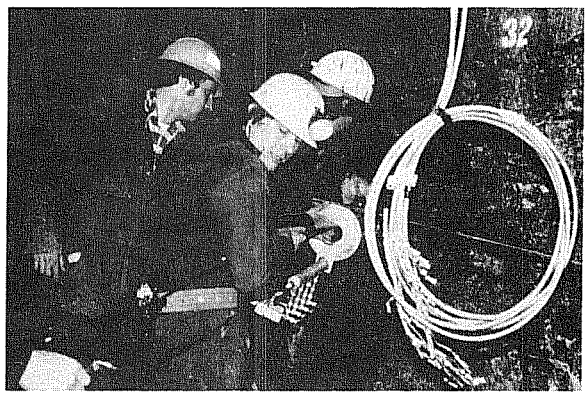

XBB 803-3398

Fig. 22. Placing extensometer in borehole.

7. Subsequent anchors each positioned by pulling on the connecting rods and then inflating the anchor
8. Collar (finish) cementing performed.

Following curing of the final cement application, the extensometer head assembly was mounted in place. This task, involving tensioning and trimming of the rods and installation of the sensing system was handled by one person. Head assembly procedure is as follows:

1. Rod spring assembly prepared and emplaced
2. Rods locked to spring assembly, tensioned, and cut to length
3. DCDT support plate mounted and DCDTs installed and wired
4. Cover plate and calibration screws installed.

This completes the extensometer installation.

2.6 Field Calibration

Extensometer calibrations are in-situ calibrations involving both data-logger and computer monitoring of displacement transducer output. The calibration includes the effects of instrument deformation (for example, rod and spring stretch) occurring during displacement measurements. The data-logger output is hand recorded and serves as both a visual check during calibrations and a calibration for use with data-logger tape values taken during the experiments. Then, the calibration is completely recorded, under the standard calibration program used at Stripa (Teknekron, Inc. 1978). Graphs of the calibration runs and computed least-squares values of slopes and standard deviation are available through the graphics routine. The slopes (calibration coefficients) and offsets entered into the sensor parameter file are listed in Appendix D.

Calibrations were performed by raising the head assembly with respect to the upper flange surface of the collar stabilizer tube (Fig. 23). Three

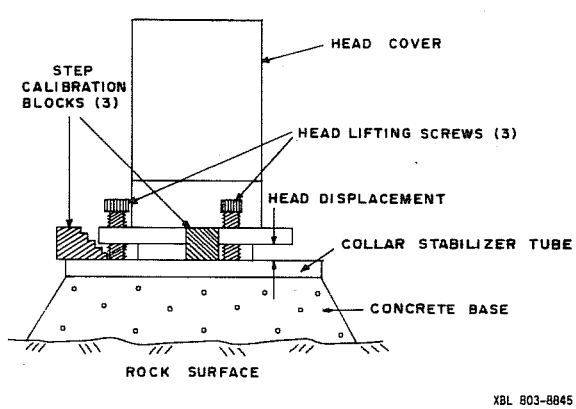

Fig. 23. Extensometer calibration set-up.

head-lifting screws provided this movement. After each lift the head was lowered onto three precision step-blocks inserted at 120° intervals between the stabilizer tube flange and the overhanging lip of the head assembly. In this way, calibrations were performed in precise steps of 5.00 mm, from 0 to 25 mm. Following calibration, the head-lifting screws were used to place the head so that the displacement sensors were near the midpoint of their range.

Sample data from an extensometer calibration are shown in Table 5 and Fig. 24. The calibration statistics are as shown below:

Time-Scale Extensometers

Average standard error = 0.041 ± 0.009 mm (20 transducers)

Highest standard error = 0.056 mm

Lowest standard error = 0.025 mm

Average slope = 2.132 ± 0.025 mm/V

Full-Scale Extensometers

(1) Vertical Extensometers

Average standard error = 0.027 ± 0.011 mm (44 transducers)

Highest standard error = 0.056 mm

Lowest standard error = 0.006 mm

Average slope = 2.132 ± 0.025 mm/V

(2) Horizontal Extensometers

Average standard error = 0.032 ± 0.011 mm (72 transducers)

Highest standard error = 0.070 mm

Lowest standard error = 0.010 mm

Average slope = 2.163 ± .023 mm/V

Table 5. Data from sample extensometer calibration, performed after installation with 5.0-mm step blocks.

Step	Distance (mm)	Voltages (V)			
		V1	V2	V3	V4
0	0.000	-5.815	-5.800	-5.840	-5.830
1	5.000	-3.485	-3.435	-3.445	-3.468
2	10.000	-1.155	-1.064	-1.050	-1.087
3	15.000	1.171	1.275	1.321	1.244
4	20.000	3.455	3.575	3.690	3.557

NOTES: Title: Extensometer calibration (full-scale) E-17

Extensometer sensor no.'s = 821, 822, 823, 824

Displacement step size = 5.000 mm

Number of displacement steps = 4

Data channel no.'s = 44, 45, 46, 47

Temperature = 15.°C

Zero readings = -5.8, -5.8, -5.8, -5.8

Standard error (mm) = 0.021, 0.033, 0.015, 0.038

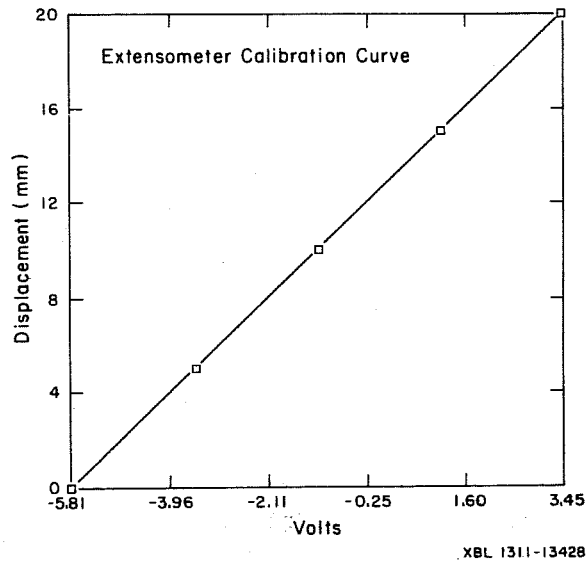

Fig. 24. Displacement versus output voltage obtained from calibration of extensometer E17A at Stripa. Calibration factor (slope) is 2.16 mm/V, with an RMS error of 21 μm.

Three extensometers (12 transducers) were recalibrated yielding an average repeatability of 0.15%.

Since the calibration curves are characteristically slightly nonlinear, the accuracy of measurements over a small range is expected to be higher than suggested by the standard errors computed over the calibrated 20-mm range.

3. USBM BOREHOLE DEFORMATION GAGES

3.1 Description of the Instrument

The USBM borehole deformation gage (Fig. 25) was developed by the U. S. Bureau of Mines to measure in-situ stress by the overcoring technique (Hooker, Aggson, and Bickel 1974). The gage measures the diametral deformation

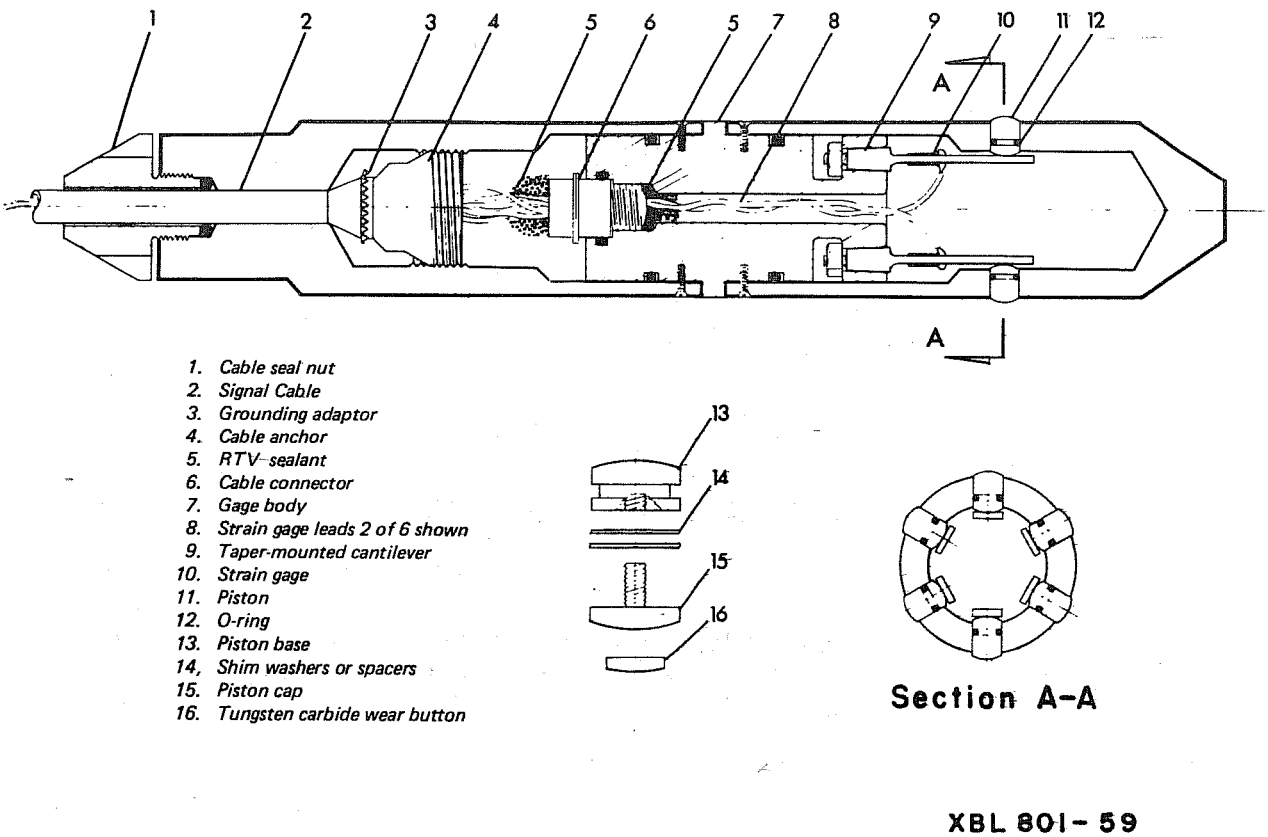

Fig. 25. U.S. Bureau of Mines (USBM) borehole deformation gage.

of an EX size (38 mm) borehole along three diameters spaced 60° apart. Each component of diameter change is measured by a pair of internally mounted cantilevers which are strain-gaged near the fixed end to produce an electrical signal proportional to the deflection of the cantilever. Each cantilever is strain-gaged on both sides to provide thermal compensation and increase the magnitude of change in gage output for a given cantilever deflection. The four strain gages are wired in a full Wheatstone bridge configuration, as shown in Fig. 26. Movement of the borehole wall is transmitted to the

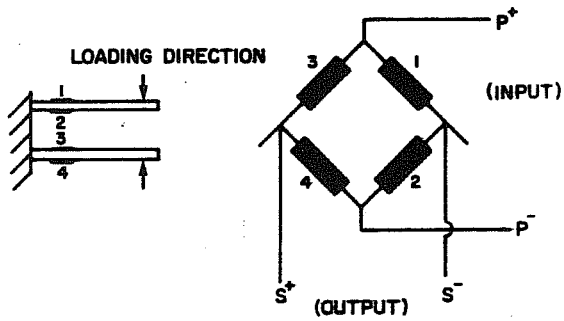

XBL 801-60

Fig. 26. Schematic of strain-gage bridge wiring on a cantilever pair for the measurement of one component of diametral deformation.

cantilevers by O-ring sealed pistons or buttons mounted through the wall of the gage body.

The measurements of borehole deformation can be converted to stress using the analytical solution for a circular hole in an infinite medium under conditions of either plain stress or plain strain (Obert and Duvall 1967). In this study the plain strain assumption was used. Conversion of borehole deformations to stress requires input of the Young's modulus and Poisson's ratio of the rock medium.

In the overcoring method, the deformation released by overcoring is used to determine the absolute stress magnitudes and orientations. In the Stripa experiments the gages are used to monitor the magnitudes and orientations of the stress changes occurring during the heating of the rock mass. Hence, the present application introduces two elements not previously considered in the use of the gage; namely, its use at elevated and changing temperature,

and its use over a time span of a year or more as compared to a few days in normal use.

In anticipation of the extended requirements, certain modifications were made in the gage material and design. These modifications include:

- Construction of the cantilever arms from 17-4 PH stainless steel instead of the beryllium copper normally used. This change was incorporated to match thermal expansions of the cantilevers to that of the gage body.
- Use of high temperature (304°C) strain gages and solder.
- Addition of individual excitation leads for all three component bridges.
- Use of teflon coated wiring and a teflon connector for cable to gage connections.
- Addition of a thermocouple installation hole in the rear body of the gage.
- Protection of electrical leads from water damage with RTV-60 silicone rubber compound.

These modifications were incorporated for gage operation up to 200°C; however, gage operation up to 250°C is probably possible. Teflon components break down at 260°C.

Each diametral strain component is measured by applying a fixed excitation voltage across the strain gage bridge and measuring the resulting bridge voltage. The diametral displacement is related to the bridge voltage by

$$u\ (\text{mm}) = C\ (V - V_s) \qquad (1)$$

where u, the diametral displacement, is given in millimeters; the slope C in millimeters per millivolt; and V, the bridge voltage, and V_S, the starting bridge voltage, are given in millivolts. If no temperature changes are expected, then gage calibration simply establishes the slope or calibration factor C. The initial voltage V_S is read after insertion of the gage into the borehole. A decrease in the borehole diameter is reckoned as a positive displacement.

The temperature dependence of the slope of the diametral displacement versus the bridge voltage response was evaluated in the laboratory for a few gages. Final calibration was performed in the field for each individual gage. In addition, temperature corrections were applied to account for the thermal expansion of the gage and the borehole. A thermocouple was installed with each gage to provide a temperature measurement at the same point as the borehole deformation measurement. All temperature corrections are incorporated into the data reduction algorithm coded on the Modcomp computer at Stripa.

3.2 Laboratory Evaluation of Temperature Effects

Calibrations for the modified USBM borehole deformation gage were conducted in the laboratory at both ambient and elevated temperatures, to determine:

- the effect of temperature on gage performance
- gage resolution and its variability among components and among gages
- procedures necessary to calibrate the gages in the field.

Complete calibrations were performed on all three components of two gages

at room temperature. In addition, these gages were calibrated at temperatures of 50°, 100°, 150°, and 200°C to determine temperature effects.

In the laboratory each gage was powered and read by means of a Vishay portable strain indicator and a switching and balancing unit with a gage factor setting of 0.40. Hence, the laboratory results are given in units of strain while the field data, which was acquired with a constant applied excitation voltage, are given with voltage as the output parameter. Since all units were fully calibrated later in the field, there was no need to relate the two units of output.

Calibrations were performed using a calibration fixture (Fig. 27) which holds the gage body firmly while depressing one component pair by means of two micrometers scaled at 0.0025 mm (0.0001 inch). After allowing the gage

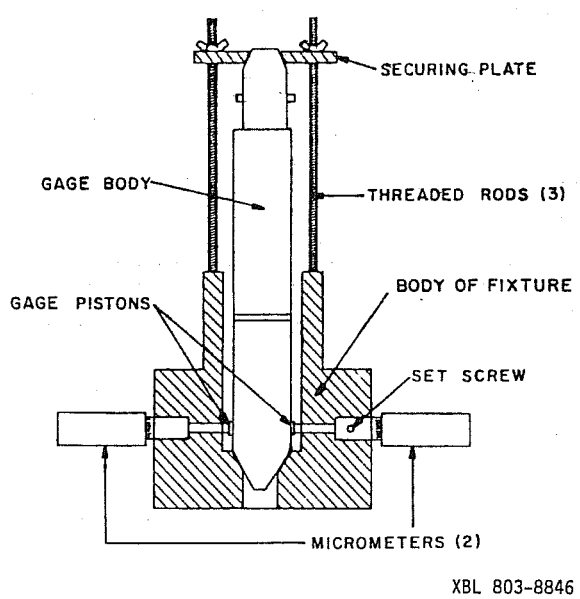

Fig. 27. USBM calibration fixture.

and calibration fixture to come to oven temperature (usually overnight), each micrometer was turned in until contact with the component pistons was made. To produce diametral change instead of radial, the micrometers were then each turned in one-half of the total incremental displacement desired. After equilibration, gage output was recorded and the process repeated. Calibrations were run over a range of 0.711 mm (0.0280 inches) of total displacement for both loading and unloading curves.

From each calibration run (loading or unloading) a calibration factor or slope was computed by least-squares linear regression. The term calibration factor as used here refers to the average change in component displacement divided by the change in component output, whether read as a voltage or as a strain.

Calibrations at elevated temperatures involved opening the oven door to permit turning of the calibration fixture micrometers. To determine the time interval required to allow the oven and gage to temperature equilibrate, a calibration run at 200°C was conducted in which readings were recorded at 0, 5, 10, 15, and 20 minutes after closing the oven door. Results of this test indicate that after the initial 5-minute lag the gage reading never changed by more than 0.0025 mm. To determine the effect of time on calibration factor, the data points from each time interval were used to compute a calibration factor. This comparison showed less than a 0.2% change in calibration factor between the 5- and 15-minute data sets. These data indicate that a 5-minute wait between readings is suitable during temperature calibration of the modified USBM gages.

Gage Calibration Factor. Typical calibration runs at room temperature and at 200°C (see Fig. 28) illustrate the linearity of the gage response with cantilever displacement. The slope of a curve is the calibration factor C, which changes only slightly with temperature. A complete listing of the calibration runs conducted in the laboratory is given in appendix Table E-1.

The results of temperature calibrations on gage number 401 for all three components is shown graphically in Fig. 29. The lines represent the least squares fit to data points representing the slopes of the calibration curves of several temperatures: the dashed lines indicate loading curves; the solid lines, unloading curves. The percent change from 20° to 200°C is also listed in Table 6.

Temperature calibrations on gage number 428 indicate a similar change

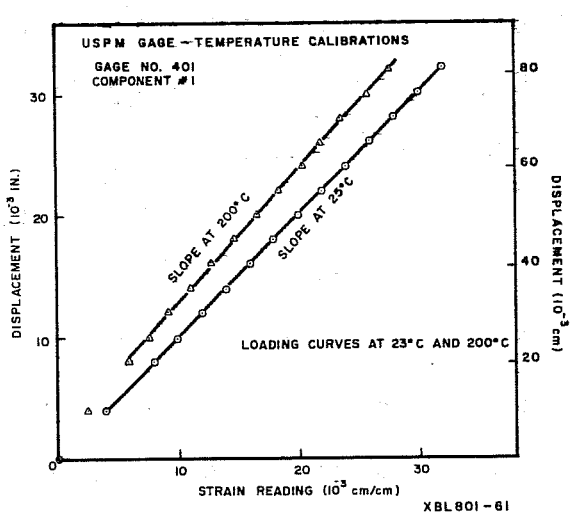

Fig. 28. USBM gage response at two temperatures, demonstrating linearity of the displacement with respect to the strain gage output. Note the small change in slope between the two temperatures. The offset between these two curves includes an offset resulting from the expansion of the calibration fixture -- see Fig. 30 for the true offset measurements.

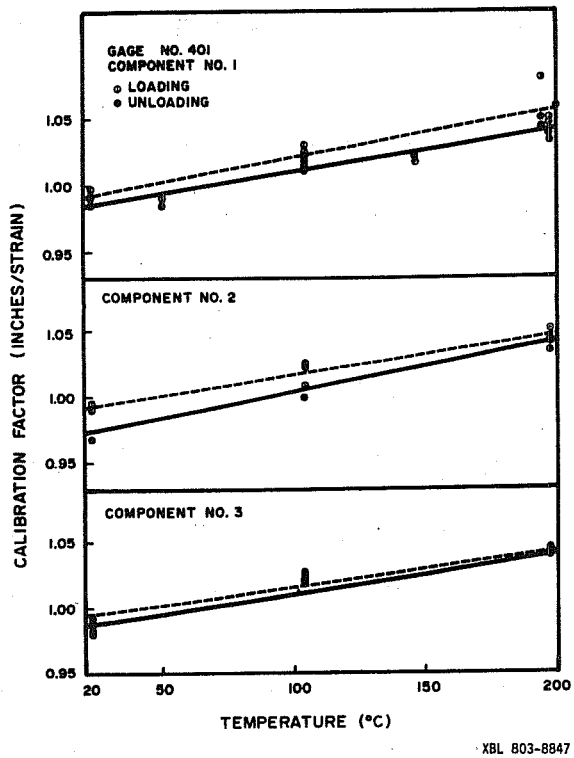

Fig. 29. USBM gage calibration factor as a function of temperature.

Table 6. Change in calibration factor with temperature for USBM gage 401.

Component number	% change (20°C - 200°C)
1	6.6 (L) 5.7 (U)
2	5.4 (L) 6.9 (U)
3	4.8 (L) 5.4 (U)
Average	5.6 (L) 6.0 (U)

in calibration factor with temperature (average 5.8% loading, 5.2% unloading). This change in calibration factor can be related to a change in gage factor for the cantilever strain gages. The gage factor is the fractional resistance change per unit mechanical strain as defined by the equation:

$$\text{Gage Factor (F)} = \frac{(\Delta R/R_o)}{(\Delta L/L_o)}$$

where: ΔR = Change in strain gage resistance (ohms)

R_o = Original strain gage resistance (ohms)

ΔL = Change in length of the strain gage filament

L_o = Original length of the strain gage filament.

The strain gages used in the manufacture of the USBM gages discussed here were Micro Measurements type WK06-125-AD350. Manufacturers' published data on the average change of gage factor with temperature indicated a 5.7% linear decrease in gage factor from 20° to 200°C. For the bridge configuration discussed here (Fig. 26) the output voltage of the unbalanced bridge is directly proportional to the gage factor. In turn, the calibration factor of each gage as defined in Eq. (1) is inversely proportional to the output voltage. Thus a 5.7% decrease in gage factor corresponds to a 5.7% increase in calibration factor, which is in direct agreement with the experimentally determined results.

Hence, the laboratory calibrations indicate that (1) the change of calibration factor with temperature is linear, (2) the change is small but not negligible, and can be taken as a 6% increase between 11° and 200°C, and (3) the change is fairly constant between different gages and different components of the same gage; that is, the change is not gage dependent.

Gage Offset. The initial bridge voltage V_0 [Eq. (1)] is also temperature dependent. This was evaluated in the laboratory at elevated temperatures and zero displacement for all three components of gages number 401 and 428. The offset referred to here is attributed to the non-compensating thermal effects of individual strain gages, and does not refer to expansion of the whole gage body against a fixed reference as discussed later.

To insure a zero displacement (no load) condition, the component pistons were removed from each gage. Both gages were then placed in an oven and brought up to 200°C from room temperature by increments of approximately 50°C. Data obtained from two runs on gage 401 are shown in Fig. 30. The

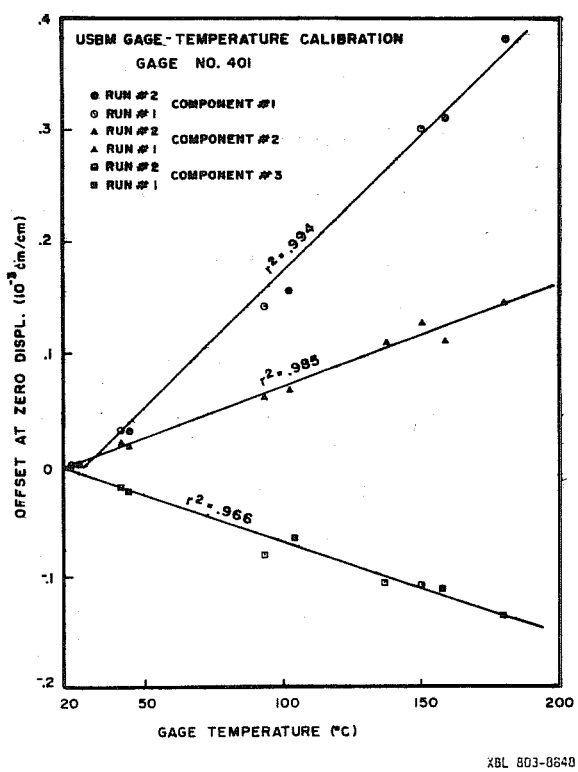

Fig. 30. Change in strain reading with temperature, cantilevers in no-load condition.

gage offset versus temperature is both linear with temperature and repeatable. This offset, unlike the change of calibration factor with temperature appears to be different for each individual component. In terms of the measured displacement,the offset correction is fairly significant as will be shown below.

Drift Measurements. Drift measurements were conducted in the laboratory on one gage to determine the stability of the gage when held at constant displacement at both room and elevated temperatures. The gage was placed in a 38-mm (i.d.) aluminum pipe causing an initial deflection of approximately 0.5 mm. Measurements were made at room temperature, and at 50°, 100°, 150°, and 200°C. Testing at 200°C was carried out for 114 hours.

Test results are shown in appendix Table E-2, as the change of gage output (millivolts) from the original, time zero, reading. After an equilibration period of about 1 hour, signal variations are generally less than 0.01 mV. The significance of this is treated below in the section on error analysis.

3.3 Computation of Displacement and Stress

Interpretation of borehole deformation from gage readings involves corrections arising from thermal effects on gage output. The following discussion involves interpretation of these thermal corrections as based on laboratory findings.

The general form of the calibration curves for USBM gauges at ambient temperature and at elevated temperature is shown in Fig.31. The calibration factors or slopes (C_i) of the calibration curves were found to be

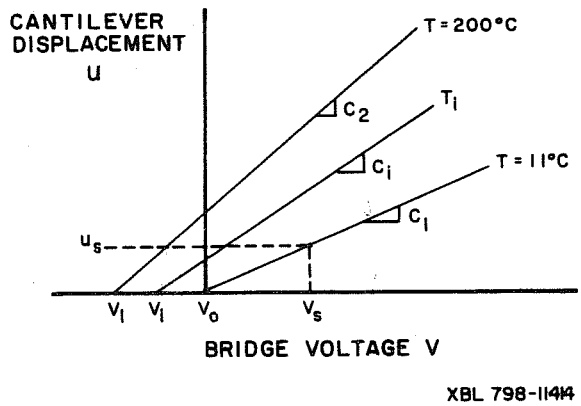

Fig. 31. General form of USBM gage calibration curves.

linear functions of temperature, thus:

$$C_i = C_1 \left[\frac{.06}{189} (T_i - 11) + 1 \right] \tag{2}$$

where

C_1 = calibration factor at 11°C

C_i = calibration factor at T_i°C.

There is an offset voltage (change of intercept) V_i, which is produced when the gage undergoes a change in temperature at <u>constant</u> displacement. This offset voltage is also linear with temperature, and the voltage change is gage dependent. The voltage change at zero displacement (component buttons removed) was evaluated at Stripa for each bridge over the temperature range 11° to 200°C. The offset voltage V_i at temperature T_i is given by Eq. (3):

$$V_i = \frac{V_1 - V_o}{189} \left[T_i - 11 \right] + V_o \tag{3}$$

where

V_0 = initial bridge voltage at 11° and zero displacement

V_1 = bridge voltage at 200°C and zero displacement.

When the gage is inserted into the borehole, the bridge voltage will change to V_s due to deflection of the cantilevers to the starting displacement u_s. The value of u_s may be computed as:

$$u_s = C_s \left[V_s - \overline{V}_s \right] \tag{4}$$

where:

$$C_s = C_1 \left[\frac{0.06}{189} \ (T_s - 11) + 1 \right] \tag{5}$$

T_s = starting temperature

$$\overline{V}_s = \frac{V_1 - V_0}{189} \left[T_s - 11 \right] + V_0 \ . \tag{6}$$

This scheme for determining u_s is valid for any starting temperature T_s; however, the procedure at Stripa assumed that T_s was 11°C, so that Eqs. (4), (5), and (6) reduce to:

$$u_s = C_i \ (V_s - V_0) \tag{7}$$

The data reduction algorithm for the USBM gages then proceeds as follows:

- Measure the new bridge voltage V_j and temperature T_j.
- Calculate the new slope and offset.

$$C_j = C_1 \left[\frac{.06}{189} \ (T_j - 11) + 1 \right] \tag{8}$$

$$\overline{V}_j = \frac{V_1 - V_0}{189} \ (T_j - 11) + V_0 \tag{9}$$

- Evaluate the displacement change u_j.

$$u_j = C_j \left[V_j - \overline{V}_j \right] - u_s \tag{10}$$

- Subtract out the difference in the thermal expansion of the rock and the gage, to obtain the real displacement u_r.

$$u_r = u_j - (\alpha_g - \alpha_r) d \ (T_j - 11) \tag{11}$$

where:

d = 38 mm, borehole diameter

$\alpha_g = 11.6 \times 10^{-6}/°C$, thermal expansion coefficient of gage body

$\alpha_r = 11.1 \times 10^{-6}/°C$, thermal expansion coefficient of rock.

Since the gage body expands against the borehole wall creating an increase in the apparent measured displacement, the contribution of gage expansion to the measured displacement must be subtracted as a correction. Similarly, the borehole diameter (in a stress-free state) increases when the temperature is raised, creating a decrease in apparent measured displacement. Thus, the contribution of borehole expansion must be added as a correction.

- Compute the biaxial stress components σ_θ, σ_r, or σ_z as outlined below.

The quantities u_1, u_2, and u_3 are the diametral displacements measured by the USBM gauges (Fig. 32). The first displacement u_1 will <u>always</u> be oriented in the tangential direction relative to the heater for both horizontal and vertical holes. The principal stress components are σ_P and σ_Q where $\sigma_P > \sigma_Q$. If the angle θ (the angle between σ_P and u_1 measured counter-

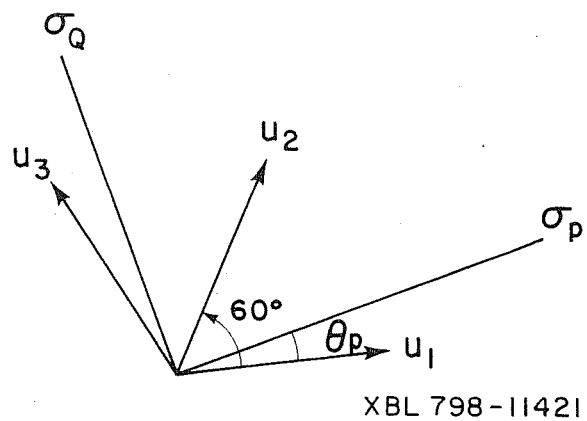

Fig. 32. Displacement and stress nomenclature for USBM gages.

clockwise from u_1) turns out to be near 90° (±10°) then the major principal stress component σ_p becomes σ_r or σ_z depending on whether the hole is vertical (σ_r) or horizontal (σ_z), and σ_Q becomes σ_θ. From Obert and Duvall (1967), the equations of interest are:

$$\sigma_p = \frac{E}{(1-\nu^2)6d} \left\{ (u_1+u_2+u_3) + \frac{\sqrt{2}}{2} \left[(u_1-u_2)^2 + (u_2-u_3)^2 + (u_3-u_1)^2 \right]^{1/2} \right\} \quad (12)$$

$$\sigma_Q = \frac{E}{(1-\nu^2)6d} \left\{ (u_1+u_2+u_3) - \frac{\sqrt{2}}{2} \left[(u_1-u_2)^2 + (u_2-u_3)^2 + (u_1-u_3)^2 \right]^{1/2} \right\} \quad (13)$$

$$\theta_p = 1/2 \tan^{-1} \left\{ \frac{3\,(u_2-u_3)}{2u_1-u_2-u_3} \right\}$$

where strain in the plane normal to the borehole is assumed to be zero.

Note that the equation for θ_p requires further inspection to determine in which quadrant the angle θ_p falls. This quadrant may be determined by examining the sign of the numerator and denominator of the right hand

portion of the expression for θ_p; +/+ = 0° - 45°, +/- = 45° - 90°, -/- = 90° - 135°, -/+ = 135° - 180°. At present, no such inspection is made by the data reduction algorithm.

3.4 Data Storage

Data for each USBM gage are stored in two ways by the computer. Short-term data, taken every 15 minutes, are stored on disk for 24 hours and can be viewed by the operators as hexadecimal values from the analog to digital converter, as voltage, and as displacement in millimeters. After each 15-minute sample, the data are written to tape for permanent storage as a coded voltage. Long-term data, an average of from 3 to 95 of the 15-minute samples, are stored as millimeters. The graphics program uses the long-term data to calculate stress values in accordance with Eqs. (12) and (13) which are displayed on the plots. Stress values are not stored by the computer.

3.5 Field Calibration and Installation

The USBM gages were calibrated on site before field installation. By calibrating on-site, the effects of the entire data acquisition system were incorporated into the calibration. This two-part calibration involved measurement of (1) thermal offset at constant displacement between 15° and 200°C, and (2) the slope of displacement versus voltage output (Fig. 33) over the displacement range of 0.71 mm at 15°C.

Thermal offset voltage was determined for each lot. First, the component buttons were removed from all gages to eliminate the influence of button expansion or friction. The gages were then placed in a forced convection oven with a resistance temperature device (RTD) as a temperature standard.

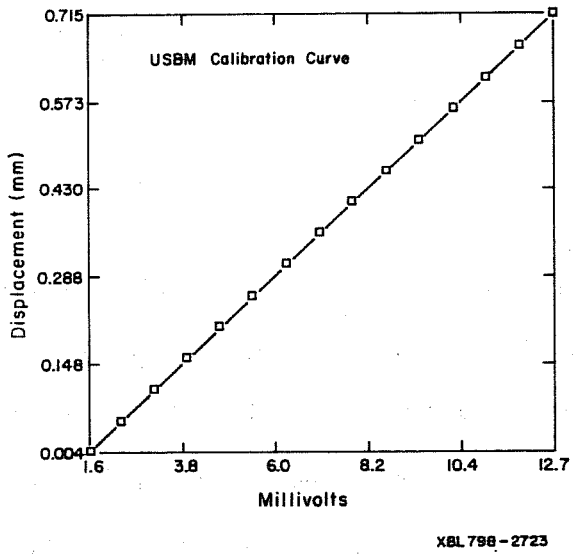

Fig. 33. Displacement versus output voltage obtained from calibration at Stripa of USBM gage U24-2. Calibration factor (slope) is 63.78 μm/mV, with an RMS error of 0.43 μm.

All gages were held at 200°C for several hours as a strain-gage annealing process, and then tested during a second heating cycle, with data taken at 20°, 80°, 140°, and 200°C, as shown in Appendix E.

The slope of displacement versus output was determined using the calibration fixture shown in Fig. 27. Each component was calibrated, at ambient temperature (15°C) only, over a range of 0.71 mm (0.0280 inch). Calibration step size was 0.051 mm (0.0020 inch).

Installation of the USBM gages involved (1) presetting the gage components, (2) assembling and attaching the associated dewatering tubes (for vertical holes only), and (3) locating the gage at the proper depth and orientation. See section 6 for a detailed discussion of the dewatering system.

The gages were preset by lowering them to a depth of 1 m and determining the necessary washer spacings to be added or subtracted to bring each component pair to the middle of its calibrated range. Spacers were available in 0.005- ,0.007- , and 0.015-inch sizes. The O-rings on the buttons as well as all other seals were lubricated with silicone vacuum grease.

Before the gage was lowered downhole, the thermocouple leads and dewatering lines were attached to the gage body and cable. The installing rods were marked at 1-m intervals for convenience. Because the small-diameter holes at Stripa are so long, the installing rods had to be modified to allow for passage of the main cable. Although slots were milled through the screw connections, twisting of the rods and wall friction often jammed the rods and cable. This problem can be avoided in future applications by redesign of the rods.

After lowering the gage to the proper depth and orienting it so that the first component was always placed in the tangential direction with respect to the cylindrical coordinate system centered on the heater, we performed a final check on the component displacement and the hole dewatering system. The rods were then removed from the hole and a fiberglass packing placed above the gage. For further detail on installation, refer to discussion of Fig. 46, section 6.4.

3.6 Sensitivity Analysis

The sensitivity of the USBM gage measurement to gage and physical property perturbations is considered in Appendix E. The analysis is undertaken in two parts: First are considered the errors in displacement caused by deviations of

the various parameters in Eqs. (7) through (11). These errors are summarized in Table E-4 for the two cases of 30°C and 90°C. It was found that the largest potential source of error lies in the thermal expansion correction. An error of 1 ppm per degree Centigrade in either the rock or gage thermal expansion coefficient results in a displacement error 3.3 μm at 90°C.

The second part of the error analysis examines the effect of parameter perturbations upon the computer stress, using a simplified version of Eqs. (12) and (13). These results are summarized in Table 7, which is reproduced from appendix Table E-5. As mentioned in Appendix E, the errors adopted for Young's modulus and Poisson's ratio are only rough estimates, representing 20% variations from the established values. Despite its preliminary nature, Table 7 contains several points of interest. The largest source of error in the computed stress is the uncertainty of Young's modulus, producing an error three times greater than the displacement measurement. Another point apparent from both appendix Table E-4 and Table 7 is that most errors increase with temperature, although the increase may not necessarily be directly proportional to temperature.

A final error analysis must refine the estimates of parameter fluctuations and especially include the effects of long-term drift. Another factor requiring assessment is the validity of the plane-strain assumption upon which Eqs. (12) and (13) are based.

3.7 Summary

For use at Stripa, equations defining the USBM gage response have been established [see Eqs. (7) through (11)] and encoded into the data reduction

Table 7. Estimated errors in stresses computed from a USBM gage measurement, due to assumed errors in the measured borehole displacement and in the mechanical moduli. Base case values at 30°C and 90°C are 15 MPa and 35 MPa.

	Magnitude of assumed error		Error in computed stress (MPa)	
	30°C	90°C	30°C	90°C
Displacement	1.1 μm	3.3 μm	+0.8	+2.3
Young's modulus	10 GPa	10 GPa	+3.0	+8.0
Poisson's ratio	0.05	0.05	+0.5	+1.0
Borehole diameter	1 mm	1 mm	-0.4	-0.9

scheme. Four temperature corrections are applied to the gage output in order to compute a borehole deformation:

1. In laboratory tests, the slope (calibration factor) C was found to increase linearly with temperature. The change is small (approximately a 6% increase between 11° and 200°C), and is uniform among different gages and among different components of the same gage--that is, the change is not gage dependent.

2. Laboratory tests showed that the offset voltage $\overline{V}$ at constant displacement changes significantly with temperature. The offset changes linearly with temperature but is gage dependent, and must be determined for each component of each gage prior to installation.

3. A correction is applied to account for the thermal expansion of the gage body. This effect is separate from the temperature dependence of the coefficients C and $\overline{V}$.

4. A correction is applied to account for the change in borehole diameter caused by thermal expansion of the rock. This effect is separate from the deformation of the borehole induced by the thermal stresses.

A preliminary error analysis shows that items 3 and 4, the thermal expansion corrections for the gage and rock, are likely to be the largest sources of error in establishing the borehole deformation caused by changes in the rock stress. As shown in appendix Table E-4, these effects appear to outweigh the uncertainties in other parameters, such as the temperature correction for the initial bridge voltage and the stability of the bridge voltage. However, long-term variations in gage properties are at present unknown and require assessment before the error analysis will be complete. A surprisingly important term is the temperature correction for the calibration factor.

To compute the stress changes associated with borehole deformation, physical property values must be used, and the uncertainty in the value of Young's modulus dominates the uncertainty in the computed stress, as shown in Table 7. Hence it appears that variations and uncertainties in physical properties overshadow measurement errors.

4. IRAD VIBRATING WIRE STRESSMETER

4.1 Description of the Instrument

Vibrating wire stressmeters are used in the Stripa heater experiments to measure stress changes in the rock mass resulting from thermal gradients developed during the heater tests. These gages were manufactured by Irad Gage, Inc. of Lebanon, New Hampshire. The original design and the operation of the gage are described by Hawkes and Bailey (1973).

Two stressmeters are wedged tightly in a 38-mm borehole which has been drilled parallel to or in the radial direction from a line heat source. The two devices are placed adjacent and at right angles to each other, and are oriented in the two principal stress directions (σ_θ, σ_r, or σ_θ, σ_z for vertical or horizontal boreholes, respectively). A total of 13 boreholes are instrumented with IRAD gages.

The vibrating wire stressmeter (see Fig. 34) operates on the principle that a change in stress of a wire causes a change in its fundamental period of vibration (Hawkes and Bailey 1973). The stressmeter consists of a highly stressed steel wire stretched across a diameter of a hollow steel cylinder. The cylinder is preloaded diametrically across the borehole, in the direction of the wire axis, by means of a sliding wedge and platen assembly. The wire undergoes a change in tension when the steel cylinder deforms as a result of changes in the force applied by the surrounding rock.

This change in wire stress is measured electronically by the IRAD MA-2 data logger or the MB-6 hand-held meter which detect the corresponding change

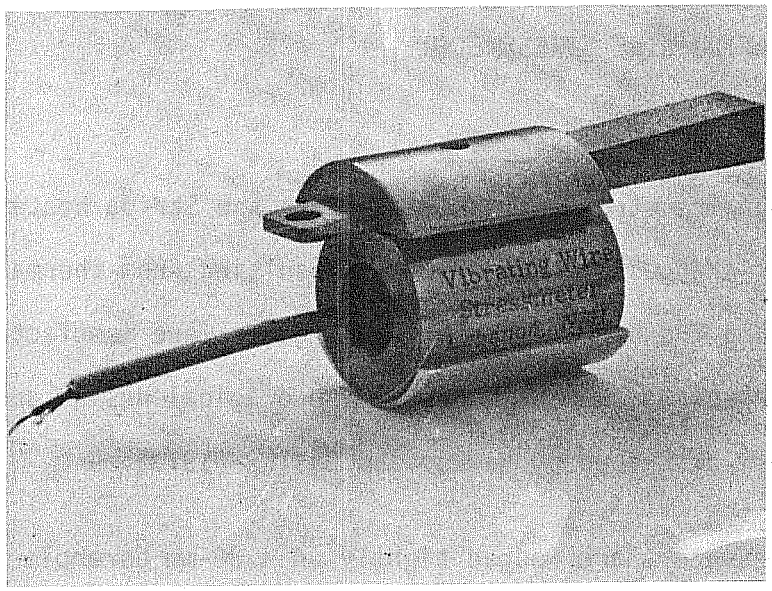

(A)

XBB 803-3400

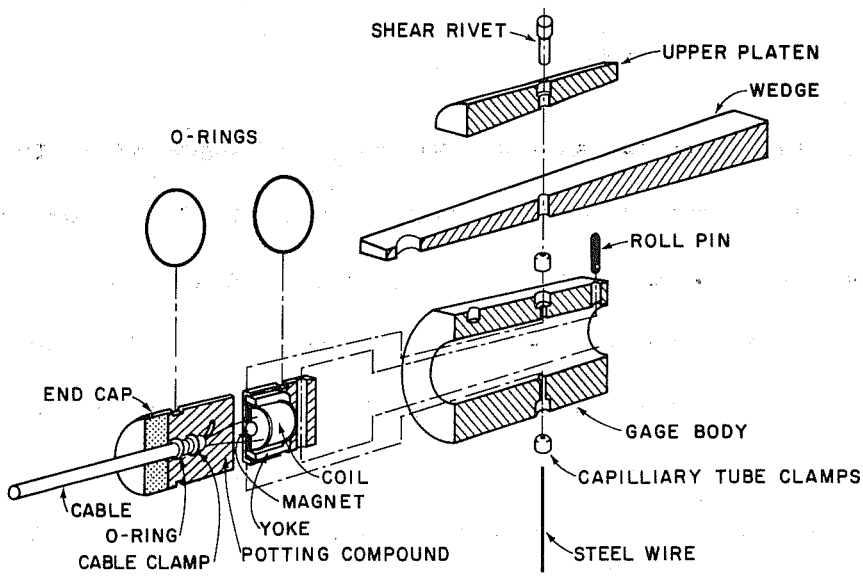

(B)

XBL 7911-13426

Fig. 34. Vibrating wire stressmeter: (A) Photograph of assembled gage with upper and lower platens, as used for soft rock. For granite, the upper platen is smaller and the lower platen is deleted (IRAD Gage, Inc. 1977). (B) Exploded sectional view.

in the wire's resonate period of vibration. These instruments provide, as readout, the digital value of the measured resonant vibratory period of the wire in units of 10^{-7} seconds. (For convenience in the following discussions and in the data reduction calculations, this period, R, shall be taken to mean the four digit meter reading rather than that number times 10^{-7} seconds. For example, R will be 2,146 units and not 2,146 x 10^{-7} seconds.)

An IRAD gage is not accurate at readings greater than about 4,000 units because the wire is then approaching a slack condition. For this reason the useful range of a specific IRAD gage is a function of its initial period of vibration. Gages of low period (high natural frequency) will provide the greatest range when installed in rock subjected to increasing compressive stresses. The distribution of the as-manufactured period, Ro, for each of the 35 gages purchased for this experiment is shown in Fig. 35.

By proper calibration of the stressmeter, the changes in gage reading can be related to stress changes in the rock at the point where the gage is installed. For the general case, three gages are required in a borehole to measure the biaxial stress changes in a plane normal to the borehole. For the Stripa project, however, the principal stress directions are assumed to be known and, hence, only two stressmeters are required for each borehole.

4.2 Gage Calibration and Evaluation of Temperature Effects

Because time was limited, it was possible to perform individual room-temperature calibration tests on less than half of the individual gages, and to perform only nine elevated-temperature (76° to 200°C) calibration tests.

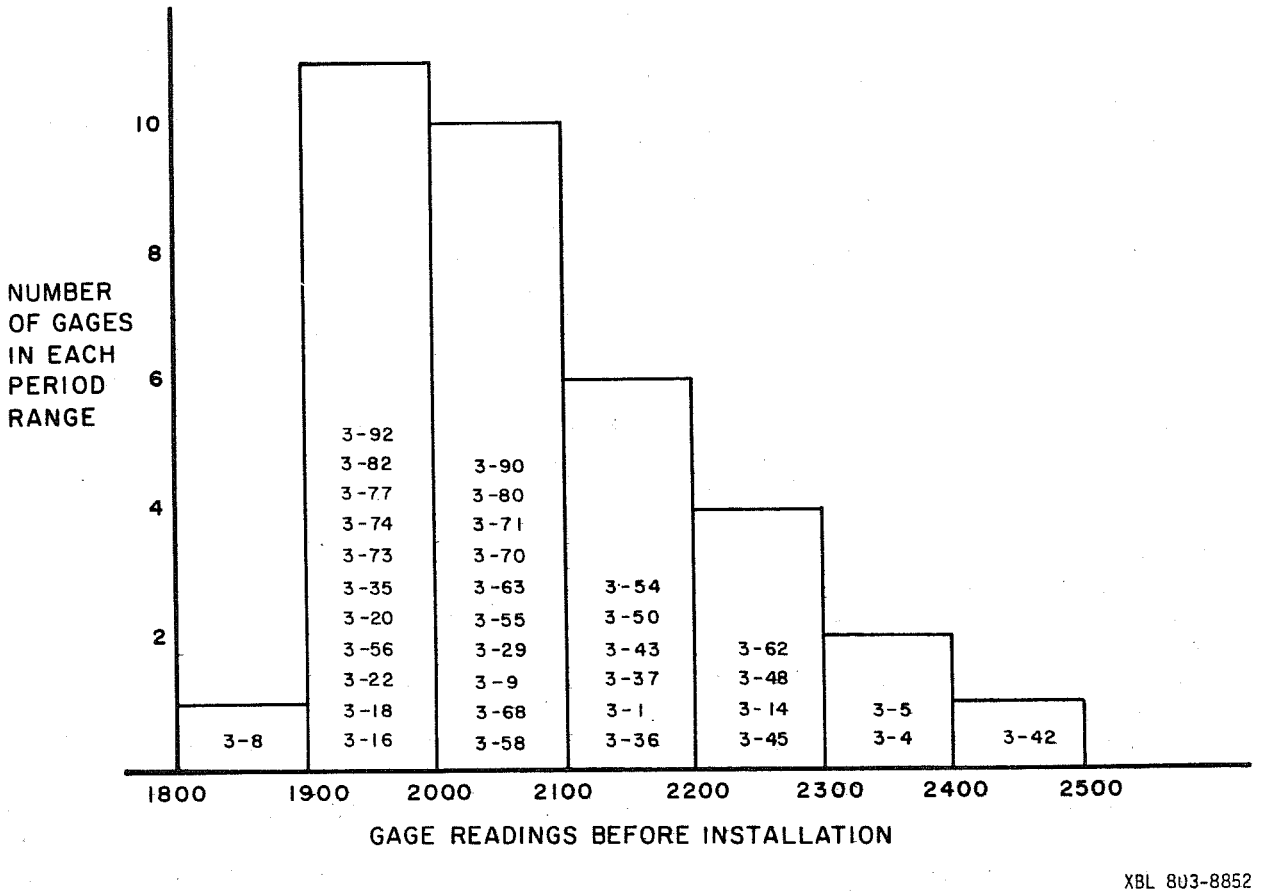

Fig. 35. Distribution of initial IRAD stressmeter readings. Individual gage numbers are noted within each group.

Gages were calibrated in the laboratory under conditions of uniaxial stress in a rock sample taken from the Stripa mine. Gages were not calibrated in the field. The calibration data provided a minimum statistical basis for the interpretation of the in-situ rock stress changes as a function of the observed gage temperatures and meter readings (vibratory period of the stressed wire).

In order to determine if any offsets in gage reading would occur when an unloaded gage (as supplied by the manufacturer) underwent a temperature

increase, two IRAD gages were placed in an oven. During rapid heat up, changes in the vibratory period were noted; after thermal equilibrium was reached at 200°C, however,the gage readings were within 5 units of the room-temperature reading. It was concluded from these measurements that gage period readings would not be significantly offset by the very slow temperature changes to which these gages would be subjected during in-situ tests at Stripa. These results are consistent with tests to 150°C reported by Hawkes and Bailey (1973).

In six additional tests (including duplicate tests on two of the gages) four IRAD gages were mounted sequentially in a sample of Stripa granite (described below) that remained free of external load. For each test, the gage reading was noted at room temperature and again after thermal equilibrium had been established at 200°C. Thermal equilibrium was assumed when the gage reading reached a steady value at the elevated furnace temperature. The coefficient of linear expansion of the Stripa granite was measured by Pratt et al. (1977) to be 11.1×10^{-6} per degree Centigrade, while a handbook value for the 4140 steel of the gage body (Smithells 1976) is 12.0×10^{-6} per degree Centrigrade. This difference in the coefficient of expansion would suggest that the period of vibration may be expected to increase slightly with increasing temperature, i.e., the gage preload is increased as a result of the temperature increase. This effect was indeed observed for most of the tests; however, for two gages a negative shift in reading was noted. The six gage offsets ranged in value from +50 units to -35 units, with an average value of +15 units.

This offset was assumed to be a linear function of temperature--as shown in Fig. 36. Future tests must locate the unidentified variables, such as wedge position, which may have caused the large scatter in these data, as well as the actual degree of linearity.

Gages were calibrated (in a Universal testing machine) by producing uniaxial compressive stress in a Stripa granite sample 22 cm long and 24 cm in diameter (Fig. 37). Sample end caps were fashioned from Little Cottonwood Stock quartz monzonite. The granite block was wrapped with electrical heater tape and thermal insulation to provide rock and instrument temperatures up to 200°C. Eighteen gages were calibrated in total. Four of these gages were tested both at ambient and at one or more elevated temperatures.

Each stressmeter was installed in the rock sample by means of a hydraulic setting tool, supplied by the gage manufacturer, which allowed control of

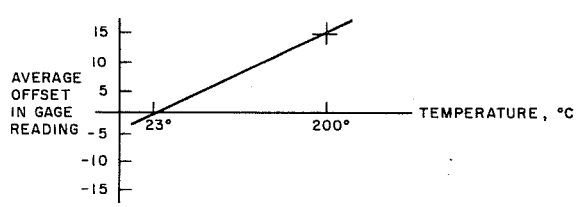

XBL 7911-13418

Fig. 36. Average response of IRAD gages when subjected to elevated temperatures while installed in Stripa granite at zero applied stress. Average offset = $R_s(T) - R_s(23)$.
$R_s(23)$ = Installed gage reading at 23°C and zero applied load.
$R_s(T)$ = Installed gage reading at T°C and zero applied load.

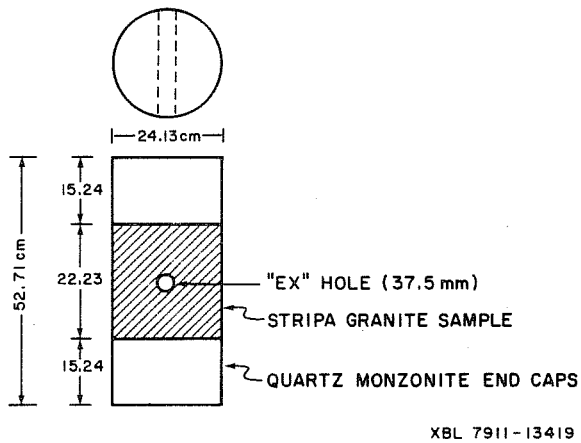

Fig. 37. Granite sample for calibration of IRAD gages under uniaxial compression.

the preset load developed by the wedging action. A preload equivalent to approximately a 100-unit change in the meter reading on the MA-2 data logger was used for these laboratory tests. For example, if the initial gage reading, Ro, was 1957, the installed gage reading, R_S, would be adusted to approximately 2057. The rock sample, with installed gage, was placed in a large test frame and loaded uniaxially to a stress of approximately 14 MPa (2,000 psi). Data were recorded in 0.70 MPa steps during both loading and unloading of the sample.

Without disturbing the gage, the sample temperature was increased by applying the appropriate current to the heat tapes, and a second calibration was performed after a new thermal equilibrium had been reached. Thermal equilibrium was reached after approximately 8 hours with a maximum heating rate of 0.2°C/minute. Thermocouples, located near the bottom, midpoint, and top of the exterior of the rock sample, as well as on the inside of the EX hole next

to the stressmeter, were used to measure sample temperatures and to verify the achievement of thermal equilibrium. At the conclusion of the testing on a given gage, it was removed and the next gage was wedged into the same hole for its calibration. Fig. 38(a) shows calibration curves obtained for gage #3-18 at 23°C and at 200°C. Additional information regarding the calibration curves is provided in Table 8.

In addition to the offset at zero load (described above), a change in the shape of the $\Delta\sigma_r$ versus R uniaxial stress calibration curve was observed as the temperature of the rock changed. In all cases tested, the calibration curves showed lower sensitivity [see definition in Eq. (14) below] at higher temperatures. That is, at any given value of R, the calibration curve for a given gage at elevated temperature has a slope which is less than the slope

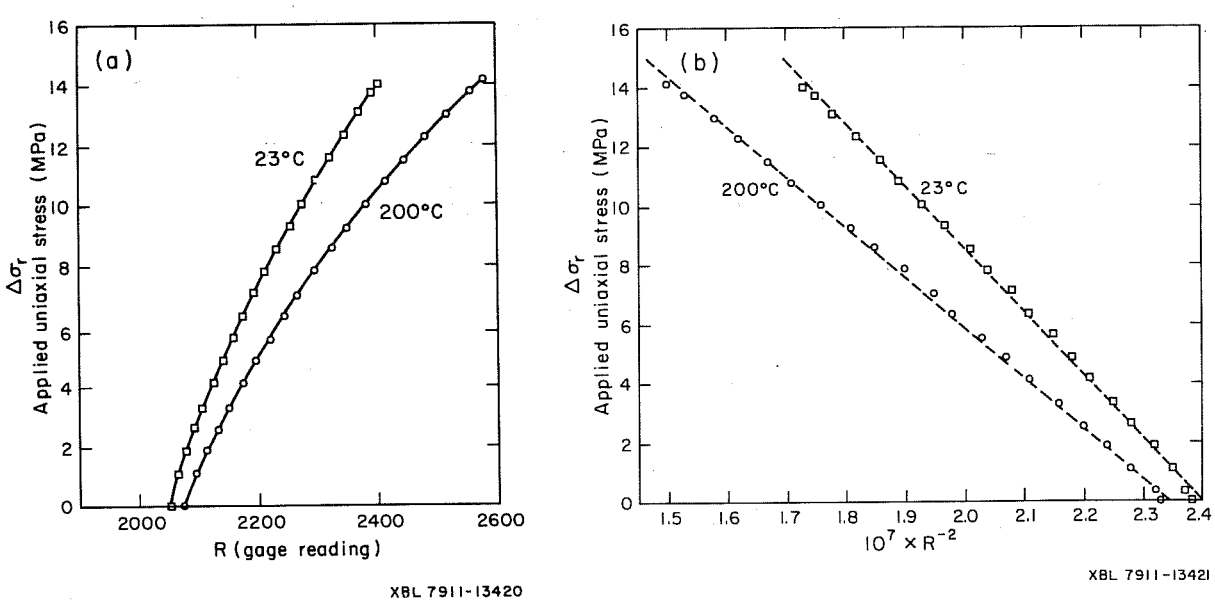

Fig. 38. Calibration curves for IRAD gage 3-18, plotted in two different planes: (A) $\Delta\sigma_r$ versus R plane with manual curve fitting. (B) $\Delta\sigma_r$ versus R^{-2} with least-squares curve fitting.

Table 8. IRAD gage calibration test results.

File name	Gage no.	Temp. (°C)	$C_2^{(23)}$ ($\times 10^0$)	$C_1^{(23)}$ ($\times 10^9$)	Standard error (MPa)	Comments
IRAD 1	3-18	23	60.03	-0.256	0.12	Max. load 7 MPa, load only
IRAD 2	3-18	23	54.00	-0.226	0.08	Max. load 7 MPa, unload only
IRAD 3	3-18	23	51.15	-0.213	0. 9	
IRAD 4	3-18	200	39.90	-0.170	0.14	Cool before unloading cycle
IRAD 5	3-42	23	47.16	-0.305	0.18	Max. load 7 MPa
IRAD 6	3-42	23	41.00	-0.260	0.24	
IRAD 7	3-42	195	30.49	-0.190	0.03	
IRAD 8	3-42	23	41.68	-0.253	0.32	
IRAD 9	3-42	108	32.42	-0.205	0.12	
IRAD 10	3-42	76	34.83	-0.219	0.16	
IRAD 11	3-42	23	42.78	-0.262	0.34	
IRAD 12	3-45	23	77.42	-0.414	0.13	Max. load 7 MPa
IRAD 13	3-45	23	62.18	-0.321	0.12	
IRAD 14	3-45	182	44.84	-0.228	0.06	
IRAD 15	3-73	23	54.40	-0.234	0.03	Max.load 7 MPa
IRAD 16	3-73	23	54.53	-0.234	0.11	Strain gaged for modulus erratic servo
IRAD 17	3-73	23	54.69	-0.233	0.04	" "
IRAD 18	3-73	88	45.70	-0.198	0.09	" "
IRAD 19	3-73	120	44.33	-0.193	0.12	Strain gage failed
IRAD 20	3-73	155	45.90	-0.196	0.02	
IRAD 21	3-73	190	46.84	-0.198	0.03	
IRAD 25	3-77	23	71.51	-0.300	0.20	
IRAD 26	3-74	23	68.53	-0.293	0.19	
IRAD 27	3-62	23	71.78	-0.383	0.22	
IRAD 28	3-71	23	68.88	-0.306	0.19	
IRAD 29	3-92	23	45.72	-0.194	0.20	
IRAD 30	3-80	23	92.01	-0.396	0.49	
IRAD 31	3-82	23	72.18	-0.305	0.15	
IRAD 32	3-90	23	84.40	-0.393	0.21	
IRAD 33	3-71	23	63.26	-0.281	0.26	
IRAD 34	3-50	23	67.17	-0.338	0.17	
IRAD 35	3-68	23	58.62	-0.267	0.17	
IRAD 36	3-16	23	67.86	-0.279	0.19	
IRAD 37	3-37	23	58.38	-0.289	0.21	
IRAD 38	3-36	23	67.17	-0.338	0.22	
IRAD 39	3-54	23	66.90	-0.344	0.23	

NOTE: Except as indicated under comments, each test included loading to 14 MPa and unloading to zero.

of the calibration curve for that gage at room temperature. The dependence of the gage calibration upon the Young's modulus of the host rock has been described by Hawkes and Bailey (1973) and by Fossum, Russell, and Hansen (1977). This loss of sensitivity would be consistent with a change in rock modulus to lower values with increasing temperature. As a check on the assumed change in rock modulus, strain gages were attached to the rock sample, and the Young's modulus was measured during a uniaxial compression test. One measurement was made at room temperature and a second measurement at 88°C. An 8.5% decrease in Young's modulus (64.8 GPa to 59.3 GPa) was observed for a 65°C increase in rock temperature. These data are consistent with independent Stripa granite measurements reported by Swan (1978). Additional modulus measurements at higher temperatures were aborted due to strain gage failure.

The calibration data were analyzed from a least squares fit of the data. A functional description of nonlinear calibration curves is easier to handle, from a data reduction point of view, than are tables of discrete calibration points for each gage, and requires less computer memory. An analysis of the data proceeds as follows:

Define the gage sensitivity γ to be:

$$\gamma = \frac{\Delta\sigma_w}{\Delta\sigma_r} \tag{14}$$

where $\Delta\sigma_w$ = change in stress of the vibrating wire

$\Delta\sigma_r$ = change in uniaxial stress of the rock.

Since:

$$\sigma_w = \frac{K_1}{R^2} \qquad \text{[See Hawkes and Bailey (1973)]} \tag{15}$$

where:

R = gage reading (period of vibration)

K_1 = constant,

then:

$$\Delta\sigma_w = K_1 \frac{1}{R^2} + K_2 \tag{16}$$

where:

$$K_2 = -K_1 \left[\frac{1}{R_S}\right]^2$$

where: R_s = installed gage reading before application of any external stress.

Combining Eqs. (14) and (16):

$$\Delta\sigma_r = \frac{1}{\gamma} \left[K_1 \left(\frac{1}{R^2}\right) + K_2\right] \tag{17}$$

or:

$$\Delta\sigma_r = C_1 \left(\frac{1}{R^2}\right) + C_2 \quad \text{(MPa)}$$

where:

$$C_1 = \frac{K_1}{\gamma}$$

$$C_2 = \frac{K_2}{\gamma} \quad .$$

If we define a new variable $\overline{R} = (R)^{-2}$ then Eq. (17) becomes a linear equation in $\overline{R}$, i.e.:

$$\Delta\sigma_r = C_1 \overline{R} + C_2 \tag{18}$$

This equation was used to fit (least square sense) the $\Delta\sigma_r$ versus R calibration data for all stressmeters tested prior to installation. See Fig. 38 for the room temperature and 200°C calibration data of gage #3 - 18.

plotted in the form of Eq. (18). The values of the constants C_1 and C_2 obtained for each least-squares curve fit and the standard errors associated with these values are listed in Table 8. The maximum standard error for any one test was 0.49 MPa (71 psi), and the average of the standard errors for all tests is less than 0.16 MPa (23 psi) over the range tested (0 to 14 MPa). This result lends credence to the use of Eq. (18) for describing vibrating wire stressmeter calibration curves. Note that, because of the least-square fit, the intercept of the $\Delta\sigma_r$ versus $\overline{R}$ curve on the $\overline{R}$ axis will not be will not be identically equal to $(R_s)^{-2}$.

There is considerable scatter in these data, and it appears that the relationship between the temperature and the values of these constants may be nonlinear; however, because of the limited amount of test data available, a linear relationship of the following form was assumed. [Note that the two slopes (4.72×10^5 and -0.0817) are averages of the least squares fit to the data shown in Fig. 39]:

$$C_1(T) = 4.72 \times 10^5 \ (T-23) + C_1(23) \tag{19}$$

$$C_2(T) = -0.0817 \ (T-23) + C_2(23) \tag{20}$$

where $C_1(23)$ and $C_2(23)$ are gage-dependent constants determined from room temperature (23^oC) calibration tests.

Further experiments need to be done to better understand the dependence of C_1 and C_2 on temperature, R_o, and other factors.

These trends in the values of the constants are consistent with results obtained by Fossum, Russell, and Hansen (1977), in which he shows that the gage sensitivity factor γ is related to the rock modulus (E_r) by

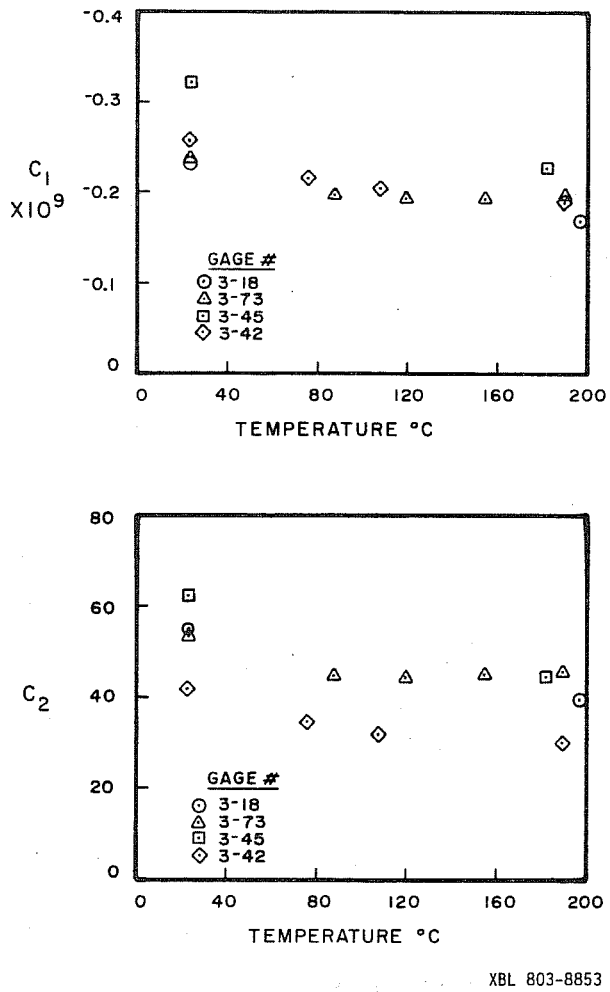

Fig. 39. Coefficients C_1 and C_2 versus temperature.

$$\gamma = \frac{d_1}{E_r \times 10^{-6} + d_2} \tag{21}$$

where d_1 and d_2 are functions of the contact angle, Poisson's ratio, and gage stiffness. Because the rock modulus E_r decreases with temperature, the value of γ, as given by Eq. (21), must increase. The absolute values of the constants C_1 and C_2 were shown previously [Eq. (17)] to be inversely

proportional to γ. Since γ increases with temperature, the absolute values values of the constants C_1 and C_2 should decrease with increasing temperature.

4.3 Interpretation of Gage Reading

The equation describing stress change as a function of meter reading for the IRAD gage is:

$$\Delta\sigma_r = C_1(T) \times R^{-2} + C_2(T) \quad \text{(Mpa)} \tag{22}$$

where R = gage reading,

T = temperature of gage and rock (in degrees Centigrade),

C_1 and C_2 are functions of temperature, as given in Eqs.(19) and (20).

Gages that could not be calibrated were matched to calibrated gages with the closest Ro values, and the uncalibrated $C_1(23)$ and $C_2(23)$ values were assumed to be equal to those of the calibrated gages. The values of $C_1(23)$ and $C_2(23)$ used at Stripa for the computerized data reduction program, ENGCON, are listed in appendix Table F-1.

In evaluating the laboratory data from four gages tested at elevated temperatures, we found that the $\Delta\sigma_r$ versus R curve, as generated using Eq. (22) and the values of the constants extrapolated [Eqs. (19) and (20)] from temperature values, yielded a curve of the same shape as the experimental data but with an offset of the entire curve in the +R direction. This offset is partly due to the overly simplified straight line, least squares fit used to correlate C_1 and C_2 versus T. The laboratory data suggest that, in addition to the temperature dependence, this offset may to some extent be dependent on gage and load history.

Lacking complete data on the response to temperature change, we have provided an offset in the value of R such that the intercept of the curve at $\Delta\sigma_r = 0$ is forced to coincide with the average offset observed for four test gages (see Fig. 36). To force this shift in the curve, Eq. (22) is modified by the addition of an ΔR term, as shown in Eq. (23) and illustrated in Fig. 40.

$$\Delta\sigma_r(R, T) = C_1(T) \times (R + \Delta R)^{-2} + C_2(T) \tag{23}$$

where:

$$\Delta R(T) = \left[\frac{-C_1(T)}{C_2(T)}\right]^{0.5} - \left[\frac{-C_1(23)}{C_2(23)}\right]^{0.5} - \left[\frac{T-23}{177}\right] \times 15 \tag{24}$$

The elements of Eq. (24) are described below.

Curve 1 in Fig. 40 represents the room temperature calibration curve generated by Eq. (22) when using $C_1(23)$ and $C_2(23)$ values derived from a least squares fit to the room temperature (23°C) calibration data. The intercept of curve 1 on the R axis is equal to $\left[-C_1(23) \div C_2(23)\right]^{0.5}$. Note

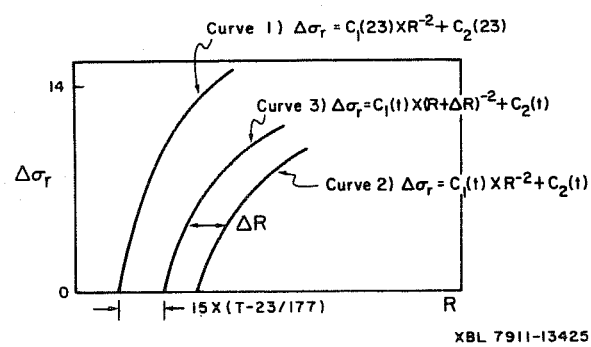

Fig. 40. Illustration of ΔR offset as used for elevated temperature data-reduction.

that, as a result of the least-squares curve fitting procedure, this intercept of the curve may not be identical with the observed value, R_s, when calibrated.

Curve 2 in Fig. 40 represents the calibration curve, for temperature (T), which would be generated by Eq. (22), when using $C_1(T)$ and $C_2(T)$ as calculated by Eqs. (19) and (20). The intercept of curve 2 on the R axis is equal to $\left[-C_1(T) \div C_2(T)\right]^{0.5}$.

Curve 3 in Fig. 40 represents the calibration curve which will be used for data reduction at Stripa. Curve 3 is generated by Eq. (23) when using $C_1(T)$ and $C_2(T)$ as calculated by Eqs. (19) and (20) and the values of ΔR as calculated by Eq. (24). This equation generates a curve in the shape of curve 2 but with its intercept to the right of curve 1 by an amount which is proportional to the <u>average</u> shift in R observed during elevated temperature testing of four gages (see Fig. 36).

Equations (19), (20), (23), and (24) are used to convert a change in vibrating wire stressmeter reading to an equivalent change in rock stress. The apparent starting rock stress (computed from the value of R and T when the gages were installed in the borehole) must be subtracted from all subsequent calculated values to obtain the next rock stress change. Figure 41 shows an example of the data reduction scheme applied to experimentally measured values on gage #3-18.

In this example, we assume the starting temperature is 23°C, the preset reading is R = 2,150, and the end point is at a value of R = 2,500 and 200°C. From Fig. 41(a) we find that the <u>calculated</u> $\Delta\sigma_r$ = 12.69 - 5.07 = 7.62 MPa.

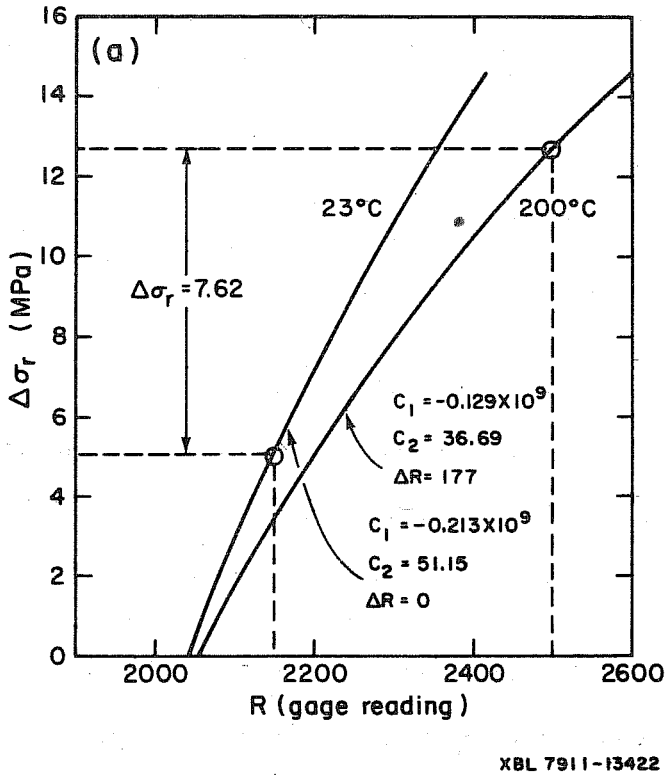

Fig. 41. (A) Comparison of calculated versus calibrated stress change values. (A) Stress change calculated by computer program ENGCON if gage 3-18 is installed at 23°C to a reading R=2150, and then later changes to R=2500 at 200°C.

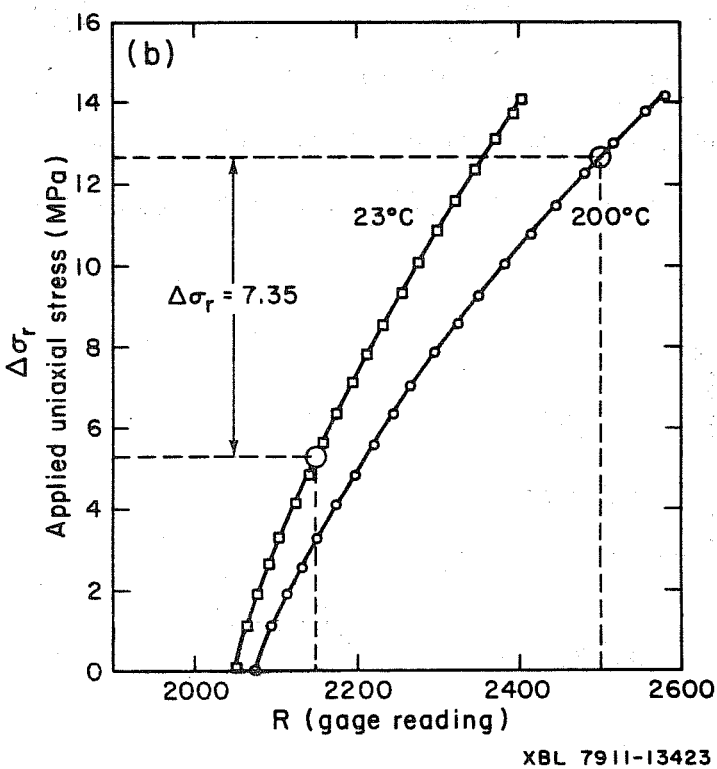

Fig. 41. (B) Comparison of calculated versus calibrated stress change values. (B) Stress change calculated by noting the stress values which were measured during the laboratory calibration of gage 3-18 at 23°C and at 200°C.

From Fig. 41(b) we find that the direct calibration data would yield $\Delta\sigma_r$ = 12.63 - 5.28 = 7.35 MPa. Although no formal error analysis was performed, comparisons based on data for other gages and for intermediate temperatures indicate that the uncertainty in indicated stress may be as large as 2 MPa at full scale for variable temperatures and cyclic loading.

In-situ stress changes for two gages are required to determine the biaxial stress change at that location in the rock mass. The stress changes sensed by these two gages, which are oriented 90° apart and in the direction of the principal stresses σ_1 and σ_2, are utilized as follows.

The equation, relating the biaxial stress changes, σ_1 and σ_2, to the stress change as sensed by an individual gage is given (IRAD Gages, Inc. 1977) as:

$$\Delta\sigma = 1/3\ (\sigma_1 + \sigma_2) + 2/3\ (\sigma_1 - \sigma_2) \cos 2\theta \qquad (25)$$

where θ is measured counter-clockwise from σ_1, as shown in Fig. 42. For the case at Stripa, the angle θ is assumed to be zero, that is, the two gages are aligned with the directions of the principal stress changes.

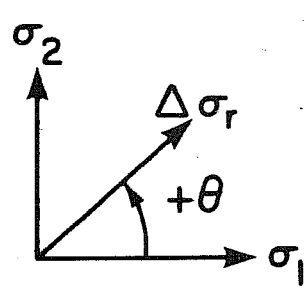

XBL 7911-13424

Fig. 42. Sign convention for angular measurements.

(Recall that this assumption is not made for the USBM gages, where three diametral components are measured.) For the vertical holes, $\sigma_1 = \sigma_\theta$ and $\sigma_2 = \sigma_r$. For the horizontal holes, $\sigma_1 = \sigma_\theta$ and $\sigma_2 = \sigma_z$.

Rewriting Eq. (25) with $\theta = 0°$ or $90°$ gives the following result for vertical holes:

$$\Delta\sigma_\theta = 1/3\ (\sigma_\theta + \sigma_r) + 2/3\ (\sigma_\theta - \sigma_r) = \sigma_\theta - 1/3\ \sigma_r \tag{26}$$

$$\Delta\sigma_r = 1/3\ (\sigma_\theta + \sigma_r) - 2/3\ (\sigma_\theta - \sigma_r) = \sigma_r - 1/3\ \sigma_\theta \tag{27}$$

where

$\Delta\sigma_\theta$ = stress change from gage oriented in the θ direction

$\Delta\sigma_r$ = stress change from gage oriented in the r direction

σ_θ, σ_r = biaxial principal stress changes in the rock.

Solving Eqs. (26) and (27) for the biaxial stress changes σ_θ and σ_r gives

$$\sigma_\theta = 9/8\ \Delta\sigma_\theta + 3/8\ \Delta\sigma_r \tag{28}$$

$$\sigma_r = 9/8\ \Delta\sigma_r + 3/8\ \Delta\sigma_\theta \tag{29}$$

Similarly for horizontal holes:

$$\sigma_\theta = 9/8\ \Delta\sigma_\theta + 3/8\ \Delta\sigma_z \tag{30}$$

$$\sigma_z = 9/8\ \Delta\sigma_z + 3/8\ \Delta\sigma_\theta \tag{31}$$

Equations (19), (20), (23), (24), and (28) through (31) are the equations used by the computer program ENGCON to convert the in-situ reading from the vibrating wire stressmeters to the equivalent biaxial stress changes in the rock.

4.4 Data Storage

Data for each IRAD gage pair are stored by the computer in two ways. Short-term data, taken every 15 minutes, are stored on disk for 24 hours and

can be viewed by the operators as the measured vibratory period of each of the two gages (in units of 10^{-7} sec) and as the principal rock stresses in MPa. After each 15-minute sample, the raw data (vibratory periods) of the gages are written to tape for permanent storage. Long-term data, an average of from 3 to 95 of the 15-minute samples, are stored as the principal rock stresses in MPa.

4.5 Field Installation

A total of 26 vibrating-wire stress gages were installed at Stripa--two per hole, 12 cm apart, and oriented in the two principal stress directions σ_θ and σ_r or σ_z, depending on the orientation of the installation hole (vertical or horizontal). Note that the gages originally intended for holes C_2, C_3, and C_4 were installed in holes U6, U15, and U17. An effort was made to pair gages that had similar initial readings. Gages were placed and preset using the standard hydraulic setting tool and installing rods provided by the manufacturer. The setting tool applies hydraulic force to pull the loading wedge and preload the gage. To mount the gage in the installing tool, the cable is first threaded through the installing tool. The gage then slides into the matched tool end and the wedge/platen assembly is fitted in place. Several strokes of the hydraulic pump draw the lever holding the wedge back towards the tool, locking the wedge, platen, and gage into place. The initial installed gage readings are given in appendix Table F-1.

Vertical Holes. IRAD gages were installed in five vertical holes in the full-scale drift. The gage to be oriented in the radial direction was always installed first.

Water was pumped from all holes, leaving the bottom half-meter of each hole filled for testing of the dewatering system (described in section 6). After each gage was lowered to the desired depth and oriented, we activated the hydraulic setting tool using the manual hydraulic pump. Gage readings were taken after each pump stroke. All gages were preloaded to approximately the same indicated stress level (7 to 10 MPa).

Gages installed in the field were thus set at a higher preload than was used for laboratory testing. This was done to accommodate expansion of the holes in response to tensile stresses anticipated during the early part of the experiment. Laboratory tests were not performed at these higher preloads to avoid tensile fracturing of the calibration rock sample.

The second or upper gage was installed in a similar manner. Both electrical cables were threaded through the setting tool. The cable from the lower gage was held tight while the setting tool, containing the second gage, was slid into place. A fiberglass packing was tamped in place following installation of the second gage. Thermocouples were installed with the pressure line of the dewatering system, as described in section 6.

Horizontal Holes. Horizontal installations were made in eight holes projecting from the extensometer drift towards the full-scale heaters. These gages were installed in an identical manner to that described for vertical boreholes. Gages oriented in the z direction were installed first. After the last gage was installed, thermocouples were attached to short (5 cm) sections of iron pipe, and one was slid into contact with each outer gage. A steel wire attached to the pipe permits easy removal of the thermocouples in the event of a thermocouple failure.

Gage Removal. If a gage must be removed, all obstructions will be taken out of the hole, including fiberglass packing, thermocouple, and de-watering tubes. A stiff length of steel pipe will be used to dislodge the wedge assembly and free the gage body. Platen and wedge assembly pieces will be removed with a magnet.

4.6 Summary

Eighteen of the IRAD vibrating wire stressmeters were calibrated at room temperature, and four at temperatures up to 200°C. Results of these experimental measurements have yielded the following results.

1. The meter reading (R_0) of a gage free of any external loads, i.e., not installed in a rock borehole, did not change by more than 5 units with an increase from room temperature to 200°C.
2. When gages were installed in a test cylinder of Stripa granite and the entire assembly heated to 200°C at zero applied axial stress, the installed-gage reading (R_S) changes varied from +50 to -35 units, with an average change of +15 units. The positive sense of the change is consistent with the fact that α gage is greater than α rock. The variation was attributed to seating of the wedges and differences in the coefficient of thermal expansion of the steel gage and the rock. For the purpose of gage reading interpretation at Stripa, this average offset in the value of R (+15 units between 23°C and 200°C) is assumed to be the best fit for all gages. The offset at other temperatures is assumed to be linearly proportional to the temperature change.

3. A curve of the form $\Delta\sigma_r = C_1 \overline{R}_2 + C_2$, where $\overline{R}$ = [meter reading]$^{-2}$, fits all the calibration data well. The average standard error for 21 calibrations using this curve fit was 0.16 MPa.
4. The changes in coefficients C_1 and C_2 with temperature were approximated as linear functions of temperature. The linearity constants were assumed to be independent of initial gage reading.

Although the individual calibration curves could be represented well by the least squares curve fitting procedure, the curves' reproducibility is uncertain. Among the factors contributing to this uncertainty are: 1) the relationship between the loading and temperature history of the granite sample and the values for its Young's modulus and its coefficient of expansion; 2) the variability in these mechanical properties at the many in-situ gage locations; 3) the long-term stability of the in-situ gage; 4) gage-to-gage variations; and 5) the impact of variations which are possible in the seating of the wedges. All IRAD gages are scheduled for recalibration at the conclusion of the field testing.

5. THERMOCOUPLES

5.1 Introduction

Temperature is measured by 273 chromel/alumel (ANSI type K) thermocouples in the full-scale experiment, and 116 type K thermocouples in the time-scale experiment. Thermocouples are attached to one or more points on each instrument for the dual purpose of rock temperature measurement and thermal compensation of the instrumentation. Others are located in independent thermocouple boreholes distributed throughout the granite to complete an

array enabling three-dimensional measurement of the thermal fields in the heater areas. Thermocouples are also mounted at several locations on each heater canister.

Three types of thermocouple clad are used: Teflon (type TFE) for temperatures up to 260°C, 304 stainless steel sheath for temperatures up to 400°C, and Inconel sheath capable of temperatures up to 1150°C. The sheathed thermocouples are electrically insulated with magnesium oxide (MgO) between wires and sheath material. Where possible thermocouples were obtained from the same chromel and alumel melts and from the same wire lots, to minimize variability due to differences in metallurgy. All thermocouples were purchased from Omega Engineering, Inc., Stamford, Connecticut.

All thermocouples are connected to ice-point temperature references manufactured by Kaye Instruments. Five model K170, 100-channel units with typical stability of ±0.01°C and guaranteed stability of ±0.025°C are used. The ice point reference outputs are connected to scanners that feed wide-range, analog-to-digital converters for digital transmission to the computer system. Parallel outputs from the ice-point references are connected to data loggers located in the experiment areas to provide computer back-up and the convenience of local readings.

5.2 Low-Temperature Thermocouples

The low-temperature thermocouples have extruded Teflon insulation over the individual wires, with fused Teflon tape over the wire pairs. TFE type Teflon was used with a maximum-continuous-use temperature of 260°C, specified by the thermocouple manufacturer. A desired precision of ±0.5°C

over a temperature range of 10° to 220°C necessitated individual calibrations in an environment as close as possible to actual operating conditions. Thermocouples that met ANSI standard-limits-of-error of ±4°F (approximately ±2.2°C) over the desired temperature range were used, since each unit was to be individually calibrated in any case.

A fourth-order-polynomial curve fit was used for each thermocouple to reduce the quantity of calibration data to five coefficients per thermocouple. This was tested using the temperature-voltage calibration data developed by the National Bureau of Standards (NBS) for type K thermocouples (ANSI 1976). A standard error of less than 0.1°C was found by a least squares fit of the fourth order polynomial to the NBS calibration data.

Several laboratory experiments were conducted to investigate protective coatings for the thermocouple junctions. The best coating found was a two component, RTV-60 silicone rubber compound manufactured by General Electric. Two thermocouples prepared with the coating were tested at high temperatures and in a 2% NaCl solution for extended periods of time. The high-temperature test was for a period of 60 days at 180°C, and the salt solution test was over 120 days at 50°C. Resistance between the thermocouple wire and the salt solution was measured periodically during the 120-day test. No measurable (<100 MΩ) resistances were ever recorded to indicate leakage of the salt water to the thermocouple junction. After installation and in most cases under elevated pressure and/or temperature, the integrity of some of the protective coatings broke down. In a few cases electrical resistance to ground became as low as several hundred ohms. However, the removal of a

reference ground in the racks eliminated the possibility of erroneous readings due to ground loops.

After data loggers, scanners, and the computer were connected and operational, the low-temperature thermocouples were wired to their ice-point references and field calibrated. Thus, calibration was done on a complete, operational, temperature measuring system. Thermocouples for the full-scale and time-scale experiments were calibrated separately in the proximity of the two instrumentation sheds. The calibration oven (Blue M, model OV-560A-2) was moved from area to area, so that the thermocouple output leads could be wired directly into the ice-point reference units located in the two instrumentation sheds.

In each case, the thermocouples were partially unrolled from their packaging coils until the open-ended leads could be laid along the cabling trays into the instrument sheds and connected to the ice-point references. The thermocouple ends were then uncoiled, tied together in a single bundle, and inserted into the top of a thick-walled aluminum vessel designed to act as a thermally stable mass that would damp out small temperature variations inside the oven (oven temperature uniformity is rated at ± 0.2°C). A platinum-resistance temperature probe (Omega Engineering Model, PR-11-3-100-1/4-18 inches E) calibrated at the Swedish Bureau of Standards to an accuracy of ± 0.05°C was also inserted into the aluminum vessel to record the actual temperature during testing. After the vessel and its contents were placed in the oven for 2 to 3 hours and allowed to reach thermal equilibrium, the first calibration data point was recorded. The oven was then turned up and permitted to stabilize for an additional 2-1/2 to 3 hours, and that calibration

point was recorded. This procedure was repeated over a temperature range of 15° to 215°C at twenty-five discrete temperatures. At each temperature the computer was instructed to scan and record the voltage values of all the thermocouples, and the resistance reading of the platinum temperature standard was manually recorded.

In this way, the calibration of each thermocouple was recorded by the computer as a series of incoming voltages, later associated with temperature values. A fourth order polynomial was curve fitted to these data, resulting in a set of five coefficients for each thermocouple record on file. The temperature for a given voltage can then be determined as follows:

$$T = C_0 + C_1 V + C_2 V^2 + C_3 V^3 + C_4 V^4$$

where C_0, C_1, C_2, C_3, C_4 are the polynomial coefficients

T is the temperature in degrees Centigrade

V is the output voltage in millivolts.

A sample graph of one of the thermocouple calibrations is shown in Fig. 43, which also lists the raw calibration data, and five polynomial coefficients.

5.3. Medium-Temperature Thermocouples

Type K thermocouples clad in stainless steel sheath were used where initial calculations indicated that rock temperature might exceed 200°C. Stainless steel was chosen over Inconel simply because of availability. Sixty of these thermocouples were used in the twelve "close-in temperature" boreholes, T13 to T24, (see Appendix A), which are within 1 m of either of the two full-scale heaters; thirty-six were used with IRAD-gages and extenso-

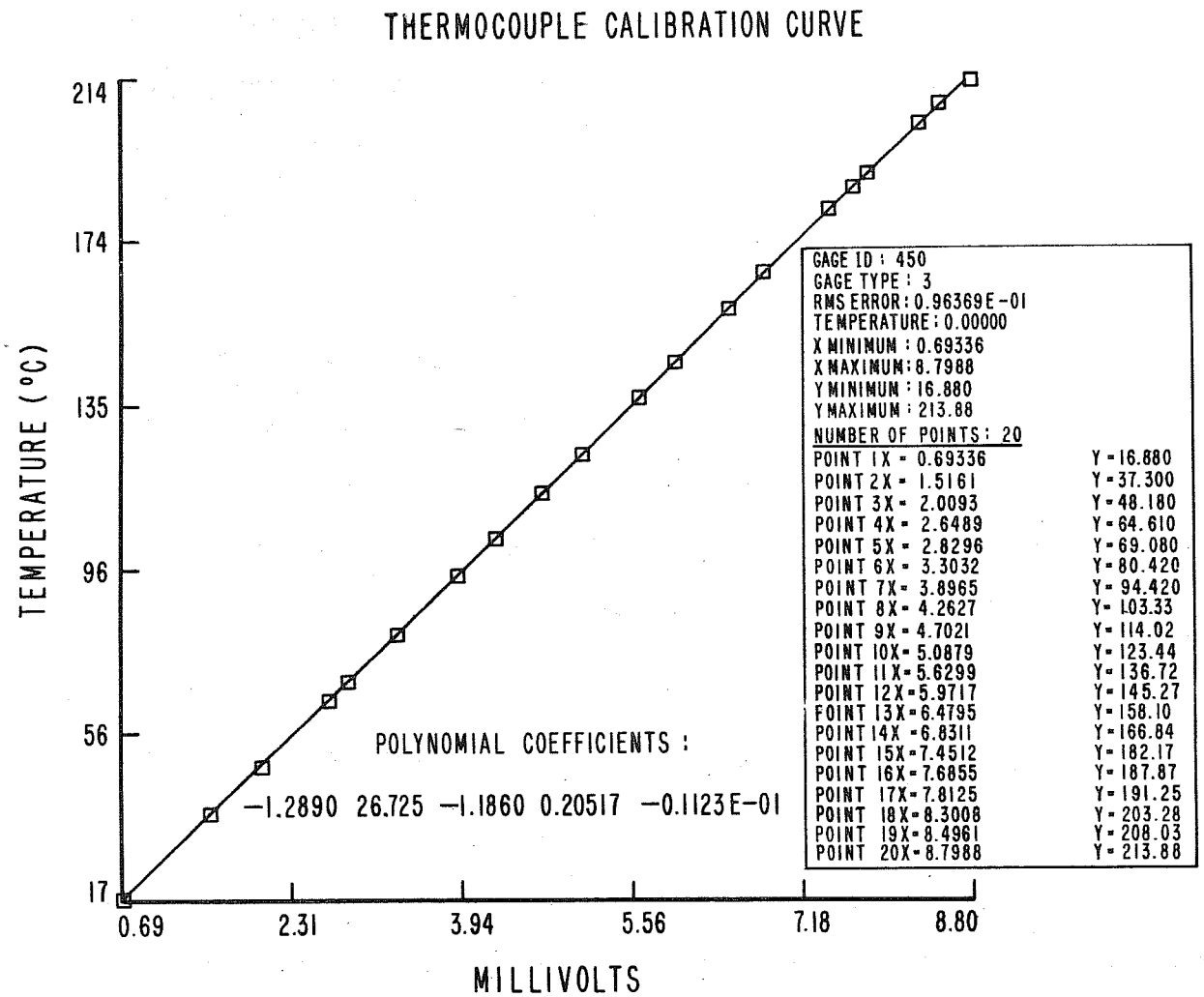

XBL 792-7367

Fig. 43. Sample plot and listing of a thermocouple calibration. The five coefficients describe the fourth order polynomial based on a least squares fit to the calibration data.

meter anchor points located within 1.5 m of the heaters; and ten were purchased as spares and calibration references.

These thermocouples, supplied by Omega Engineering, were fabricated from 1/16-inch-diameter thermocouple wire, sheathed in 304 stainless steel, and

were from a single special-limits-of-error lot. Specified lengths allowed the sheathed wire to exit any borehole into an ambient temperature environment (10° to 20°C) before going into a transition junction, where it was joined to Teflon insulated, AWG No. 24, type K extension wire that met ANSI standard-limits-of-error specifications. The transition junction between clad and teflon covered wire was welded and strain relieved. The teflon was sandblasted, and the junction potted with epoxy. The epoxy was then coated with silicone for added moisture resistance.

ANSI special-limits-of-error specify an initial tolerance of ±2°F (approximately ±1.1°C) to 530°F (277°C) and ±3/8% above 277°C. However, if chromel-alumel accumulates 5 to 10 hours at 500° to 600°C, chromium in the chromel precipitates out along the grain boundaries as chromium carbide, causing an increase in temperature readings. This precipitation is complete after about 30 hours.

The 106 stainless-steel clad thermocouples were, therefore, stabilized by heat treatment at just below 600°C for 50 hours. Five samples, calibrated from 0° to 300°C before the heat treatment, matched the NBS curves to better than -0.5°C at 0°C, and +1.0°C at 300°C. After heat treatment, they showed negligible shift at 0°C, with a linearly increasing shift to +2° to +2.5°C from the NBS curve at 300°C. A second heat-treatment cycle of two of these samples caused no further shift.

The heat treatment process may have lead to the subsequent failure of many of the thermocouples in the close-in temperature boreholes (T13 to T24) because of corrosion of the stainless steel clad. It was discovered, after

installation, that this same process also caused chromium to be precipitated out into the grain boundaries of stainless steel as chromium carbide, thus leaving the steel sensitized to corrosion. The cause of intergranular corrosion is summarized in the section on corrosion failures in the Metals Handbook (American Society for Metals 1975). Holding at temperatures as low as about 400°C for prolonged periods has been reported to cause sensitization of austenitic stainless steel. Future use of stainless-steel sheathed thermocouples in a repository or test facility should probably be avoided.

Because of limitations in the maximum temperature capability of the calibration oven used in Sweden, the medium- and high-temperature range thermocouples could not be calibrated in the field beyond about 215°C. The five coefficients for a fourth order temperature-voltage polynomial were, therefore, computed from data contained in the NBS tables of type K thermocouple voltage-temperature characteristics. Laboratory measurements on several heat-treated sample thermocouples showed that these thermocouples did not exactly match the NBS data. These sample measurements indicated an error of up to 1°C near ambient temperature, which increased linearly to 3°C at 300°C.

5.4 High-Temperature Thermocouples

Type K thermocouples clad in Inconel-600, and capable of temperatures up to 1150°C, were used to monitor heater canister temperatures. Initial calculations indicated these temperatures might exceed 500°C. Sixteen thermocouples were used on the two full-scale heaters, twenty-four on the eight peripheral heaters, and twenty-four on the eight time-scale

heaters. Additional units were purchased as spares and for calibration purposes.

These thermocouples were fabricated by Omega Engineering from 1/16-inch diameter, Inconel-clad stock, with a transition junction to heavier, AWG No. 20 size, teflon-insulated extension wire. The high-temperature thermocouples were fabricated to the same general specifications as the medium-temperature thermocouples, with the exception that units for the time-scale and peripheral heater were from a lot of standard-limits-of-error thermocouple wire.

These thermocouples were heat treated with the same process as was used for the medium-temperature units, and with nearly identical results. Five samples, calibrated from 0°C to 300°C before heat treatment, matched the NBS tables with an error of less than -0.5°C at 0°C and +1.0°C at 300°C. After heat treatment there was no measurable shift at 0°C, with an increasing shift (proportional to temperature) of between +2° and +3°C from the NBS tables at 300°C.

The Inconel-clad thermocouples have proven to be reliable and rugged, and there has been no problem with corrosion. However, solid-solution, nickel-base alloys such as Inconel 600 are subject to grain-boundary carbide precipitation if held at or slowly cooled through the temperature range of 540° to 760°C (American Society for Metals 1975). If thus sensitized, they are susceptible to intergranular corrosion in hot, caustic solutions and in high-temperature water containing low concentrations of chlorides or other salts.

The same voltage-to-temperature conversion polynomial derived from the NBS tables for the medium-temperature thermocouples was used for these Inconel-clad thermocouples,with essentialy the same error and correction capabilities.

5.5 Data Storage

Data for each thermocouple are stored by the computer in two ways. Short-term data, taken every 15 minutes, are stored on disk for 24 hours and can be viewed by the operators as a hexadecimal value, a voltage, and a temperature in degrees Centigrade. After each 15 minute sample, the data are written to tape for permanent storage as a coded voltage. Long-term data, an average of from 3 to 95 of the 15-minute samples, are stored as degrees Centigrade.

5.6 Field Installation

Time-Scale Experiment. Because the rock in the time-scale experiment was highly fractured, dewatering schemes were unsuccessful in the time-scale instrumentation holes, as described in section 6. Borehole depth (14 m) and size (38-mm diameter) ruled out vacuum or downhole pumping alternatives. All thermocouples were therefore grouted in place, with the disadvantages of (1) inability to remove and replace thermocouples, and (2) loss of the hole for geophysical logging after the test was completed.

Installation was relatively simple. First, the thermocouples were uncoiled and fastened tightly together with teflon tape so that the spacing between them was precisely as it should be down the hole. Next, a small piece of metal was hung from the lowest thermocouple as a weight to tension the

thermocouples as they were lowered into the hole. When the proper depth was reached, the string of thermocouples was grouted in place using a standard cement/sand mix. This completed installation, except for occasional "topping" of the holes with grout as drying required.

Full-Scale Experiment. The thermocouples in the full-scale experiment were installed and attached to the dewatering system in each hole. As in the time-scale experiment, they were laid out with the proper spacing and fastened together before being lowered into the holes. A description of the dewatering apparatus and its installation and removal is included in section 6. After installation, all holes were backfilled with sand.

6. DEWATERING SYSTEM

6.1 Introduction

Infiltration of water into the instrumentation holes, even at very low flow rates, posed two problems for the proper operation of borehole instrumentation. Firstly the IRAD and USBM gages, particularly the latter, were not proven to be watertight and it was desired that the electrical components of the gages be kept as dry as possible. Secondly, convection of fluid within the borehole would produce temperature anomalies not related to the true temperature of the rock. This latter problem was addressed both with the dewatering installation and with the emplacement of a sand backfill or a fiberglass packing. Dewatering systems were also installed in the heater holes (Burleigh et al. 1979), but for a different reason. There it was realized the vaporized water would cause uncertainties in the amount and distribution of heat delivered to the rock. The dewatering systems for the

heater holes are completely different and separate from the systems used for the instrumentation holes.

To avoid extra cost and reduce maintenance, it was desirable that the dewatering system be as simple as possible. Due to the hole depths and frictional line losses in pumping out water, a simple suction system alone was not sufficient; therefore, it was planned to pressurize the borehole with air and force the water to exit upwards through a small copper tube. Because they offered the least clearance for the passage of dewatering tubes, the USBM gages posed the biggest problem in design. A laboratory mock-up, using PVC pipe as a borehole, established minimum pressure requirements and relative flow rates. Very small (1/16 inch)-diameter tubing was selected to bypass the gage. Final testing and design was done in the field. The final system used both air pressure and vacuum extraction, as described below.

In the field the small-diameter boreholes were tested to see if they would hold air pressure adequately. The procedure was to plug a hole near the collar, apply air pressure by means of a tube passing through the plug, and allow water to vent through a second tube passing through the plug. In some instances, air leakage could be observed as air bubbles escaping from the top of the water column in nearby holes, or as air bubbles escaping from wetted cracks on the surface in the vicinity of the air injection hole. In the time-scale drift, the thermocouple holes around heater hole H3 were found to be interconnected to one another and to H3 through fractures. As a result, the holes would not hold pressure well enough to permit installation of the dewatering system; therefore, the thermocouples in the T-holes in the time-scale room were grouted. In the full-scale drift, no such gross inter-

hole connections existed, although in a few cases some escape of air through surface cracks could be seen. Hence all the small-diameter (38 mm) holes in the full-scale drift were outfitted with dewatering tubes. None of the extensometer holes were so outfitted, since all extensometers were grouted. Nor were any of the horizontal holes (from the extensometer drift) as they had all been drilled on a slightly upwards incline for the very purpose of permitting drainage. Hence, the following descriptions apply only to the vertical U, C, and T holes of 38-mm diameter in the full-scale drift.

The dewatering systems in the USBM, IRAD, and thermocouple holes are quite similar. There is a suction tube to a point near the bottom of each hole, and an air pressure line to a point near the top of each hole which assists the vacuum system by increasing the pressure in the entire hole. In most cases, either the vacuum or the pressure applied to a particular hole could be used to dewater it; however, the redundancy helps to speed the process and provides a safeguard in case either the air compressor or the vacuum pump fails.

6.2 Thermocouple Holes

A schematic diagram of the dewatering system used in all thermocouple holes is shown in Fig. 44. The bottom thermocouple is seen fastened to a fiberglass plug wedged between two steel washers, soldered to the 1/8-inch o.d. copper vacuum and pressure lines. Above this plug, the boreholes were backfilled with sand to reduce heat convection along the hole. Any water entering one of the holes filters down through the sand, through the fiberglass, and into the empty chamber at the bottom, where the vacuum line sucks

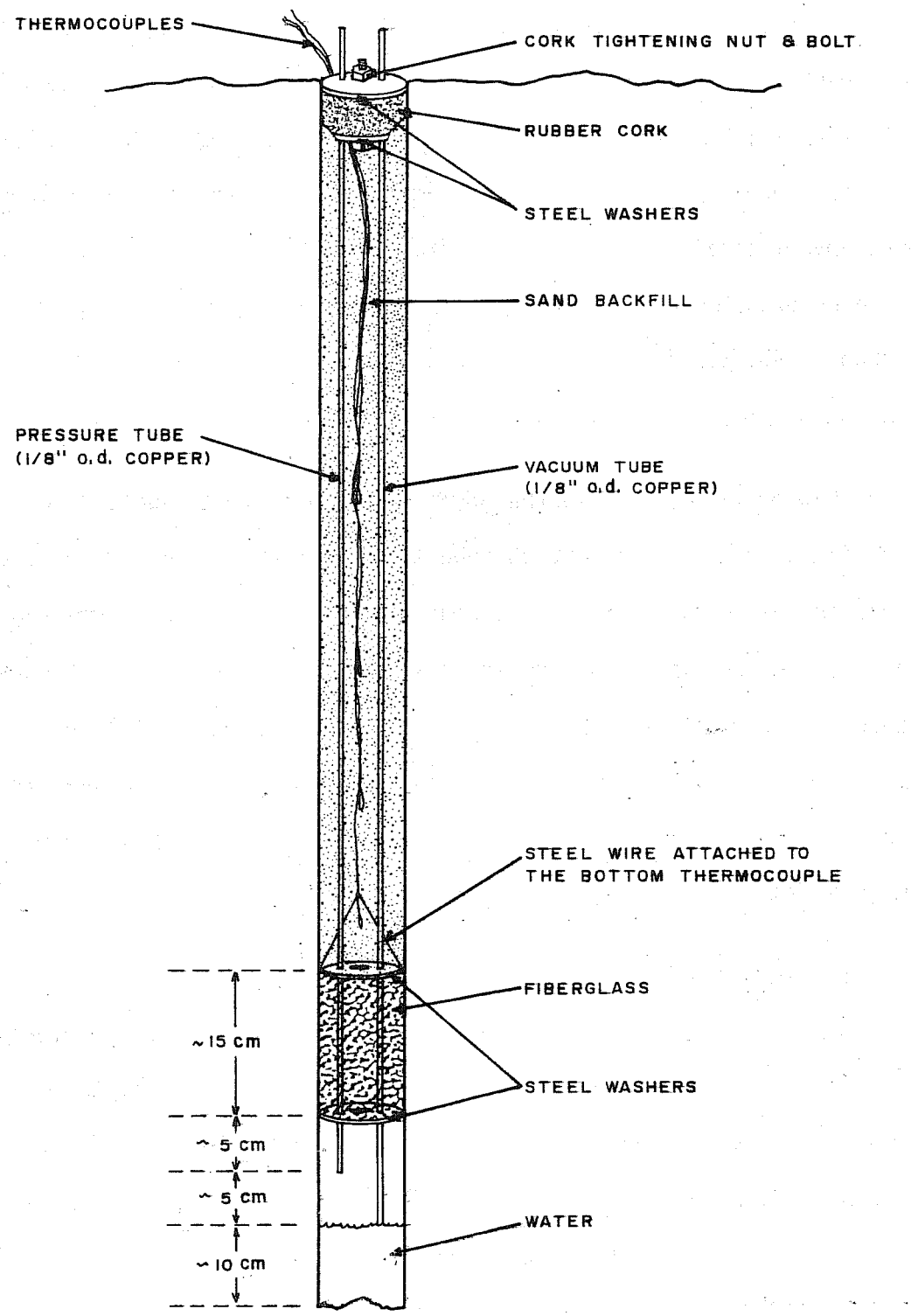

XBL 803-453

Fig. 44. Thermocouple hole dewatering tubes.

it up and out of the hole with the aid of the pressure assist tube. The fiberglass plug acts as a filter to trap the sand backfill.

At the top of each hole, a rubber plug was placed, which could be sealed effectively in the hole by tightening the upper 3/8-inch nut, forcing the two constraining washers closer together. This made it possible to pressurize all of the holes, and substantially improve the rate at which water could be removed.

Installation. The dewatering tubes and the thermocouples in each hole were installed simultaneously. First, the thermocouples were uncoiled and their ends positioned at the proper distances with respect to one another. They were then fastened together with high-temperature teflon tape. The bottom thermocouple was next secured to the fiberglass plug by means of a small steel wire. Finally, the entire assembly was pushed into the hole using the hollow-cored CSM cell-positioning rods. When the bottom thermocouple reached its proper location, the installing rods were removed, the holes were backfilled with sand, and the air-tight rubber plug was secured into the top of the hole. It was standard procedure to dewater each hole almost entirely just before the installation of the thermocouple assembly, usually leaving enough water in the bottom of the hole to test the system before backfilling with sand.

Removal. In case it becomes necessary to remove a thermocouple, the rubber cork should be removed, the hole blown completely free of sand above the fiberglass plug, and the assembly lifted out of the hole by pulling on

the copper tubes. There should be some resistive force due to the friction between the fiberglass and the walls of the hole.

6.3 IRAD Holes

The dewatering tubing in the IRAD gage holes is very simple (Fig. 45), consisting of a 1/4-inch o.d. copper vacuum tube pushed down below the gage locations (almost to the hole bottom) and a 1/8-inch o.d. pressure tube placed directly at the gage locations. A packing of fiberglass is lightly pushed on top of the gages to help limit heat transfer by natural convection. In the case of gages C3 and C4 (in holes U15 and U17) the holes were backfilled with sand; however, this procedure was discontinued because it made later removal of the gages extremely difficult. This was discovered when one of the gages in hole U17 had to be removed.

Installation. The IRAD gages were first installed according to the procedure described in section 4. Then the copper vacuum line was pushed down past the two gages, relying on trial and error to find sufficient space between them for insertion of the tube. Next, a shorter pressure line with a thermocouple attached to its end was lowered down past the first gage and allowed to rest on the second. Finally, a fiberglass packing was positioned just above the upper gage, and a rubber cork was fastened in the top of the hole just as in the thermocouple holes.

Removal. If there is any need to remove an IRAD gage, the cork should be removed, the holes blown free of fiberglass (and sand in holes U15 and U17), and the copper tubes pulled out.

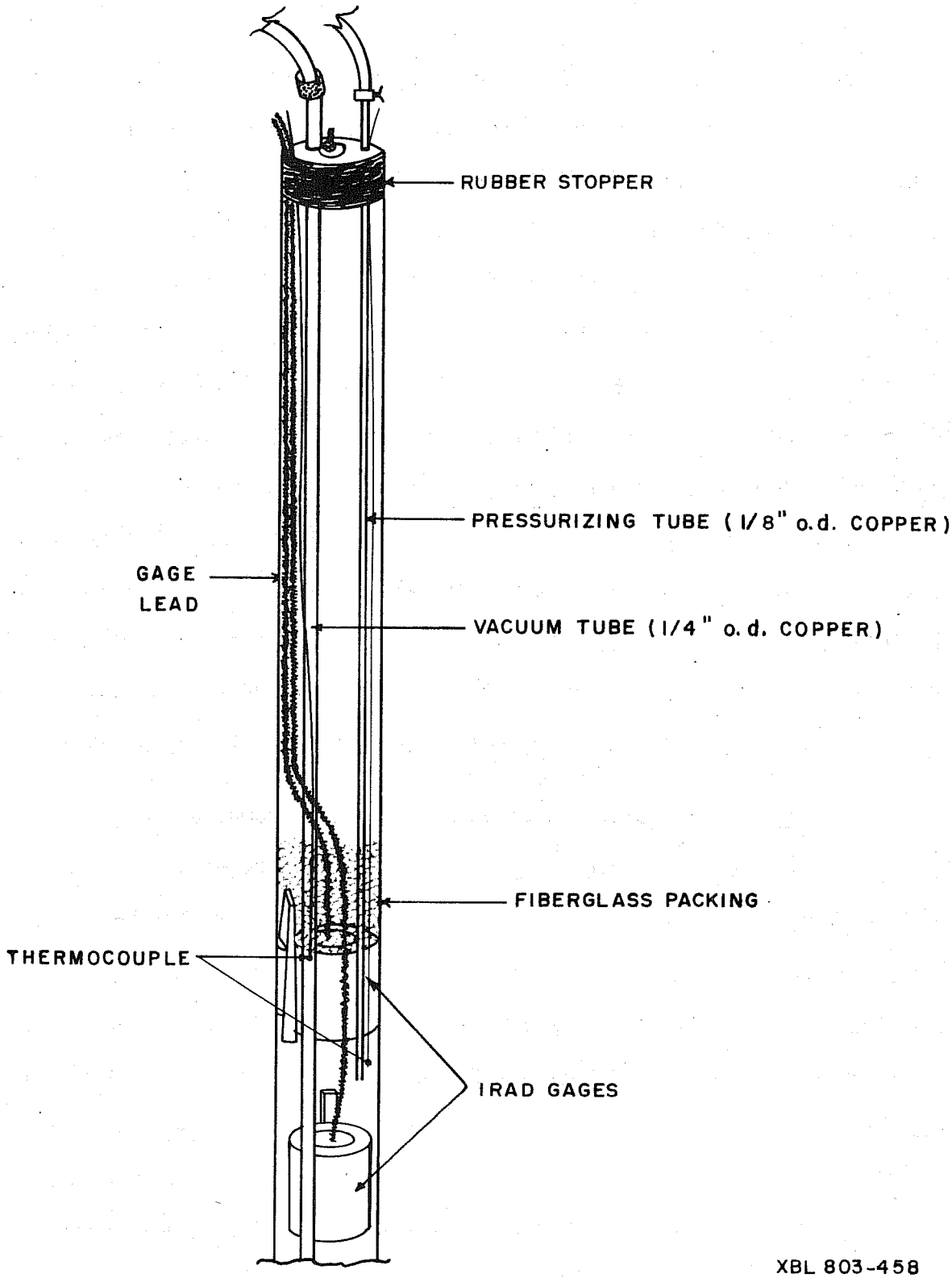

Fig. 45. IRAD gages and dewatering tubes.

6.4 USBM Holes

A schematic diagram of a USBM gage and its dewatering system are seen in Fig. 46. As in the IRAD and thermocouple holes, there is a short pressure tube and a longer vacuum line extending beyond the gage; however, in this case it was necessary to reduce the 1/8-inch o.d. vacuum line to a 1/16-inch o.d. tube in order to pass between the gage body and the borehole wall. USBM installations were completed around the H10 heater initially, leaving only a short section of the slender brass tubing extending below the gages. This extension of about 0.7 m did not prove sufficient, however, as certain gages were "submerged" in water when dewatering was not performed over a 2-day period, such as a weekend. So, for subsequent gage installations, a section of 1/8-inch o.d. copper tube several meters in length was added below the 1/16-inch o.d. brass tube, and extended down near the bottom of each hole. This procedure was followed with all USBMs around the H9 heater, and with gages U16, U13, U14, and U20, which had to be reinstalled around H10.

Installation. Installation of USBM gages was a comparatively slow task (about 3.5 gages per day), and at times required several attempts to achieve proper positioning in the holes. It was necessary that both the gages and their dewatering tubes be placed down the hole simultaneously. The first step was to preset the USBM gage components by adjusting the washers in the six sensory buttons according to the procedures described under USBM installation. Next, a vacuum line had to be fabricated for each gage consisting of a 1/8-inch o.d. copper tube measured to the depth of the particular gage, a section of 1/16-inch o.d. brass tubing long enough to bypass the gage body, and a further extension of 1/8-inch o.d. tubing to reach the bottom of the

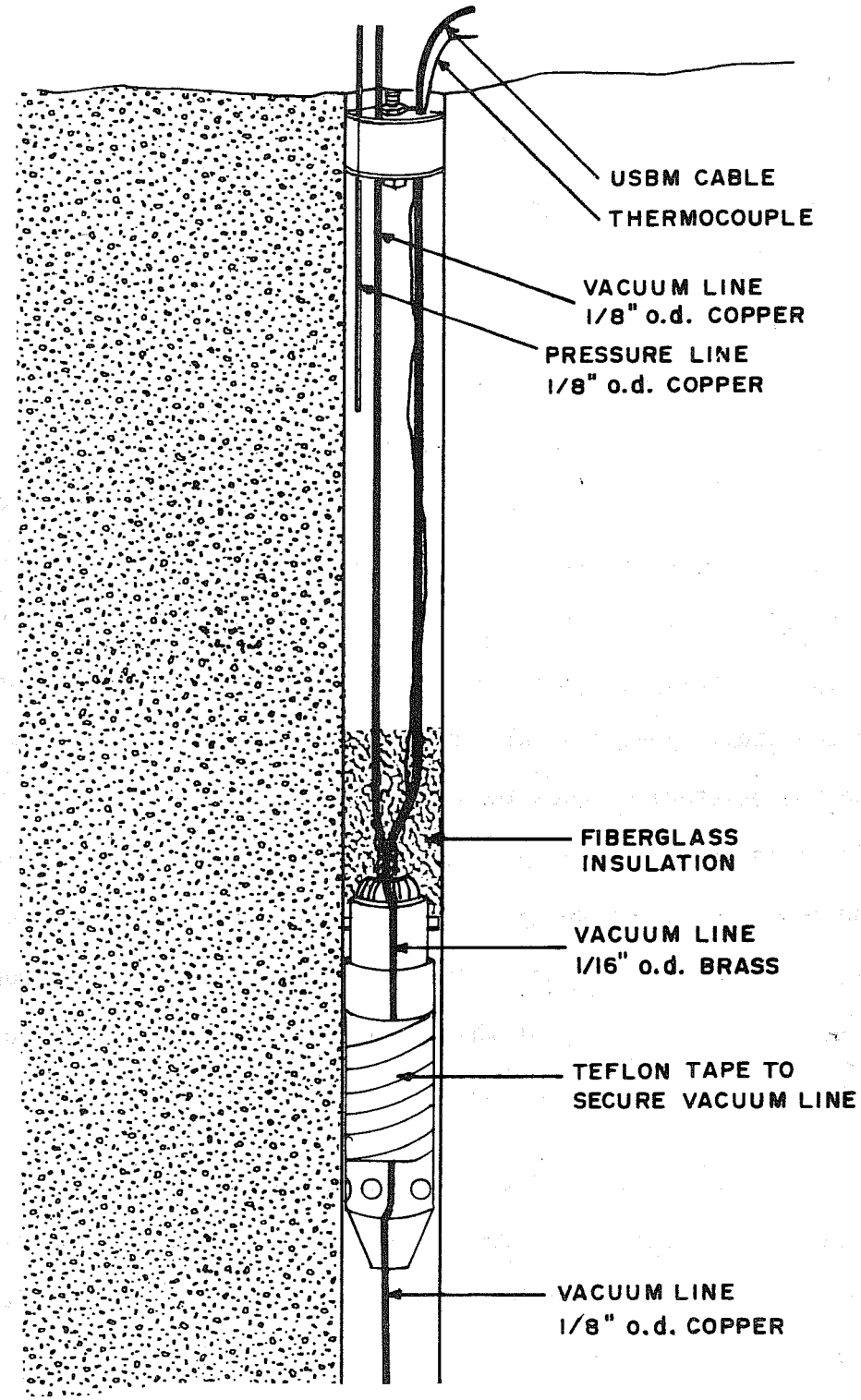

XBL 803-459

Fig. 46. USBM gage and dewatering tubes.

hole. The narrow section of this tube was then fastened along the gage with high-temperature teflon tape, and positioned with respect to the small pins on the rear of the gages so that the slot in the installing tool could be rotated on and off freely during installation. The vacuum tube was further secured to the USBM cable where it entered the gage, and at intervals about 1 m apart. After this was accomplished, the gage and its dewatering tube were ready to go down the hole. The hole was dewatered to a level just above where the lower end of the copper suction tube would finally be positioned. The gage was pushed down the hole slowly until the predetermined depth was reached, and the orientation was then set by rotating the gage until the upper handle on the installing tool pointed in the proper direction. The data logger reading was next checked against the calibration curves to verify an acceptable preset of all three channels and, finally, a pull was applied to the dewatering tubes to make certain that they were in fact, at the correct level in the hole. Only after this check list was completed was the installing tool disengaged and removed from the hole. A loose packing of fiberglass was next pushed down to the gage level and, lastly, a rubber stopper was placed in the top of the hole with a short section (about 1 m) of 1/8-inch o.d. copper tube extending through it as a pressure line.

Suggested Alternatives. The small, 1/16-inch o.d. brass tube that was implemented to bypass the USBM gage bodies caused several problems during both installation and subsequent dewatering. Its inside diameter was so small that it restricted and retarded the dewatering procedure greatly. One suggestion for the future is to mill a small groove in the gage body so that a larger-diameter tube could be used, or to substitute a thin-walled

tubing which could be flattened between the gage and the wall and still provide a large aperture for water to pass through.

Removal. The task of removing the USBM gages will not be an easy one. One must first remove the cork at the top of the hole, blow out the fiberglass packing completely, and carefully lower the installing rods down the hole. It will be necessary to "feel" very carefully with the rods to make sure the slot in the end aligns with the dewatering tube before the tool can be slipped down completely over the back of the gage and locked in place. Once this is accomplished, one can pull the gage up, keeping a steady tension on the cable and dewatering tube. Despite these precautions, the gage may still become abruptly jammed in the hole on the way up. Jamming was experienced two or three times when it became necessary to remove a gage during the installation proceedings. If jamming occurs, it is probably due to the small dewatering tube becoming twisted and wedged against some portion of the gage, usually the pistons. In such a case, one must work the gage up and down while trying to rotate it, using as much force as necessary. Eventually the gage will free itself.

6.5 Dewatering Control System

The dewatering of all instrumentation holes is centrally controlled by two pumping stations (see Fig. 47)--one on the H9 side, and one on the H10 side of the full-scale shed. A small Gast pump (Model MAA-108-HO) creates a vacuum which can be selectively connected to each hole by individual valves on a collective header system. Positive pressure is applied to several holes simultaneously through a pressure regulator which reduces the mine air pressure from 150 psi to about 40 psi. In both the H9 and H10 areas, there

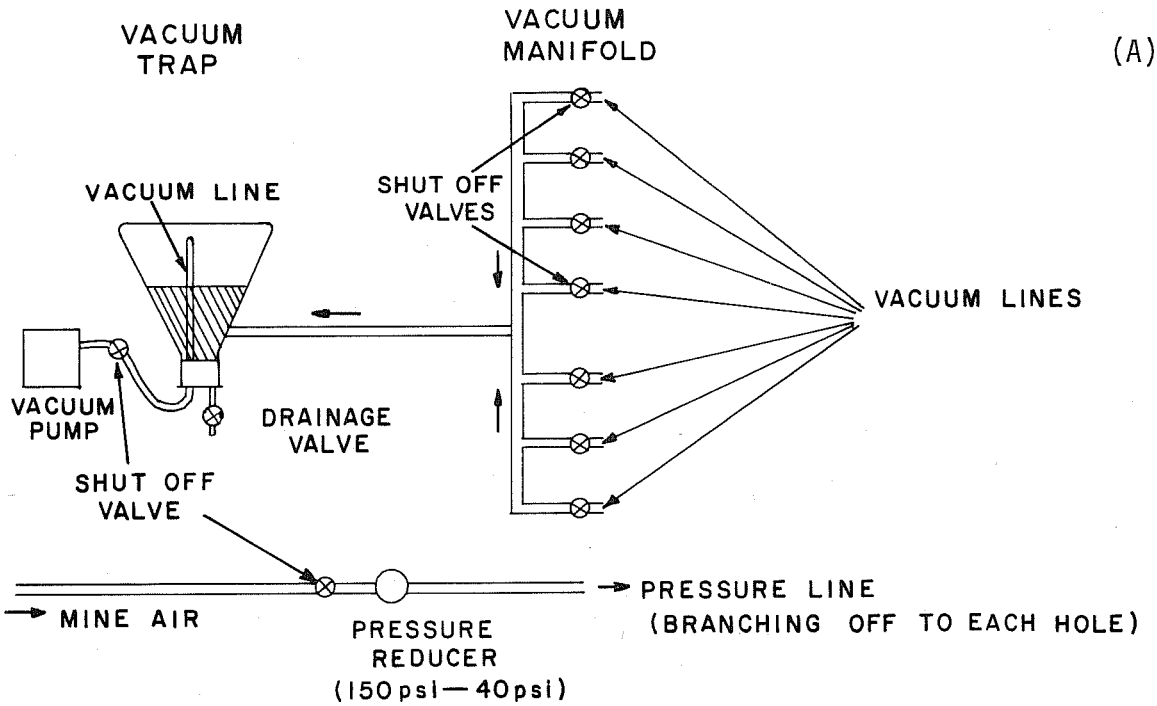

XBL 803-8854

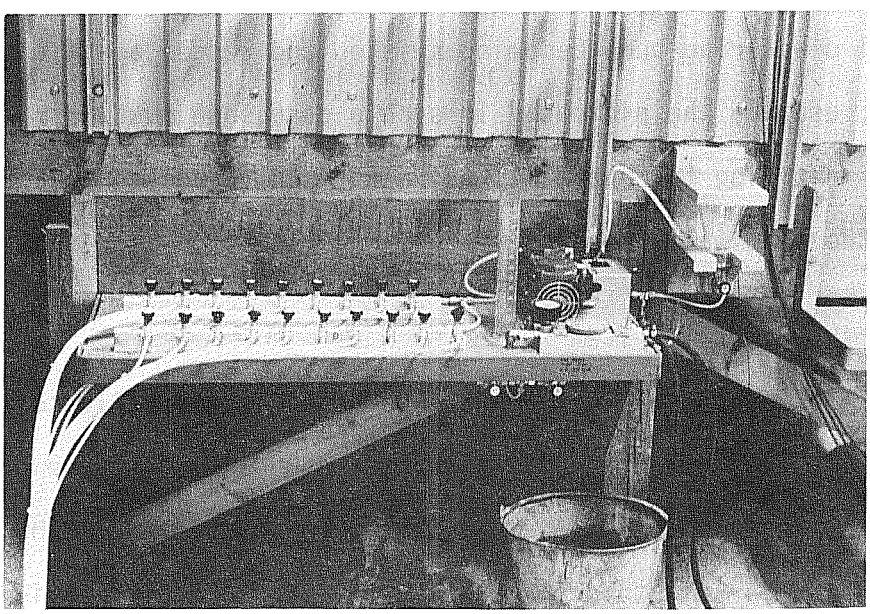

(B)

XBB 803-3399

Fig. 47. Dewatering control station. (A) Schematic of control station plumbing. Each valve, in sequence, is opened for 1 hour. (B) Photograph of the control station.

are two groups of holes that are pressurized separately when dewatering is in progress. These hole groupings are listed in Table 9.

Table 9. Pressurized hole groupings for dewatering.

H-9 area		H-10 area	
Pressure valve #1	Pressure valve #2	Pressure valve #1	Pressure valve #2
T-19, T-22, T-23,	T-20, T-21	T-16, T-17, T-18	U-2, U-5,
T-24, U-11, U-12,	U-19, C-5	C-11, C-2, U-1,	U-9
U-13, U-14, U-15,		U-3, U-4, U-6,	
U-16, U-17, U-18,		U-7, U-8, U-10,	
C-3, C-4.		T-13, T-14, T-15	

Those holes that were almost completely air tight were placed in one grouping (pressure valve #1), while those that leaked air through open fractures were placed in a second grouping (valve #2). Water from each hole is collected in a glass flask, which acts as a vacuum trap, then emptied into a graduated cylinder to record the rate of inflow into the holes.

7. WORK IN PROGRESS

The instrumentation for Stripa was evaluated and installed in a short time, considering that this was an experimental project to be operated in a hostile environment for 1-1/2 years. As would be expected in a measurement system of this magnitude, a number of operational problems have been encountered. The more significant so far have been:

a) Many of the USBM gages installed in the vertical boreholes have failed due to the infiltration of water and consequent corrosion of components. Very few gages have been lost in the horizontal boreholes where water drainage was provided.

b) Frictional sticking effects occur on many extensometers at low displacements and at low displacement rates. The lower limit of resolution has not yet been established for various rod lengths and geometries.

c) Heat-treated thermocouples sheathed in stainless steel have corroded (see section 5), necessitating their replacement around the H9 and H10 heater experiments.

d) Only a very limited amount of physical property data was available early in the experiment for input to some of the data reduction algorithms. Thermal expansion values and the rock mass moduli, for example, require further experimental work.

We are now trying to resolve these and lesser problems that have affected the data. Instrumentation and data acquisition routines are being checked and improved during the heater experiments:

- Failed components are inspected visually, modified, and replaced if practical. Down-time is recorded as an indicator of long-term reliability.
- Tests are underway to determine accuracy and resolution of instrumentation, and to better ascertain the parameters needed for data reduction. For example, the USBM gages are cycled to several temperatures in cylinders of rock and metal to determine the correct thermal expansion coefficients, and to examine temperature hysteresis effects.

- Using a mechanical load, an in-situ calibration with the instrumentation still in place after the heater experiments have terminated will provide a determination of calibration constants independent of thermal effects.
- Post-experiment calibration of individual thermocouples, stress gages, and extensometers will permit the assessment of long-term drift for the four basic types of sensors employed in the heater experiments.
- Additional physical and thermal property tests are being conducted to provide more accurate values for input into the data reduction algorithms.

The final reporting on the instrumentation performance will document long-term stability, final calibration results, and the measurement accuracy for each instrument type.

8. ACKNOWLEDGMENTS

N.G.W. Cook and T. Chan provided design guidance for the instrumentation layout. M. McEvoy contributed to the coordinate calculation and put the survey data into computer format.

Oak Ridge National Laboratories very helpfully supplied consultation and design drawings based on their experience with similar heater experiments.

Careful assistance with the calibration and installation by L. Bills, H. Selden, and particularly R. Lingle was critical to the timely operation of the experiment.

9. APPENDICES

APPENDIX A. Sensor Locations

Description of Coordinate Systems

The sensor locations were originally specified in a local coordinate system unique to each of the three experimental sites. The local coordinate system in the time-scale drift is inherently a rectangular system, while both coordinate systems in the full-scale drift are inherently cylindrical. As described by Kurfurst, Hugo-Persson, and Rudolph (1978), the local borehole coordinates were converted to mine coordinates for the drilling and surveying operations. Figure A-1 shows the spatial relationship among the three coordinate systems. Note that the mine coordinate system specifies z as positive downwards, while the local system specifies z as positive upwards. Table A-1 gives the mathematical relationships among the three systems and also gives the origin of each of the local systems in mine coordinates. The local systems are centered on H9, H10, and E1 as indicated in Figure A1. The z_0 coordinate given in Table A-1 refers to the midplane of the heaters. All distances and lengths are given in meters; angles are in degrees with 360° in a circle (the borehole survey by VIAK used 400 grads to a circle).

Borehole Locations

The borehole layout and survey coordinates of the top and bottom of the holes have been given by Kurfurst, Hugo-Persson, and Rudolph (1978). For ready reference, the Kurfurst borehole layout figures are shown here as Figs. A-2 through A-4. The only change from the figures presented by Kurfurst is the deletion of boreholes C9 and C13, which were not drilled although they were originally specified. Borehole nomenclature has remained as it was

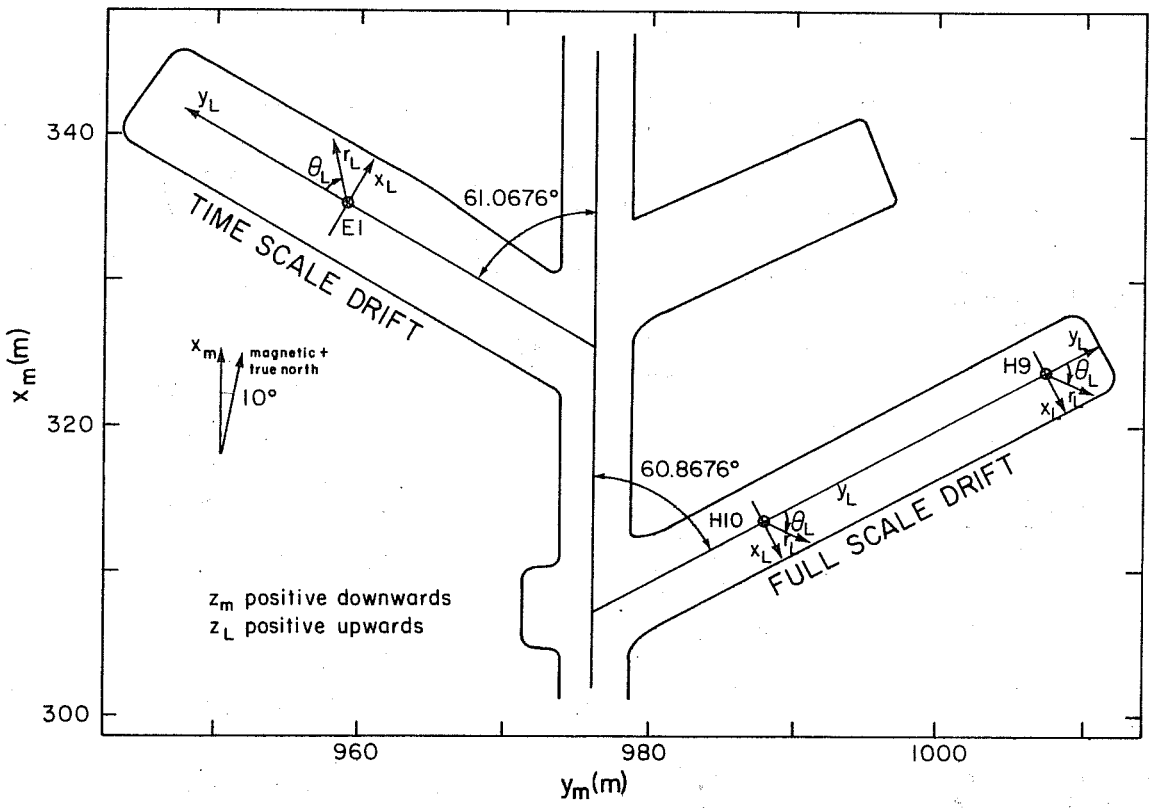

XBL 798-11422

Fig. A-1. Relationships among the mine coordinate system (x_m, y_m, z_m) and the three local rectangular (x_L, y_L, z_L) and local cylindrical (r_L, θ_L, z_L) systems. All rectangular systems are right handed; cylindrical systems are left handed.

Table A-1. Transform equations relating to the mine and experimental coordinate systems. Numerical values in meters and degrees.

	Full-scale drift		Time-scale drift
From mine coordinates to local cylindrical	$r_L = (X_m - X_o)/\cos(60.8676° + \theta_L)$		$r_L = (X_m - X_o)/\cos(\theta_L - 61.0676°)$
	$\theta_L = \tan^{-1}\frac{Y_m - Y_o}{X_m - X_o} - 60.8676°$		$\theta_L = \tan^{-1}\frac{Y_m - Y_o}{X_m - X_o} + 61.0676°$
	$Z_L = Z_o - Z_m$		$Z_L = Z_o - Z_m$
From local cylindrical to mine coordinates	$X_m = r_L \cos\alpha + X_o$		$X_m = r_L \cos\alpha + X_o$
	$Y_m = r_L \sin\alpha + Y_o$		$Y_m = r_L \sin\alpha + Y_o$
	$Z_m = Z_o - Z_L$		$Z_m = Z_o - Z_L$
	$\alpha = 60.8676° + \theta_L$		$\alpha = \theta_L - 61.0676°$
From local rectangular to mine coordinates	$X_m = X_o + X_L \frac{\cos\alpha}{\sin\theta_L}$		$X_m = X_o + X_L \frac{\cos\alpha}{\sin\theta_L}$
	$Y_m = Y_o + Y_L \frac{\sin\alpha}{\cos\theta_L}$		$Y_m = Y_o + Y_L \frac{\sin\alpha}{\cos\theta_L}$
	$Z_m = Z_o - Z_L$		$Z_m = Z_o - Z_L$
	H9	H10	
Center of local coordinate systems (in mine coordinates)	$X_o = 323.412$	$X_o = 312.715$	$X_o = 334.714$
	$Y_o = 1007.251$	$Y_o = 988.025$	$Y_o = 959.083$
	$Z_o = 343.0$	$Z_o = 343.0$	$Z_o = 347.0$

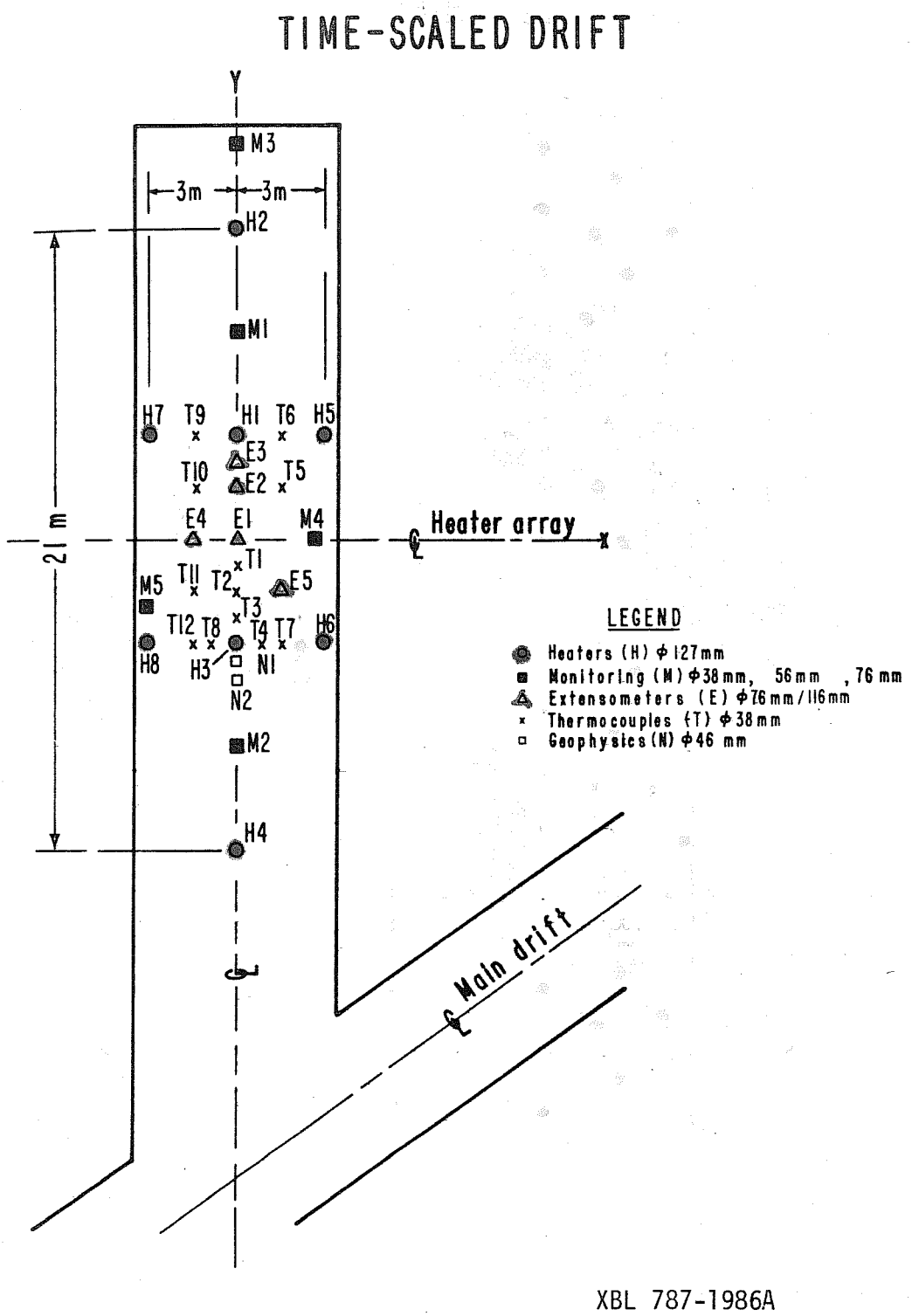

Fig. A-2. Borehole layout in the time-scaled drift.

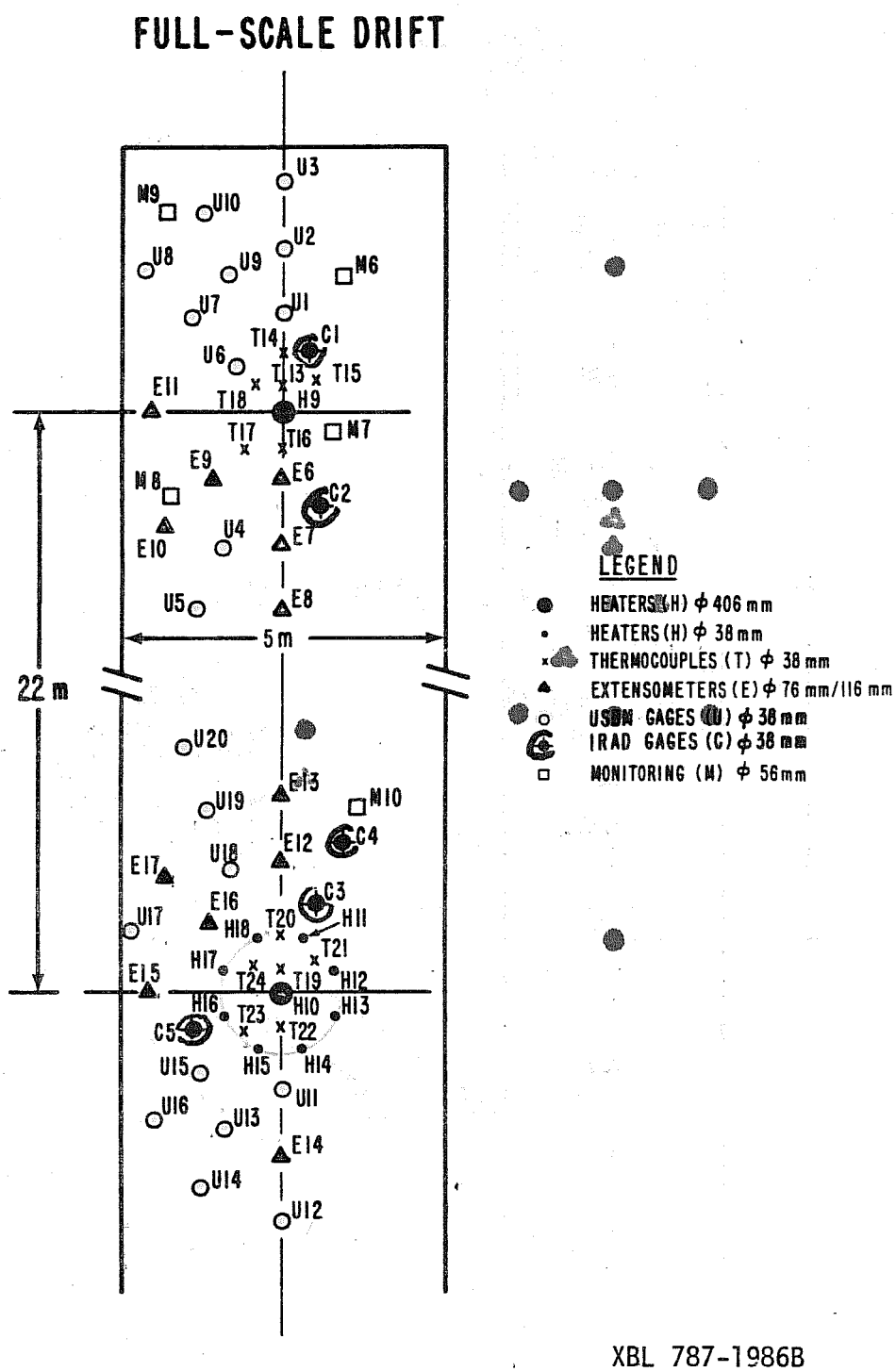

Fig. A-3. Borehole layout in the full-scale drift.

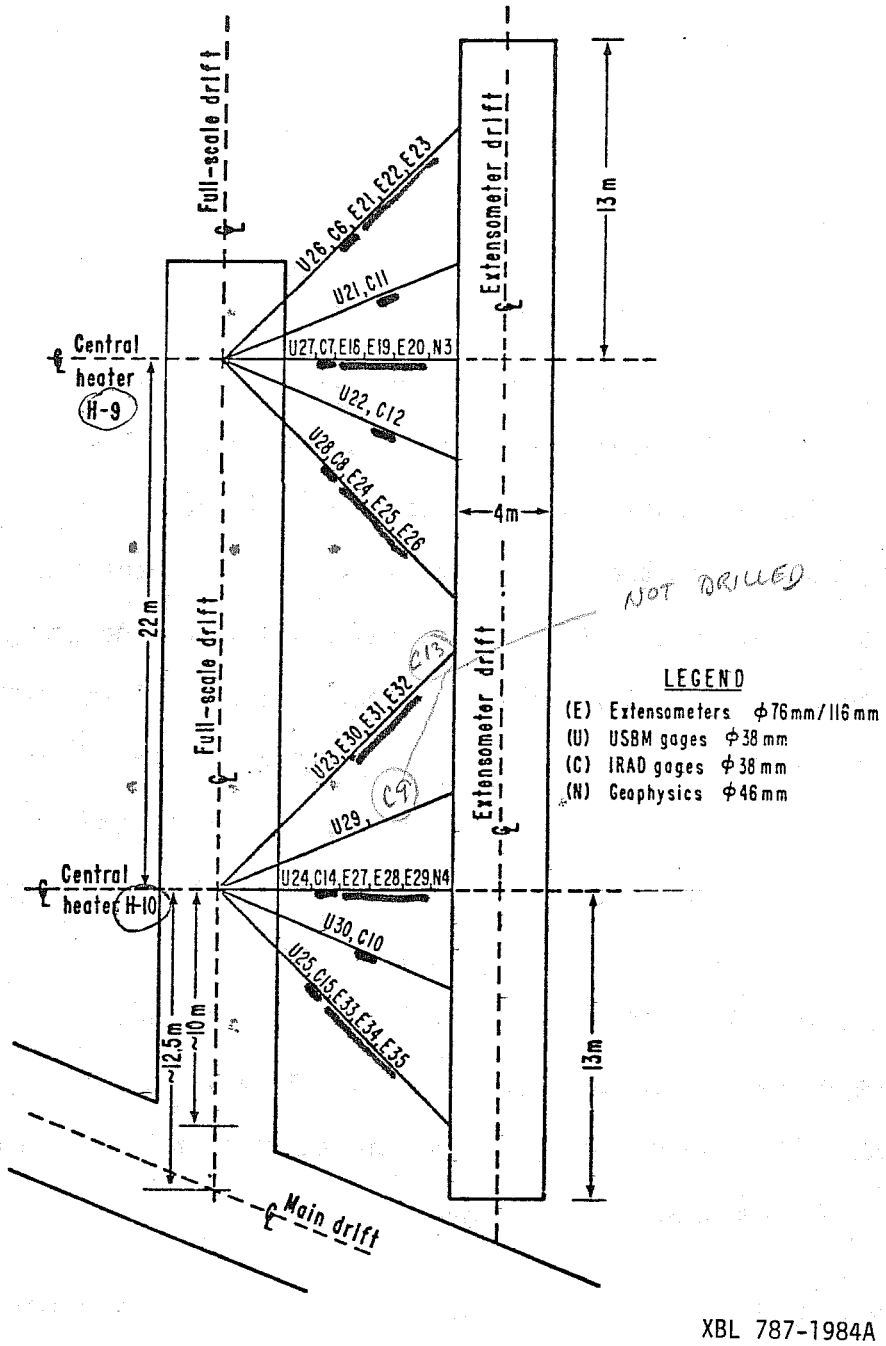

XBL 787-1984A

Fig. A-4. Borehole layout in the extensometer drift.

initially specified even though some gages were installed in different holes than originally intended.

Description of Sensor Locations

Table A-2 is a list of all the sensors (one or more sensors make up an instrument) and their locations for the three heater experiments at Stripa. The mine coordinates for each sensor are determined from its depth in the hole and the mine coordinates of the top and bottom of the hole. The line through the top and bottom of the hole is calculated in the mine coordinate system; then, using the sensor's depth in the hole, the mine coordinates of the sensor are calculated. Using the calculated mine coordinates and the transforms given in Table A-1, the local cylindrical and rectangular coordinates are calculated. The error in a sensor's coordinates is due to the error in the measurement of the sensor's depth, because the borehole-surveying accuracy is greater than the accuracy of sensor positioning. This error varies for the different sensors as follows:

Thermocouples ∓ 1 cm, depth is to center of thermocouple

Extensometers ∓ 2.5 cm, depth is to center of anchor point

USBM gage ∓ 1 cm, depth is to the button location in the instrument

IRAD gage ∓ 1 cm, depth is to midpoint between IRAD sensors.

In Table A-2 all coordinates are given to the nearest centimeter, except for the horizontal coordinates of the time-scale heater thermocouples. These are given to the nearest tenth of a meter because the orientation of the heater was not recorded at installation. The error of these thermocouple locations is at most the diameter of the heater, 9 cm.

A few of the sensor numbers allocated to thermocouples in Table A-2 do not get their data from an actual sensor in the specified location, but instead get it from a thermocouple in another location where the temperature is judged to be equivalent. Temperatures obtained in this fashion are used to correct for the thermal expansion of the extensometer rods. In such cases, the sensor label is assigned a prefix "RF," designating it as a referenced sensor. For example, on the first page of Table A-2, the temperature for sensor number 130 in hole E6 is actually measured by sensor number 128, which is located at the collar of E7. This was done because the air temperature in the drift is the same at all collar locations, and needed to be measured at only one location. Similarly, sensor 572 measures the air temperature in the extensometer drift at the collar of hole E31, and the data are used for all the horizontal extensometer corrections, as shown by the entry "RF572" in the sensor label column.

The hole identification (first column in Table A-2) corresponds with the hole labeling used in Figs. A-2 through A-4. The sensor label (fourth column) in most cases is the same as the hole identification, with the additional refinement of a prefix or suffix to further identify the sensor type or position in a hole. However, in a few cases the hole identification differs from the sensor label, because the gages were installed in the wrong hole. The gages which were switched are:

Gage (sensor label)	Hole Identifier
U6	C2
C2	U6
U15	C3
C3	U15
U17	C4
C4	U17

The sensor number given in the third column of Table A-1 identifies each sensor uniquely in the sensor parameter file, in the stored data, and in the subsequent appendices of this report.

Table A-2. List of all sensors and their locations for the three heater experiments at Stripa.

SENSOR LOCATIONS FOR EXPERIMENT 1, FULL SCALE HEATER H9

HOLE ID	SENSOR TYPE	SENSOR NUMBER	SENSOR LABEL	CYLINDRICAL COORDINATES RHO	THETA	Z	LOCAL X	RECTANGULAR Y	Z	MINE X	RECTANGULAR Y	Z	DEPTH	HOLE LENGTH
C1	IRAD GAGE	271	C1	.99	22.1	.85	.37	.92	.85	323.53	1008.24	342.15	3.42	7.12
C1	IRAD GAGE	272	C1	.99	22.1	.85	.37	.92	.85	323.53	1008.24	342.15	3.42	7.12
C1	THERMOCOUPLE	77	C1	.99	22.1	.85	.37	.92	.85	323.53	1008.24	342.15	3.42	7.12
C2	USBM	216	U6	1.48	157.6	-.65	.57	-1.37	-.65	322.25	1006.33	343.65	4.93	7.15
C2	USBM	217	U6	1.48	157.6	-.65	.57	-1.37	-.65	322.25	1006.33	343.65	4.93	7.15
C2	USBM	218	U6	1.48	157.6	-.65	.57	-1.37	-.65	322.25	1006.33	343.65	4.93	7.15
C2	THERMOCOUPLE	7	U6	1.48	157.6	-.65	.57	-1.37	-.65	322.25	1006.33	343.65	4.93	7.15
C6	IRAD GAGE	275	C6	2.50	47.5	.65	1.84	1.69	.65	322.62	1009.62	342.35	11.64	13.18
C6	IRAD GAGE	276	C6	2.50	47.5	.65	1.84	1.69	.65	322.62	1009.62	342.35	11.64	13.18
C6	THERMOCOUPLE	79	C6	2.50	47.5	.65	1.84	1.69	.65	322.62	1009.62	342.35	11.64	13.18
C7	IRAD GAGE	277	C7	2.00	90.1	.66	2.00	-.00	.66	321.66	1008.22	342.34	8.08	9.09
C7	IRAD GAGE	278	C7	2.00	90.1	.66	2.00	-.00	.66	321.66	1008.22	342.34	8.08	9.09
C7	THERMOCOUPLE	80	C7	2.00	90.1	.66	2.00	-.00	.66	321.66	1008.22	342.34	8.08	9.09
C8	IRAD GAGE	279	C8	3.01	134.8	.70	2.13	-2.12	.70	320.52	1006.44	342.30	11.20	13.16
C8	IRAD GAGE	280	C8	3.01	134.8	.70	2.13	-2.12	.70	320.52	1006.44	342.30	11.20	13.16
C8	THERMOCOUPLE	81	C8	3.01	134.8	.70	2.13	-2.12	.70	320.52	1006.44	342.30	11.20	13.16
C11	IRAD GAGE	281	C11	3.99	67.8	-.85	3.69	1.51	-.85	320.92	1010.37	343.85	6.50	9.49
C11	IRAD GAGE	282	C11	3.99	67.8	-.85	3.69	1.51	-.85	320.92	1010.37	343.85	6.50	9.49
C11	THERMOCOUPLE	82	C11	3.99	67.8	-.85	3.69	1.51	-.85	320.92	1010.37	343.85	6.50	9.49
C12	IRAD GAGE	283	C12	3.48	112.7	-.87	3.21	-1.34	-.87	319.95	1007.64	343.87	7.53	8.02
C12	IRAD GAGE	284	C12	3.48	112.7	-.87	3.21	-1.34	-.87	319.95	1007.64	343.87	7.53	8.02
C12	THERMOCOUPLE	83	C12	3.48	112.7	-.87	3.21	-1.34	-.87	319.95	1007.64	343.87	7.53	8.02
E6	EXTENSOMETER	291	E6A	1.00	180.8	2.23	-.01	-1.00	2.23	322.94	1006.37	340.77	1.97	12.95
E6	EXTENSOMETER	292	E6B	1.00	180.9	-.02	-.02	-1.00	-.02	322.94	1006.37	343.02	4.22	12.95
E6	EXTENSOMETER	293	E6C	1.00	180.9	-2.27	-.02	-1.00	-2.27	322.94	1006.37	345.27	6.47	12.95
E6	EXTENSOMETER	294	E6D	1.00	181.1	-7.32	-.02	-1.00	-7.32	322.94	1006.37	350.33	11.53	12.95
E6	THERMOCOUPLE	17	E6A	1.00	180.8	2.43	-.01	-1.00	2.43	322.94	1006.37	340.58	1.78	12.95
E6	THERMOCOUPLE	18	E6B	1.00	180.9	-.82	-.02	-1.00	-.82	322.94	1006.37	343.83	5.03	12.95
E6	THERMOCOUPLE	19	E6C	1.00	180.9	-2.07	-.02	-1.00	-2.07	322.94	1006.37	345.08	6.28	12.95
E6	THERMOCOUPLE	20	E6D	1.00	181.1	-7.32	-.02	-1.00	-7.32	322.94	1006.37	350.33	11.53	12.95
E6	THERMOCOUPLE	122	TE6F	1.00	180.9	.18	-.02	-1.00	.18	322.94	1006.37	342.83	4.03	12.95
E6	THERMOCOUPLE	123	TE6G	1.00	181.0	-4.70	-.02	-1.00	-4.70	322.94	1006.37	347.71	8.91	12.95
E6	THERMOCOUPLE	130	RF128	1.00	180.8	4.20	-.01	-1.00	4.20	322.94	1006.37	338.80	0.	12.95
E7	EXTENSOMETER	295	E7A	2.00	180.4	2.22	-.01	-2.00	2.22	322.45	1005.50	340.78	2.11	12.69
E7	EXTENSOMETER	296	E7B	2.00	180.4	-.03	-.01	-2.00	-.03	322.45	1005.50	343.03	4.36	12.69
E7	EXTENSOMETER	297	E7C	2.00	180.4	-2.28	-.01	-2.00	-2.28	322.45	1005.49	345.28	6.61	12.69
E7	EXTENSOMETER	298	E7D	2.01	180.3	-7.50	-.01	-2.01	-7.50	322.44	1005.49	350.50	11.83	12.69
E7	THERMOCOUPLE	21	E7A	2.00	180.4	-1.02	-.01	-2.00	-1.02	322.45	1005.50	344.02	5.35	12.69
E7	THERMOCOUPLE	22	E7B	2.00	180.4	-2.25	-.01	-2.00	-2.25	322.45	1005.49	345.25	6.58	12.69
E7	THERMOCOUPLE	23	E7C	2.01	180.4	-4.88	-.01	-2.01	-4.88	322.45	1005.49	347.88	9.21	12.69
E7	THERMOCOUPLE	24	E7D	2.01	180.3	-7.50	-.01	-2.01	-7.50	322.44	1005.49	350.50	11.83	12.69
E7	THERMOCOUPLE	124	TE7F	2.00	180.4	2.26	-.01	-2.00	2.26	322.45	1005.50	340.75	2.08	12.69
E7	THERMOCOUPLE	125	TE7G	2.00	180.4	0.01	-.01	-2.00	0.01	322.45	1005.50	343.00	4.33	12.69
E7	THERMOCOUPLE	128	E7	2.00	180.4	4.33	-.01	-2.00	4.33	322.45	1005.50	338.67	0.	12.69
E8	EXTENSOMETER	299	E8A	2.99	180.2	2.25	-.01	-2.99	2.25	321.97	1004.63	340.75	2.07	12.67
E8	EXTENSOMETER	300	E8B	2.99	180.3	.00	-.01	-2.99	.00	321.97	1004.63	343.00	4.32	12.67
E8	EXTENSOMETER	301	E8C	2.99	180.3	-2.26	-.01	-2.99	-2.26	321.97	1004.63	345.26	6.58	12.67
E8	EXTENSOMETER	302	E8D	2.98	180.3	-7.48	-.02	-2.98	-7.48	321.98	1004.64	350.48	11.80	12.67
E8	THERMOCOUPLE	25	E8A	2.99	180.2	2.27	-.01	-2.99	2.27	321.97	1004.63	340.73	2.05	12.67
E8	THERMOCOUPLE	26	E8B	2.99	180.3	.02	-.01	-2.99	.02	321.97	1004.63	342.98	4.30	12.67
E8	THERMOCOUPLE	27	E8C	2.99	180.3	-2.23	-.01	-2.99	-2.23	321.97	1004.63	345.23	6.55	12.67
E8	THERMOCOUPLE	28	E8D	2.98	180.3	-7.48	-.02	-2.98	-7.48	321.98	1004.64	350.48	11.80	12.67
E8	THERMOCOUPLE	132	RF128	3.00	180.2	4.32	-.01	-3.00	4.32	321.96	1004.63	338.68	0.	12.67
E9	EXTENSOMETER	303	E9A	1.51	225.3	2.23	-1.07	-1.06	2.23	323.83	1005.80	340.77	2.01	12.58

SENSOR LOCATIONS FOR EXPERIMENT 1, FULL SCALE HEATER H9

HOLE ID	SENSOR TYPE	SENSOR NUMBER	SENSOR LABEL	CYLINDRICAL COORDINATES RHO	THETA	Z	LOCAL RECTANGULAR X	Y	Z	MINE RECTANGULAR X	Y	Z	DEPTH	HOLE LENGTH
E9	EXTENSOMETER	304	E9B	1.50	225.2	-.02	-1.07	-1.06	-.02	323.83	1005.81	343.02	4.26	12.58
E9	EXTENSOMETER	305	E9C	1.50	225.2	-2.27	-1.07	-1.06	-2.27	323.83	1005.81	345.27	6.51	12.58
E9	EXTENSOMETER	306	E9D	1.50	225.0	-7.42	-1.06	-1.06	-7.42	323.82	1005.81	350.42	11.66	12.58
E9	THERMOCOUPLE	29	E9A	1.51	225.3	2.39	-1.07	-1.06	2.39	323.83	1005.80	340.61	1.85	12.58
E9	THERMOCOUPLE	30	E9B	1.50	225.2	.14	-1.07	-1.06	.14	323.83	1005.81	342.86	4.10	12.58
E9	THERMOCOUPLE	31	E9C	1.50	225.2	-.86	-1.07	-1.06	-.86	323.83	1005.81	343.86	5.10	12.58
E9	THERMOCOUPLE	32	E9D	1.50	225.2	-2.11	-1.07	-1.06	-2.11	323.83	1005.81	345.11	6.35	12.58
E9	THERMOCOUPLE	133	RF128	1.51	225.4	4.24	-1.07	-1.06	4.24	323.83	1005.80	338.76	0.	12.58
E9	THERMOCOUPLE	160	RF 24	1.50	225.0	-7.42	-1.06	-1.06	-7.42	323.82	1005.81	350.42	11.66	12.58
E10	EXTENSOMETER	307	E10A	2.51	225.1	2.23	-1.78	-1.77	2.23	324.10	1004.84	340.77	2.03	12.63
E10	EXTENSOMETER	308	E10B	2.51	225.0	-.02	-1.78	-1.77	-.02	324.10	1004.84	343.02	4.28	12.63
E10	EXTENSOMETER	309	E10C	2.51	225.0	-2.21	-1.78	-1.78	-2.21	324.10	1004.83	345.21	6.47	12.63
E10	EXTENSOMETER	310	E10D	2.52	224.9	-7.49	-1.78	-1.78	-7.49	324.10	1004.83	350.49	11.75	12.63
E10	THERMOCOUPLE	33	E10A	2.51	225.1	2.26	-1.78	-1.77	2.26	324.10	1004.84	340.74	2.00	12.63
E10	THERMOCOUPLE	34	E10B	2.51	225.0	.01	-1.78	-1.77	.01	324.10	1004.84	342.99	4.25	12.63
E10	THERMOCOUPLE	35	E10C	2.51	225.0	-.99	-1.78	-1.77	-.99	324.10	1004.84	343.99	5.25	12.63
E10	THERMOCOUPLE	36	E10D	2.51	225.0	-2.24	-1.78	-1.78	-2.24	324.10	1004.83	345.24	6.50	12.63
E10	THERMOCOUPLE	134	RF128	2.51	225.1	4.26	-1.78	-1.77	4.26	324.10	1004.84	338.74	0.	12.63
E10	THERMOCOUPLE	161	RF 24	2.52	224.9	-7.49	-1.78	-1.78	-7.49	324.10	1004.83	350.49	11.75	12.63
E11	EXTENSOMETER	311	E11A	2.01	270.1	2.23	-2.01	.00	2.23	325.17	1006.27	340.77	2.00	12.54
E11	EXTENSOMETER	312	E11B	2.01	270.1	-.03	-2.01	.00	-.03	325.17	1006.28	343.03	4.26	12.54
E11	EXTENSOMETER	313	E11C	2.01	270.1	-2.28	-2.01	.00	-2.28	325.17	1006.28	345.28	6.51	12.54
E11	EXTENSOMETER	314	E11D	2.00	270.1	-7.44	-2.00	.00	-7.44	325.17	1006.28	350.44	11.67	12.54
E11	THERMOCOUPLE	37	E11A	2.01	270.1	2.31	-2.01	.00	2.31	325.17	1006.27	340.69	1.92	12.54
E11	THERMOCOUPLE	38	E11B	2.01	270.1	.06	-2.01	.00	.06	325.17	1006.28	342.94	4.17	12.54
E11	THERMOCOUPLE	39	E11C	2.01	270.1	-2.19	-2.01	.00	-2.19	325.17	1006.28	345.19	6.42	12.54
E11	THERMOCOUPLE	40	E11D	2.00	270.1	-7.44	-2.00	.00	-7.44	325.17	1006.28	350.44	11.67	12.54
E11	THERMOCOUPLE	135	RF128	2.01	270.1	4.23	-2.01	.00	4.23	325.17	1006.27	338.77	0.	12.54
E18	EXTENSOMETER	315	HE18D	7.06	90.0	1.40	7.06	.00	1.40	317.25	1010.69	341.60	3.00	9.03
E18	EXTENSOMETER	316	HE18A	1.63	89.7	1.96	1.63	.01	1.96	321.99	1008.05	341.04	8.46	9.03
E18	EXTENSOMETER	317	HE18B	3.05	89.9	1.81	3.05	.01	1.81	320.75	1008.74	341.19	7.03	9.03
E18	EXTENSOMETER	318	HE18C	4.30	89.9	1.68	4.30	.01	1.68	319.66	1009.35	341.32	5.77	9.03
E18	THERMOCOUPLE	41	HE18D	8.10	90.0	1.30	8.10	.00	1.30	316.34	1011.19	341.70	1.96	9.03
E18	THERMOCOUPLE	42	HE18C	4.36	89.9	1.68	4.36	.01	1.68	319.60	1009.38	341.32	5.71	9.03
E18	THERMOCOUPLE	43	HE18B	3.12	89.9	1.80	3.12	.01	1.80	320.69	1008.78	341.20	6.96	9.03
E18	THERMOCOUPLE	44	HE18A	1.63	89.7	1.96	1.63	.01	1.96	321.99	1008.05	341.04	8.46	9.03
E18	THERMOCOUPLE	142	RF572	10.04	90.0	1.10	10.04	.00	1.10	314.64	1012.14	341.90	0.	9.03
E19	EXTENSOMETER	319	HE19C	3.49	89.9	-.06	3.49	.01	-.06	320.36	1008.96	343.06	6.42	8.90
E19	EXTENSOMETER	320	HE19B	2.53	89.8	-.01	2.53	.01	-.01	321.21	1008.49	343.01	7.39	8.90
E19	EXTENSOMETER	321	HE19A	1.23	89.5	.05	1.23	.01	.05	322.35	1007.86	342.95	8.69	8.90
E19	EXTENSOMETER	322	HE19D	5.01	89.9	-.14	5.01	.01	-.14	319.04	1009.70	343.14	4.90	8.90
E19	THERMOCOUPLE	45	HE19D	4.97	89.9	-.14	4.97	.01	-.14	319.07	1009.68	343.14	4.94	8.90
E19	THERMOCOUPLE	46	HE19C	3.47	89.9	-.06	3.47	.01	-.06	320.38	1008.95	343.06	6.44	8.90
E19	THERMOCOUPLE	47	HE19B	2.48	89.8	-.01	2.48	.01	-.01	321.25	1008.46	343.01	7.44	8.90
E19	THERMOCOUPLE	48	HE19A	1.23	89.5	.05	1.23	.01	.05	322.35	1007.86	342.95	8.69	8.90
E19	THERMOCOUPLE	143	RF572	9.91	90.0	-.39	9.91	.00	-.39	314.76	1012.07	343.39	0.	8.90
E20	EXTENSOMETER	323	HE20D	5.97	89.9	-2.04	5.97	.01	-2.04	318.20	1010.17	345.04	3.72	11.12
E20	EXTENSOMETER	324	HE20C	2.01	89.5	-1.93	2.01	.02	-1.93	321.66	1008.25	344.93	7.68	11.12
E20	EXTENSOMETER	325	HE20B	1.01	88.9	-1.90	1.01	.02	-1.90	322.54	1007.76	344.90	8.68	11.12
E20	EXTENSOMETER	326	HE20A	.97	271.4	-1.84	-.97	.02	-1.84	324.27	1006.80	344.84	10.66	11.12
E20	THERMOCOUPLE	49	HE20D	6.03	89.9	-2.04	6.03	.01	-2.04	318.15	1010.20	345.04	3.66	11.12
E20	THERMOCOUPLE	50	HE20C	2.03	89.5	-1.93	2.03	.02	-1.93	321.65	1008.25	344.93	7.66	11.12
E20	THERMOCOUPLE	51	HE20B	1.03	88.9	-1.90	1.03	.02	-1.90	322.52	1007.77	344.90	8.66	11.12
E20	THERMOCOUPLE	52	HE20A	.04	271.3	-1.87	.03	.02	-1.87	323.39	1007.29	344.87	9.66	11.12

SENSOR LOCATIONS FOR EXPERIMENT 1, FULL SCALE HEATER H9

HOLE ID	SENSOR TYPE	SENSOR NUMBER	SENSOR LABEL	CYLINDRICAL COORDINATES RHO	THETA	Z	LOCAL RECTANGULAR X	Y	Z	MINE RECTANGULAR X	Y	Z	DEPTH	HOLE LENGTH
E20	THERMOCOUPLE	144	RF572	9.69	90.0	-2.14	9.69	.00	-2.14	314.95	1011.97	345.14	0.	11.12
E21	EXTENSOMETER	327	HE21D	6.96	44.9	1.63	4.91	4.93	1.63	321.52	1013.95	341.37	7.29	13.28
E21	EXTENSOMETER	328	HE21C	4.24	44.8	1.83	2.98	3.01	1.83	322.27	1011.33	341.17	10.02	13.28
E21	EXTENSOMETER	329	HE21B	3.00	44.7	1.92	2.11	2.13	1.92	322.61	1010.14	341.08	11.26	13.28
E21	EXTENSOMETER	330	HE21A	1.49	44.3	2.03	1.04	1.07	2.03	323.02	1008.69	340.97	12.77	13.28
E21	THERMOCOUPLE	53	HE21D	7.98	44.9	1.55	5.63	5.65	1.55	321.24	1014.93	341.45	6.27	13.28
E21	THERMOCOUPLE	54	HE21C	4.24	44.8	1.83	2.98	3.01	1.83	322.27	1011.33	341.17	10.02	13.28
E21	THERMOCOUPLE	55	HE21B	2.99	44.7	1.92	2.10	2.13	1.92	322.61	1010.13	341.08	11.27	13.28
E21	THERMOCOUPLE	56	HE21A	1.49	44.3	2.03	1.04	1.07	2.03	323.02	1008.69	340.97	12.77	13.28
E21	THERMOCOUPLE	145	RF572	14.23	45.0	1.09	10.06	10.07	1.09	319.53	1020.94	341.91	0.	13.28
E22	EXTENSOMETER	331	HE22D	5.03	44.8	-.06	3.54	3.57	-.06	322.05	1012.09	343.06	8.99	13.01
E22	EXTENSOMETER	332	HE22C	3.51	44.7	-.00	2.47	2.49	-.00	322.47	1010.63	343.00	10.51	13.01
E22	EXTENSOMETER	333	HE22B	2.52	44.5	.03	1.77	1.80	.03	322.74	1009.68	342.97	11.50	13.01
E22	EXTENSOMETER	334	HE22A	1.29	44.0	.08	.90	.93	.08	323.08	1008.50	342.92	12.73	13.01
E22	THERMOCOUPLE	57	HE22D	5.04	44.8	-.06	3.55	3.57	-.06	322.05	1012.10	343.06	8.98	13.01
E22	THERMOCOUPLE	58	HE22C	3.54	44.7	-.00	2.49	2.52	-.00	322.46	1010.66	343.00	10.48	13.01
E22	THERMOCOUPLE	59	HE22B	2.54	44.5	.03	1.78	1.81	.03	322.74	1009.70	342.97	11.48	13.01
E22	THERMOCOUPLE	60	HE22A	1.29	44.0	.08	.90	.93	.08	323.08	1008.50	342.92	12.73	13.01
E22	THERMOCOUPLE	146	RF572	14.01	45.0	-.40	9.90	9.91	-.40	319.59	1020.73	343.40	0.	13.01
E23	EXTENSOMETER	335	HE23D	6.00	44.9	-1.98	4.23	4.25	-1.98	321.78	1013.03	344.98	7.88	12.85
E23	EXTENSOMETER	336	HE23C	3.02	44.7	-1.92	2.13	2.15	-1.92	322.60	1010.16	344.92	10.86	12.85
E23	EXTENSOMETER	337	HE23B	2.00	44.5	-1.90	1.40	1.43	-1.90	322.88	1009.18	344.90	11.88	12.85
E23	EXTENSOMETER	338	HE23A	1.07	44.1	-1.88	.75	.77	-1.88	323.14	1008.29	344.88	12.81	12.85
E23	THERMOCOUPLE	61	HE23D	6.07	44.9	-1.98	4.28	4.30	-1.98	321.77	1013.09	344.98	7.81	12.85
E23	THERMOCOUPLE	62	HE23C	3.07	44.7	-1.92	2.16	2.18	-1.92	322.59	1010.21	344.92	10.81	12.85
E23	THERMOCOUPLE	63	HE23B	2.07	44.6	-1.90	1.45	1.48	-1.90	322.86	1009.25	344.90	11.81	12.85
E23	THERMOCOUPLE	64	HE23A	1.07	44.1	-1.88	.75	.77	-1.88	323.14	1008.29	344.88	12.81	12.85
E23	THERMOCOUPLE	147	RF572	13.88	45.0	-2.15	9.81	9.82	-2.15	319.63	1020.60	345.15	0.	12.85
E24	EXTENSOMETER	339	HE24B	2.99	134.2	1.93	2.14	-2.09	1.93	320.52	1006.47	341.07	11.25	13.25
E24	EXTENSOMETER	340	HE24C	4.26	134.5	1.83	3.04	-2.99	1.83	319.31	1006.12	341.17	9.98	13.25
E24	EXTENSOMETER	341	HE24D	6.99	134.8	1.63	4.96	-4.93	1.63	316.68	1005.36	341.37	7.24	13.25
E24	EXTENSOMETER	342	HE24A	1.48	133.2	2.04	1.08	-1.01	2.04	321.98	1006.89	340.96	12.77	13.25
E24	THERMOCOUPLE	65	HE24D	7.96	134.9	1.56	5.64	-5.61	1.56	315.75	1005.09	341.44	6.27	13.25
E24	THERMOCOUPLE	66	HE24C	4.22	134.5	1.84	3.01	-2.96	1.84	319.35	1006.13	341.16	10.02	13.25
E24	THERMOCOUPLE	67	HE24B	2.97	134.2	1.93	2.13	-2.07	1.93	320.54	1006.48	341.07	11.27	13.25
E24	THERMOCOUPLE	68	HE24A	1.48	133.2	2.04	1.08	-1.01	2.04	321.98	1006.89	340.96	12.77	13.25
E24	THERMOCOUPLE	148	RF572	14.21	135.0	1.09	10.04	-10.05	1.09	309.75	1003.36	341.91	0.	13.25
E25	EXTENSOMETER	343	HE25D	4.96	134.6	-.04	3.54	-3.49	-.04	318.63	1005.93	343.04	9.42	13.38
E25	EXTENSOMETER	344	HE25C	3.47	134.3	.01	2.48	-2.42	.01	320.07	1006.34	342.99	10.92	13.38
E25	EXTENSOMETER	345	HE25B	2.48	133.9	.05	1.78	-1.72	.05	321.02	1006.62	342.95	11.91	13.38
E25	EXTENSOMETER	346	HE25A	1.25	132.6	.10	.92	-.84	.10	322.20	1006.96	342.90	13.14	13.38
E25	THERMOCOUPLE	69	HE25D	4.99	134.6	-.05	3.56	-3.51	-.05	318.60	1005.92	343.05	9.39	13.38
E25	THERMOCOUPLE	70	HE25C	3.50	134.3	.01	2.50	-2.44	.01	320.04	1006.34	342.99	10.89	13.38
E25	THERMOCOUPLE	71	HE25B	2.50	133.9	.05	1.80	-1.73	.05	321.00	1006.61	342.95	11.89	13.38
E25	THERMOCOUPLE	72	HE25A	1.25	132.6	.10	.92	-.84	.10	322.20	1006.96	342.90	13.14	13.38
E25	THERMOCOUPLE	149	RF572	14.38	135.0	-.41	10.16	-10.17	-.41	309.59	1003.31	343.41	0.	13.38
E26	EXTENSOMETER	347	HE26D	6.04	134.7	-1.98	4.29	-4.25	-1.98	317.60	1005.63	344.98	8.06	13.08
E26	EXTENSOMETER	348	HE26C	3.04	134.2	-1.91	2.18	-2.12	-1.91	320.48	1006.46	344.91	11.06	13.08
E26	EXTENSOMETER	349	HE26B	2.05	133.7	-1.89	1.48	-1.42	-1.89	321.43	1006.74	344.89	12.05	13.08
E26	EXTENSOMETER	350	HE26A	1.09	132.4	-1.87	.80	-.73	-1.87	322.35	1007.00	344.87	13.01	13.08
E26	THERMOCOUPLE	73	HE26D	6.09	134.7	-1.98	4.32	-4.28	-1.98	317.55	1005.61	344.98	8.01	13.08
E26	THERMOCOUPLE	74	HE26C	3.09	134.2	-1.91	2.21	-2.15	-1.91	320.43	1006.45	344.91	11.01	13.08
E26	THERMOCOUPLE	75	HE26B	2.09	133.8	-1.89	1.51	-1.44	-1.89	321.39	1006.72	344.89	12.01	13.08
E26	THERMOCOUPLE	76	HE26A	1.09	132.4	-1.87	.80	-.73	-1.87	322.35	1007.00	344.87	13.01	13.08

SENSOR LOCATIONS FOR EXPERIMENT 1, FULL SCALE HEATER H9

HOLE ID	SENSOR TYPE	SENSOR NUMBER	SENSOR LABEL	CYLINDRICAL COORDINATES RHO	THETA	Z	LOCAL RECTANGULAR X	Y	Z	MINE RECTANGULAR X	Y	Z	DEPTH	HOLE LENGTH
E26	THERMOCOUPLE	150	RF572	14.09	135.0	-2.15	9.96	-9.97	-2.15	309.86	1003.39	345.15	0.	13.08
H9	HEATER CURRENT	351												
H9	HEATER VOLTAGE	352												
H9	HEATER POWER	353												
H9	HEATER CURRENT	354												
H9	HEATER VOLTAGE	355												
H9	HEATER POWER	356												
H9	HEATER CURRENT	357												
H9	HEATER VOLTAGE	358												
H9	HEATER POWER	359												
H9	HEATER CURRENT	360												
H9	HEATER VOLTAGE	361												
H9	HEATER POWER	362												
H9	HEATER POWER	363												
H9	THERMOCOUPLE	114	TH9A	.00	0.	-.51	.00	-.00	-.51	323.41	1007.25	343.51	4.73	5.60
H9	THERMOCOUPLE	115	TH9B	.00	0.	-.51	.00	-.00	-.51	323.41	1007.25	343.51	4.73	5.60
H9	THERMOCOUPLE	116	TH9C	0.	0.	.10	0.	0.	.10	323.41	1007.25	342.90	4.12	5.60
H9	THERMOCOUPLE	117	TH9D	0.	0.	.10	0.	0.	.10	323.41	1007.25	342.90	4.12	5.60
H9	THERMOCOUPLE	118	TH9E	.00	0.	.71	.00	.00	.71	323.41	1007.25	342.29	3.51	5.60
H9	THERMOCOUPLE	119	TH9F	.00	0.	.71	.00	.00	.71	323.41	1007.25	342.29	3.51	5.60
H9	THERMOCOUPLE	120	TH9G	.00	273.3	2.44	-.00	.00	2.44	323.42	1007.25	340.56	1.78	5.60
H9	THERMOCOUPLE	121	TH9H	.00	273.3	2.44	-.00	.00	2.44	323.42	1007.25	340.56	1.78	5.60
T13	THERMOCOUPLE	84	T13A	.40	357.9	3.00	-.01	.40	3.00	323.62	1007.59	340.01	1.27	7.64
T13	THERMOCOUPLE	85	T13B	.40	357.8	1.50	-.02	.40	1.50	323.62	1007.59	341.51	2.77	7.64
T13	THERMOCOUPLE	86	T13C	.40	357.6	-.01	-.02	.40	-.01	323.62	1007.59	343.01	4.27	7.64
T13	THERMOCOUPLE	87	T13D	.40	357.4	-1.51	-.02	.40	-1.51	323.62	1007.59	344.51	5.77	7.64
T13	THERMOCOUPLE	88	T13E	.40	357.2	-3.01	-.02	.40	-3.01	323.62	1007.59	346.01	7.27	7.64
T14	THERMOCOUPLE	89	T14A	.90	0.	3.00	-.01	.90	3.00	323.86	1008.03	340.00	1.30	7.70
T14	THERMOCOUPLE	90	T14B	.89	0.	1.50	-.01	.89	1.50	323.85	1008.03	341.50	2.80	7.70
T14	THERMOCOUPLE	91	T14C	.89	0.	.00	-.01	.89	.00	323.85	1008.02	343.00	4.30	7.70
T14	THERMOCOUPLE	92	T14D	.89	0.	-1.50	-.01	.88	-1.50	323.85	1008.02	344.50	5.80	7.70
T14	THERMOCOUPLE	93	T14E	.88	0.	-3.00	-.01	.88	-3.00	323.85	1008.02	346.00	7.30	7.70
T15	THERMOCOUPLE	94	T15A	.69	44.2	3.00	.48	.49	3.00	323.23	1007.92	340.01	1.25	7.64
T15	THERMOCOUPLE	95	T15B	.69	44.1	1.50	.48	.49	1.50	323.24	1007.91	341.51	2.75	7.64
T15	THERMOCOUPLE	96	T15C	.68	44.1	-.01	.47	.49	-.01	323.24	1007.91	343.01	4.25	7.64
T15	THERMOCOUPLE	97	T15D	.68	44.0	-1.51	.47	.49	-1.51	323.24	1007.91	344.51	5.75	7.64
T15	THERMOCOUPLE	98	T15E	.67	43.9	-3.01	.47	.49	-3.01	323.24	1007.90	346.01	7.25	7.64
T16	THERMOCOUPLE	99	T16A	.50	182.8	3.00	-.02	-.50	3.00	323.19	1006.81	340.00	1.15	7.57
T16	THERMOCOUPLE	100	T16B	.50	184.3	1.50	-.04	-.49	1.50	323.20	1006.80	341.50	2.65	7.57
T16	THERMOCOUPLE	101	T16C	.50	186.0	.00	-.05	-.49	.00	323.22	1006.79	343.00	4.15	7.57
T16	THERMOCOUPLE	102	T16D	.50	187.6	-1.50	-.07	-.49	-1.50	323.23	1006.79	344.50	5.65	7.57
T16	THERMOCOUPLE	103	T16E	.50	189.1	-3.00	-.08	-.49	-3.00	323.24	1006.78	346.00	7.15	7.57
T17	THERMOCOUPLE	104	T17A	.81	225.7	3.00	-.58	-.56	3.00	323.64	1006.48	340.00	1.23	7.64
T17	THERMOCOUPLE	105	T17B	.81	226.0	1.50	-.58	-.56	1.50	323.65	1006.48	341.50	2.73	7.64
T17	THERMOCOUPLE	106	T17C	.81	226.2	.00	-.58	-.56	.00	323.65	1006.48	343.00	4.23	7.64
T17	THERMOCOUPLE	107	T17D	.81	226.4	-1.50	-.59	-.56	-1.50	323.65	1006.48	344.50	5.73	7.64
T17	THERMOCOUPLE	108	T17E	.81	226.7	-3.00	-.59	-.55	-3.00	323.66	1006.48	346.00	7.23	7.64
T18	THERMOCOUPLE	109	T18A	.61	314.5	3.00	-.44	.43	3.00	324.00	1007.41	340.00	1.32	7.72
T18	THERMOCOUPLE	110	T18B	.62	314.6	1.50	-.44	.43	1.50	324.01	1007.42	341.50	2.82	7.72
T18	THERMOCOUPLE	111	T18C	.62	314.7	.00	-.44	.44	.00	324.01	1007.42	343.00	4.32	7.72
T18	THERMOCOUPLE	112	T18D	.62	314.8	-1.50	-.44	.44	-1.50	324.01	1007.42	344.50	5.82	7.72
T18	THERMOCOUPLE	113	T18E	.63	314.8	-3.00	-.44	.44	-3.00	324.02	1007.42	346.00	7.32	7.72
U1	USBM	201	U1	1.51	0.	.85	-.02	1.51	.85	324.16	1008.56	342.15	3.50	7.45
U1	USBM	202	U1	1.51	0.	.85	-.02	1.51	.85	324.16	1008.56	342.15	3.50	7.45

SENSOR LOCATIONS FOR EXPERIMENT 1, FULL SCALE HEATER H9

HOLE ID	SENSOR TYPE	SENSOR NUMBER	SENSOR LABEL	CYLINDRICAL COORDINATES RHO	THETA	Z	LOCAL RECTANGULAR X	Y	Z	MINE RECTANGULAR X	Y	Z	DEPTH	HOLE LENGTH
U1	USBM	203	U1	1.51	0.	.85	-.02	1.51	.85	324.16	1008.56	342.15	3.50	7.45
U1	THERMOCOUPLE	2	U1	0.	0.	0.	0.	0.	0.	0.	0.	0.	3.50	7.45
U2	USBM	204	U2	2.49	0.	-.65	-.01	2.49	-.65	324.64	1009.42	343.65	5.03	7.77
U2	USBM	205	U2	2.49	0.	-.65	-.01	2.49	-.65	324.64	1009.42	343.65	5.03	7.77
U2	USBM	206	U2	2.49	0.	-.65	-.01	2.49	-.65	324.64	1009.42	343.65	5.03	7.77
U2	THERMOCOUPLE	3	U2	2.49	0.	-.65	-.01	2.49	-.65	324.64	1009.42	343.65	5.03	7.77
U3	USBM	207	U3	3.49	0.	.85	-.01	3.49	.85	325.12	1010.30	342.15	3.54	7.46
U3	USBM	208	U3	3.49	0.	.85	-.01	3.49	.85	325.12	1010.30	342.15	3.54	7.46
U3	USBM	209	U3	3.49	0.	.85	-.01	3.49	.85	325.12	1010.30	342.15	3.54	7.46
U3	THERMOCOUPLE	4	U3	3.49	0.	.85	-.01	3.49	.85	325.12	1010.30	342.15	3.54	7.46
U4	USBM	210	U4	2.25	202.6	.85	-.86	-2.08	.85	323.15	1005.01	342.15	3.32	7.04
U4	USBM	211	U4	2.25	202.6	.85	-.86	-2.08	.85	323.15	1005.01	342.15	3.32	7.04
U4	USBM	212	U4	2.25	202.6	.85	-.86	-2.08	.85	323.15	1005.01	342.15	3.32	7.04
U4	THERMOCOUPLE	5	U4	2.25	202.6	.85	-.86	-2.08	.85	323.15	1005.01	342.15	3.32	7.04
U5	USBM	213	U5	3.27	202.8	-.65	-1.26	-3.01	-.65	323.05	1004.00	343.65	4.99	7.22
U5	USBM	214	U5	3.27	202.8	-.65	-1.26	-3.01	-.65	323.05	1004.00	343.65	4.99	7.22
U5	USBM	215	U5	3.27	202.8	-.65	-1.26	-3.01	-.65	323.05	1004.00	343.65	4.99	7.22
U5	THERMOCOUPLE	6	U5	3.27	202.8	-.65	-1.26	-3.01	-.65	323.05	1004.00	343.65	4.99	7.22
U6	IRAD GAGE	273	C2	1.01	314.8	-.65	-.72	.71	-.65	324.38	1007.52	343.65	4.96	7.42
U6	IRAD GAGE	274	C2	1.01	314.8	-.65	-.72	.71	-.65	324.38	1007.52	343.65	4.96	7.42
U6	THERMOCOUPLE	78	C2	1.01	314.8	-.65	-.72	.71	-.65	324.38	1007.52	343.65	4.96	7.42
U7	USBM	219	U7	2.00	314.6	-.65	-1.42	1.40	-.65	325.34	1007.78	343.65	4.90	7.34
U7	USBM	220	U7	2.00	314.6	-.65	-1.42	1.40	-.65	325.34	1007.78	343.65	4.90	7.34
U7	USBM	221	U7	2.00	314.6	-.65	-1.42	1.40	-.65	325.34	1007.78	343.65	4.90	7.34
U7	THERMOCOUPLE	8	U7	2.00	314.6	-.65	-1.42	1.40	-.65	325.34	1007.78	343.65	4.90	7.34
U8	USBM	222	U8	3.01	314.7	-.65	-2.14	2.12	-.65	326.32	1008.06	343.65	4.90	7.14
U8	USBM	223	U8	3.01	314.7	-.65	-2.14	2.12	-.65	326.32	1008.06	343.65	4.90	7.14
U8	USBM	224	U8	3.01	314.7	-.65	-2.14	2.12	-.65	326.32	1008.06	343.65	4.90	7.14
U8	THERMOCOUPLE	9	U8	3.01	314.7	-.65	-2.14	2.12	-.65	326.32	1008.06	343.65	4.90	7.14
U9	USBM	225	U9	2.28	337.1	.85	-.89	2.10	.85	325.21	1008.66	342.15	3.41	7.14
U9	USBM	226	U9	2.28	337.1	.85	-.89	2.10	.85	325.21	1008.66	342.15	3.41	7.14
U9	USBM	227	U9	2.28	337.1	.85	-.89	2.10	.85	325.21	1008.66	342.15	3.41	7.14
U9	THERMOCOUPLE	10	U9	2.28	337.1	.85	-.89	2.10	.85	325.21	1008.66	342.15	3.41	7.14
U10	USBM	228	U10	3.25	337.2	.95	-1.26	3.00	.95	325.97	1009.26	342.05	3.32	7.19
U10	USBM	229	U10	3.25	337.2	.95	-1.26	3.00	.95	325.97	1009.26	342.05	3.32	7.19
U10	USBM	230	U10	3.25	337.2	.95	-1.26	3.00	.95	325.97	1009.26	342.05	3.32	7.19
U10	THERMOCOUPLE	11	U10	3.25	337.2	.85	-1.26	3.00	.85	325.97	1009.26	342.15	3.42	7.19
U21	USBM	231	U21	2.49	67.9	.62	2.31	.94	.62	321.85	1009.19	342.38	8.26	9.75
U21	USBM	232	U21	2.49	67.9	.62	2.31	.94	.62	321.85	1009.19	342.38	8.26	9.75
U21	USBM	233	U21	2.49	67.9	.62	2.31	.94	.62	321.85	1009.19	342.38	8.26	9.75
U21	THERMOCOUPLE	12	U21	2.49	67.9	.62	2.31	.94	.62	321.85	1009.19	342.38	8.26	9.75
U22	USBM	234	U22	3.49	112.7	.68	3.22	-1.35	.68	319.94	1007.64	342.32	7.58	8.08
U22	USBM	235	U22	3.49	112.7	.68	3.22	-1.35	.68	319.94	1007.64	342.32	7.58	8.08
U22	USBM	236	U22	3.49	112.7	.68	3.22	-1.35	.68	319.94	1007.64	342.32	7.58	8.08
U22	THERMOCOUPLE	13	U22	3.49	112.7	.68	3.22	-1.35	.68	319.94	1007.64	342.32	7.58	8.08
U26	USBM	237	U26	2.48	46.2	-.82	1.79	1.72	-.82	322.68	1009.63	343.82	11.47	12.91
U26	USBM	238	U26	2.48	46.2	-.82	1.79	1.72	-.82	322.68	1009.63	343.82	11.47	12.91
U26	USBM	239	U26	2.48	46.2	-.82	1.79	1.72	-.82	322.68	1009.63	343.82	11.47	12.91
U26	THERMOCOUPLE	14	U26	2.48	46.2	-.82	1.79	1.72	-.82	322.68	1009.63	343.82	11.47	12.91
U27	USBM	240	U27	2.00	90.9	-.83	2.00	-.03	-.83	321.65	1008.20	343.83	7.85	8.83
U27	USBM	241	U27	2.00	90.9	-.83	2.00	-.03	-.83	321.65	1008.20	343.83	7.85	8.83
U27	USBM	242	U27	2.00	90.9	-.83	2.00	-.03	-.83	321.65	1008.20	343.83	7.85	8.83
U27	THERMOCOUPLE	15	U27	2.00	90.9	-.83	2.00	-.03	-.83	321.65	1008.20	343.83	7.85	8.83
U28	USBM	243	U28	2.99	135.3	-.84	2.10	-2.13	-.84	320.54	1006.42	343.84	11.27	13.24

SENSOR LOCATIONS FOR EXPERIMENT 1, FULL SCALE HEATER H9

HOLE ID	SENSOR TYPE	SENSOR NUMBER	SENSOR LABEL	CYLINDRICAL COORDINATES RHO	THETA	Z	LOCAL RECTANGULAR X	Y	Z	MINE RECTANGULAR X	Y	Z	DEPTH	HOLE LENGTH
U28	USBM	244	U28	2.99	135.3	-.84	2.10	-2.13	-.84	320.54	1006.42	343.84	11.27	13.24
U28	USBM	245	U28	2.99	135.3	-.84	2.10	-2.13	-.84	320.54	1006.42	343.84	11.27	13.24
U28	THERMOCOUPLE	16	U28	2.99	135.3	-.84	2.10	-2.13	-.84	320.54	1006.42	343.84	11.27	13.24

SENSOR LOCATIONS FOR EXPERIMENT 2, FULL SCALE HEATER H10

HOLE ID	SENSOR TYPE	SENSOR NUMBER	SENSOR LABEL	CYLINDRICAL COORDINATES RHO	THETA	Z	LOCAL RECTANGULAR X	Y	Z	MINE RECTANGULAR X	Y	Z	DEPTH	HOLE LENGTH
C3	USBM	723	U15	1.59	21.6	-.53	.59	1.48	-.53	312.92	989.60	343.53	4.73	7.09
C3	USBM	724	U15	1.59	21.6	-.53	.59	1.48	-.53	312.92	989.60	343.53	4.73	7.09
C3	USBM	725	U15	1.59	21.6	-.53	.59	1.48	-.53	312.92	989.60	343.53	4.73	7.09
C3	THERMOCOUPLE	431	U15	1.59	21.6	-.53	.59	1.48	-.53	312.92	989.60	343.53	4.73	7.09
C4	USBM	729	U17	2.50	22.6	-.57	.96	2.31	-.57	313.00	990.51	343.57	4.89	7.20
C4	USBM	730	U17	2.50	22.6	-.57	.96	2.31	-.57	313.00	990.51	343.57	4.89	7.20
C4	USBM	731	U17	2.50	22.6	-.57	.96	2.31	-.57	313.00	990.51	343.57	4.89	7.20
C4	THERMOCOUPLE	433	U17	2.50	22.6	-.57	.96	2.31	-.57	313.00	990.51	343.57	4.89	7.20
C5	IRAD GAGE	865	C5	1.51	247.9	.85	-1.39	-.57	.85	313.66	986.85	342.15	3.10	6.80
C5	IRAD GAGE	866	C5	1.51	247.9	.85	-1.39	-.57	.85	313.66	986.85	342.15	3.10	6.80
C5	THERMOCOUPLE	504	C5	1.51	247.9	.85	-1.39	-.57	.85	313.66	986.85	342.15	3.10	6.80
C10	IRAD GAGE	869	C10	4.02	112.5	.65	3.72	-1.54	.65	308.72	988.49	342.35	6.56	9.58
C10	IRAD GAGE	870	C10	4.02	112.5	.65	3.72	-1.54	.65	308.72	988.49	342.35	6.56	9.58
C10	THERMOCOUPLE	506	C10	4.02	112.5	.65	3.72	-1.54	.65	308.72	988.49	342.35	6.56	9.58
C14	IRAD GAGE	873	C14	1.50	90.9	-.82	1.50	-.02	-.82	311.40	988.73	343.82	8.12	8.59
C14	IRAD GAGE	874	C14	1.50	90.9	-.82	1.50	-.02	-.82	311.40	988.73	343.82	8.12	8.59
C14	THERMOCOUPLE	508	C14	1.50	90.9	-.82	1.50	-.02	-.82	311.40	988.73	343.82	8.12	8.59
C15	IRAD GAGE	875	C15	3.00	135.2	-.81	2.11	-2.13	-.81	309.84	987.19	343.81	11.00	12.99
C15	IRAD GAGE	876	C15	3.00	135.2	-.81	2.11	-2.13	-.81	309.84	987.19	343.81	11.00	12.99
C15	THERMOCOUPLE	509	C15	3.00	135.2	-.81	2.11	-2.13	-.81	309.84	987.19	343.81	11.00	12.99
E12	EXTENSOMETER	801	E12B	1.99	0.	-.07	.01	1.99	-.07	313.68	989.77	343.07	4.28	12.58
E12	EXTENSOMETER	802	E12C	1.98	0.	-2.24	.01	1.98	-2.24	313.68	989.76	345.24	6.45	12.58
E12	EXTENSOMETER	803	E12D	1.97	0.	-7.39	.01	1.97	-7.39	313.67	989.74	350.39	11.60	12.58
E12	EXTENSOMETER	804	E12A	2.00	0.	2.24	.01	2.00	2.24	313.68	989.77	340.76	1.97	12.58
E12	THERMOCOUPLE	442	E12A	2.00	0.	2.36	.01	2.00	2.36	313.68	989.77	340.64	1.85	12.58
E12	THERMOCOUPLE	443	E12B	1.99	0.	.11	.01	1.99	.11	313.68	989.77	342.89	4.10	12.58
E12	THERMOCOUPLE	444	E12C	1.99	0.	-.89	.01	1.99	-.89	313.68	989.76	343.89	5.10	12.58
E12	THERMOCOUPLE	445	E12D	1.98	0.	-2.14	.01	1.98	-2.14	313.68	989.76	345.14	6.35	12.58
E12	THERMOCOUPLE	573	E12	2.00	0.	4.21	.01	2.00	4.21	313.69	989.78	338.79	0.	12.58
E12	THERMOCOUPLE	163	RF457	1.96	0.	-7.39	.00	1.96	-7.39	313.67	989.74	350.39	11.60	12.58
E13	EXTENSOMETER	805	E13A	3.00	0.	2.23	.01	3.00	2.23	314.17	990.65	340.77	1.87	12.30
E13	EXTENSOMETER	806	E13B	3.00	0.	-.02	.01	3.00	-.02	314.17	990.65	343.02	4.12	12.30
E13	EXTENSOMETER	807	E13C	3.00	0.	-2.27	.00	3.00	-2.27	314.17	990.65	345.27	6.37	12.30
E13	EXTENSOMETER	808	E13D	3.00	0.	-7.52	.00	3.00	-7.52	314.17	990.65	350.52	11.62	12.30
E13	THERMOCOUPLE	446	E13A	3.00	0.	-1.02	.01	3.00	-1.02	314.17	990.65	344.02	5.12	12.30
E13	THERMOCOUPLE	447	E13B	3.00	0.	-2.27	.00	3.00	-2.27	314.17	990.65	345.27	6.37	12.30
E13	THERMOCOUPLE	448	E13C	3.00	0.	-4.90	.00	3.00	-4.90	314.17	990.65	347.90	9.00	12.30
E13	THERMOCOUPLE	449	E13D	3.00	0.	-7.52	.00	3.00	-7.52	314.17	990.65	350.52	11.62	12.30
E13	THERMOCOUPLE	126		3.00	0.	-0.02	.00	3.00	-0.02	314.17	990.65	343.02	4.12	12.30
E13	THERMOCOUPLE	127		3.00	0.	2.23	.01	3.00	2.23	314.17	990.65	340.77	1.87	12.30
E13	THERMOCOUPLE	136	RF573	3.00	0.	4.10	.01	3.00	4.10	314.17	990.65	338.90	0.	12.30
E14	EXTENSOMETER	809	E14A	2.50	179.8	2.26	.01	-2.50	2.26	311.49	985.85	340.74	1.92	12.57
E14	EXTENSOMETER	810	E14B	2.50	179.8	-.00	.01	-2.50	-.00	311.49	985.85	343.00	4.18	12.57
E14	EXTENSOMETER	811	E14C	2.50	179.8	-2.29	.01	-2.50	-2.29	311.49	985.85	345.29	6.47	12.57
E14	EXTENSOMETER	812	E14D	2.50	179.7	-7.47	.01	-2.50	-7.47	311.49	985.85	350.47	11.65	12.57
E14	THERMOCOUPLE	450	E14A	2.50	179.8	2.28	.01	-2.50	2.28	311.49	985.85	340.72	1.90	12.57
E14	THERMOCOUPLE	451	E14B	2.50	179.8	.03	.01	-2.50	.03	311.49	985.85	342.97	4.15	12.57
E14	THERMOCOUPLE	452	E14C	2.50	179.8	-2.22	.01	-2.50	-2.22	311.49	985.85	345.22	6.40	12.57
E14	THERMOCOUPLE	453	E14D	2.50	179.7	-7.47	.01	-2.50	-7.47	311.49	985.85	350.47	11.65	12.57
E14	THERMOCOUPLE	138	RF573	2.50	179.8	4.18	.01	-2.50	4.18	311.49	985.85	338.82	0.	12.57
E15	EXTENSOMETER	813	E15A	1.99	270.2	2.25	-1.99	.01	2.25	314.46	987.06	340.75	1.77	12.38
E15	EXTENSOMETER	814	E15D	1.98	270.6	-7.50	-1.98	.02	-7.50	314.46	987.08	350.50	11.52	12.38
E15	EXTENSOMETER	815	E15C	1.99	270.4	-2.26	-1.99	.01	-2.26	314.46	987.07	345.26	6.28	12.38
E15	EXTENSOMETER	816	E15B	1.99	270.3	.01	-1.99	.01	.01	314.46	987.07	342.99	4.01	12.38

SENSOR LOCATIONS FOR EXPERIMENT 2, FULL SCALE HEATER H10

HOLE ID	SENSOR TYPE	SENSOR NUMBER	SENSOR LABEL	CYLINDRICAL COORDINATES RHO	THETA	Z	LOCAL RECTANGULAR X	Y	Z	MINE RECTANGULAR X	Y	Z	DEPTH	HOLE LENGTH
E15	THERMOCOUPLE	454	E15A	1.99	270.2	2.25	-1.99	.01	2.25	314.46	987.06	340.75	1.77	12.38
E15	THERMOCOUPLE	455	E15B	1.99	270.3	0.	-1.99	.01	0.	314.46	987.07	343.00	4.02	12.38
E15	THERMOCOUPLE	456	E15C	1.99	270.4	-2.25	-1.99	.01	-2.25	314.46	987.07	345.25	6.27	12.38
E15	THERMOCOUPLE	457	E15D	1.98	270.6	-7.50	-1.98	.02	-7.50	314.46	987.08	350.50	11.52	12.38
E15	THERMOCOUPLE	139	RF573	1.99	270.1	4.02	-1.99	.00	4.02	314.46	987.06	338.98	0.	12.38
E16	EXTENSOMETER	817	E16A	1.50	315.4	2.27	-1.05	1.07	2.27	314.15	988.44	340.73	1.81	12.47
E16	EXTENSOMETER	818	E16B	1.50	315.4	.02	-1.05	1.07	.02	314.16	988.45	342.98	4.06	12.47
E16	EXTENSOMETER	819	E16C	1.50	315.5	-2.23	-1.05	1.07	-2.23	314.16	988.45	345.23	6.31	12.47
E16	EXTENSOMETER	820	E16D	1.51	315.6	-7.46	-1.06	1.08	-7.46	314.16	988.45	350.46	11.54	12.47
E16	THERMOCOUPLE	458	E16A	1.50	315.4	2.29	-1.05	1.07	2.29	314.15	988.44	340.71	1.79	12.47
E16	THERMOCOUPLE	459	E16B	1.50	315.4	.04	-1.05	1.07	.04	314.16	988.45	342.96	4.04	12.47
E16	THERMOCOUPLE	460	E16C	1.50	315.4	-.96	-1.05	1.07	-.96	314.16	988.45	343.96	5.04	12.47
E16	THERMOCOUPLE	461	E16D	1.50	315.5	-2.13	-1.05	1.07	-2.13	314.16	988.45	345.13	6.21	12.47
E16	THERMOCOUPLE	140	RF573	1.50	315.3	4.08	-1.05	1.06	4.08	314.15	988.44	338.92	0.	12.47
E16	THERMOCOUPLE	162	RF457	1.51	315.6	-7.46	-1.06	1.08	-7.46	314.16	988.45	350.46	11.54	12.47
E17	EXTENSOMETER	821	E17A	2.50	315.2	2.22	-1.76	1.77	2.22	315.11	988.72	340.78	1.93	12.55
E17	EXTENSOMETER	822	E17B	2.50	315.3	.08	-1.76	1.78	.08	315.12	988.72	342.92	4.07	12.55
E17	EXTENSOMETER	823	E17C	2.50	315.5	-2.27	-1.75	1.78	-2.27	315.12	988.73	345.27	6.42	12.55
E17	EXTENSOMETER	824	E17D	2.51	315.8	-7.50	-1.75	1.80	-7.50	315.12	988.74	350.50	11.65	12.55
E17	THERMOCOUPLE	462	E17A	2.50	315.2	2.25	-1.76	1.77	2.25	315.11	988.72	340.75	1.90	12.55
E17	THERMOCOUPLE	463	E17B	2.50	315.3	-.00	-1.76	1.78	-.00	315.12	988.72	343.00	4.15	12.55
E17	THERMOCOUPLE	464	E17C	2.50	315.4	-1.00	-1.76	1.78	-1.00	315.12	988.73	344.00	5.15	12.55
E17	THERMOCOUPLE	465	E17D	2.50	315.5	-2.25	-1.75	1.78	-2.25	315.12	988.73	345.25	6.40	12.55
E17	THERMOCOUPLE	141	RF573	2.50	315.1	4.15	-1.76	1.77	4.15	315.11	988.71	338.85	0.	12.55
E17	THERMOCOUPLE	164	RF457	2.51	315.7	-7.50	-1.75	1.79	-7.50	315.12	988.74	350.50	11.65	12.55
E27	EXTENSOMETER	825	HE27D	6.97	89.9	1.41	6.97	.01	1.41	306.63	991.42	341.59	3.11	9.08
E27	EXTENSOMETER	826	HE27C	4.23	89.8	1.68	4.23	.01	1.68	309.02	990.10	341.32	5.86	9.08
E27	EXTENSOMETER	827	HE27B	2.98	89.7	1.81	2.98	.01	1.81	310.12	989.49	341.19	7.12	9.08
E27	EXTENSOMETER	828	HE27A	1.47	89.4	1.96	1.47	.02	1.96	311.44	988.75	341.04	8.64	9.08
E27	THERMOCOUPLE	466	HE27D	7.93	90.0	1.31	7.93	.01	1.31	305.79	991.89	341.69	2.14	9.08
E27	THERMOCOUPLE	467	HE27C	4.20	89.8	1.69	4.20	.01	1.69	309.05	990.08	341.31	5.89	9.08
E27	THERMOCOUPLE	468	HE27B	2.96	89.7	1.81	2.96	.01	1.81	310.14	989.48	341.19	7.14	9.08
E27	THERMOCOUPLE	469	HE27A	1.47	89.4	1.96	1.47	.02	1.96	311.44	988.75	341.04	8.64	9.08
E27	THERMOCOUPLE	151	RF572	10.06	90.0	1.10	10.06	.01	1.10	303.93	992.93	341.90	0.	9.08
E28	EXTENSOMETER	829	HE28D	4.95	89.8	-.14	4.95	.01	-.14	308.40	990.44	343.14	4.71	8.62
E28	EXTENSOMETER	830	HE28C	3.46	89.7	-.06	3.46	.02	-.06	309.70	989.72	343.06	6.20	8.62
E28	EXTENSOMETER	831	HE28B	2.46	89.5	-.01	2.46	.02	-.01	310.58	989.24	343.01	7.20	8.62
E28	EXTENSOMETER	832	HE28A	1.22	88.9	.06	1.22	.02	.06	311.66	988.64	342.94	8.44	8.62
E28	THERMOCOUPLE	470	HE28D	4.96	89.9	-.14	4.96	.01	-.14	308.39	990.45	343.14	4.69	8.62
E28	THERMOCOUPLE	471	HE28C	3.47	89.7	-.06	3.47	.02	-.06	309.70	989.73	343.06	6.19	8.62
E28	THERMOCOUPLE	472	HE28B	2.47	89.6	-.01	2.47	.02	-.01	310.57	989.24	343.01	7.19	8.62
E28	THERMOCOUPLE	473	HE28A	1.22	88.9	.06	1.22	.02	.06	311.66	988.64	342.94	8.44	8.62
E28	THERMOCOUPLE	152	RF572	9.65	90.0	-.38	9.65	.01	-.38	304.29	992.72	343.38	0.	8.62
E29	EXTENSOMETER	833	HE29D	6.00	89.9	-2.04	6.00	.01	-2.04	307.48	990.96	345.04	3.63	11.02
E29	EXTENSOMETER	834	HE29C	2.00	89.3	-1.93	2.00	.02	-1.93	310.98	989.02	344.93	7.63	11.02
E29	EXTENSOMETER	835	HE29B	.99	88.5	-1.91	.99	.03	-1.91	311.86	988.53	344.91	8.64	11.02
E29	EXTENSOMETER	836	HE29A	1.01	271.8	-1.85	-1.01	.03	-1.85	313.61	987.56	344.85	10.64	11.02
E29	THERMOCOUPLE	474	HE29D	5.99	89.9	-2.04	5.99	.01	-2.04	307.49	990.95	345.04	3.64	11.02
E29	THERMOCOUPLE	475	HE29C	1.99	89.3	-1.93	1.99	.02	-1.93	310.99	989.01	344.93	7.64	11.02
E29	THERMOCOUPLE	476	HE29B	.99	88.5	-1.91	.99	.03	-1.91	311.86	988.53	344.91	8.64	11.02
E29	THERMOCOUPLE	477	HE29A	.03	271.8	-1.88	-.01	.03	-1.88	312.74	988.04	344.88	9.64	11.02
E29	THERMOCOUPLE	153	RF572	9.63	89.9	-2.14	9.63	.01	-2.14	304.31	992.72	345.14	0.	11.02
E30	EXTENSOMETER	837	HE30D	7.12	45.1	1.63	5.04	5.02	1.63	310.76	994.87	341.38	7.17	13.23
E30	EXTENSOMETER	838	HE30C	4.35	45.2	1.83	3.09	3.07	1.83	311.51	992.21	341.17	9.94	13.23

SENSOR LOCATIONS FOR EXPERIMENT 2, FULL SCALE HEATER H10

HOLE ID	SENSOR TYPE	SENSOR NUMBER	SENSOR LABEL	CYLINDRICAL COORDINATES RHO	THETA	Z	LOCAL RECTANGULAR X	Y	Z	MINE RECTANGULAR X	Y	Z	DEPTH	HOLE LENGTH
E30	EXTENSOMETER	839	HE30B	3.13	45.3	1.92	2.22	2.20	1.92	311.84	991.03	341.08	11.17	13.23
E30	EXTENSOMETER	840	HE30A	1.61	45.7	2.03	1.15	1.12	2.03	312.26	989.57	340.97	12.69	13.23
E30	THERMOCOUPLE	478	HE30D	8.09	45.1	1.55	5.73	5.71	1.55	310.49	995.81	341.45	6.19	13.23
E30	THERMOCOUPLE	479	HE30C	4.35	45.2	1.83	3.09	3.07	1.83	311.51	992.21	341.17	9.94	13.23
E30	THERMOCOUPLE	480	HE30B	3.11	45.3	1.92	2.21	2.18	1.92	311.85	991.01	341.08	11.19	13.23
E30	THERMOCOUPLE	481	HE30A	1.61	45.7	2.03	1.15	1.12	2.03	312.26	989.57	340.97	12.69	13.23
E30	THERMOCOUPLE	154	RF572	14.27	45.0	1.09	10.08	10.09	1.09	308.81	1001.75	341.91	0.	13.23
E31	EXTENSOMETER	841	HE31D	4.98	45.1	-.04	3.53	3.52	-.04	311.35	992.82	343.04	9.21	13.13
E31	EXTENSOMETER	842	HE31B	2.24	45.2	.07	1.59	1.58	.07	312.09	990.18	342.93	11.95	13.13
E31	EXTENSOMETER	843	HE31A	1.23	45.4	.11	.87	.86	.11	312.37	989.20	342.89	12.97	13.13
E31	EXTENSOMETER	844	HE31C	3.45	45.1	.02	2.45	2.44	.02	311.76	991.34	342.98	10.74	13.13
E31	THERMOCOUPLE	482	HE31D	4.97	45.1	-.04	3.52	3.51	-.04	311.35	992.81	343.04	9.22	13.13
E31	THERMOCOUPLE	483	HE31C	3.47	45.1	.02	2.46	2.45	.02	311.76	991.36	342.98	10.72	13.13
E31	THERMOCOUPLE	484	HE31B	2.47	45.2	.06	1.76	1.74	.06	312.03	990.40	342.94	11.72	13.13
E31	THERMOCOUPLE	485	HE31A	1.23	45.4	.11	.87	.86	.11	312.37	989.20	342.89	12.97	13.13
E31	THERMOCOUPLE	572	HE31	14.18	45.0	-.40	10.03	10.03	-.40	308.83	1001.67	343.40	0.	13.13
E32	EXTENSOMETER	845	HE32D	6.00	44.9	-1.97	4.24	4.25	-1.97	311.08	993.80	344.98	8.11	13.11
E32	EXTENSOMETER	846	HE32C	3.02	44.8	-1.91	2.13	2.15	-1.91	311.90	990.94	344.91	11.09	13.11
E32	EXTENSOMETER	847	HE32B	2.04	44.6	-1.89	1.44	1.46	-1.89	312.17	989.99	344.89	12.07	13.11
E32	EXTENSOMETER	848	HE32A	1.15	44.3	-1.87	.81	.83	-1.87	312.41	989.14	344.87	12.96	13.11
E32	THERMOCOUPLE	486	HE32D	6.15	44.9	-1.98	4.35	4.36	-1.98	311.04	993.95	344.98	7.96	13.11
E32	THERMOCOUPLE	487	HE32C	3.15	44.8	-1.91	2.22	2.24	-1.91	311.86	991.06	344.91	10.96	13.11
E32	THERMOCOUPLE	488	HE32B	2.15	44.7	-1.89	1.51	1.53	-1.89	312.14	990.10	344.89	11.96	13.11
E32	THERMOCOUPLE	489	HE32A	1.15	44.3	-1.87	.81	.83	-1.87	312.41	989.14	344.87	12.96	13.11
E32	THERMOCOUPLE	156	RF572	14.11	45.0	-2.15	9.97	9.98	-2.15	308.85	1001.60	345.15	0.	13.11
E33	EXTENSOMETER	849	HE33D	7.03	134.5	1.63	5.02	-4.93	1.63	305.93	986.16	341.37	7.33	13.36
E33	EXTENSOMETER	850	HE33C	4.24	133.9	1.83	3.06	-2.94	1.83	308.61	986.94	341.17	10.13	13.36
E33	EXTENSOMETER	851	HE33B	2.99	133.3	1.93	2.17	-2.05	1.93	309.82	987.29	341.07	11.39	13.36
E33	EXTENSOMETER	852	HE33A	1.48	131.1	2.04	1.12	-.97	2.04	311.27	987.72	340.96	12.90	13.36
E33	THERMOCOUPLE	490	HE33D	7.96	134.6	1.56	5.67	-5.59	1.56	305.04	985.90	341.44	6.40	13.36
E33	THERMOCOUPLE	491	HE33C	4.22	133.9	1.83	3.04	-2.93	1.83	308.63	986.95	341.17	10.15	13.36
E33	THERMOCOUPLE	492	HE33B	2.98	133.3	1.93	2.17	-2.04	1.93	309.83	987.30	341.07	11.40	13.36
E33	THERMOCOUPLE	493	HE33A	1.48	131.1	2.04	1.12	-.97	2.04	311.27	987.72	340.96	12.90	13.36
E33	THERMOCOUPLE	157	RF572	14.34	134.9	1.09	10.16	-10.13	1.09	298.92	984.11	341.91	0.	13.36
E34	EXTENSOMETER	853	HE34D	5.02	134.4	-.05	3.59	-3.51	-.05	307.87	986.70	343.05	9.04	13.02
E34	EXTENSOMETER	854	HE34C	3.53	134.0	.01	2.54	-2.45	.01	309.30	987.12	342.99	10.53	13.02
E34	EXTENSOMETER	855	HE34B	2.49	133.5	.05	1.81	-1.72	.05	310.30	987.41	342.95	11.57	13.02
E34	EXTENSOMETER	856	HE34A	1.23	131.7	.10	.92	-.82	.10	311.51	987.76	342.90	12.83	13.02
E34	THERMOCOUPLE	494	HE34D	4.98	134.4	-.04	3.56	-3.48	-.04	307.91	986.71	343.04	9.08	13.02
E34	THERMOCOUPLE	495	HE34C	3.48	134.0	.02	2.50	-2.42	.02	309.35	987.13	342.99	10.58	13.02
E34	THERMOCOUPLE	496	HE34B	2.48	133.5	.05	1.80	-1.71	.05	310.31	987.41	342.95	11.58	13.02
E34	THERMOCOUPLE	497	HE34A	1.23	131.7	.10	.92	-.82	.10	311.51	987.76	342.90	12.83	13.02
E34	THERMOCOUPLE	158	RF572	14.05	134.9	-.39	9.95	-9.93	-.39	299.20	984.19	343.39	0.	13.02
E35	EXTENSOMETER	857	HE35D	6.02	134.5	-1.97	4.29	-4.22	-1.97	306.91	986.43	344.97	7.70	12.70
E35	EXTENSOMETER	858	HE35C	3.05	133.8	-1.91	2.20	-2.11	-1.91	309.76	987.25	344.91	10.67	12.70
E35	EXTENSOMETER	859	HE35B	2.05	133.0	-1.89	1.50	-1.40	-1.89	310.72	987.53	344.89	11.67	12.70
E35	EXTENSOMETER	860	HE35A	1.10	131.0	-1.87	.83	-.72	-1.87	311.64	987.80	344.87	12.62	12.70
E35	THERMOCOUPLE	498	HE35D	6.10	134.5	-1.97	4.35	-4.28	-1.97	306.84	986.41	344.98	7.62	12.70
E35	THERMOCOUPLE	499	HE35C	3.10	133.8	-1.91	2.24	-2.14	-1.91	309.72	987.24	344.91	10.62	12.70
E35	THERMOCOUPLE	500	HE35B	2.10	133.0	-1.89	1.54	-1.43	-1.89	310.68	987.52	344.89	11.62	12.70
E35	THERMOCOUPLE	501	HE35A	1.10	131.0	-1.87	.83	-.72	-1.87	311.64	987.80	344.87	12.62	12.70
E35	THERMOCOUPLE	159	RF572	13.72	134.9	-2.14	9.71	-9.69	-2.14	299.52	984.28	345.14	0.	12.70
H10	HEATER CURRENT	624												
H10	HEATER VOLTAGE	625												

SENSOR LOCATIONS FOR EXPERIMENT 2, FULL SCALE HEATER H10

HOLE ID	SENSOR TYPE	SENSOR NUMBER	SENSOR LABEL	CYLINDRICAL COORDINATES RHO	THETA	Z	LOCAL RECTANGULAR X	Y	Z	MINE RECTANGULAR X	Y	Z	DEPTH	HOLE LENGTH
H10	HEATER POWER	626												
H10	HEATER CURRENT	627												
H10	HEATER VOLTAGE	628												
H10	HEATER POWER	629												
H10	HEATER CURRENT	630												
H10	HEATER VOLTAGE	631												
H10	HEATER POWER	632												
H10	HEATER CURRENT	633												
H10	HEATER VOLTAGE	634												
H10	HEATER POWER	635												
H10	HEATER POWER	636												
H10	THERMOCOUPLE	540	TH10A	0.	0.	-.50	0.	0.	-.05	312.72	988.03	343.50	4.55	5.43
H10	THERMOCOUPLE	541	TH10B	0.	0.	-.50	0.	0.	-.05	312.72	988.03	343.50	4.55	5.43
H10	THERMOCOUPLE	542	TH10C	.00	0.	.10	.00	.00	.10	312.72	988.03	342.90	3.95	5.43
H10	THERMOCOUPLE	543	TH10D	.00	0.	.10	.00	.00	.10	312.72	988.03	342.90	3.95	5.43
H10	THERMOCOUPLE	544	TH10E	.00	0.	.70	.00	.00	.70	312.72	988.03	342.30	3.35	5.43
H10	THERMOCOUPLE	545	TH10F	.00	0.	.70	.00	.00	.70	312.72	988.03	342.30	3.35	5.43
H10	THERMOCOUPLE	546	TH10G	.00	0.	2.44	.00	.00	2.44	312.71	988.03	340.56	1.61	5.43
H10	THERMOCOUPLE	547	TH10H	.00	0.	2.44	.00	.00	2.44	312.71	988.03	340.56	1.61	5.43
H11	HEATER CURRENT	600												
H11	HEATER VOLTAGE	601												
H11	HEATER POWER	602												
H11	THERMOCOUPLE	548	TH11A	.91	22.8	-1.22	.35	.83	-1.22	312.82	988.93	344.22	5.42	6.49
H11	THERMOCOUPLE	549	TH11B	.91	22.8	0.61	.35	.83	0.61	312.82	988.93	342.39	3.59	6.49
H11	THERMOCOUPLE	550	TH11C	.91	22.8	2.34	.35	.83	2.34	312.82	988.93	340.66	1.86	6.49
H12	HEATER CURRENT	603												
H12	HEATER VOLTAGE	604												
H12	HEATER POWER	605												
H12	THERMOCOUPLE	551	TH12A	.91	67.4	-1.22	.84	.35	-1.22	312.15	988.74	344.31	5.55	6.55
H12	THERMOCOUPLE	552	TH12B	.91	67.4	0.61	.84	.35	0.61	312.15	988.74	342.39	3.63	6.55
H12	THERMOCOUPLE	553	TH12C	.91	67.4	2.34	.84	.35	2.34	312.15	988.74	340.66	1.90	6.55
H13	HEATER CURRENT	606												
H13	HEATER VOLTAGE	607												
H13	HEATER POWER	608												
H13	THERMOCOUPLE	554	TH13A	.91	112.0	-1.22	.84	-.34	-1.22	311.82	988.14	344.22	5.31	6.37
H13	THERMOCOUPLE	555	TH13B	.91	112.0	0.61	.84	-.34	0.61	311.82	988.14	342.40	3.49	6.37
H13	THERMOCOUPLE	556	TH13C	.91	112.0	2.34	.84	-.34	2.34	311.82	988.14	340.67	1.76	6.37
H14	HEATER CURRENT	609												
H14	HEATER VOLTAGE	610												
H14	HEATER POWER	611												
H14	THERMOCOUPLE	557	TH14A	.90	157.2	-1.22	.35	-.83	-1.22	312.01	987.47	344.22	5.35	6.42
H14	THERMOCOUPLE	558	TH14B	.90	157.2	0.61	.35	-.83	0.61	312.01	987.47	342.39	3.52	6.42
H14	THERMOCOUPLE	559	TH14C	.90	157.2	2.34	.35	-.83	2.34	312.01	987.47	340.66	1.79	6.42
H15	HEATER CURRENT	612												
H15	HEATER VOLTAGE	613												
H15	HEATER POWER	614												
H15	THERMOCOUPLE	560	TH15A	.89	202.5	-1.22	-.34	-.83	-1.22	312.61	987.14	344.22	5.34	6.37
H15	THERMOCOUPLE	561	TH15B	.89	202.5	0.61	-.34	-.83	0.61	312.61	987.14	342.39	3.51	6.37
H15	THERMOCOUPLE	562	TH15C	.89	202.5	2.34	-.34	-.83	2.34	312.61	987.14	340.66	1.78	6.37
H16	HEATER CURRENT	615												
H16	HEATER VOLTAGE	616												
H16	HEATER POWER	617												
H16	THERMOCOUPLE	563	TH16A	.90	247.6	-1.22	-.83	-.34	-1.22	313.27	987.32	344.22	5.13	6.17
H16	THERMOCOUPLE	564	TH16B	.90	247.6	0.61	-.83	-.34	0.61	313.27	987.32	342.39	3.30	6.17

SENSOR LOCATIONS FOR EXPERIMENT 2, FULL SCALE HEATER H10

HOLE ID	SENSOR TYPE	SENSOR NUMBER	SENSOR LABEL	CYLINDRICAL COORDINATES RHO	THETA	Z	LOCAL RECTANGULAR X	Y	Z	MINE RECTANGULAR X	Y	Z	DEPTH	HOLE LENGTH
H16	THERMOCOUPLE	565	TH16C	.90	247.6	2.34	-.83	-.34	2.34	313.27	987.32	340.66	1.57	6.17
H17	HEATER CURRENT	618												
H17	HEATER VOLTAGE	619												
H17	HEATER POWER	620												
H17	THERMOCOUPLE	566	TH17A	.90	292.8	-1.22	-.83	.35	-1.22	313.61	987.93	344.22	5.27	6.32
H17	THERMOCOUPLE	567	TH17B	.90	292.8	0.61	-.83	.35	0.61	313.61	987.93	342.39	3.44	6.32
H17	THERMOCOUPLE	568	TH17C	.90	292.8	2.34	-.83	.35	2.34	313.61	987.93	340.67	1.72	6.32
H18	HEATER CURRENT	621												
H18	HEATER VOLTAGE	622												
H18	HEATER POWER	623												
H18	THERMOCOUPLE	569	TH18A	.91	337.6	-1.22	-.34	.84	-1.22	313.42	988.59	344.22	5.31	6.39
H18	THERMOCOUPLE	570	TH18B	.91	337.6	0.61	-.34	.84	0.61	313.42	988.59	342.39	3.48	6.39
H18	THERMOCOUPLE	571	TH18C	.91	337.6	2.34	-.34	.84	2.34	313.42	988.59	340.66	1.75	6.39
T19	THERMOCOUPLE	510	T19A	.40	0.	3.00	.00	.40	3.00	312.91	988.37	340.00	1.10	7.47
T19	THERMOCOUPLE	511	T19B	.40	0.	1.50	.00	.40	1.50	312.91	988.37	341.50	2.60	7.47
T19	THERMOCOUPLE	512	T19C	.40	0.	-.00	-.00	.40	-.00	312.91	988.38	343.00	4.10	7.47
T19	THERMOCOUPLE	513	T19D	.40	0.	-1.50	-.00	.40	-1.50	312.91	988.38	344.50	5.60	7.47
T19	THERMOCOUPLE	514	T19E	.41	0.	-3.00	-.00	.41	-3.00	312.91	988.38	346.00	7.10	7.47
T20	THERMOCOUPLE	515	T20A	.91	0.	3.00	-.00	.91	3.00	313.16	988.82	340.00	1.22	7.58
T20	THERMOCOUPLE	516	T20B	.91	0.	1.50	-.01	.91	1.50	313.16	988.82	341.50	2.72	7.58
T20	THERMOCOUPLE	517	T20C	.91	0.	-.00	-.01	.91	-.00	313.17	988.82	343.00	4.22	7.58
T20	THERMOCOUPLE	518	T20D	.92	0.	-1.50	-.02	.92	-1.50	313.18	988.82	344.50	5.72	7.58
T20	THERMOCOUPLE	519	T20E	.92	358.7	-3.00	-.02	.92	-3.00	313.18	988.82	346.00	7.22	7.58
T21	THERMOCOUPLE	520	T21A	.70	44.7	3.00	.49	.50	3.00	312.53	988.70	340.00	1.21	7.69
T21	THERMOCOUPLE	521	T21B	.70	44.5	1.50	.49	.50	1.50	312.53	988.70	341.50	2.71	7.69
T21	THERMOCOUPLE	522	T21C	.69	44.2	.00	.48	.50	.00	312.53	988.70	343.00	4.21	7.69
T21	THERMOCOUPLE	523	T21D	.69	44.0	-1.50	.48	.50	-1.50	312.54	988.69	344.50	5.71	7.69
T21	THERMOCOUPLE	524	T21E	.69	43.8	-3.00	.48	.50	-3.00	312.54	988.69	346.00	7.21	7.69
T22	THERMOCOUPLE	525	T22A	.50	179.8	3.00	.00	-.50	3.00	312.47	987.59	340.00	1.03	7.40
T22	THERMOCOUPLE	526	T22B	.50	179.3	1.50	.01	-.50	1.50	312.47	987.60	341.50	2.53	7.40
T22	THERMOCOUPLE	527	T22C	.50	178.7	.00	.01	-.50	.00	312.46	987.60	343.00	4.03	7.40
T22	THERMOCOUPLE	528	T22D	.49	178.1	-1.50	.02	-.49	-1.50	312.46	987.60	344.50	5.53	7.40
T22	THERMOCOUPLE	529	T22E	.49	177.6	-3.00	.02	-.49	-3.00	312.46	987.61	346.00	7.03	7.40
T23	THERMOCOUPLE	530	T23A	.79	224.8	3.00	-.56	-.56	3.00	312.93	987.26	340.00	1.01	7.38
T23	THERMOCOUPLE	531	T23B	.79	224.5	1.50	-.55	-.56	1.50	312.92	987.27	341.50	2.51	7.38
T23	THERMOCOUPLE	532	T23C	.78	224.3	-.00	-.55	-.56	-.00	312.92	987.27	343.00	4.01	7.38
T23	THERMOCOUPLE	533	T23D	.78	224.1	-1.50	-.54	-.56	-1.50	312.92	987.27	344.50	5.51	7.38
T23	THERMOCOUPLE	534	T23E	.78	223.9	-3.00	-.54	-.56	-3.00	312.91	987.27	346.00	7.01	7.38
T24	THERMOCOUPLE	535	T24A	.60	315.2	3.00	-.43	.43	3.00	313.30	988.19	340.00	.98	7.38
T24	THERMOCOUPLE	536	T24B	.61	315.4	1.50	-.43	.43	1.50	313.30	988.20	341.50	2.48	7.38
T24	THERMOCOUPLE	537	T24C	.62	315.6	.00	-.43	.44	.00	313.31	988.20	343.00	3.98	7.38
T24	THERMOCOUPLE	538	T24D	.62	315.7	-1.50	-.44	.45	-1.50	313.31	988.20	344.50	5.48	7.38
T24	THERMOCOUPLE	539	T24E	.63	315.9	-3.00	-.44	.45	-3.00	313.32	988.21	346.00	6.98	7.38
U11	USBM	711	U11	1.51	180.1	.85	-.00	-1.51	.85	311.99	986.71	342.15	3.20	6.88
U11	USBM	712	U11	1.51	180.1	.85	-.00	-1.51	.85	311.99	986.71	342.15	3.20	6.88
U11	USBM	713	U11	1.51	180.1	.85	-.00	-1.51	.85	311.99	986.71	342.15	3.20	6.88
U11	THERMOCOUPLE	427	U11	1.51	180.1	.85	-.00	-1.51	.85	311.99	986.71	342.15	3.20	6.88
U12	USBM	714	U12	3.48	180.2	-.65	-.01	-3.48	-.65	311.03	984.98	343.65	4.71	6.95
U12	USBM	715	U12	3.48	180.2	-.65	-.01	-3.48	-.65	311.03	984.98	343.65	4.71	6.95
U12	USBM	716	U12	3.48	180.2	-.65	-.01	-3.48	-.65	311.03	984.98	343.65	4.71	6.95
U12	THERMOCOUPLE	428	U12	3.48	180.2	-.65	-.01	-3.48	-.65	311.03	984.98	343.65	4.71	6.95
U13	USBM	717	U13	2.26	202.0	-.65	-.85	-2.10	-.65	312.43	985.78	343.65	4.71	6.95
U13	USBM	718	U13	2.26	202.0	-.65	-.85	-2.10	-.65	312.43	985.78	343.65	4.71	6.95
U13	USBM	719	U13	2.26	202.0	-.65	-.85	-2.10	-.65	312.43	985.78	343.65	4.71	6.95

SENSOR LOCATIONS FOR EXPERIMENT 2, FULL SCALE HEATER H10

HOLE ID	SENSOR TYPE	SENSOR NUMBER	SENSOR LABEL	CYLINDRICAL COORDINATES RHO	THETA	Z	LOCAL RECTANGULAR X	Y	Z	MINE RECTANGULAR X	Y	Z	DEPTH	HOLE LENGTH
U13	THERMOCOUPLE	429	U13	2.26	202.0	-.65	-.85	-2.10	-.65	312.43	985.78	343.65	4.71	6.95
U14	USBM	720	U14	3.22	202.0	-.65	-1.21	-2.98	-.65	312.32	984.83	343.65	4.87	7.12
U14	USBM	721	U14	3.22	202.0	-.65	-1.21	-2.98	-.65	312.32	984.83	343.65	4.87	7.12
U14	USBM	722	U14	3.22	202.0	-.65	-1.21	-2.98	-.65	312.32	984.83	343.65	4.87	7.12
U14	THERMOCOUPLE	430	U14	3.22	202.0	-.65	-1.21	-2.98	-.65	312.32	984.83	343.65	4.87	7.12
U15	IRAD GAGE	861	C3	1.71	225.6	-.65	-1.22	-1.20	-.65	313.20	986.38	343.65	4.73	6.92
U15	IRAD GAGE	862	C3	1.71	225.6	-.65	-1.22	-1.20	-.65	313.20	986.38	343.65	4.73	6.92
U15	THERMOCOUPLE	502	C3	1.71	225.6	-.65	-1.22	-1.20	-.65	313.20	986.38	343.65	4.73	6.92
U16	USBM	726	U16	2.77	224.8	.85	-1.95	-1.97	.85	313.46	985.36	342.15	3.26	7.01
U16	USBM	727	U16	2.77	224.8	.85	-1.95	-1.97	.85	313.46	985.36	342.15	3.26	7.01
U16	USBM	728	U16	2.77	224.8	.85	-1.95	-1.97	.85	313.46	985.36	342.15	3.26	7.01
U16	THERMOCOUPLE	432	U16	2.77	224.8	.85	-1.95	-1.97	.85	313.46	985.36	342.15	3.26	7.01
U17	IRAD GAGE	863	C4	2.46	292.7	-.65	-2.27	.95	-.65	315.16	987.75	343.65	4.89	7.13
U17	IRAD GAGE	864	C4	2.46	292.7	-.65	-2.27	.95	-.65	315.16	987.75	343.65	4.89	7.13
U17	THERMOCOUPLE	503	C4	2.46	292.7	-.65	-2.27	.95	-.65	315.16	987.75	343.65	4.89	7.13
U18	USBM	732	U18	1.99	337.9	.85	-.75	1.85	.85	314.27	989.27	342.15	3.31	7.06
U18	USBM	733	U18	1.99	337.9	.85	-.75	1.85	.85	314.27	989.27	342.15	3.31	7.06
U18	USBM	734	U18	1.99	337.9	.85	-.75	1.85	.85	314.27	989.27	342.15	3.31	7.06
U18	THERMOCOUPLE	434	U18	1.99	337.9	.85	-.75	1.85	.85	314.27	989.27	342.15	3.31	7.06
U19	USBM	735	U19	3.00	337.8	.85	-1.14	2.78	.85	315.06	989.90	342.15	3.29	7.04
U19	USBM	736	U19	3.00	337.8	.85	-1.14	2.78	.85	315.06	989.90	342.15	3.29	7.04
U19	USBM	737	U19	3.00	337.8	.85	-1.14	2.78	.85	315.06	989.90	342.15	3.29	7.04
U19	THERMOCOUPLE	435	U19	3.00	337.8	.85	-1.14	2.78	.85	315.06	989.90	342.15	3.29	7.04
U20	USBM	738	U20	4.01	338.2	-.65	-1.49	3.73	-.65	315.83	990.55	343.65	4.80	7.04
U20	USBM	739	U20	4.01	338.2	-.65	-1.49	3.73	-.65	315.83	990.55	343.65	4.80	7.04
U20	USBM	740	U20	4.01	338.2	-.65	-1.49	3.73	-.65	315.83	990.55	343.65	4.80	7.04
U20	THERMOCOUPLE	436	U20	4.01	338.2	-.65	-1.49	3.73	-.65	315.83	990.55	343.65	4.80	7.04
U23	USBM	741	U23	2.50	46.6	.66	1.82	1.72	.66	311.96	990.41	342.34	11.65	13.12
U23	USBM	742	U23	2.50	46.6	.66	1.82	1.72	.66	311.96	990.41	342.34	11.65	13.12
U23	USBM	743	U23	2.50	46.6	.66	1.82	1.72	.66	311.96	990.41	342.34	11.65	13.12
U23	THERMOCOUPLE	437	U23	2.50	46.6	.66	1.82	1.72	.66	311.96	990.41	342.34	11.65	13.12
U24	USBM	744	U24	2.00	90.4	.66	2.00	-.01	.66	310.96	988.99	342.34	8.00	8.93
U24	USBM	745	U24	2.00	90.4	.66	2.00	-.01	.66	310.96	988.99	342.34	8.00	8.93
U24	USBM	746	U24	2.00	90.4	.66	2.00	-.01	.66	310.96	988.99	342.34	8.00	8.93
U24	THERMOCOUPLE	438	U24	2.00	90.4	.66	2.00	-.01	.66	310.96	988.99	342.34	8.00	8.93
U25	USBM	747	U25	2.99	134.5	.62	2.13	-2.09	.62	309.83	987.23	342.38	11.31	13.29
U25	USBM	748	U25	2.99	134.5	.62	2.13	-2.09	.62	309.83	987.23	342.38	11.31	13.29
U25	USBM	749	U25	2.99	134.5	.62	2.13	-2.09	.62	309.83	987.23	342.38	11.31	13.29
U25	THERMOCOUPLE	439	U25	2.99	134.5	.62	2.13	-2.09	.62	309.83	987.23	342.38	11.31	13.29
U29	USBM	750	U29	3.50	67.7	-.85	3.24	1.33	-.85	310.53	990.76	343.85	7.36	9.84
U29	USBM	751	U29	3.50	67.7	-.85	3.24	1.33	-.85	310.53	990.76	343.85	7.36	9.84
U29	USBM	752	U29	3.50	67.7	-.85	3.24	1.33	-.85	310.53	990.76	343.85	7.36	9.84
U29	THERMOCOUPLE	440	U29	3.50	67.7	-.85	3.24	1.33	-.85	310.53	990.76	343.85	7.36	9.84
U30	USBM	753	U30	2.26	112.4	-.83	2.09	-.86	-.83	310.47	988.29	343.83	8.18	9.37
U30	USBM	754	U30	2.26	112.4	-.83	2.09	-.86	-.83	310.47	988.29	343.83	8.18	9.37
U30	USBM	755	U30	2.26	112.4	-.83	2.09	-.86	-.83	310.47	988.29	343.83	8.18	9.37
U30	THERMOCOUPLE	441	U30	2.26	112.4	-.83	2.09	-.86	-.83	310.47	988.29	343.83	8.18	9.37

SENSOR LOCATIONS FOR EXPERIMENT 3, TIME SCALE HEATERS

HOLE ID	SENSOR TYPE	SENSOR NUMBER	SENSOR LABEL	CYLINDRICAL COORDINATES RHO	THETA	Z	LOCAL RECTANGULAR X	Y	Z	MINE RECTANGULAR X	Y	Z	DEPTH	HOLE LENGTH
E1	EXTENSOMETER	1081	E1A	.01	164.3	7.04	.00	-.01	7.04	334.71	959.09	339.96	2.73	13.99
E1	EXTENSOMETER	1082	E1B	.01	186.8	3.04	-.00	-.01	3.04	334.71	959.09	343.96	6.73	13.99
E1	EXTENSOMETER	1083	E1C	.01	195.3	.05	-.00	-.01	.05	334.71	959.09	346.95	9.72	13.99
E1	EXTENSOMETER	1084	E1D	.02	203.3	-2.90	-.01	-.01	-2.90	334.70	959.09	349.90	12.67	13.99
E1	THERMOCOUPLE	902	E1A	.01	186.8	3.10	-.00	-.01	3.10	334.71	959.09	343.90	6.67	13.99
E1	THERMOCOUPLE	903	E1B	.01	187.9	2.10	-.00	-.01	2.10	334.71	959.09	344.90	7.67	13.99
E1	THERMOCOUPLE	904	E1C	.01	191.6	1.10	-.00	-.01	1.10	334.71	959.09	345.90	8.67	13.99
E1	THERMOCOUPLE	905	E1D	.01	195.3	.10	-.00	-.01	.10	334.71	959.09	346.90	9.67	13.99
E1	THERMOCOUPLE	985	E1	.01	144.4	9.77	.00	-.01	9.77	334.72	959.09	337.23	0.	13.99
E1	THERMOCOUPLE	1014	TE1F	.01	164.3	7.10	.00	-.01	7.10	334.71	959.09	339.90	2.67	13.99
E1	THERMOCOUPLE	1015	TE1G	.01	170.5	5.35	.00	-.01	5.35	334.71	959.09	341.65	4.42	13.99
E2	EXTENSOMETER	1085	E2A	1.74	0.	7.01	-.00	1.74	7.01	335.56	957.56	339.99	2.94	14.17
E2	EXTENSOMETER	1086	E2B	1.74	0.	3.02	-.01	1.74	3.02	335.55	957.56	343.98	6.93	14.17
E2	EXTENSOMETER	1087	E2C	1.74	0.	.05	-.01	1.74	.05	335.55	957.56	346.95	9.90	14.17
E2	EXTENSOMETER	1088	E2D	1.74	0.	-2.93	-.01	1.74	-2.93	335.54	957.56	349.93	12.88	14.17
E2	THERMOCOUPLE	906	E2A	1.74	0.	7.07	-.00	1.74	7.07	335.56	957.56	339.93	2.88	14.17
E2	THERMOCOUPLE	907	E2B	1.74	0.	3.07	-.01	1.74	3.07	335.55	957.56	343.93	6.88	14.17
E2	THERMOCOUPLE	908	E2C	1.74	0.	1.07	-.01	1.74	1.07	335.55	957.56	345.93	8.88	14.17
E2	THERMOCOUPLE	909	E2D	1.74	0.	.07	-.01	1.74	.07	335.55	957.56	346.93	9.88	14.17
E2	THERMOCOUPLE	989	E2	1.74	0.	9.95	.00	1.74	9.95	335.56	957.56	337.05	0.	14.17
E3	EXTENSOMETER	1089	E3A	2.61	0.	7.00	.01	2.61	7.00	335.98	956.80	340.00	3.07	14.64
E3	EXTENSOMETER	1090	E3B	2.60	0.	2.98	.00	2.60	2.98	335.98	956.81	344.02	7.09	14.64
E3	EXTENSOMETER	1091	E3C	2.60	0.	.01	.00	2.60	.01	335.98	956.81	346.99	10.06	14.64
E3	EXTENSOMETER	1092	E3D	2.60	0.	-2.97	.00	2.60	-2.97	335.97	956.81	349.97	13.04	14.64
E3	THERMOCOUPLE	910	E3A	2.60	0.	2.98	.00	2.60	2.98	335.98	956.81	344.02	7.09	14.64
E3	THERMOCOUPLE	911	E3B	2.60	0.	2.01	.00	2.60	2.01	335.98	956.81	344.99	8.06	14.64
E3	THERMOCOUPLE	912	E3C	2.60	0.	1.01	.00	2.60	1.01	335.98	956.81	345.99	9.06	14.64
E3	THERMOCOUPLE	913	E3D	2.60	0.	.01	.00	2.60	.01	335.98	956.81	346.99	10.06	14.64
E3	THERMOCOUPLE	993	E3	2.61	0.	10.07	.01	2.61	10.07	335.98	956.80	336.93	0.	14.64
E3	THERMOCOUPLE	1016	TE3F	2.61	0.	7.00	.01	2.61	7.00	335.98	956.80	340.00	3.07	14.64
E3	THERMOCOUPLE	1017	TE3G	2.61	0.	5.23	.00	2.61	5.23	335.98	956.80	341.77	4.84	14.64
E4	EXTENSOMETER	1093	E4A	1.50	269.6	7.01	-1.50	-.01	7.01	333.40	958.37	339.99	2.92	14.57
E4	EXTENSOMETER	1094		1.50	269.8	3.01	-1.50	-.01	3.01	333.40	958.36	343.99	6.92	14.57
E4	EXTENSOMETER	1095		1.50	270.0	-.01	-1.50	-.00	-.01	333.40	958.36	347.01	9.94	14.57
E4	EXTENSOMETER	1096		1.50	270.2	-2.93	-1.50	.00	-2.93	333.40	958.35	349.93	12.86	14.57
E4	THERMOCOUPLE	914	E4A	1.50	269.6	7.07	-1.50	-.01	7.07	333.40	958.37	339.93	2.86	14.57
E4	THERMOCOUPLE	915	E4B	1.50	269.8	3.07	-1.50	-.01	3.07	333.40	958.36	343.93	6.86	14.57
E4	THERMOCOUPLE	916	E4C	1.50	269.9	1.07	-1.50	-.00	1.07	333.40	958.36	345.93	8.86	14.57
E4	THERMOCOUPLE	917	E4D	1.50	270.0	.07	-1.50	-.00	.07	333.40	958.36	346.93	9.86	14.57
E4	THERMOCOUPLE	997	E4	1.50	269.4	9.93	-1.50	-.02	9.93	333.40	958.37	337.07	0.	14.57
E5	EXTENSOMETER	1097		2.31	139.5	6.97	1.50	-1.76	6.97	335.18	961.34	340.03	2.81	14.00
E5	EXTENSOMETER	1098		2.30	139.8	2.96	1.49	-1.76	2.96	335.16	961.34	344.04	6.82	14.00
E5	EXTENSOMETER	1099		2.30	139.9	-.04	1.48	-1.76	-.04	335.16	961.34	347.04	9.82	14.00
E5	EXTENSOMETER	1100		2.29	140.1	-3.00	1.47	-1.76	-3.00	335.15	961.33	350.00	12.78	14.00
E5	THERMOCOUPLE	918	E5A	2.31	139.5	7.00	1.50	-1.76	7.00	335.18	961.34	340.00	2.78	14.00
E5	THERMOCOUPLE	919	E5B	2.30	139.8	3.00	1.49	-1.76	3.00	335.17	961.34	344.00	6.78	14.00
E5	THERMOCOUPLE	920	E5C	2.30	139.9	1.00	1.48	-1.76	1.00	335.16	961.34	346.00	8.78	14.00
E5	THERMOCOUPLE	921	E5D	2.30	139.9	-.00	1.48	-1.76	-.00	335.16	961.34	347.00	9.78	14.00
E5	THERMOCOUPLE	1001	E5	2.31	139.4	9.78	1.51	-1.76	9.78	335.18	961.35	337.22	0.	14.00
H1	HEATER CURRENT	1101												
H1	HEATER VOLTAGE	1102												
H1	HEATER POWER	1103												
H1	HEATER CURRENT	1104												
H1	HEATER VOLTAGE	1105												

SENSOR LOCATIONS FOR EXPERIMENT 3, TIME SCALE HEATERS

HOLE ID	SENSOR TYPE	SENSOR NUMBER	SENSOR LABEL	CYLINDRICAL COORDINATES RHO	THETA	Z	LOCAL RECTANGULAR X	Y	Z	MINE RECTANGULAR X	Y	Z	DEPTH	HOLE LENGTH
H1	HEATER POWER	1106												
H1	HEATER POWER	1107												
H1	CALIPER	1157		3.49	0.	7.09	.00	3.49	7.09	336.41	956.03	339.91	10.22	11.17
H1	CALIPER	1158		3.48	0.	-1.91	.01	3.48	-1.91	336.41	956.04	348.91	10.22	11.17
H1	CALIPER	1159		3.49	0.	10.09	.00	3.49	10.09	336.40	956.03	336.91	10.22	11.17
H1	CALIPER	1160		3.49	0.	10.09	.00	3.49	10.09	336.40	956.03	336.91	10.37	11.17
H1	CALIPER	1161		3.49	0.	10.09	.00	3.49	10.09	336.40	956.03	336.91	10.37	11.17
H1	CALIPER	1162		3.49	0.	10.09	.00	3.49	10.09	336.40	956.03	336.91	10.37	11.17
H1	THERMOCOUPLE	982	TH1A	3.49	0.	.00	.01	3.49	.00	336.41	956.04	347.00	10.09	11.17
H1	THERMOCOUPLE	983	TH1B	3.49	0.	.00	.01	3.49	.00	336.41	956.04	347.00	10.09	11.17
H1	THERMOCOUPLE	984	TH1C	3.49	0.	.91	.01	3.49	.91	336.41	956.04	346.09	9.18	11.17
H2	HEATER CURRENT	1108												
H2	HEATER VOLTAGE	1109												
H2	HEATER POWER	1110												
H2	HEATER CURRENT	1111												
H2	HEATER VOLTAGE	1112												
H2	HEATER POWER	1113												
H2	HEATER POWER	1114												
H2	THERMOCOUPLE	986	TH2A	10.48	0.	0.	-.01	10.48	0.	339.78	949.91	347.00	10.44	11.77
H2	THERMOCOUPLE	987	TH2B	10.48	0.	0.	-.01	10.48	0.	339.78	949.91	347.00	10.44	11.77
H2	THERMOCOUPLE	988	TH2C	10.48	0.	.92	-.01	10.48	.92	339.78	949.91	346.08	9.52	11.77
H3	HEATER CURRENT	1115												
H3	HEATER VOLTAGE	1116												
H3	HEATER POWER	1117												
H3	HEATER CURRENT	1118												
H3	HEATER VOLTAGE	1119												
H3	HEATER POWER	1120												
H3	HEATER POWER	1121												
H3	WEIGHING PAN	1165		3.51	179.9	9.73	.01	-3.51	9.73	333.02	962.16	337.27	10.10	10.83
H3	WEIGHING PAN	1166		3.51	179.9	9.73	.01	-3.51	9.73	333.02	962.16	337.27	10.10	10.83
H3	WEIGHING PAN	1167		3.51	179.9	9.73	.01	-3.51	9.73	333.02	962.16	337.27	10.10	10.83
H3	THERMOCOUPLE	990	TH3A	3.47	180.0	0.	.00	-3.47	0.	333.04	962.12	347.00	9.73	10.83
H3	THERMOCOUPLE	991	TH3B	3.47	180.0	0.	.00	-3.47	0.	333.04	962.12	347.00	9.73	10.83
H3	THERMOCOUPLE	992	TH3C	3.47	179.9	.91	.00	-3.47	.91	333.04	962.12	346.09	8.82	10.83
H4	HEATER CURRENT	1122												
H4	HEATER VOLTAGE	1123												
H4	HEATER POWER	1124												
H4	HEATER CURRENT	1125												
H4	HEATER VOLTAGE	1126												
H4	HEATER POWER	1127												
H4	HEATER POWER	1128												
H4	THERMOCOUPLE	994	TH4A	10.50	180.0	.00	-.00	-10.50	.00	329.64	968.27	347.00	9.65	10.55
H4	THERMOCOUPLE	995	TH4B	10.50	180.0	.00	-.00	-10.50	.00	329.64	968.27	347.00	9.65	10.55
H4	THERMOCOUPLE	996	TH4C	10.50	180.0	.91	-.00	-10.50	.91	329.64	968.27	346.09	8.74	10.55
H5	HEATER CURRENT	1129												
H5	HEATER VOLTAGE	1130												
H5	HEATER POWER	1131												
H5	HEATER CURRENT	1132												
H5	HEATER VOLTAGE	1133												
H5	HEATER POWER	1134												
H5	HEATER POWER	1135												

SENSOR LOCATIONS FOR EXPERIMENT 3, TIME SCALE HEATERS

HOLE ID	SENSOR TYPE	SENSOR NUMBER	SENSOR LABEL	CYLINDRICAL COORDINATES RHO	THETA	Z	LOCAL RECTANGULAR X	Y	Z	MINE RECTANGULAR X	Y	Z	DEPTH	HOLE LENGTH
H5	THERMOCOUPLE	998	TH5A	4.58	41.4	0.	3.03	3.44	0.	339.03	957.54	347.00	9.90	11.07
H5	THERMOCOUPLE	999	TH5B	4.58	41.4	0.	3.03	3.44	0.	339.03	957.54	347.00	9.90	11.07
H5	THERMOCOUPLE	1000	TH5C	4.58	41.4	.91	3.03	3.44	.91	339.03	957.54	346.09	8.99	11.07
H6	HEATER CURRENT	1136												
H6	HEATER VOLTAGE	1137												
H6	HEATER POWER	1138												
H6	HEATER CURRENT	1139												
H6	HEATER VOLTAGE	1140												
H6	HEATER POWER	1141												
H6	HEATER POWER	1142												
H6	THERMOCOUPLE	1002	TH6A	4.65	139.5	0.	3.02	-3.54	0.	335.64	963.64	347.00	9.78	10.80
H6	THERMOCOUPLE	1003	TH6B	4.65	139.5	0.	3.02	-3.54	0.	335.64	963.64	347.00	9.78	10.80
H6	THERMOCOUPLE	1004	TH6C	4.65	139.5	.91	3.02	-3.53	.91	335.64	963.63	346.09	8.87	10.80
H7	HEATER CURRENT	1143												
H7	HEATER VOLTAGE	1144												
H7	HEATER POWER	1145												
H7	HEATER CURRENT	1146												
H7	HEATER VOLTAGE	1147												
H7	HEATER POWER	1148												
H7	HEATER POWER	1149												
H7	THERMOCOUPLE	1006	TH7A	4.61	319.4	0.	-3.00	3.50	0.	333.78	954.57	347.00	9.97	11.18
H7	THERMOCOUPLE	1007	TH7B	4.61	319.4	0.	-3.00	3.50	0.	333.78	954.57	347.00	9.97	11.18
H7	THERMOCOUPLE	1008	TH7C	4.61	319.4	.91	-3.00	3.50	.91	333.78	954.57	346.09	9.06	11.18
H8	HEATER CURRENT	1150												
H8	HEATER VOLTAGE	1151												
H8	HEATER POWER	1152												
H8	HEATER CURRENT	1153												
H8	HEATER VOLTAGE	1154												
H8	HEATER POWER	1155												
H8	HEATER POWER	1156												
H8	THERMOCOUPLE	1010	TH8A	4.65	220.0	0.	-2.99	-3.56	0.	330.37	960.75	347.00	9.83	10.92
H8	THERMOCOUPLE	1011	TH8B	4.65	220.0	0.	-2.99	-3.56	0.	330.37	960.75	347.00	9.83	10.92
H8	THERMOCOUPLE	1012	TH8C	4.65	220.0	.91	-2.99	-3.56	.91	330.37	960.75	346.09	8.92	10.92
T1	THERMOCOUPLE	922	T1E	.95	181.1	-2.00	-.02	-.95	-2.00	334.24	959.91	349.00	11.86	13.22
T1	THERMOCOUPLE	923	T1A	.92	180.2	5.00	-.00	-.92	5.00	334.27	959.88	342.00	4.86	13.22
T1	THERMOCOUPLE	924	T1C	.94	180.7	1.00	-.01	-.94	1.00	334.25	959.90	346.00	8.86	13.22
T1	THERMOCOUPLE	925	T1B	.93	180.5	3.00	-.01	-.93	3.00	334.26	959.89	344.00	6.86	13.22
T1	THERMOCOUPLE	926	T1D	.94	180.9	.00	-.01	-.94	.00	334.25	959.90	347.00	9.86	13.22
T2	THERMOCOUPLE	927	T2E	1.79	180.1	-2.01	-.00	-1.79	-2.01	333.85	960.65	349.01	11.75	12.86
T2	THERMOCOUPLE	928	T2D	1.79	180.1	-.01	-.00	-1.79	-.01	333.85	960.64	347.01	9.75	12.86
T2	THERMOCOUPLE	929	T2C	1.78	180.1	.99	-.00	-1.78	.99	333.85	960.64	346.01	8.75	12.86
T2	THERMOCOUPLE	930	T2B	1.78	180.0	3.00	-.00	-1.78	3.00	333.85	960.64	344.01	6.75	12.86
T2	THERMOCOUPLE	931	T2A	1.77	180.0	5.00	.00	-1.77	5.00	333.86	960.64	342.01	4.75	12.86
T3	THERMOCOUPLE	932	T3E	2.58	177.9	-2.00	.10	-2.58	-2.00	333.55	961.38	349.00	11.69	12.79
T3	THERMOCOUPLE	933	T3D	2.59	178.2	0.	.08	-2.59	0.	333.53	961.38	347.00	9.69	12.79
T3	THERMOCOUPLE	934	T3C	2.59	178.4	1.00	.07	-2.59	1.00	333.52	961.39	346.00	8.69	12.79
T3	THERMOCOUPLE	935	T3B	2.60	178.7	3.00	.06	-2.60	3.00	333.51	961.39	344.00	6.69	12.79
T3	THERMOCOUPLE	936	T3A	2.61	179.1	5.00	.04	-2.61	5.00	333.49	961.39	342.00	4.69	12.79
T4	THERMOCOUPLE	937	T4E	3.66	166.1	-2.00	.88	-3.56	-2.00	333.77	962.62	349.00	11.69	12.82
T4	THERMOCOUPLE	938	T4D	3.66	166.1	0.	.88	-3.55	0.	333.77	962.61	347.00	9.69	12.82
T4	THERMOCOUPLE	939	T4C	3.65	166.1	1.00	.88	-3.54	1.00	333.77	962.61	346.00	8.69	12.82
T4	THERMOCOUPLE	940	T4B	3.64	166.0	3.00	.88	-3.54	3.00	333.77	962.60	344.00	6.69	12.82
T4	THERMOCOUPLE	941	T4A	3.64	166.1	5.00	.88	-3.53	5.00	333.77	962.60	342.00	4.69	12.82
T5	THERMOCOUPLE	942	T5E	2.24	40.8	-3.00	1.46	1.70	-3.00	336.82	958.31	350.00	12.76	13.99

SENSOR LOCATIONS FOR EXPERIMENT 3, TIME SCALE HEATERS

HOLE ID	SENSOR TYPE	SENSOR NUMBER	SENSOR LABEL	CYLINDRICAL COORDINATES RHO	THETA	Z	LOCAL RECTANGULAR X	Y	Z	MINE RECTANGULAR X	Y	Z	DEPTH	HOLE LENGTH
T5	THERMOCOUPLE	943	T5D	2.25	40.8	0.	1.47	1.71	0.	336.83	958.30	347.00	9.76	13.99
T5	THERMOCOUPLE	944	T5C	2.27	40.8	4.00	1.48	1.72	4.00	336.85	958.30	343.00	5.76	13.99
T5	THERMOCOUPLE	945	T5B	2.28	40.8	6.00	1.49	1.72	6.00	336.85	958.30	341.00	3.76	13.99
T5	THERMOCOUPLE	946	T5A	2.29	40.9	8.00	1.50	1.73	8.00	336.86	958.29	339.00	1.76	13.99
T6	THERMOCOUPLE	947	T6E	3.78	23.5	-2.00	1.51	3.47	-2.00	337.71	956.78	349.00	12.06	13.28
T6	THERMOCOUPLE	948	T6D	3.78	23.5	0.	1.51	3.47	0.	337.71	956.78	347.00	10.06	13.28
T6	THERMOCOUPLE	949	T6C	3.78	23.5	1.00	1.51	3.47	1.00	337.71	956.78	346.00	9.06	13.28
T6	THERMOCOUPLE	950	T6B	3.78	23.4	3.00	1.51	3.47	3.00	337.71	956.77	344.00	7.06	13.28
T6	THERMOCOUPLE	951	T6A	3.79	23.4	5.00	1.51	3.47	5.00	337.71	956.77	342.00	5.06	13.28
T7	THERMOCOUPLE	952	T7E	3.86	157.4	-2.00	1.48	-3.57	-2.00	334.29	962.92	349.00	11.67	12.81
T7	THERMOCOUPLE	953	T7D	3.86	157.3	0.	1.49	-3.56	0.	334.30	962.92	347.00	9.67	12.81
T7	THERMOCOUPLE	954	T7C	3.85	157.2	1.00	1.49	-3.55	1.00	334.30	962.91	346.00	8.67	12.81
T7	THERMOCOUPLE	955	T7B	3.84	157.1	3.00	1.49	-3.54	3.00	334.31	962.90	344.00	6.67	12.81
T7	THERMOCOUPLE	956	T7A	3.84	157.0	5.00	1.50	-3.53	5.00	334.32	962.90	342.00	4.67	12.81
T8	THERMOCOUPLE	957	T8E	3.72	194.1	-2.00	-.91	-3.61	-2.00	332.17	961.80	349.00	11.67	12.76
T8	THERMOCOUPLE	958	T8D	3.70	194.1	0.	-.90	-3.59	0.	332.19	961.79	347.00	9.67	12.76
T8	THERMOCOUPLE	959	T8C	3.69	194.1	1.00	-.90	-3.58	1.00	332.20	961.78	346.00	8.67	12.76
T8	THERMOCOUPLE	960	T8B	3.68	194.0	3.00	-.89	-3.57	3.00	332.21	961.77	344.00	6.67	12.76
T8	THERMOCOUPLE	961	T8A	3.66	194.0	5.00	-.88	-3.55	5.00	332.22	961.76	342.00	4.67	12.76
T9	THERMOCOUPLE	962	T9E	3.81	336.7	-2.00	-1.50	3.50	-2.00	335.09	955.30	349.00	11.92	13.54
T9	THERMOCOUPLE	963	T9D	3.80	336.7	0.	-1.50	3.49	0.	335.09	955.30	347.00	9.92	13.54
T9	THERMOCOUPLE	964	T9C	3.80	336.7	1.00	-1.50	3.49	1.00	335.09	955.30	346.00	8.92	13.54
T9	THERMOCOUPLE	965	T9B	3.80	336.7	3.00	-1.50	3.49	3.00	335.09	955.30	344.00	6.92	13.54
T9	THERMOCOUPLE	966	T9A	3.80	336.8	5.00	-1.50	3.49	5.00	335.09	955.30	342.00	4.92	13.54
T10	THERMOCOUPLE	967	T10E	2.24	319.8	-2.65	-1.45	1.71	-2.65	334.28	956.89	349.65	12.63	13.10
T10	THERMOCOUPLE	968	T10D	2.25	319.6	.05	-1.46	1.71	.05	334.27	956.88	346.95	9.93	13.10
T10	THERMOCOUPLE	969	T10C	2.27	319.5	3.95	-1.47	1.72	3.95	334.26	956.86	343.05	6.03	13.10
T10	THERMOCOUPLE	970	T10B	2.27	319.4	5.95	-1.48	1.73	5.95	334.26	956.86	341.05	4.03	13.10
T10	THERMOCOUPLE	971	T10A	2.28	319.3	7.95	-1.49	1.73	7.95	334.25	956.85	339.05	2.03	13.10
T11	THERMOCOUPLE	972	T11E	2.25	218.5	-3.00	-1.40	-1.76	-3.00	332.64	959.94	350.00	12.76	13.98
T11	THERMOCOUPLE	973	T11D	2.26	219.0	0.	-1.42	-1.76	0.	332.62	959.94	347.00	9.76	13.98
T11	THERMOCOUPLE	974	T11C	2.29	219.5	4.00	-1.45	-1.76	4.00	332.59	959.92	343.00	5.76	13.98
T11	THERMOCOUPLE	975	T11B	2.30	219.8	6.00	-1.47	-1.76	6.00	332.57	959.92	341.00	3.76	13.98
T11	THERMOCOUPLE	976	T11A	2.31	220.1	8.00	-1.49	-1.77	8.00	332.56	959.91	339.00	1.76	13.98
T12	THERMOCOUPLE	977	T12E	3.84	202.5	-2.00	-1.47	-3.55	-2.00	331.71	961.48	349.00	11.77	12.93
T12	THERMOCOUPLE	978	T12D	3.84	202.6	0.	-1.47	-3.54	0.	331.71	961.47	347.00	9.77	12.93
T12	THERMOCOUPLE	979	T12C	3.84	202.6	1.00	-1.48	-3.54	1.00	331.71	961.47	346.00	8.77	12.93
T12	THERMOCOUPLE	980	T12B	3.83	202.7	3.00	-1.48	-3.53	3.00	331.71	961.46	344.00	6.77	12.93
T12	THERMOCOUPLE	981	T12A	3.83	202.8	5.00	-1.49	-3.53	5.00	331.71	961.45	342.00	4.77	12.93

APPENDIX B. Sensor Parameter File

Description of File

The sensor parameter file is the master computer record of information on all sensors in the Stripa experiment. Each sensor is assigned an individual record containing 90 fields. These labeled fields contain numerical or alphanumerical information such as calibration values and input channels. These parameters are for use both as a general record and for executing the graphics and engineering conversion computer programs.

File Input

Much of the file input can be performed before computer facilities are set up in the field; however, corrections, changes, calibration data, exact instrument locations (coordinates and depths), and sensor activation must be performed in the field. Details of the sensor parameter program activation and workings are given by Teknekron, Inc. (1978). The following information concerning each field is of note.

Field 1	Record No.	A permanent field and identifying tag of this record. This field's value is the sensor's disc record number in the long-term data file.
Field 2	Active Sensor	Activates sensor for wide record scans on a timed interval to be activated only by site personnel.
Field 3	Sensor Name	Identifies sensor type.
Field 4	Qualifier Note	Identifies if sensor has been placed in another hole, is used for temperature correction, or uses data from another sensor (dummy thermocouples).

Field 8	Pair/Length Code	Indicates component number of instruments with more than one sensor.
Field 9	Input Channel	Identifies REMAC channel number.
Field 10	REMAC Number	Identifies REMAC unit.
Field 11	Data Logger	Identifies data logger unit.
Field 12	Experiment Code	Indicates which experiment sensor is associated with.
Field 13	Hole I.D.	Indicates hole number in which sensor was placed.
Field 14, 15, 16	Sensor's Cylindrical Coordinates	Local coordinates: rho, theta, and z, in m.
Field 17	Depth	Distance from sensor to borehole top.
Field 18	Engineering Units	Indicates units to which sensor output is converted: for USBM = mm, IRAD = MPa, extensometer = mm, thermocouples = ^{o}C.
Field 19	Quantity	Indicates quantity measured by instrument: for USBM = displacement, IRAD = stress, extensometer = displacement, thermocouples = temperature.
Field 22	Temperature @ Time Zero	For USBM, IRAD, and extensometers = ambient rock temperature.
Field 24	Diameter	Indicates hole diameter for USBM gages, in mm.
Field 25, 26, 27		Indicates record numbers of associated sensors (excluding thermocouples in borehole, not needed for thermocouple records).
Field 28, 29, 30, 31, 32		Indicates record numbers of associated thermocouples (for USBM and IRAD gages and extensometer thermocouples only).

Field 38, 39, 40	Sensor's Local X, Y, Z Coordinates	Used only for graphics - calculated by sensor parameter program from the local cylindrical coordinates (fields 14-16).
Field 44	Orientation Code	Indicates hole orientation (vertical or horizontal for extensometers).
Field 51	Sensor Calibration (T or F)	Indicates if sensor has been calibrated.
Field 54	Zero Offset	Indicates zero (starting) voltage for extemsometer DCDTs and USBM gages, indicates zero reading for IRAD gages.
Field 55	Rezero Offset	Indicates USBM gage voltage with buttons removed.
Field 57	Slope	Calibration slope: for DCDTs and USBM = mm/volt.
Field 58	Coefficient A	Calibration coefficient: for USBM gages = coefficient of thermal expansion (gage); IRAD gages = coefficient $C_1(23)$; thermocouples = X° term coefficient.
Field 59	Coefficient B	Calibration coefficient: for USBM gages = coefficient of thermal expansion (rock); IRAD gages = coefficient $C_2(23)$; thermocouples = X^1 term coefficient.
Field 60, 61, 62	Coefficient C, D, E	Calibration coefficient: for thermocouple X^2, X^3, and X^4 terms.
Field 80	Data Logger Channel	Indicates sensor's data logger channel.
Field 86	Temperature Correction Const.	Indicates voltage offset for USBM gages between ambient temperature and 200°C.

APPENDIX C. Properties of Pressurizing Fluids for Extensometer Anchors

Properties of Heat Transfer of Fluids

Table C-1 shows a comparison of five heat-transfer oils tested for thermal degradation in a study by Seifert, Jackson, and Sech (1972). These tests were conducted on samples placed in a sealed stainless steel tube purged by nitrogen gas. Following the test periods at the indicated temperatures, the samples were cooled in dry ice and removed for examination and testing. Table C-1 indicates the percentage of the sample lost (handling losses are less than 4% by volume) and the physical states present in the sample.

A comparison of the physical properties of several heat-transfer fluids is shown in Table C-2. The comparison shows surprising similarities between the six oils with the exception of Dowtherm A, which exhibits a high freezing point and a relatively low fire point. Thermal expansion curves for several heat-transfer fluids, as shown in Fig.C-1, also indicate few differences.

Table C-1. Thermal degradation of five heat-transfer oils.

Compound	Test length (weeks)	Temperature (°C)	Sample lost (%)	Physical state*	Color
Therminol 66	0	--	--	L	Yellow
	8	343	2.5	L	Brown
	2	371	10.6	L	Brown
	4	371	10.3	L	Brown
	2	385	9.4	L	Brown
	4	385	11.9	L	Black
	1	399	42.7	L & S	Black
Dowtherm A	0	--	--	L	Lt. Yellow
	3	413	1.9	L	Yellow
Dowtherm G	0	--	--	L	Yellow
	8	343	2-4	L	Brown
	4	371	2-4	L	Brown
	3	399	2-4	L	Brown
	3	413	2-4	L	Brown
Humbletherm 500	0	--	--	L	Yellow
	2	343	8.3	L	Brown
	4	343	57.6	L & S	Brown
Mobiltherm 500	0	--	--	L	Brown
	2	343	8.5	L	Brown
	4	343	77.2	L & S	Brown

*L = liquid, S = solid.

Table C-2. Physical properties of heat-transfer fluids.

Oil type	Freeze (F) or pour (P) E- point	Flash point (°C)	Fire point (°C)	Auto ignition temp. (°C)	Recommended use range (°C)
Dowtherm A--73.5% Dipheryl oxide, 26.5% Biphonyl	12.0 (F)	116	135	621	16 to 400
Dowtherm G--Mix of di- and triaryl ethers	-30.0 (P)	133	157	554	4 to 340
Mobiltherm 600--Petroleum based mineral oil	-18.0 (P)	177	--	--	Up to 316
Caloria HT-43	- 9.0 (P)	204	--	--	Up to 316 (to 191 when air is present)
Dow Corning X2-1162--Silicone based	5.0 (F)	154	199	--	
Therminol 66--Modified Terphenyl	-28.0	180	194	374	0 to 340

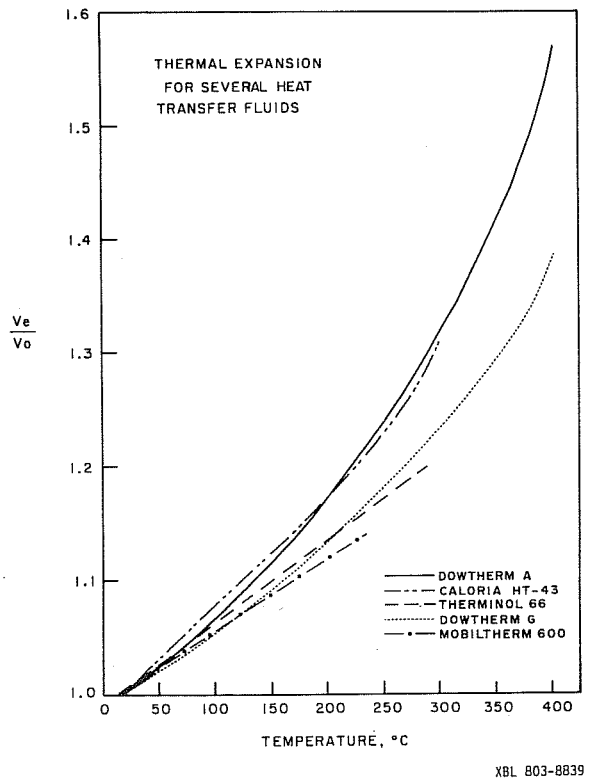

Fig. C-1. Thermal expansion for several heat-transfer fluids.

APPENDIX D. Extensometer Calibration Data

Appendix D shows voltage offsets V_0 (volts) and calibration coefficients C (mm/volt) for the 35 extensometers in the time-scale and full-scale experiments. The first triplet gives the coefficients for the anchor nearest the collar, the fourth triplet for the anchor farthest from the collar. Hence, each of the columns gives data for comparable rod lengths.

		Sensor number	V_o	C	Sensor number	V_o	C	Sensor number	V_o	C	Sensor number	V_o	C
	E1	1081	-1.2600	2.1766	1082	-1.2375	2.1303	1083	-1.2300	2.1406	1084	-1.2438	2.1217
TS	E2	1085	-1.4188	2.2111	1086	-1.2800	2.1394	1087	-1.2950	2.1196	1088	-1.3100	2.1210
	E3	1089	-1.2363	2.1351	1090	-1.2250	2.1247	1091	-1.2613	2.1383	1092	-1.1850	2.1042
	E4	1093	-1.3200	2.1476	1094	-1.2813	2.1056	1095	-1.2300	2.1216	1096	-1.2300	2.1295
	E5	1097	-1.2525	2.1258	1098	-1.2763	2.1274	1099	-1.2300	2.1207	1100	-1.2050	2.1011
	E6	291	-1.2350	2.2220	292	-1.1638	2.1869	293	-1.1313	2.1674	294	-1.1688	2.1618
	E7	295	-1.1613	2.1642	296	-1.1338	2.1670	297	-1.1013	2.1487	298	-1.3363	2.2207
	E8	299	-1.2913	2.2467	300	-1.1625	2.1654	301	-1.1913	2.1797	302	-1.1113	2.1469
H9	E9	303	-1.1413	2.1710	304	-1.1213	2.1575	305	-1.1313	2.1532	306	-1.1438	2.1572
Vertical	E10	307	-1.2263	2.2143	308	-1.0150	2.1486	309	-1.1400	2.1658	310	-1.1238	2.1464
	E11	311	-0.0373	2.3353	312	-0.0277	2.4546	313	-0.0205	2.2141	314	-0.0103	2.5510
	E12	802	-1.2540	2.2273	803	-1.1038	2.1148	804	-0.9438	2.1017	801	-1.4300	2.2205
	E13	805	-1.1713	2.1996	806	-1.1500	2.6272	807	-1.0638	2.1488	808	-1.0638	2.1365
	E14	809	-1.0913	2.1787	810	-1.0425	2.1295	811	-0.9169	2.1104	812	-1.0263	2.1270
H10	E15	813	-1.1063	2.1912	816	-1.0050	2.1334	815	-1.0363	2.1363	814	-1.0688	2.1278
Vertical	E16	817	-1.3513	2.2586	818	-1.0900	2.1698	819	-1.0975	2.1489	820	-1.0650	2.1683
	E17	821	-1.1213	2.1555	822	-1.0300	2.1312	823	-1.0300	2.0985	824	-1.0550	2.1295
	E18	315	-1.1525	2.1669	318	-1.0363	2.1270	317	-1.1338	2.1626	316	-1.1400	2.1533
	E19	322	-1.1963	2.1829	319	-1.2350	2.2116	320	-1.1950	2.1688	321	-1.0950	2.1422
	E20	323	-1.2075	2.1963	324	-1.0575	2.1489	325	-1.1363	2.1734	326	-1.1325	2.1734
	E21	327	-1.1650	2.1852	328	-1.0875	2.1590	329	-1.1213	2.1648	330	-1.1663	2.1640
H9	E22	331	-1.1125	2.1878	332	-1.1225	2.1694	333	-1.0913	2.1476	334	-1.0925	2.1537
Hori-	E23	335	-1.1888	2.1871	336	-1.2263	2.1655	337	-1.2300	2.1995	338	-1.2400	2.1627
zontal	E24	341	-1.0750	2.1454	340	-1.1200	2.1505	339	-1.2138	2.1820	342	-1.1050	2.1379
	E25	343	-1.0750	2.1645	344	-1.1263	2.1657	345	-1.1063	2.1543	346	-1.0563	2.1231
	E26	347	-1.1250	2.1800	348	-1.0825	2.1608	349	-1.1313	2.1569	350	-1.0725	2.1486
	E27	825	-1.0963	2.1836	826	-1.0825	2.1808	827	-1.0600	2.1639	828	-1.0788	2.1490
	E28	829	-1.1625	2.1673	830	-1.1938	2.1898	831	-1.1100	2.1591	832	-1.0075	2.1091
	E29	833	-0.8588	2.1418	834	-0.8431	2.1515	835	-0.8969	2.1244	836	-0.8188	2.1100
	E30	837	-1.2100	2.2057	838	-1.1775	2.1972	839	-1.1888	2.1616	840	-1.1613	2.1659
H10	E31	841	-1.1350	2.1768	844	-1.0788	2.1398	842	-1.1588	2.1768	843	-1.1475	2.1775
hori-	E32	845	-1.1013	2.1833	846	-1.0863	2.1604	847	-1.1200	2.1694	848	-1.0400	2.1409
zontal	E33	849	-1.1388	2.1895	850	-1.0438	2.1305	851	-1.0300	2.1231	852	-1.0513	2.1262
	E34	853	-1.1875	2.1849	854	-1.2000	2.1814	855	-1.1313	2.1584	856	-1.1213	2.1534
	E35	857	-1.0425	2.1425	858	-1.1113	2.1750	859	-1.0375	2.1248	860	-0.9763	2.1125

APPENDIX E. USBM Gage Test Data, Calibration Data, and Error Analysis

Table E-1 summarizes all laboratory calibrations of gage displacement versus output, using the procedures described in the text. Indicated from left to right are: 1) the test identification, 2) the serial number of the tested gage, 3) the gage component tested, 4) the range of displacement (inches) over which the gage was tested, 5) the incremental displacements (inches) for which gage output was recorded, 6) the temperature at which the calibration was performed, and 7) the slope or calibration factor (inches/unit strain reading) determined by a linear regression fit to the recorded data for both loading and unloading.

In Table E-2, the change with time in voltage readings of a gage installed in an aluminum pipe is noted with respect to an initial time zero reading. Time zero readings were taken after allowing a few hours for temperature equilibration at the test temperature shown.

The offset voltages shown in Table E-3 were recorded at four temperatures, with buttons removed from the gages. A least squares fit of the offset voltages was used to establish $V_1 - V_0$. V_0 was again measured just before installation at ambient temperature with the buttons removed. The starting voltage V_s was averaged from several readings over a 2-day period prior to turn on. The slope C was established at ambient temperature using the calibration fixture. All voltages are given in millivolts, C is given in millimeters per millivolt.

Table E-1. USBM gage-temperature calibration listing.

Run no.	Gage no.	Component no.	Loading range (inches)	Loading increments. (inches)	Temp (°C)	Calibration factor (inches/strain)
1	401	1	0 to 0 032	0.002	23	0.993 (L) 0.985 (U)
2	401	2	0 to 0.020	0.002	23	0.988 (L) 0.992 (U)
3	401	3	0 to 0.032	0.002	23	0.995 (L) 0.992 (L) 0.981 (U)
4	401	3	0 to 0.020	0.004	23	0.989 (L) 0.984 (U)
5	401	1	0 to 0.032	0.002	50	0.995 (L) 0.984 (U)
6	401	1	0 to 0.032	0.002	104	1.015 (L) 1.011 (U)
7	401	1	0 to 0.032	0.004	104	1.030 (L) 1.025 (U) 1.015 (L) 1.018 (U) 1.021 (L) 1.010 (U)
8	401	2	0 to 0.032	0.004	104	1.024 (L) 1.022 (U) 1.008 (L) 0.999 (U)
9	401	3	0 to 0.032	0.004	104	1.027 (L) 1.024 (U) 1.022 (L) 1.019 (U)
10	401	1	0 to 0.032	0.002	146	1.018 (L) 1.021 (U)
11	401	1	0 to 0.032	0.002	194	1.043 (U)
12	401	1	0 to 0.032	0.004	199	1.080 (L) 1.050 (U)
13	401	1	0 to 0.032	0.004	197	1.049 (L) 1.037 (U) 1.046 (L) 1.033 (U)
14	401	2	0 to 0.032	0.004	197	1.050 (L) 1.041 (U) 1.040 (L) 1.034 (U)
15	401	3	0 to 0.032	0.004	197	1.037 (L) 1.036 (U) 1.037 (L) 1.034 (U)

*(L) = loading, (U) = unloading.

(continued)

Table E-1 (continued)

Run no.	Gage no.	Component no.	Loading range (inches)	Loading increments (inches)	Temp (°C)	Calibration factor (inches/strain)
16	401	1	0 to 0.032	0.008	23	0.994 (L) 0.996 (U)
17	401	2	0 to 0.032	0.008	23	0.990 (L) 0.967 (U)
18	401	3	0 to 0.032	0.008	23	0.992 (L) 0.980 (U)
19	401	1	0 to 0.032	0.008	51	1.004 (U)
20	401	1	0 to 0.032	0.008	102	1.054 (L) 1.020 (U)
21	401	2	0 to 0.032	0.008	102	1.053 (L) 1.019 (U)
22	401	3	0 to 0.032	0.008	102	1.142 (L) 1.040 (L)
23	401	1	0 to 0.032	0.008	150	1.031 (L) 1.019 (U)
24	401	2	0 to 0.032	0.008	150	1.033 (L) 1.022 (U)
25	401	3	0 to 0.032	0.008	150	1.086 (L) 1.080 (U)
26	401	1	0 to 0.032	0.008	199	1.089 (L) 1.046 (U)
27	428	1	0 to 0.032	0.002	23	0.995 (L) 0.987 (U) 0.994 (L) 0.989 (U) 0.988 (L) 0.980 (U) 0.983 (L) 0.982 (U) 0.986 (L) 0.984 (U) 0.986 (L) 0.983 (U)
28	428	2	0 to 0.032	0.002	23	0.966 (L) 0.955 (U) 0.962 (L) 0.959 (U)
29	428	3	0 to 0.032	0.002	23	1.016 (L) 1.007 (U) 1.012 (L) 1.007 (U)

*(L) = loading, (U) = unloading.

Table E-1 (concluded)

Run no.	Gage no.	Component no.	Loading range (inches)	Loading increments (inches)	Temp (°C)	Calibration factor (inches/strain)
30	428	1	0 to 0.032	0.004	184	1.048 (L) 1.050 (U) 1.025 (U) 1.049 (U)
31	428	2	0 to 0.032	0.004	184	1.002 (L) 1.027 (L) 0.999 (U)
32	428	3	0 to 0.032	0.004	184	1.026 (U) 1.033 (L) 1.062 (L) 1.011 (U) 1.064 (U)

*(L) = loading, (U) = unloading.

Table E-2. USBM gage-drift measurements.

Time (hours)	Temperature (°C)	Change in component (mV)) #1	#2	#3
0	23	0	0	0
1/2	"	-0.11	0	+0.11
2-1/4	"	-0.11	0	+0.11
3-1/4	"	-0.11	0	+0.11
4-3/4	"	-0.11	0	+0.11
0	52	0	0	0
16-1/2	"	+0.05	+0.03	-0.03
18-1/2	"	+0.04	+0.03	-0.03
23-1/2	"	+0.05	+0.03	-0.03
0	102	0	0	0
1/2	"	-0.01	0	0
2	"	-0.01	-0.01	0
3	"	-0.01	-0.04	0
4	"	-0.01	0	0
5	"	-0.01	0	0
6	"	-0.01	0	0
7	"	-0.01	0	0
21-1/2	"	-0.01	0	0
0	147	0	0	0
3-1/2	"	+0.04	+0.09	+0.08
4-1/2	"	+0.03	+0.09	+0.08
6-1/2	"	+0.01	+0.08	+0.08
7-1/2	"	+0.01	+0.08	+0.12
0	188	0	0	0
3	"	-0.01	+0.01	+0.01
5	"	-0.04	-0.07	-0.06
0	192	0	0	0
1-1/2	"	0	+0.01	0
44	"	-0.03	-0.06	-0.03
92	"	-0.04	-0.08	-0.04
114	"	-0.04	-0.08	-0.04

Table E-3. USBM gage offset measurements. (H9)

Number			Offset voltages (mV)				Voltage			Slope
Gage (hole)	Sensor number	Component	12°C	87°C	137°C	190°C	V_0† (mV)	V_1-V_0†† (mV)	V_s§ (mV)	C $\frac{mm}{mV}$
U1	201	1	0.063	-0.043	-0.192	-0.219	0.106	-0.320	7.471	0.0686
	202	2	-0.063	-0.104	-0.156	-0.192	-0.038	-0.140	7.578	0.0665
	203	3	2.395	2.435	2.465	2.478	2.445	0.090	10.732	0.0662
U2	204	1	0.205	0.199	0.202	0.217	0.207	0.012	5.571	0.0658
	205	2	0.134	0.140	0.095	0.090	0.188	-0.054	5.947	0.0657
	206	*3	---	---	---	---	0.445	---	6.772	0.0649
U3	207	1	-0.109	-0.079	-0.046	-0.041	-0.11	0.076	7.041	0.0645
	208	2	2.111	2.100	2.068	2.072	2.14	-0.047	7.627	0.0656
	209	3	-0.295	-0.307	-0.332	-0.358	-0.264	-0.067	8.603	0.0646
U4	210	1	0.166	0.229	0.346	0.380	0.197	0.242	7.666	0.0642
	211	2	-0.305	-0.233	-0.139	-0.095	-0.252	0.231	4.946	0.0659
	212	3	0.285	0.299	0.280	0.258	0.397	0.0	4.894	0.0655
U5	213	1	0.273	0.277	0.283	0.278	0.299	0.006	5.947	0.0651
	214	2	-0.241	-0.253	-0.271	-0.253	-0.235	0.042	5.561	0.0658
	215	3	2.724	2.746	2.770	2.766	2.750	0.043	7.891	0.0637
U6	216	1	-0.004	0.002	0.014	-0.002	0.046	0.029	6.143	0.0682
(C2)	217	2	0.354	0.338	0.334	0.336	0.362	-0.017	6.895	0.0661
	218	3	0.280	0.345	0.410	0.429	0.304	0.165	7.334	0.0653
U7	219	1	-0.246	-0.279	-0.327	-0.361	-0.233	-0.124	7.227	0.0697
	220	2	-0.034	-0.189	-0.217	-0.231	-0.038	-0.208	8.193	0.0632
	221	3	0.610	0.592	0.568	0.578	0.631	-0.039	6.602	0.0668
U8	222	1	0.073	0.062	0.043	0.014	0.073	-0.061	8.281	0.0649
	223	2	0.183	0.197	0.224	0.234	0.216	0.058	8.623	0.0641
	224	3	-0.095	-0.077	-0.073	-0.046	-0.040	0.048	8.125	0.0639
U9	225	1	-0.515	-0.445	-0.354	-0.329	-0.463	0.200	5.244	0.0581
	226	2	-0.070	-0.069	-0.058	-0.065	-0.033	0.008	7.334	0.0695
	227	3	0.561	0.601	0.624	0.649	0.630	0.093	7.529	0.0671
U10	228	1	0.034	0.012	0.007	0.009	-0.057	-0.026	4.844	0.0651
	229	2	-0.170	-0.150	-0.090	-0.095	-0.154	0.091	5.02	0.0662
	230	3	0.021	0.017	0.683	0.107	0.097	0.0	6.563	0.0658

(continued)

*Calibration unsuccessful.

†V_0 = initial bridge voltage at 11°C and zero displacement.

††V_1 = bridge voltage at 200°C and zero displacement.

§V_s = bridge voltage as installed in the borehole.

Table E-3 (continued)

(H10)

Number			Offset voltages (mV)				Voltage			Slope
Gage (hole)	Sensor number	Component	21°C	83°C	142°C	209°C	V_o (mV)	V_1-V_o (mV)	V_s (mV)	C $\left(\frac{mm}{mV}\right)$
U11	711	1	0.146	0.146	0.168	0.175	0.177	0.033	7.617	0.0645
	712	2	0.241	0.234	0.227	0.188	0.262	-0.058	6.336	0.0656
	713	3	1.777	1.750	1.745	1.701	1.765	0.070	6.049	0.0657
U12	714	1	-0.004	0.022	0.031	0.007	-0.040	0.057	4.585	0.0666
	715	2	0.178	0.151	0.083	-0.034	0.118	0.214	4.406	0.0650
	716	3	0.043	-0.022	-0.048	-0.134	0.021	0.171	5.884	0.0675
U13	717	1	-0.065	-0.043	-0.024	-0.041	-0.073	0.064	---†	0.0650
	718	2	-0.058	-0.085	-0.129	-0.185	-0.072	-0.128	---	0.0658
	719	3	0.061	0.080	0.114	0.1099	0.044	0.083	---	0.0642
U14	720	1	0.119	0.148	0.212	0.249	0.128	0.136	5.629	0.0645
	721	2	-0.141	-0.185	-0.241	-0.324	-0.152	-0.183	6.406	0.0644
	722	3	-0.148	-0.146	-0.156	-0.173	-0.190	-0.025	6.712	0.0643
U15	723	1	-0.178	-0.202	-0.202	-0.271	-0.190	-0.086	4.671	0.0666
(C3)	724	2	0.109	0.124	0.124	0.087	0.105	0.022	5.323	0.0683
	725	3	0.097	0.170	0.246	0.302	0.081	0.208	6.703	0.0692
U16	726	1	-1.339	-1.423	-1.435	-1.516	-1.354	-0.146	4.803	0.0657
	727	2	0.080	0.087	0.102	0.070	0.066	0.034	7.027	0.0691
	728	3	0.329	0.249	0.168	0.068	0.327	-0.261	5.611	0.0659
U17	729	*1	--	--	--	--	-0.221	--	8.242	0.0645
(C4)	730	2	-0.148	-0.134	-0.107	-0.114	0.117	0.038	6.000	0.0655
	731	3	-0.075	-0.100	-0.146	-0.190	-0.079	-0.117	7.736	0.0635
U18	732	1	0.017	-0.043	-0.065	-0.156	0.008	-0.165	6.264	0.0640
	733	2	0.029	-0.007	-0.041	-0.124	0.049	-0.151	6.360	0.0647
	734	3	-0.524	-0.551	-0.595	-0.642	-0.485	-0.120	6.244	0.0645
U19	735	1	-0.246	-0.261	-0.283	-0.293	-0.100	-0.049	4.826	0.0637
	736	2	0.312	0.253	0.244	0.151	0.331	-0.149	6.404	0.0656
	737	3	-0.705	-0.754	-0.798	-0.883	-0.698	-0.175	5.089	0.0655
U20	738	1	0.092	0.112	0.105	0.105	0.065	0.008	5.473	0.0655
	739	2	0.512	0.534	0.534	0.512	0.522	0.0	5.735	0.0643
	740	3	-0.043	-0.031	0.012	-0.004	-0.052	0.087	5.871	0.0666

*Calibration unsuccessful.

†Gage failed early - no starting voltage.

Table E-3 (concluded)

(Extensometer Drift)

Number			Offset voltages (mV)				Voltage			Slope
Gage (hole)	Sensor number	Component	10°C	84°C	144°C	201°C	V_o (mV)	V_1-V_o (mV)	V_s (mV)	C $\left(\frac{mm}{mV}\right)$
U21	231	1	-0.051	-0.022	-0.078	-0.109	-0.003	-0.054	4.331	0.0713
	232	2	-0.273	-0.310	-0.332	-0.349	-0.258	-0.074	3.716	0.0694
	233	3	-0.064	-0.119	-0.231	-0.312	0.003	-0.252	5.669	0.0667
U22	234	1	-0.229	-0.261	-0.322	-0.302	-0.166	-0.085	5.063	0.0661
	235	2	-0.446	-0.422	-0.427	-0.397	-0.418	0.042	4.971	0.0673
	236	3	-1.577	-1.606	-1.630	-1.643	-1.53	-0.065	4.248	0.0666
U23	741	1	-0.014	-0.019	-0.134	-0.200	-0.0146	-0.195	6.121	0.068
	742	2	1.560	1.613	1.6189	1.677	1.56	0.114	8.389	0.0667
	743	3	0.007	-0.0026	0.017	0.029	0.007	0.020	7.374	0.0678
U24	744	1	1.713	1.696	1.647	1.657	1.714	-0.065	6.806	0.0631
	745	2	-0.283	-0.312	-0.412	-0.461	-0.283	-0.186	3.287	0.0638
	746	3	-0.297	-0.278	-0.239	-0.195	-0.298	0.101	5.049	0.0655
U25	747	1	-0.344	-0.266	-0.449	-0.400	-0.344	-0.100	6.118	0.0641
	748	2	0.153	0.127	0.144	0.127	0.153	-0.019	7.169	0.0642
	749	3	-0.898	-0.908	-0.983	-0.930	-0.898	-0.032	5.427	0.0648
U26	237	1	-0.202	-0.148	-0.178	-0.131	0.290	0.055	5.537	0.0641
	238	2	0.302	0.293	----	0.295	0.763	-0.006	8.242	0.0655
	239	3	-0.231	-0.266	----	-0.217	0.242	0.020	6.079	0.0643
U27	240	1	0.034	0.000	-0.073	-0.105	0.518	-0.139	4.643	0.0626
	241	2	-0.068	-0.053	-0.053	-0.039	0.454	0.026	5.337	0.0631
	242	3	-0.197	-0.134	-0.119	-0.056	-0.141	0.130	6.592	0.065
U28	243	1	0.078	0.004	-0.041	-0.083	0.079	-0.158	4.648	0.0625
	244	2	-1.596	-1.623	-1.684	-1.704	-1.58	-0.113	6.772	0.0663
	245	3	-0.622	-0.617	-0.661	-0.634	-0.589	0.0	5.898	0.0666
U29	750	1	0.368	0.378	0.376	0.371	0.369	-0.024	4.991	0.0674
	751	2	-0.236	-0.363	-0.505	-0.610	-0.237	-0.374	3.459	0.0687
	752	3	-0.061	0.158	0.190	0.280	0.061	0.205	4.812	0.066
U30	753	1	-0.307	-0.244	-0.224	-0.170	-0.308	0.128	7.156	0.0668
	754	2	-0.085	-0.092	-0.139	-0.148	-0.085	-0.069	5.209	0.0661
	755	3	-0.346	-0.239	-0.200	-0.114	-0.347	0.219	8.918	0.0687

Sensitivity Analysis of the USBM gage

The equations given in section 3 can be used to evaluate the sensitivity of the computed stress to errors in measurement, errors in parameter evaluation, and to parameter changes due to temperature effects. This evaluation is best done in two steps: first by assessing the possible errors in the measured displacement of the borehole wall as corrected for temperature effects, and secondly by examining the errors associated with computing the stresses from the displacements.

For example, consider the gage in horizontal hole U24. This gage measures the vertical and tangential components of stress at a radial distance of 2 m from the center of the 5-kW heater in heater hole H10, as given in Appendix A. In the first 200 days of operation the stress levels are predicted to rise about 15 MPa and the temperature to increase about 30°C. After the peripheral heaters are turned on, the stresses and temperature at U24 will rise again, for total expected increases of about 35 MPa and 90°C. Isotropic stress increases of 15 and 35 MPa induce bridge voltage increases of about 0.33 and 0.77 mV, respectively, for the gage in hole U24. Hence the following analysis addresses the impact of the variation of individual parameters upon the computed displacements and stresses for the two cases (30°C, 0.33 mV, 15 MPa) and (90°C, 0.77 mV, 35 MPa).

Equations (7) through (11) in section 3 can be rewritten to give

$$u_r = C_1 (1 + \delta C/C_1) (V - V_o - \delta V_o) - C_1 (V_s - V_o) - (\alpha_g - \alpha_r) d\delta T \qquad \text{(E-1)}$$

where the three temperature-dependent terms are:

$$\delta T = T\text{-}11$$

$$\delta V_o = \frac{V_1 - V_o}{189} \quad (T\text{-}11)$$

$$\delta C/C_1 = \frac{0.06}{189} \quad (T\text{-}11) \ .$$

For this analysis $\delta C/C_1$ is ignored with respect to unity, and δV is ignored with respect to $V-V_o$.

a) Bridge voltage V and starting voltage V_s. From Eq. (E-1) an error in the bridge voltage affects the displacement by the calibration factor C_1, which for gage U24 has the value 64 μm/mV,

$$\Delta u = C_1 \ \Delta V \ . \qquad \text{(E-2)}$$

Two factors affecting the bridge voltage stability are the bridge excitation voltage and the analog-to-digital conversion stability. A change in excitation voltage produces an equivalent fractional change in the signal. Stability of the excitation voltage is no better than 0.1% for a 30-hour time period, which corresponds to 7 μv for a 7 mV operating point. The overall stability of the analog-to-digital converter is given as ±5 μV. In addition, the drift measurements discussed previously also indicate a drift of less than 10 μV. Hence a 10 μV figure seems reasonable for the electronic stability, producing a displacement error of 0.6 μm. An error in V_s will be of opposite sign to an error in V, hence a voltage measurement error affecting both V and V_s equally will very nearly cancel [see Eq. (E-1)].

b) Offset voltage V_o. Errors due to a change in the magnitude of V_o will be quite small because the C_1 terms in Eq. (E-1) cancel, leaving

$$\Delta u \simeq -\delta C \ \Delta V_o \ .$$

At 90°C the value of δC is 0.025 x 64 μm/mV or 1.6 μm/mV. The drift measurements (refer to the discussion of Table E-2 in section 3) indicate a value of 0.01 mV for ΔV_0; however, the repeat reading done at Stripa just before installation (Table E-3) indicates that 0.05 mV is a more realistic value. Using these values in Eq. (E-2) gives a displacement error of -0.08 μm at 90°C and -0.025 μm at 30°C.

c) Temperature correction term δV_0. The error due to δV_0 will be

$$\Delta u \simeq -C_1 \quad \Delta(\delta V_0) \tag{E-3}$$

Since a linear fit is used to evaluate δV_0, the error is best assessed by evaluating the deviation from that linear fit. The average standard deviation of all the linear regression fits to the offset voltage data of Table E-3 is 0.0096 mV. Hence the displacement error is -0.61 μm, which does not seem to be much affected by temperature.

d) Calibration factor C_1. The errors due to variations in C_1 will be

$$\Delta u = (V-V_s)\Delta C_1 \ . \tag{E-4}$$

As given above, $V-V_s$ will be 0.33 mV and 0.77 mV for the two temperatures considered here. Repeat measurements in the laboratory (see Run No. 27 in Table E-1) and repeat calibrations on five gage components in the field, yielded a repeatability of about 0.5% for C_1. Hence ΔC_1 will be 0.005 x 64 μm/mV, or 0.32 μm/mV. From Eq. (E-4), the displacement errors for 30°C and 90°C are 0.11 μm and 0.25 μm, respectively.

e) Calibration factor correction term δC_1. The errors from δC_1 are

$$\Delta u \simeq (V-V_0) \ \Delta \ (\delta C_1) \ . \tag{E-5}$$

Comparing with Eq. (E-4), it is apparent that the correction term is more important as an error source than the calibration factor itself, because $V-V_0$ is considerably greater than $V-V_s$. Hence, to minimize this error source the operating point should be as close to V_0 as possible. For our case $V-V_0$ is 5.2 mV, and the correction term is judged to be about 6% ± 1%, so that

$$\begin{aligned}\Delta u &= 5.2 \times 0.01 \times 64 \times (T-11)/189 \\ &= 0.53\ \mu m\ (30°C) \\ &= 1.58\ \mu m\ (90°C)\ .\end{aligned}$$

f) Thermal expansion coefficient α. Except for sign, the gage and rock expansion coefficients can be treated together. An error of 10%, or 1 ppm per degree Centigrade seems a reasonable precision for α. Hence, the error in the displacement will be

$$\begin{aligned}\Delta u &= -d\ (\delta T)\ \Delta\alpha_g \\ &= -38 \times 10^{-3} \times 30 \times 10^{-6} \\ &= -1.1\ \mu m\ .\end{aligned} \tag{E-6}$$

For the 90°C case, the displacement error will be -3.3 μm for α_g.

g) Temperature T. Differentiating Eq. (E-1) with respect to T gives

$$\begin{aligned}\Delta u &= \left\{\frac{0.06}{189}\ C_1\ (V-V_o - \delta V_o) - C_1\ (1 + \delta C/C_1)\left[\frac{V_1-V_o}{189}\right] - (\alpha_g-\alpha_r)\ d\right\}\Delta T. \\ &= 0.14\Delta T\end{aligned} \tag{E-7}$$

This correction does not change much with temperature. Assuming a measurement accuracy of ± 2°C (see discussion in section 5) gives a displacement error of 0.28 μm.

h) Borehole diameter d. Since an error in the diameter affects both the gage and rock thermal corrections, we have

$$\begin{aligned} \Delta u &= -(\alpha_g - \alpha_r)\ \delta T \Delta d \\ &= -0.5 \times 10^{-6} \times 90 \times 10^{-3} \\ &= -0.045\ \mu m \end{aligned} \qquad \text{(E-8)}$$

where the diameter error Δd is assumed to be 1 mm. So, the displacement error is -0.015 μm and -0.045 μm for the 30°C and 90°C cases, respectively.

This completes the error analysis of the measured displacements. The results of steps a) through h) are summarized in Table E-4. It is clear that the thermal expansion correction produces the largest uncertainty in the displacement measurements, and that this source of error is temperature dependent. Next in order of importance are the errors associated with the bridge voltage reading V, and the temperature correction for the voltage offset V_0. In addition, at high temperature, errors in the calibration factor can be significant as this contribution is highly temperature dependent. Unimportant are the errors contributed by the offset voltage, the temperature, and the borehole diameter. Note that the maximum error in Table E-4 (3.3 μm) is about 6% of the total displacement of 56 μm as calculated from Eq. (E-1).

Note that the correction for thermal expansion applied in Eq. (E-1) is potentially a large correction to the displacement term. Ignoring secondary temperature corrections, the ratio of the thermal expansion term to the voltage term is $(\alpha_g - \alpha_r)\ \delta T / C_1\ (V - V_s)$. Using the values given above for the 90°C case gives a fraction of 0.035; so the thermal expansion

Table E-4. Summary of estimated errors in the USBM gage measurement of borehole displacement, including temperature compensation terms.

			Error in corrected displacement (μm)		
	Base case values	Magnitude of assumed error	(30°C)	(90°C)	Temperature independent
Bridge voltage V, V_s	5.61 mV 5.05 mV	10 μV			+0.6 -0.6
Offset voltage V_o	0.38 mV	50 μV	-0.025	-0.08	
Temperature correction for offset, δV_o	-0.15 mV	10 μV			-0.6
Calibration factor C_1	64 μm/mv	0.32 μm/mv (0.5%)	+0.11	+0.25	
Calibration factor correction $\delta C_1/C_1$	0.06	0.01	+0.5	+1.6	
Thermal expansion coefficients α_g α_r	11.5×10^{-6} 11.0×10^{-6}	1×10^{-6}	-1.1 +1.1	-3.3 +3.3	
Temperature T	30°, 90°	2°C			+0.28
Borehole diameter d	38 mm	1 mm	-0.015	-0.045	

Notes: The base case values apply to gage U24 located 2 m from heater H10. If the errors do not appear to be temperature dependent, they are listed in the third column. For comparison, the total displacements computed from Eq. E-1 are 21 μm and 48 μm for the 30° and 90°C base cases.

correction is only 3.5% of the total. However, since the precision in α_g and α_r is no better than $\pm 1 \times 10^{-6}$, the value of $\alpha_g - \alpha_r$ could easily be 2.5×10^{-6} per degree Centigrade instead of 0.5×10^{-6} per degree Centigrade, thereby increasing its contribution to 15%. At higher temperatures this contribution is of course increased even more.

The next step is relating the errors in displacement and in the mechanical moduli to the computed stress. This is done by assuming that the gage is subjected to a uniform stress so all three components are deformed equally and respond equally to any perturbation. If this is the case, then Eq. (12) in section 3 simplifies to

$$\sigma = \frac{Eu}{2(1-\nu^2)d} \quad . \tag{E-9}$$

The values E = 52 GPa, ν = 0.23, and d = 38 mm, assumed for the theoretical models, will be used in the following analysis.

i) Displacement u. The contribution of displacement error to the stress error is

$$\Delta\sigma = \frac{E}{2(1-\nu^2)d} \Delta u$$

$$= 0.7\Delta u \text{ (MPa/μm)}.$$

From Table E-4, the largest expected displacement error of 3.3 μm gives a stress error of 2.3 MPa.

j) Young's modulus E. Equation (E-9) gives

$$\Delta\sigma = \frac{u}{2(1-\nu^2)d} \Delta E \tag{E-10}$$

$$= 0.78 \times 10^{-3} \Delta E \text{ (90°C case)}$$

$$= 0.29 \times 10^{-3} \Delta E \text{ (30°C case)}.$$

Uncertainties in the determination of Young's modulus stem from geological neterogeneity and temperature dependence. Borehole measurements with the CSM cell reported in Nelson et al. (1979) show standard deviations of E as large as ± 10 GPa, and a mean value that varies with the fracture intensity. Laboratory data by Swan (1978) show a decrease of Young's modulus with temperature of -13.3 GPa per 100°C, but give average values greater than those obtained in situ. For present purposes, a figure of 10 GPa for the uncertainty in modulus is used, corresponding to a stress uncertainty of 3 MPa and 8 MPa for the two cases.

k) Poisson's ratio ν. The error due to ν is assessed by evaluating Eq. (E-9) directly rather than by differentiating. Assuming a variation of ± 20% in ν gives values of 0.18, 0.23 (base case), and 0.28. Insertion of these values in Eq. (E-9) gives errors of about 0.5 MPa and 1.0 MPa for the 30° and 90°C cases.

l) Borehole diameter d. Borehole diameter affects both the displacement, already assessed above, and the computed stress:

$$\Delta\sigma = -\frac{Eu}{2(1-\nu^2)d^2}\,\Delta d$$

$$= -0.91\ \Delta d\ (\text{mm})\ (90°\text{C})$$

$$= -0.40\ \Delta d\ (\text{mm})\ (30°\text{C})\ .$$

For 1 mm error of borehole diameter, the stress errors are 0.4 and 0.9 MPa.

Table E-5 summarizes the contributions of errors in the measured borehole deformation and in the mechanical moduli upon the computed stress for the hydrostatic stress field assumed for Eq. (E-9). The values used for the

Table E-5. Estimated errors in stresses computed from a USBM gage measurement due to assumed errors in the measured borehole displacement and in the mechanical moduli. Base case values at 30°C and 90°C are 15 MPa and 35 MPa.

	Magnitude of assumed error		Error in computed stress (MPa)	
	30°C	90°C	30°C	90°C
Displacement	1.1 μm	3.3 μm	+0.8	+2.3
Young's modulus	10 GPa	10 GPa	+3.0	+8.0
Poisson's ratio	0.05	0.05	+0.5	+1.0
Borehole diameter	1 mm	1 mm	-0.4	-0.9

borehole displacement are the maximum values given in Table E-4, which are attributed to the thermal expansion coefficients. The errors adopted for the Young's modulus and Poisson's ratio are only rough estimates, representing fluctuations of ± 20% in the established values. As shown in Table E-5, the error in displacement measurement contributes less to the overall stress error than the uncertainty in Young's modulus. Unaccounted for in Table E-5 is the effect of long-term drift upon the measurement accuracy. Another source of uncertainty is the plane strain assumption used in deriving Eqs. (12) and (13) in section 3, which relate the measured borehole displacements to the stresses.

APPENDIX F. IRAD Gauge Installation Data

H10 area

Gage no.	Gage (hole)	Sensor number	Orientation	$C_1(23)$ $\times 10^9$	$C_2(23)$	Initial period, R_o	Installed period, R_s	
3-73*	C3 (U15)	862	R	-.233	54.69	1961	2180	220
3-77*	C3 (U15)	861	O	-.300	71.51	1969	2167	197
3-63	C4 (U17)	864	R	-.396	92.01	2036	2165	130
3-8	C4 (U17)	863	O	-.279	67.86	1868	2047	177
3-35	C5	866	R	-.279	67.86	1907	2086	180
3-82*	C5	865	O	-.305	72.18	1980	2151	170
3-45*	C10	870	Z	-.321	62.18	2204	2431	230
3-14	C10	869	O	-.383	71.78	2244	2476	230
3-29	C14	874	Z	-.194	45.72	2010	2166	156
3-9	C14	873	O	-.194	45.72	2005	2194	190
3-36	C15	876	Z	-.338	67.17	2165	2350	185
3-50*	C15	875	O	-.338	67.17	2161	2371	210

H9 area

3-20	C1	272	R	-.279	67.86	1926	2082	155
3-22	C1	271	O	-.279	67.86	1926	2053	127
3-16*	C2 (U6)	274	R	-.279	67.86	1937	2131	194
3-18*	C2 (U6)	273	O	-.213	51.15	1958	2091	133
3-68*	C6	276	Z	-.267	58.62	2044	2277	
3-55*	C6	275	O	-.267	58.62	2044	2276	
3-74*	C7	278	Z	-.293	68.53	1985	2195	
3-92*	C7	277	O	-.194	45.72	1973	2161	
3-58	C8	280	Z	-.296	65.59	2051	2249	
3-90*	C8	279	O	-.393	84.40	2072	2276	
3-37*	C11	282	Z	-.289	58.38	2139	2324	
3-1	C11	281	O	-.289	58.38	2131	2318	
3-43	C12	284	Z	-.344	66.90	2195	2376	
3-48	C12	283	O	-.383	71.78	2285	2515	

NOTES: Damaged gages = 3-56, 3-80*, 3-71, 3-70*, 3-54*, 3-62*.

Extra gages = 3-42, 3-4, 3-5 (high Ro values).

The initial and installed periods are in gage reading units (10^{-7} sec).

*Calibrated gages.

APPENDIX G. Thermocouple Calibration Coefficients

THERMOCOUPLE POLYNOMIAL COEFFICIENTS FOR EXPERIMENT 1

HOLE	SENSOR NUMBER	POLYNOMIAL COEFFICIENTS C0	C1	C2	C3	C4
C6	79	-.72491	26.53800	-1.019300	.154750	-.007271000
C7	80	-.72491	26.53800	-1.019300	.154750	-.007271000
C8	81	-.53194	25.49380	-.645966	.103520	-.005080310
C11	82	-.72491	26.53800	-1.019300	.154750	-.007271000
C12	83	-.53194	25.49380	-.645966	.103520	-.005080310
E6	122	-1.90683	28.02560	-1.721950	.282717	-.014919600
E6	123	-1.63638	27.53450	-1.480530	.241607	-.012630600
E6	130	-1.17568	26.41170	-.995426	.153588	-.007442650
E7	21	-1.31435	26.83150	-1.249910	.210827	-.011294800
E7	22	-1.25915	26.74020	-1.170130	.200259	-.010827000
E7	23	-.81369	25.94120	-.808877	.131111	-.006576890
E7	24	-1.24845	26.72850	-1.193370	.200932	-.010697400
E7	124	-1.35600	27.04960	-1.258340	.203125	-.010393300
E7	125	-1.03025	26.42100	-1.043540	.162625	-.007946600
E7	128	-1.17570	26.41200	-.995430	.153590	-.007442650
E7	131	-1.17568	26.41170	-.995426	.153588	-.007442650
E8	25	-1.24168	26.72920	-1.195980	.200310	-.010636000
E8	26	-1.48172	27.12260	-1.342220	.225867	-.012097200
E8	27	-1.20746	26.62440	-1.097420	.184149	-.009772720
E8	28	-.92167	26.13000	-.870671	.144857	-.007488220
E8	132	-1.17568	26.41170	-.995426	.153588	-.007442650
E9	133	-1.17568	26.41170	-.995426	.153588	-.007442650
E9	160	-1.24850	26.72800	-1.193400	.200930	-.010697000
E10	33	-.99973	26.29760	-.968988	.165488	-.008858970
E10	34	-1.37030	26.91490	-1.234830	.205791	-.010911500
E10	35	-1.07070	26.37570	-.990399	.164096	-.008514420
E10	36	-1.02736	26.29080	-.946101	.156072	-.008041750
E10	134	-1.17568	26.41170	-.995426	.153588	-.007442650
E10	161	-1.24850	26.72800	-1.193400	.200930	-.010697000
E11	37	-.82313	25.93580	-.786083	.126966	-.006305740
E11	38	-1.10127	26.44450	-1.031640	.172328	-.009039790
E11	39	-1.31975	26.88860	-1.245310	.212139	-.011456200
E11	40	-1.08173	26.43410	-1.044730	.173603	-.009060480
E11	135	-1.17568	26.41170	-.995426	.153588	-.007442650
E18	41	-1.35764	26.84930	-1.245290	.208904	-.011122500
E18	42	-1.17579	26.58820	-1.111870	.187277	-.009932520
E18	43	-.96611	26.23170	-.931314	.160526	-.008639030
E18	142	-1.12666	26.56190	-.094943	.155351	-.007930390
E19	45	-1.27504	26.78310	-1.203200	.203537	-.010888100
E19	46	-1.33471	26.87490	-1.184250	.202253	-.010926600
E19	47	-1.13048	26.52020	-1.065870	.182176	-.009801600
E19	143	-1.12666	26.56190	-.094943	.155351	-.007930390

E20	49	-.83995	26.15460	-.935847	.156132	-.008118330
E20	50	-.94411	26.21090	-.927744	.154832	-.008061830
E20	144	-1.12666	26.56190	-.094943	.155351	-.007930390
E21	53	-1.17437	26.76050	-1.168470	.184168	-.009200370
E21	54	-.97932	26.29580	-1.024520	.170759	-.008961380
E21	55	-1.30135	26.81900	-1.213480	.208459	-.011308600
E21	145	-1.12666	26.56190	-.094943	.155351	-.007930390
E22	57	-.92702	26.28250	-.980563	.162286	-.008392080
E22	58	-1.29387	26.81860	-1.215540	.207717	-.011238800
E22	59	-1.13387	26.53080	-1.120160	.188272	-.009950420
E22	146	-1.12666	26.56190	-.094943	.155351	-.007930390
E23	61	-1.04406	26.36820	-1.020670	.173188	-.009225710
E23	62	-1.10258	26.56830	-1.100980	.190164	-.010327800
E23	63	-.93837	26.21300	-.963400	.159676	-.008295930
E23	147	-1.12666	26.56190	-.094943	.155351	-.007930390
E24	65	-1.39580	26.87620	-1.252350	.209888	-.011146400
E24	66	-1.07491	26.45240	-1.074140	.180127	-.009502930
E24	67	-.90922	26.14260	-.905065	.146358	-.007557310
E24	148	-1.12666	26.56190	-.094943	.155351	-.007930390
E25	69	-1.14555	26.47480	-1.059140	.174550	-.009017820
E25	70	-1.12775	26.40410	-1.001240	.166847	-.008754000
E25	71	-.99990	26.30540	-.993481	.164984	-.008553620
E25	149	-1.12666	26.56190	-.094943	.155351	-.007930390
E26	73	-1.49002	27.02160	-1.295310	.224122	-.012335600
E26	74	-1.47539	26.99110	-1.298830	.224228	-.012295600
E26	75	-1.42315	26.93080	-1.285900	.217687	-.011689000
E26	150	-1.12666	26.56190	-.094943	.155351	-.007930390
U2	3	-1.73705	27.72970	-1.626510	.267041	-.014076900
U3	4	-1.68781	27.64970	-1.552940	.257666	-.013682200
U4	5	-1.11940	26.69020	-1.179270	.187490	-.009444590
U5	6	-1.73705	27.72970	-1.626510	.267041	-.014076900
U7	8	-1.11940	26.69020	-1.179270	.187490	-.009444590
U9	10	-1.68781	27.64970	-1.552940	.257666	-.013682200
U10	11	-1.11940	26.69020	-1.179270	.187490	-.009444590
U21	12	-1.73705	27.72970	-1.626510	.267041	-.014076900
U22	13	-1.68781	27.64970	-1.552940	.257666	-.013682200
U26	14	-1.11940	26.69020	-1.179270	.187490	-.009444590
U27	15	-1.73705	27.72970	-1.626510	.267041	-.014076900
U28	16	-1.68781	27.64970	-1.552940	.257666	-.013682200

THERMOCOUPLE POLYNOMIAL COEFFICIENTS FOR EXPERIMENT 1

THE FOLLOWING THERMOCOUPLES USE THE NBS STANDARD CURVE
COEFFICIENTS .31595 23.92680 .151074 -.010743 .000197998

HOLE	SENSOR NUMBER	HOLE	SENSOR NUMBER	HOLE	SENSOR NUMBER	HOLE	SENSOR NUMBER
C1	77	C2	7	E6	17	E6	18
E6	19	E6	20	E9	29	E9	30
E9	31	E9	32	E18	44	E19	48
E20	51	E20	52	E21	56	E22	60
E23	64	E24	68	E25	72	E26	76
H9	114	H9	115	H9	116	H9	117
H9	118	H9	119	H9	120	H9	121
T13	84	T13	85	T13	86	T13	87
T13	88	T14	89	T14	90	T14	91
T14	92	T14	93	T15	94	T15	95
T15	96	T15	97	T15	98	T16	99
T16	100	T16	101	T16	102	T16	103
T17	104	T17	105	T17	106	T17	107
T17	108	T18	109	T18	110	T18	111
T18	112	T18	113	U1	2	J6	78
U8	9						

THERMOCOUPLE POLYNOMIAL COEFFICIENTS FOR EXPERIMENT 2

HOLE	SENSOR NUMBER	POLYNOMIAL COEFFICIENTS C0	C1	C2	C3	C4
C4	433	-1.61187	27.74970	-1.606480	.264657	-.013971100
C10	506	-1.92615	28.05190	-1.738620	.293608	-.015974700
C14	508	-1.52682	27.48770	-1.503190	.247396	-.013060300
C15	509	-1.59953	27.59180	-1.538090	.252242	-.013183900
E12	442	-1.33880	26.91300	-1.296130	.216796	-.011720200
E12	443	-1.27056	26.78550	-1.230230	.207373	-.011055000
E12	444	-1.37816	26.94970	-1.295070	.218337	-.011688500
E12	445	-1.36184	26.94200	-1.282040	.222817	-.012255300
E12	573	-1.07050	26.74400	-1.193300	.192500	-.009784250
E13	446	-1.44362	27.05310	-1.289650	.219397	-.011901500
E13	447	-1.30567	26.87390	-1.262330	.212712	-.011355000
E13	448	-1.30419	26.94550	-1.287600	.219141	-.011807800
E13	449	-1.15155	26.56080	-1.107230	.187638	-.009999060
E14	450	-1.28901	26.72470	-1.186010	.205168	-.011224700
E14	451	-1.16788	26.47430	-1.056630	.175622	-.009162070
E14	452	-1.38411	26.86660	-1.240260	.208857	-.011123300
E14	453	-1.42970	26.95190	-1.283720	.221027	-.012068300
E15	454	-1.16444	26.48190	-1.054130	.176428	-.009268020
E15	455	-1.14648	26.44960	-1.060520	.176973	-.009272390
E15	456	-1.22312	26.61040	-1.131440	.190229	-.010121000
E15	457	-1.24916	26.62960	-1.128230	.195013	-.010611900
E17	462	-1.21919	26.69020	-1.184310	.200593	-.010715600
E17	463	-1.21013	26.67540	-1.172960	.196408	-.010403100
E17	464	-1.21996	26.69050	-1.174230	.198659	-.010638900
E17	465	-1.36162	26.91420	-1.221230	.208509	-.011306000
E27	466	-1.24551	26.61330	-1.129810	.191420	-.010272600
E27	467	-1.40950	26.79120	-1.209550	.202032	-.010666000
E27	468	-1.34896	26.68160	-1.155870	.192891	-.010209500
E28	470	-.47697	25.17040	-.465173	.071657	-.003229050
E28	471	-1.26696	26.64720	-1.152140	.195178	-.010506700
E28	472	-1.49832	27.04560	-1.341290	.227647	-.012292700
E29	474	-1.57797	27.16330	-1.326600	.225809	-.012252700
E29	475	-1.14156	26.41100	-1.017680	.174990	-.009477290
E30	478	-.60657	25.66560	-.660577	.112408	-.005830010
E30	479	-1.18540	26.71240	-1.176070	.205563	-.011352700
E30	480	-1.26794	26.74850	-1.188150	.205828	-.011293200
E31	482	-1.09527	26.36000	-.982885	.167808	-.009024230
E31	483	-1.19665	26.62700	-1.139760	.197211	-.010820600
E31	484	-1.29098	26.87910	-1.244650	.215245	-.011820700
E31	572	-1.12670	26.56200	-.094943	.155350	-.007930390

E32	486	-.92140	26.26930	-1.023020	.172424	-.009204090
E32	487	-1.14331	26.64950	-1.155160	.194619	-.010364700
E32	488	-.47697	25.17040	-.465173	.071657	-.003229050
E33	490	-.59494	25.64650	-.656615	.104988	-.005077240
E33	491	-.86932	26.24780	-.956820	.162851	-.008669010
E33	492	-.61153	25.79070	-.736020	.126828	-.006702370
E34	494	-1.29284	26.89310	-1.230700	.207439	-.011128500
E34	495	-.47697	25.17040	-.465173	.071657	-.003229050
E34	496	-.47697	25.17040	-.465173	.071657	-.003229050
E35	498	-1.21122	26.75020	-1.138870	.194787	-.010583900
E35	499	-1.12218	26.68740	-1.143230	.193752	-.010404900
E35	500	-1.09942	26.52720	-1.086200	.182349	-.009631600
U12	428	-1.72291	27.74210	-1.616350	.263653	-.013781300
U13	429	-.76521	26.12790	-.888034	.136164	-.006435750
U14	430	-.47697	25.17040	-.465173	.071657	-.003229050
U16	432	-1.43258	27.42780	-1.452050	.236733	-.012302000
U17	503	-1.75217	27.88040	-1.618420	.270862	-.014557000
U18	434	-1.08490	26.95590	-1.254580	.202474	-.010334800
U19	435	-1.44471	27.49130	-1.505030	.245077	-.012767300
U20	436	-1.53517	27.72520	-1.595840	.262860	-.013893000
U23	437	-1.41305	26.94640	-1.253030	.194891	-.009640070
U24	438	-1.28803	26.97570	-1.291600	.206867	-.010549000
U25	439	-1.17437	26.76050	-1.168470	.184168	-.009200370
U29	440	-1.24616	26.85630	-1.193630	.188764	-.009442220
U30	441	-1.67514	27.63320	-1.573100	.257699	-.013511500

THERMOCOUPLE POLYNOMIAL COEFFICIENTS FOR EXPERIMENT 2

THE FOLLOWING THERMOCOUPLES USE THE NBS STANDARD CURVE
COEFFICIENTS .31595 23.92680 .151074 -.010743 .000197998

HOLE	SENSOR NUMBER	HOLE	SENSOR NUMBER	HOLE	SENSOR NUMBER	HOLE	SENSOR NUMBER
C5	504	E16	458	E16	459	E16	460
E16	461	E27	469	E28	473	E29	476
E29	477	E30	481	E31	485	E32	489
E33	493	E34	497	E35	501	H10	540
H10	541	H10	542	H10	543	H10	544
H10	545	H10	546	H10	547	H11	548
H11	549	H11	550	H12	551	H12	552
H12	553	H13	554	H13	555	H13	556
H14	557	H14	558	H14	559	H15	560
H15	561	H15	562	H16	563	H16	564
H16	565	H17	566	H17	567	H17	568
H18	569	H18	570	H18	571	T19	510
T19	511	T19	512	T19	513	T19	514
T20	515	T20	516	T20	517	T20	518
T20	519	T21	520	T21	521	T21	522
T21	523	T21	524	T22	525	T22	526
T22	527	T22	528	T22	529	T23	530
T23	531	T23	532	T23	533	T23	534
T24	535	T24	536	T24	537	T24	538
T24	539	U11	427	U15	502		

THERMOCOUPLE POLYNOMIAL COEFFICIENTS FOR EXPERIMENT 3

HOLE	SENSOR NUMBER	POLYNOMIAL COEFFICIENTS C0	C1	C2	C3	C4
E1	902	-.45256	25.84430	-.766434	.125494	-.006242670
E1	903	-.45256	25.84430	-.766434	.125494	-.006242670
E1	904	-.45256	25.84430	-.766434	.125494	-.006242670
E1	905	-.45256	25.84430	-.766434	.125494	-.006242670
E1	985	-.45256	25.84430	-.766434	.125494	-.006242670
E1	1014	-.45256	25.84430	-.766434	.125494	-.006242670
E1	1015	-.45256	25.84430	-.766434	.125494	-.006242670
E2	906	-.45256	25.84430	-.766434	.125494	-.006242670
E2	907	-.45256	25.84430	-.766434	.125494	-.006242670
E2	908	-.45256	25.84430	-.766434	.125494	-.006242670
E2	909	-.45256	25.84430	-.766434	.125494	-.006242670
E2	989	-.45256	25.84430	-.766434	.125494	-.006242670
E3	910	-.45256	25.84430	-.766434	.125494	-.006242670
E3	911	-.45256	25.84430	-.766434	.125494	-.006242670
E3	912	-.45256	25.84430	-.766434	.125494	-.006242670
E3	913	-.45256	25.84430	-.766434	.125494	-.006242670
E3	993	-.45256	25.84430	-.766434	.125494	-.006242670
E3	1016	-.45256	25.84430	-.766434	.125494	-.006242670
E3	1017	-.45256	25.84430	-.766434	.125494	-.006242670
E4	914	-.45256	25.84430	-.766434	.125494	-.006242670
E4	915	-.45256	25.84430	-.766434	.125494	-.006242670
E4	916	-.45256	25.84430	-.766434	.125494	-.006242670
E4	917	-.45256	25.84430	-.766434	.125494	-.006242670
E4	997	-.45256	25.84430	-.766434	.125494	-.006242670
E5	918	-.45256	25.84430	-.766434	.125494	-.006242670
E5	919	-.45256	25.84430	-.766434	.125494	-.006242670
E5	920	-.45256	25.84430	-.766434	.125494	-.006242670
E5	921	-.45256	25.84430	-.766434	.125494	-.006242670
E5	1001	-.45256	25.84430	-.766434	.125494	-.006242670
T1	922	-.58581	26.33050	-.926792	.136299	-.006248000
T1	923	-.71480	26.54860	-1.008110	.157155	-.007623940
T1	924	-.87672	26.70630	-1.104110	.162297	-.007305010
T1	925	-.82407	26.63900	-.982284	.143282	-.006207990
T1	926	-.70847	26.56460	-1.001040	.153261	-.007260490
T2	927	-.62020	26.49750	-.963762	.147527	-.007026640
T2	928	-.81349	26.73920	-1.122870	.166770	-.007632650
T2	929	-.91419	26.74280	-1.044380	.156386	-.007168630
T2	930	-.79013	26.66730	-1.057610	.162417	-.007722040
T2	931	-.69822	26.49740	-.943611	.142027	-.006564960
T3	932	-.76050	26.61170	-1.043590	.159149	-.007494030
T3	933	-.70914	26.59900	-1.020840	.155047	-.007160690
T3	934	-.66775	26.53720	-1.017250	.147750	-.006480330
T3	935	-.83314	26.72540	-1.087850	.166833	-.007865160
T3	936	-.80508	26.69620	-1.073660	.164878	-.007789620

T4	937	-.84659	26.71940	-1.023530	.152415	-.006877180
T4	938	-.65464	26.40050	-.895835	.131573	-.005830540
T4	939	-.62048	26.48820	-.972951	.148153	-.006941150
T4	940	-.81265	26.71650	-1.078260	.165495	-.007873890
T4	941	-.66411	26.45380	-.959364	.144655	-.006700880
T5	942	-.68550	26.56770	-1.056090	.158318	-.007321920
T5	943	-.60552	26.46620	-1.009210	.150732	-.006975040
T5	944	-.71250	26.64270	-1.086290	.162900	-.007559380
T5	945	-.71480	26.48990	-1.003150	.146797	-.006476800
T5	946	-.83247	26.73460	-1.074620	.163964	-.007661870
T6	947	-.75563	26.52250	-.997581	.154706	-.007478130
T6	948	-.73233	26.56840	-1.009500	.155246	-.007394480
T6	949	-.85510	26.73710	-1.033160	.153620	-.006956160
T6	950	-.80150	26.66960	-1.067860	.162781	-.007607620
T6	951	-.84799	26.71900	-1.022080	.152196	-.006913940
T7	952	-.81774	26.75360	-1.087700	.167066	-.007923740
T7	953	-.85124	26.76340	-1.095760	.166963	-.007764840
T7	954	-.70359	26.52810	-.991926	.151748	-.007213510
T7	955	-.66988	26.46910	-1.009360	.151204	-.007062690
T7	956	-.62647	26.40000	-.954224	.138478	-.006155100
T8	957	-.88243	26.79200	-1.108090	.168953	-.007849910
T8	958	-.89492	26.77720	-1.107190	.170318	-.008123400
T8	959	-.89397	26.73270	-1.074140	.162505	-.007511080
T8	960	-.91206	26.77050	-1.048310	.156430	-.007184260
T8	961	-.82390	26.70680	-1.060440	.160850	-.007470170
T9	962	-.68819	26.51290	-1.013260	.150617	-.006965650
T9	963	-.74459	26.58220	-1.011730	.155201	-.007378390
T9	964	-.62877	26.43370	-.991892	.148102	-.006916520
T9	965	-.79562	26.69310	-1.077300	.164396	-.007770040
T9	966	-.48633	25.87580	-.711803	.113401	-.005513340
T10	967	-.50381	25.91910	-.765287	.124220	-.006195730
T10	968	-.48997	25.92690	-.794088	.130505	-.006530240
T10	969	-.43004	25.80300	-.745619	.123661	-.006265920
T10	970	-.46158	25.88080	-.769336	.126847	-.006433010
T10	971	-.45256	25.84430	-.766434	.125494	-.006242670
T11	972	-.47832	25.87700	-.730124	.117400	-.005733200
T11	973	-.44690	25.87830	-.799771	.126428	-.006188850
T11	974	-.59387	26.07070	-.856127	.140582	-.007023730
T11	975	-.40758	25.75560	-.717725	.117594	-.005830890
T11	976	-.55819	25.94500	-.737732	.113986	-.005134730
T12	977	-.48661	25.88020	-.766725	.123372	-.005935650
T12	978	-.58357	26.07090	-.883788	.137078	-.006424460
T12	979	-.50230	25.86090	-.708688	.110353	-.005047370
T12	980	-.52067	25.90470	-.797073	.121159	-.005417800
T12	981	-.55086	25.99960	-.826386	.134041	-.006542780

THERMOCOUPLE POLYNOMIAL COEFFICIENTS FOR EXPERIMENT 3

THE FOLLOWING THERMOCOUPLES USE THE NBS STANDARD CURVE
COEFFICIENTS .31595 23.92680 .151074 -.010743 .0001979

HOLE	SENSOR NUMBER	HOLE	SENSOR NUMBER	HOLE	SENSOR NUMBER	HOLE	SENSOR NUMBER
H1	982	H1	983	H1	984	H2	986
H2	987	H2	988	H3	990	H3	991
H3	992	H4	994	H4	995	H4	996
H5	998	H5	999	H5	1000	H6	1002
H6	1003	H6	1004	H7	1006	H7	1007
H7	1008	H8	1010	H8	1011	H8	1012

10. REFERENCES

American Society for Metals. 1975. Metals Handbook. 8th ed. Vol.I (Properties & Selection of Metals). Metals Park, Ohio: ASM.

ANSI. 1976. American National Standard for Temperature Measurement Thermocouples. ANSI-MC 96.1-1975. Pittsburgh: Instrument Society of America.

Burleigh, R.H., E.P. Binnall, A.O. DuBois, D.U. Norgren, and A.R. Ortiz. 1979. Electrical Heaters for Thermo-mechanical Tests at the Stripa Mine. Lawrence Berkeley Laboratory report LBL-7063,SAC-13. Berkeley, California.

Chan, Tin, Neville G.W. Cook, and Chin-Fu Tsang. 1978. Theoretical Temperature Fields for the Stripa Heater Project. Lawrence Berkeley Laboratory report LBL-7082, SAC-09. Berkeley, California.

Fossum, A. F., J. E. Russell, and F. D. Hansen. 1977. Analysis of a Vibrating Wire Stress Gage in Soft Rock. Exp. Mech. 17(7):261-264.

Hawkes, I. and W.V. Bailey. 1973. Design, Develop, Fabricate, Test, and Demonstrate Permissible Low Cost Cylindrical Stress Gages and Associated Components Capable of Measuring Change of Stress as a Function of Time in Underground Coal Mines. U.S. Bureau of Mines Contract Report (H0220050). Washington, D.C.

Hooker, V., J. Aggson, and D. Bickel. 1974. Improvements in the Three-Component Borehole Deformation Gage and Overcoring Technique. U.S. Bureau of Mines Report of Investigations #7894. Washington, D.C.

IRAD Gage, Inc. 1977. Vibrating Wire Stress Meter Instruction Manual. Lebanon, New Hampshire.

Kurfurst, Pavel J., T. Hugo-Persson, and G. Rudolph. 1978. Borehole Drilling and Related Activities at the Stripa Mine. Lawrence Berkeley Laboratory report LBL-7080, SAC-05. Berkeley, California.

Marshall, C.W. and R.E. Maringer. 1976. Dimensional Stability, An Introduction. New York: Pergamon Press.

McEvoy, Maurice B. 1979. Data Acquisition, Handling, and Display for the Heater Experiments at Stripa. Lawrence Berkeley Laboratory report LBL-7062, SAC-14. Berkeley, California.

Nelson, P., B. Paulsson, R. Rachiele, L. Andersson, T. Schrauf, W. Hustrulid, O. Duran, and K. A. Magnusson. 1979. Preliminary Report on Geophysical and Mechanical Borehole Measurements at Stripa. Lawrence Berkeley Laboratory report LBL-8280, SAC-16. Berkeley, California.

Obert, L. and W.I. Duvall. 1967. Rock Mechanics and the Design of Structures in Rock. New York: John Wiley and Sons.

Pratt, H.R., T.A. Schrauf, L.A. Bills, and W.A. Hustrulid. 1977. Thermal and Mechanical Properties of Granite, Stripa, Sweden. Terra Tek report #TR77-92. Salt Lake City, Utah.

Seifert, W.F., L.L. Jackson, and C.F. Sech. 1972. Design and Operational Consideration for High Temperature Organic Heat Transfer Systems. In Process Heat Transfer Syymposium, Dallas, Texas. American Institute of Chemical Engineers.

Smithells, Colin J., editor. 1976. Metals Reference Book. 5th ed. London & Boston: Butterworths.

Swan, Graham. 1978. The Mechanical Properties of Stripa Granite. Lawrence Berkeley Laboratory report LBL-7074, SAC-03. Berkeley, California.

Teknekron, Inc. 1978. Geotechnical Graphical and Data Acquisition System User's Manual. Berkeley, California.